The Application of Radiowave Tomography for the Characterization of Fractured Rock Aquifers

R Meyer • E Wedepohl • G Mitchell • B Pitts

Report to the Water Research Commission
by the
Division of Water, Environment and Forestry Technology, CSIR
and
Division of Mining Technology, CSIR

WRC Report No 516/1/98

THE APPLICATION OF RADIOWAVE TOMOGRAPHY FOR THE CHARACTERIZATION OF FRACTURED ROCK AQUIFERS

Report to the

WATER RESEARCH COMMISSION

on the Project "The Application of Seismic Tomography and Ground Penetrating Radar for the Detection of Fractures and the Determination of Hydraulic Properties of Fractured Rock Aquifers

by

R Meyer, E Wedepohl, G Mitchell and B Pitts
Division of Water, Environment and Forestry Technology
and
Division of Mining Technology, CSIR

WRC Project No 516/1/98
ISBN 1 86845 445 2

EXECUTIVE SUMMARY

1. Introduction

Research into secondary aquifers has been identified by the Water Research Commission as one of its primary focus areas for ground water research and forms part of a longer term ground water research programme. Fractured rock aquifers play a major role in South African geohydrology as more than 80% of the country's ground water reserves are found in such aquifers. The physical nature and behaviour of fractured rock aquifers, however, are not well understood. South African researchers are therefore in a unique position to conduct research into this category of aquifers and thereby make a valuable contribution to our knowledge base of these aquifers. In addition, fractured rock aquifers are present in different forms in South Africa. They range from Protorozoic crystalline type rocks that have undergone a long history of tectonic change, chemically deposited formations where secondary aquifer conditions have been developed through karstification processes enhanced by a long tectonic history, to relatively young fractured sedimentary rocks.

The behaviour of fractured aquifers in general cannot be described by the traditionally used theory of porous flow. Botha (1992) has shown through theoretical derivation of flow formulae that almost identical time drawdown relations are observed in phreatic and in two layer confined aquifers. This leads to the formulation of incorrect conceptual models during the investigation of aquifers, which in turn may lead to totally incorrect aquifer parameters being calculated. Management of aquifers can therefore be based on incorrect assumptions made and may lead to serious consequences in the long term for providing a sustainable water supply or to control or remediate aquifer pollution.

2. Purpose of the study

The investigation was primarily focussed to gain a better understanding of the physical nature of hardrock aquifers through the application of sophisticated geophysical techniques not generally applied in ground water research. Initially it was envisaged that seismic borehole tomography and borehole radar imaging techniques would be applied. Although both these techniques were used, the main emphasis shifted during the course of the project to the application of Radiowave Tomography (RT). However, despite changing to different techniques, the primary objectives remained the same. These were:

(a) To investigate the above mentioned geophysical techniques as fracture detection and characterisation techniques, through theoretical modelling studies for different fracture geometries and distributions. The aim of this investigation was to gain knowledge on the theoretical limitations of the techniques when used as tools to study secondary aquifers.

(b) To collaborate with the Institute of Groundwater Studies (IGS) at the University of the Orange Free State in their WRC projects related to fractured aquifer research and in particular as it relates to the Campus Test Site. The results from packer tests, cross hole test data, detailed geological investigations and other information collected for the test site were to be incorporated in the research programme.

(c) To relate the geophysical characteristics obtained from seismic tomography and radar technologies to the storage coefficient and hydraulic conductivity.

(d) To compare the accuracy and reliability of the methods regarding their representation of the physical conditions and hydraulic characteristics.

(e) To use geostatistical techniques for the three dimensional interpolation of the data, as well as to define the accuracy and certainty with which the data represent the geology.

(f) To assess the cost of applying the methods versus the reliability for a cost benefit analysis.

The final report on the project was to include a description of the techniques used during the project for fracture detection and characterisation highlighting the areas where deficiencies in our current knowledge of the methodologies exist and to which future research should be directed.

The progress report tabled at the first Steering Committee meeting in 1993 (Brandt and Coetsee, 1993) highlighted the difficulties with seismic tomography and especially the approach the researchers initially envisaged using in the characterisation of secondary aquifers and in particular, fracture characterisation.

To obtain the in situ stress and related fracture distribution in the rock, seismic techniques are often used. One such technique which is investigated intensively in the oil exploration industry, is to detect seismic anisotropy primarily caused by fractures and horizontal layering. This techniques can be employed to determine the strike of vertical fractures, fracture density, fluid content of fractures and the aspect ratio. Three main effects of anisotropy on seismic wave propagation are, (i) shear wave splitting, (ii) polarization and (iii) velocity variations. The Vertical Seismic Profiling (VSP) technique in particular was identified and proposed as a technique that could be used to study seismic anisotropy. One of the problems associated with the VSP technique identified during the literature study was that the best results are only achieved when this technique is applied in fairly deep boreholes, typically a few hundred metres deep. Concerns were raised by the Steering Committee as to whether the results achieved at these depths still relate to the geohydrology of fractured rock aquifers at the depths that the ground water industry is usually exploring.

The Steering Committee also had some reservations about the applicability of this technique in fractured aquifer research, particularly in the South African context. A Technical

Subcommittee, appointed by the Steering Committee, together with the project team, investigated other options in the seismic field that could be used during this research. As a result of extensive discussions held in meetings of the Technical Subcommittee during 1993, as well as further literature studies, a decision was taken not to continue with the seismic tomography approach as initially intended and that further investigations in terms of the VSP technique should be abandoned. The Technical Subcommittee recommended that the future direction of the project should be to rather concentrate on the Radiowave Tomography (RT) and radar techniques and that these would form the basis of the future work plans. This recommendation was accepted by the Steering Committee.

As a result of the decision referred to above, two areas were identified for detailed field investigations. One of the sites was the Vaalputs radioactive waste disposal facility where extensive geological, geohydrological and geotechnical investigations had been conducted by the Atomic Energy Corporation. The other site selected was the test site developed by the Institute for Groundwater Studies at the University of the Orange Free State. Both these sites were selected because a large amount of data had already been accumulated for these sites that could be of major benefit to the current investigation. It was further felt that rather than start at a new site where the geological conditions were not known and where new boreholes would first have to be drilled at a considerable cost, the study should concentrate on these two terrains. Active and fruitful cooperation between the CSIR, the IGS and the Department of Geology at UOFS resulted following this decision.

3. Description of the techniques used

Ground Penetrating Radar (GPR) operates on the principle that electromagnetic waves, emitted from a transmitter antenna, are reflected from buried objects and detected at another antenna, called the receiver. The signals recorded at the receiver provide a map, or cross section of the subsurface that is similar in appearance to those obtained with the well-known seismic reflection technique used widely in the oil industry. GPR is a high-resolution geophysical technique which is similar to normal radar, with the exception that the electromagnetic pulses are transmitted through the ground rather than through free space.

Radiowave tomography (RT) is a novel geophysical technique which utilizes radiowaves to interpolate geological information between boreholes by producing attenuation images of the intervening rockmass. Since radiowave attenuation rate is primarily a function of conductivity, geological features which correlate to changes in conductivity are mapped.

The RT equipment comprises of five logical units. These are down borehole radiowave transmitter (Tx) and receiver (Rx) probes, a radiowave receiver unit located at the borehole collar, cabling and winches for lowering the two probes down the boreholes, a PC based control unit and fibre optics link for recording the data and controlling the transmitter and receiver units, and data processing software.

In general, RT is applied at frequencies of between 1 and 30 MHz. However, for this project, frequencies of up to 90 MHz were used. At 90 MHz the radio wavelength in granite is approximately 1 metre, providing a survey resolution of between 25 and 50 cm.

Different scanning modes were applied. These included *Reconnaissance parallel scans*, used *to determine operating ranges and frequencies*, *Background imaging* used for lithology characterization, *Differential tomography* to produce images of the gradient of the attenuation of the rockmass with respect to frequency, and *Alterant tomography* which is used to track tracer flow directly, thereby giving an indication of flow paths and the porosity of the medium. In general the technique is most applicable to mapping conductive features in resistive country rocks. Features which fall into this category are weathered zones, fissures filled with saline water, base metal mineralization, and electrically distinct lithologies such as clays and sandstones.

The principle of **seismic tomography (ST)** is similar to that of RT. Whereas in RT the variations in electrical conductivity are mapped, the variation in seismic velocity is what is mapped in ST. Similar to RT, a seismic source (Tx) is lowered in one borehole, while geophones (Rx) are lowered in the second borehole. Seismic borehole tomography provides a propagation seismic velocity section in the borehole plane, which can lead ultimately to the respective geologic section, using all other available information to construct a meaningful geological picture of the rockmass between the two boreholes.

Similar to GPR, **borehole radar** operates on the principle that electromagnetic waves, emitted from a transmitter antenna, are reflected from surfaces and objects in the rock and detected at another antenna, the receiver antenna. The differences are, however, mainly in the design where one of the challenges is to design suitable antennae that can fit into a borehole. Using radar tomography, the presence of fresh water can be mapped. Here radar travel time is measured in transmission mode, and images of radiowave velocity instead of attenuation rate, are produced. Radar tomography, although originally included in the research programme was, however, not applied extensively in this project.

The system can be used in two modes: single-hole reflection or cross-hole measurements. In single-hole reflection application the transmitter and receiver are lowered into the same hole, along with fibre-glass rods used as separators. Optical fibres are used for transmission of signals between the control computer and the borehole probes and to transfer data from the receiver to the control unit. The advantage of optical fibres are that they have no electrical conductivity and therefore do not cause wave propagation along the borehole. Moreover, since optical fibres are never disturbed by electrical noise, signals do not deteriorate along the cable, and signal quality is thus completely independent of cable length.

4. Field studies

Field studies were concentrated on the Vaalputs Nuclear Waste Repository Site in the Northern Cape Province and the Karoo Aquifer Test Site of the Institute for Groundwater Studies (IGS) on the campus of the University of the Free State. In addition borehole radar experiments were conducted at the newly established waste disposal facility at Chloorkop near Midrand. These sites were selected because a great deal of information had already been gathered for each site which would reduce the drilling of additional and expensive boreholes, and it presented the opportunity to test the technique under different geological environments. Furthermore, in the case of the IGS site, the results gathered during the project would assist the IGS staff greatly in their research on the Karoo aquifers and improve their understanding of the aquifer behaviour.

At Vaalputs the techniques employed consisted of ground magnetic and electromagnetic surveys, and a wide variety of different radiowave tomography scan configurations. Radiowave tomography scans at definite time intervals were also observed while an electrically conductive tracer was introduced into a borehole and the migration with time was studied. This presented the opportunity to observe the preferential flow paths of water in the fractured medium.

At the IGS site, the experiments concentrated on the use of radiowave techniques. The experiments were designed in such a way as to get high resolution results over relatively short distances. Borehole selection was specifically done in such a way that three dimensional constructions of the geohydrological environment between boreholes could be achieved. As in the case of Vaalputs, the injection of conductive tracers was also done and provided good insight into the flow paths and interconnection of fractures and bedding [planes in the sedimentary Karoo aquifer.

Also at this site, some of the radiowave tomography experiments were repeated, although at much reduced intensity, using the seismic tomography and borehole radar experiments. The seismic tomography technique produced good results but the borehole radar results were less successful.

5. Conclusions and recommendations

In terms of the main objectives of the project, the following main conclusions of a general nature can be made from the information presented in this research report:

- Three pilot studies using the high resolution geophysical techniques of Radiowave and Seismic Tomography, have been conducted successfully to test whether these techniques can assist in characterizing the nature of aquifers on a micro-scale (over ranges of metres, with resolutions of 10's of centimetres) compared to the more traditional geohydrological techniques available. This work was supported by the use of more conventional geophysical techniques.

- The Radiowave Tomography results proved that it is a flexible technique that not only finds application in secondary-phase mineral exploration, for which it was originally been developed, but can equally well be applied in the environmental field. In particular, fractured aquifer research can benefit from the application of RT.

- Radiowave and Seismic Tomography (RT and ST), in contrast to other more conventional geophysical techniques, demonstrated the potential to interpolate the aquifer geometry between boreholes. This was proven in two contrasting geological environments, namely fractured Proterozoic granite gneiss and Karoo age sedimentary successions.

- The characterisation of the physical nature of the aquifer can be done indirectly by pin-pointing lithological controls on the aquifer geometry, and directly by using alterant tomography to track water flow. It was demonstrated that RT and ST, when used in combination, have the ability to map different lithologies and lateral variations therein, major fractures, and water flow directly. Alterant scans confirmed that the water flow could be directly mapped using a conductive tracer.

- RT is at a stage where the efficiency, consistency and repeatability of results is sufficiently high to render the technique useful as a monitoring tool. The technique produces information essential in the development of both geologic and geohydrological models, and can be used in combination with Seismic Tomography, to further constrain these models.

- RT has proved itself in the field of geohydrology and may facilitate a major advance in the formulation of geohydrological models of flow, which are usually derived from sparse and often incomplete datasets. It can be applied to the identification and delineation of flow paths within aquifers as an aid to the identification, definition and refinement of appropriate geohydrological models.

- No surface geophysical technique (including GPR, seismic reflection and refraction, magnetics, and frequency domain EM) can, at present, characterize aquifers directly on this scale. These techniques can, however, provide useful background information. Since these techniques are fast and inexpensive to apply, it is suggested that they are used routinely in future studies, but in a supporting rather than a primary role.

From the limited borehole radar experiments done during this project, the more important and general observations made include the following:

- Best results are achieved when the host rock is electrically resistive. The RAMAC system delivered good ranges in the Witwatersrand quartzites, Halfway House granites, and other resistive hosts, but gave very little penetration in various Karoo sediments.

- If there is layering, with the borehole crossing resistive and conductive layers, the resistive layers should be substantially thicker than the antenna system is long. In the Karoo aquifer for example, the resistive layer was not thick enough for effective use of the borehole radar.

- The target should be semi-parallel to the borehole. In the Karoo aquifer, the target crossed the borehole at right angles, so the radargram provided no more information than conventional borehole logging, or even careful core logging. By contrast, some fractures in the Witwatersrand quartzites could be well imaged because of their semi-vertical nature.

- The borehole should be long enough for profiling and of small diameter. Radar returns echo from any discontinuity encountered. Only by profiling a sufficiently long borehole can desired echoes be separated from short discontinuities. Borehole radar works most successfully in small diameter holes. In larger holes, such as the 150 mm holes at the Chloorkop waste site, the holes cause reverberations which reduce the data quality.

- The borehole radar feasibility study has shown that this technique is an exciting new tool available to ground water researchers. In terms of ground water applications, the applications will be governed by the economics of the project and will probably be best suited for applications in a research environment, and not so much the production side.

More detailed and site specific conclusions emanating from the studies done are included in the conclusions of the main text.

Some recommendations resulting from this project are the following:

- The results of the RT and ST experiments have been very promising and it is recommended that these techniques be employed as the prime high-resolution geophysical tool in obtain detailed information on rock and aquifer structure when the demands on the project are such that detailed information is required.

- More surveys of this nature will have to be conducted to test the technique under different geological and geohydrological environments in order to become more familiar with the interpretation of the results in terms of their geohydrological meaning.

- One aspect that was not addressed in this project although initially envisaged, was to develop techniques to calculate from RT derived information, hydraulic parameters for the aquifer or specific sections thereof. Much more work in this respect will be required in terms of the development of the necessary theoretical base for such calculations, the effect that the geological environment has on the calculated values, and ultimately on the the verification of the calculated values. Geostatistical techniques may perhaps be a suitable route to follow in this regard. In this respect, more emphasis should be placed on the application of Seismic Tomography, as some work has already been done in the oil exploration industry to determine permeability and storage from cross borehole seismic surveys.

As a final and overall conclusion it can be said that the results obtained using RT in a Karoo geological environment indicated that the physical nature of the aquifer agrees in broad terms with the current geohydrological thinking. Significant deviations from this were, however, identified, such as flow along non-horizontal fracturing which now needs to be incorporated into the conceptual model, as well as taken into account when developing any mathematical techniques to analyse fluid flow in fractured rocks of this nature.

The project further demonstrated the importance and power of working as a team comprising members from a wide variety of disciplines (geohydrologists, geophysicists, geologists (structural geologists, sedimentologists), mathematicians, electronic engineers, numerical data specialists). In many cases there was no direct interaction between these disciplines and there may be no reference to their work in this report, but in some way their expertise was incorporated into the end product. In this regard the workshops and field visits of South African researchers in fractured rock aquifers organised and funded by the Water Research Commission plays a vital role and needs to be further supported and expanded.

ACKNOWLEDGEMENTS

The research described in this report emanated from a project funded by the Water Research Commission entitled:

The application of seismic tomography and ground penetrating radar for the detection of fractures and the determination of hydraulic properties of fractured rock aquifers.

The Steering Committee responsible for this project consisted of the following persons:

Mr A G Reynders	Water Research Commission (Chairman)
Mr H M du Plessis	Water Research Commission
Mr N Andersen	Atomic Energy Commission
Prof J F Botha	Institute for Groundwater Studies
Prof W J Botha	University of Pretoria
Mr VdA Coetsee	GeoHydro Technologies cc
Dr E Stettler	Council for Geoscience
Mr J M C Weaver	CSIR
Mr F P Marais	Water Research Commission (Secretary)

The financing of the project by the Water Research Commission and the contributions of the members of the Steering Committee and their representatives are gratefully acknowledged.

The input made by the members of the Technical Subcommittee during the early stages of the project and which gave valuable direction to the project is highly appreciated.

Numerous formal and informal discussions were held with many researches in the course of this project. In particular, the authors would like to thank the staff at the Institute for Groundwater Studies, and in particular Prof J F Botha and Mr J Verwey, for the stimulating discussions on the behaviour of and ground water movement in Karoo aquifers. Likewise, the discussions on many technical aspects of the geophysical techniques with various staff at Miningtek, CSIR, and in particular Mr Rolf Frankenhauser, is appreciated.

Finally, the authors would like to express their sincere appreciation to all persons involved in fractured aquifer research in South Africa, who, through their research efforts, contribute to increase our knowledge base on the complex issues of fractured aquifers. It is our belief that only through approaching this problem in a multi-disciplinary fashion, will we achieve positive results. We appreciate the contributions by all working in this interesting and challenging field.

CONTENTS

Page

1. STRUCTURE OF THE REPORT ... 1

2. INTRODUCTION ... 1

3. AIMS ... 2

4. CHANGE IN RESEARCH APPROACH ... 3

5. BROAD PRINCIPLES OF TECHNIQUES USED DURING THE PROJECT ... 4
   - 5.1 Principles of the Ground Penetrating Radar (GPR) Technique ... 5
   - 5.2 Principles of the Radiowave Tomography (RT) Technique ... 6
   - 5.3 Principles of seismic tomography ... 8
   - 5.4 The RAMAC Borehole Radar System ... 8

6. EQUIPMENT AND FIELD PROCEDURE FOR RADIOWAVE AND SEISMIC TOMOGRAPHY ... 8
   - 6.1 Radiowave tomography ... 8
     - 6.1.1 General ... 8
     - 6.1.2 Different RT systems used ... 10
     - 6.1.3 Scanning modes ... 10
   - 6.2 Seismic tomography ... 11
     - 6.2.1 Equipment and data acquisition ... 11
     - 6.2.2 Data processing ... 11
   - 6.3 Borehole radar equipment ... 12

7. RADIOWAVE TOMOGRAPHY AND GROUND PENETRATING RADAR INVESTIGATIONS AT THE VAALPUTS SITE ... 13
   - 7.1 Description of the site and research programme ... 13
   - 7.2 Ground magnetic survey ... 14
   - 7.3 Frequency Domain Electromagnetic (FDEM) profiling with the EM34 system ... 14
     - 7.3.1 Survey design and procedures ... 14
     - 7.3.2 Presentation and discussion of results ... 14
   - 7.4 Ground Penetrating Radar (GPR) ... 15
     - 7.4.1 Survey design and procedures ... 15
     - 7.4.2 Presentation and interpretation of results ... 16
   - 7.5 Summary of results from surface techniques ... 16

7.6 **Radio Wave Tomography (RT)** . . . 17
7.6.2 Presentation of results . . . 18
7.6.2.1 Signal strength and attenuation images . . . 18
7.6.2.2 Alterant Tomography: Scans V1 and V3 (Figures 10a and 10b) . . . 18
7.6.2.3 Low yielding boreholes: RT scan V5 (Figure 10c) . . . 19
7.6.2.4 High yielding boreholes: RT Scan V4 (Figure 10d) . . . 20
7.6.2.5 Low yielding/high yielding borehole combination: RT scan V2 . . . 20
7.7 **Correlation between packer test and RT results** . . . 21
7.8 **Discussion of results** . . . 21

8. TOMOGRAPHY INVESTIGATION AT THE IGS SITE AT BLOEMFONTEIN . . . 22
8.1 **Geology and geohydrology at the IGS site** . . . 22
8.2 **Objectives and programme at the IGS site** . . . 24
8.3 **Field programme and results for first series of experiments** . . . 25
8.3.1. Results from the GPR survey . . . 25
8.3.2 Presentation and analysis of Radiowave Tomography results . . . 25
8.3.3 Phase (i): RT background calibrations and range tests . . . 26
8.3.3.2 Lithological characterization . . . 27
8.3.3.3 Lateral changes . . . 28
8.3.3.4 System calibration, data repeatability and data consistency . . . 28
8.3.4 Phase (ii): Background tomographic imaging for lithology characterization . . . 29
8.3.4.1 Lithological characterization . . . 29
8.3.4.2 Lateral changes . . . 31
8.3.4.3 Consistency of results . . . 31
8.3.5 Phase (iii): Alterant tomography to track water movement directly . . . 31
8.3.5.1 Injection from borehole UO7 . . . 32
8.3.5.2 Injection from borehole UO4 . . . 32
8.3.5.3 Alterant scan between boreholes UO3-UO5, and boreholes UO5-UO6 . . . 33
8.3.5.4 Alterant scan between boreholes UO20-UO7 . . . 34

9. SECOND RADIOWAVE TOMOGRAPHY SURVEY AT THE IGS . . . 35
9.1 **Objectives** . . . 35
9.2 **Equipment and field procedure specific to the Phase 2 experiments** . . . 35
9.3 **Presentation of results** . . . 37

9.3.1 System calibration, range tests and penetration . . . 37
9.3.1.1 The 50 MHz system . . . 37
9.3.1.2 The 30 MHz system . . . 37
9.3.2.1 Lithological characterisation and lateral variations . . . 38
9.3.2.2 Background imaging . . . 40
9.3.3 Differential tomography . . . 42
9.3.3.1 30 MHz differential images . . . 42
9.3.4 Alterant tomography to track water movement directly . . . 42
9.3.4.1 Continuous monitoring of the tracer . . . 42
9.3.4.2 50 MHz alterant scans . . . 44
9.3.4.4 30 MHz alterant scans . . . 46
9.4 Results from the seismic tomography experiments . . . 46
9.5 Correlation between RT and Packer test results . . . 47

10. BOREHOLE RADAR EXPERIMENTS . . . 48
10.1 Background information . . . 48
10.2 Discussion of results . . . 49
10.2.1 Chloorkop Waste Disposal Site . . . 49
10.4.2 Aquifer Test Site: Bloemfontein . . . 50

11. CONCLUSIONS AND RECOMMENDATIONS . . . 51

REFERENCES . . . 58

LIST OF FIGURES

Figure 1: Instrument layout for cross borehole Radiowave Tomography surveys.
Figure 2: Example of a RT "fan-beam profile" between two boreholes.
Figure 3: Schematic diagram to illustrate the "radiowave shadow zone" being cast behind a body between the Transmitter (Tx) and Receiver (Rx).
Figure 4: Locality map for the Vaalputs survey area.
Figure 5: Grid layout at Vaalputs indicating the survey lines for the surface geophysical surveys.
Figure 6: Contoured residual ground magnetic field intensity in nT over the survey grid at Vaalputs.
Figure 7a: Contoured apparent electrical conductivity values in mS/m for the 10 m spacing EM34 vertical dipole mode at Vaalputs.
Figure 7b: Contoured apparent electrical conductivity values in mS/m for the 10 m spacing EM34 horizontal dipole mode at Vaalputs.
Figure 7c: Contoured apparent electrical conductivity values in mS/m for the 20 m spacing EM34 vertical dipole mode at Vaalputs.
Figure 7d: Contoured apparent electrical conductivity values in mS/m for the 20 m spacing EM34 horizontal dipole mode at Vaalputs.
Figure 7e: Contoured apparent electrical conductivity values in mS/m for the 40 m spacing EM34 vertical dipole mode at Vaalputs.
Figure 7f: Contoured apparent electrical conductivity values in mS/m for the 40 m spacing EM34 horizontal dipole mode at Vaalputs.
Figure 8a: 50 MHz bistatic antennae GPR Radargram (S-N) along Line 0 (Figure 5), Vaalputs.
Figure 8b: 25 MHz bistatic antennae GPR Radargram (S-N) along Line 0 (Figure 5), Vaalputs.
Figure 8c: 12,5 MHz bistatic antennae GPR Radargram (S-N) along Line 0 (Figure 5), Vaalputs.
Figure 8d: 25 MHz bistatic antennae GPR Radargram (S-N) along Line 25 (Figure 5), Vaalputs.
Figure 8e: 12,5 MHz bistatic antennae GPR Radargram (S-N) along Line 25 (Figure 5), Vaalputs.
Figure 8f: 25 MHz bistatic antennae GPR Radargram (S-N) along Line 50 (Figure 5), Vaalputs.
Figure 8g: 12,5 MHz bistatic antennae GPR Radargram (S-N) along Line 50 (Figure 5), Vaalputs.
Figure 8h: 25 MHz bistatic antennae GPR Radargram (S-N) along Line 75(Figure 5), Vaalputs.
Figure 8i: 12,5 MHz bistatic antennae GPR Radargram (S-N) along Line 75 (Figure 5), Vaalputs.
Figure 9a: Representative RT signal strength profile from Scan V1 at Vaalputs.

Figure 9b: Representative RT signal strength profile from Scan V3 at Vaalputs.
Figure 9c: Representative RT signal strength profile from Scan V5 at Vaalputs.
Figure 9d: Representative RT signal strength profile from Scan V4 at Vaalputs.
Figure 9e: Representative RT signal strength profile from Scan V2 at Vaalputs.
Figure 10a: Tomographic images from scan between boreholes FW26 and FW27, Vaalputs, before injection of saline water.
Figure 10b: Tomographic images from scan between boreholes FW26 and FW27, Vaalputs, after injection of saline water.
Figure 10c: Tomographic images from scan between boreholes GWB9 and PBH16, Vaalputs.
Figure 10d: Tomographic images from scan between boreholes GWB3 and GWB8, Vaalputs.
Figure 10e: Tomographic images from scan between boreholes GWB7 and GWB5, Vaalputs.
Figure 11: Results of Packer testing on borehole GWB3, Vaalputs.
Figure 12: Results of Packer testing on borehole GWB5, Vaalputs.
Figure 13: Results of Packer testing on borehole PBH16, Vaalputs.
Figure 14: Representative geological section at the IGS Test Site.
Figure 15: Map showing the positions and types of boreholes drilled on the Campus Test Site at the University of the Orange Free State.
Figure 16: Enlarged section of part of Figure 15 showing the positions of the boreholes where the RT work was concentrated, IGS Test Site.
Figure 17: Geological profiles of the percussion boreholes on the UOFS Campus Test Site.
Figure 18: Parallel scans between boreholes UO3 and UO5, and UO5 and UO6, IGS Test Site.
Figure 19: RT images between boreholes UO3 and UO5, and between UO5 and UO6 before and after salt water injection, together with the resulting alterant images, IGS Test Site.
Figure 20: Background and parallel tomographic scans between boreholes UO7 and UO6, IGS Test Site.
Figure 21: Background images between boreholes UO14 and UO20 and between boreholes UO20 and UO7, IGS Test Site.
Figure 22: Imaging of boreholes UO20 to UO7 before and after salt water injection, together with the alterant image, IGS Test Site.
Figure 23: 50 MHz calibrated background parallel scan.
Figure 24: 30 MHz background parallel scans between boreholes UO3 and UO5.
Figure 25: 30 MHz background parallel scans between boreholes UO3 and UO6.
Figure 26: Typical 50 MHz background image (Boreholes UO8 to UO5).
Figure 27: 50 MHz background images.
Figure 28: 50 MHz post-injection images
Figure 29: 30 MHz background images (boreholes UO3 to UO5) at three frequencies.
Figure 30: 30 MHz post-injection images (boreholes UO3 to UO5) at three frequencies.
Figure 31: 30 MHz background images (boreholes UO3 to UO6) at five frequencies.

Figure 32: 30 MHz post-injection images (boreholes UO3 to UO6) at five frequencies.
Figure 33: 30 MHz background difference images (between boreholes UO3 and UO5).
Figure 34: 30 MHz post-injection difference images (between boreholes UO3 and UO5).
Figure 35: 30 MHz background difference images (between boreholes UO3 and UO6).
Figure 36: 30 MHz post-injection difference images (between boreholes UO3 and UO6).
Figure 37a: 50 MHz tracer progression monitoring (between boreholes UO3 and UO5).
Figure 37b: Difference to background image (between boreholes UO9 and UO5).
Figure 38a: 50 MHz tracer progression monitoring (between boreholes UO9 and UO5).
Figure 38b: Difference to background image (between boreholes UO9 and UO5).
Figure 39a: 50 MHz tracer progression monitoring (between boreholes UO8 and UO5).
Figure 39b: Difference to background image (between boreholes UO8 and UO5).
Figure 40: 50 MHz alterant images from salt water injection at borehole UO5.
Figure 41: 50 MHz alterant images from salt water injection at borehole UO8.
Figure 42: Composite diagram showing all 50 MHz alterant images.
Figure 43a: Parallel seismic scan between boreholes UO5 and UO6.
Figure 43b: Parallel seismic scan between boreholes UO5 and UO6.
Figure 43c: Parallel seismic scan between boreholes UO5 and UO6.
Figure 44: Tomographic images for boreholes UO3-UO4 reconstructed from the seismic scans.
Figure 45: Correlation between travel time data between boreholes UO3 and UO4 interpreted with two different software packages. Upper scan interpreted with a seismic software package, and theJower scan interpreted with a RT software package adapted for seismic data.
Figure 46: A graphical representation of the distribution of the hydraulic conductivity of borehole UO5, using the data from a single borehole, double packer test.
Figure 47: Vertical sections where cross borehole packer tests were conducted. The thickness of the connecting lines indicates the relative magnitude of the hydraulic connection between the boreholes.
Figure 48: A graphical representation of the connections observed during the cross borehole packer tests.
Figure 49: Radargram form Chloorkop Borehole Ch-15, 60 MHz dipole antenna.
Figure 50: Radargram form Chloorkop Borehole Ch-15, 60 MHz dipole antenna.
Figure 51: Radargram form Chloorkop Borehole Ch-17, 60 MHz dipole antenna.
Figure 52: Radargram form Chloorkop Borehole Ch-27, 60 MHz dipole antenna.
Figure 53: Radargram form Chloorkop Borehole Ch-31, 60 MHz dipole antenna.
Figure 54: Radargram form IGS Karoo Test Site Borehole C1, 60 MHz dipole antenna.
Figure 55: Radargram form IGS Karoo Test Site Borehole C2, 60 MHz dipole antenna.
Figure 56: Radargram form IGS Karoo Test Site Borehole UO5, 60 MHz dipole antenna.
Figure 57: Radargram form IGS Karoo Test Site Borehole UO8, 60 MHz dipole antenna.
Figure 58: Radargram form IGS Karoo Test Site Borehole UO20, 60 MHz dipole antenna.
Figure 59: Radargram form IGS Karoo Test Site Borehole UO5, 60 MHz dipole antenna, parallel scan.

LIST OF TABLES

Table 5.1: Relative permittivity of some common materials (From Kraus, 1983).
Table 7.1: Summary of RT survey geometry at Vaalputs.
Table 8.1: Summary of different scans completed during first survey.
Table 8.2: Summary of scan geometry.
Table 9.1: *Range test at a borehole separation of 25.2 m* (UO6-UO14).
Table 9.2: Range test at a borehole separation of 50.6 m (UO6-UO10).
Table 10.1: Correlation between radargrams and weathering depth, Chloorkop.

1. STRUCTURE OF THE REPORT

Following a short introduction (Chapter 2) in which some background and motivation to the project is presented, the aims of the project, as contained in the project proposal submitted to and approved by the WRC are presented in Chapter 3. Early on in the project, some difficulties with the seismic tomography were highlighted which resulted in a change in the originally envisaged research approach and methods that were to be followed. This led to the appointment of a Technical Subcommittee to make recommendations as to the direction the research should rather take to avoid becoming deadlocked in highly technical investigations. The recommendations of this subcommittee are presented in Chapter 4 and eventually resulted in a change in the research approach adopted for the project.

Chapters 5 and 6 describe the broad principles of the four basic techniques used during the project and some of the equipment and field procedures used in radiowave and seismic tomography. The techniques described are Ground Penetrating Radar (GPR), Radiowave Tomography (RT), Seismic Tomography and Borehole Radar.

In Chapters 7 to 10 the application of, and results obtained by applying the techniques to three geologically and geohydrologically different test sites are discussed. The sites where the different techniques were applied were the South African low level nuclear waste repository site at Vaalputs in the Northern Cape Province, the Karoo fractured aquifer test site at the Institute for Groundwater Studies (IGS) on the campus of the University of the Free State in Bloemfontein, and at Chloorkop, a newly developed waste disposal site on the Halfway House Granite Complex near Johannesburg.

Finally, the conclusions reached during the project and recommendations for future research are contained in Chapter 11.

2. INTRODUCTION

The Water Research Commission has as part of its long term ground water research programme identified secondary aquifers as being one of its primary focus areas for ground water research. Fractured rock aquifers play a major role in South African geohydrology as more than 80% of the country's ground water reserves are found in such aquifers. The physical nature and behaviour of fractured rock aquifers, however, are not well understood. South African researchers are therefore in a unique position to conduct research into this category of aquifers and thereby make a valuable contribution to our knowledge base of these aquifers. In addition, fractured rock aquifers are present in different forms in South Africa. They range from Protorozoic crystalline type rocks that have undergone a long history of tectonic change, chemically deposited formations where secondary aquifer conditions have been developed through karstification processes enhanced by a long tectonic history, to relatively young fractured sedimentary rocks.

The behaviour of fractured aquifers in general cannot be described by the traditionally used theory of porous flow. The reason why porous flow theory is widely applied to explain and interpret for example aquifer test results, is due to a lack of understanding of the physical nature of fractured aquifers. Botha (1992) has shown through theoretical derivation of flow formulae that almost identical time drawdown relations are observed in phreatic and in two layer confined aquifers. This leads to the formulation of incorrect conceptual models during the investigation of aquifers, which in turn may lead to totally incorrect aquifer parameters being calculated. Management of aquifers can therefore be based on incorrect assumptions made and may lead to serious consequences in the long term for providing a sustainable water supply or to control or remediate aquifer pollution.

3. AIMS

The main aim of this project as stated in the original contract document was to investigate the physical nature of hardrock aquifers using the seismic borehole tomography and borehole radar methods as geophysical tools. In particular, the following aspects were to be addressed:

(a) To investigate the above mentioned geophysical techniques as fracture detection and characterisation techniques, through theoretical modelling studies for different fracture geometries and distributions. The aim of this investigation was to gain knowledge on the theoretical limitations of the techniques when used as tools to study secondary aquifers.

(b) To collaborate with the Institute of Ground Water Studies (IGS) at the University of the Orange Free State in their WRC projects related to fractured aquifer research and in particular as it relates to the Campus Test Site. The results from packer tests, cross hole test data, detailed geological investigations and other information collected for the test site were to be incorporated in the present study.

(c) To relate the geophysical characteristics obtained from seismic tomography and radar technologies to the storage coefficient and hydraulic conductivity.

(d) To compare the accuracy and reliability of the methods regarding their representation of the physical conditions and hydraulic characteristics.

(e) To use geostatistical techniques for the three dimensional interpolation of the data, as well as to define the accuracy and certainty with which the data represent the geology.

(f) To assess the cost of applying the methods versus the reliability for a cost benefit analysis.

The final report on the project was to include a description of the seismic tomography and borehole radar method for fracture detection and characterisation, highlighting the areas where deficiencies in our current knowledge of the methodologies exist and to which future research should be directed.

4. CHANGE IN RESEARCH APPROACH

The progress report tabled at the first Steering Committee meeting in 1993 (Brandt and Coetsee, 1993) highlighted the difficulties with seismic tomography and especially the approach the researchers initially envisaged using in the characterisation of secondary aquifers and in particular, fracture characterisation.

To obtain the in situ stress and related fracture distribution in the rock, seismic techniques are often used. One such technique which is investigated intensively in the oil exploration industry, is to detect seismic anisotropy primarily caused by horizontal layering and fractures (Crampin and Lovell, 1991). This techniques can be employed to determine the strike of vertical fractures, fracture density, fluid content of fractures and the aspect ratio (Crampin and Lovell, 1991). In an anisotropic medium the physical properties of that medium are directional dependant. Three main effects of anisotropy on seismic wave propagation are, (i) shear wave splitting, (ii) polarization and (iii) velocity variations. The Vertical Seismic Profiling (VSP) technique in particular was identified and proposed as a technique that could be used to study seismic anisotropy. One of the problems associated with the VSP technique identified during the literature study was that the best results are only achieved when this technique is applied in fairly deep boreholes, typically a few hundred metres deep. Concerns were raised by the Steering Committee as to whether the results achieved at these depths still relate to the geohydrology of fractured rock aquifers at the depths that the ground water industry is usually exploring.

The Steering Committee also had some reservations about the applicability of this technique in fractured aquifer research, particularly in the South African context. A Technical Subcommittee was appointed which together with the research team were requested to discuss this matter in more detail and to investigate the other options in the seismic field that could be used during this research. As a result of extensive discussions held in meetings of the Technical Subcommittee during 1993, as well as further literature studies, a decision was taken not to continue with the seismic tomography approach as initially intended. This committee recommended that further investigations in terms of the VSP technique should be abandoned. Several reasons for this decision were put forward. The initial proposal was seen to be overambitious and not achievable within the approved budget of the project due to unforseen limitations of the seismic borehole tomography techniques which were initially thought could be applied. During a thorough investigation of the theoretical aspect of this technique, it was decided not to pursue this technique any further.

The Technical Subcommittee recommended that the future direction of the project should be to rather concentrate on the Radiowave Tomography (RT) and radar techniques and that these would form the basis of the future work plans. After thorough consideration by the Technical

Subcommittee as well as the Steering Committee, it was agreed that the original emphasis of the project should be changed with radio tomography being substituted for seismic tomography. In view of this, the originally planned work programme had to be amended. This recommendation was accepted by the Steering Committee.

However, seismic tomography instrumentation developed at the US Bureau of Mines (USBM) was made available to the CSIR by the USBM for a limited period during late 1995 and early 1996. Because of the limited time the instrumentation was made available, only one pair of boreholes could be imaged. The results, although limited, are also included in this report.

At the Technical Subcommittee meeting in 1993 it was recommended to change the original work programme and to focus on the application of Radiowave Tomography (RT) and Ground Penetrating Radar (GPR) at sites where the geological conditions are well known, reasonably "homogeneous" and where sufficient geohydrological data were already available from previous studies. As a result of the decision referred to above, two areas were identified for detailed field investigations. One of the sites was the Vaalputs radioactive waste disposal facility where extensive geological, geohydrological and geotechnical investigations had been conducted by the Atomic Energy Corporation. The other site that was selected is the test site developed by the Institute for Groundwater Studies at the University of the Orange Free State. Both these sites were selected because a large amount of data had already been accumulated for these sites that could be of major benefit to the current investigation. It was further felt that rather than start at a new site where the geological conditions were not known and where new boreholes would first have to be drilled at a considerable cost, the study should concentrate on these two terrains.

During a workshop and field visit by members of the Technical Committee appointed to advise on the Research Programme on Fractured Rock Aquifers of the Water Research Commission and researchers involved in some of the WRC's research projects in this programme, held during early 1994 at the IGS in Bloemfontein, it was decided that current and future WRC projects on fractured rocks should preferably use the two test sites currently being developed by the IGS at the University campus and at Dewetsdorp as widely as possible, instead of conducting research on a large variety of different fractured rock aquifers. This sentiment echoed the decision taken by the Technical Subcommittee the previous year in respect of the future test site for the tomography project. At the time of the workshop, the Vaalputs site had already been investigated.

Active and fruitful cooperation between the CSIR, the IGS and the Department of Geology at UOFS resulted following this decision.

5. BROAD PRINCIPLES OF TECHNIQUES USED DURING THE PROJECT

Tomography is a mathematical inversion process that uses data generally obtained at the boundaries of a region and produces an image of the physical property within the region.

Apart from the emphasis on the Radiowave Tomography technique in this project, limited use was also made of electromagnetic and ground magnetic technique surveys to provide additional background information. As these techniques are well known and find wide use in geophysical exploration programmes, the basic principles will not be repeated here. Seismic tomography was employed on a limited scale and some attention will also be given to explain the basic principles as well as equipment, field procedure and data acquisition.

5.1 Principles of the Ground Penetrating Radar (GPR) Technique

Ground Penetrating Radar (GPR) is a high-resolution geophysical technique which is similar to normal radar, with the exception that the electromagnetic pulses are transmitted through the ground rather than through free space. The output of the technique is a so-called "radargram" of subsurface radar reflectors, and is analogous to a seismogram. These reflectors relate to interfaces at which there is a change in the intrinsic impedance which, in turn is caused by a change in electromagnetic parameters such as the dielectric constant and the conductivity of adjacent layers.

The propagation of electromagnetic waves through material is determined by the movement of electrical charges, and the two phenomena that describe the movement of electrical charge to the propagation of an electromagnetic wave through the material are: 1) conduction, and 2) displacement (or polarization). An external electric field applied to a *conductor* will cause electrical charges to move continuously through the material. An external electric field applied to a *dielectric* causes charges of opposite polarity to separate, which creates an electric field that opposes the external field. The opposing electric field in the dielectric will eventually cancel the effects of the external field, creating a balance that is called charge polarization. The two principle electrical properties that affect the attenuation and propagation of electromagnetic waves are conductivity and dielectric permittivity Dielectric permittivity is often incorrectly referred to as dielectric constant (Daniels, 1990). Both the conductivity and dielectric permittivity affect wave propagation in the frequency range for GPR.

Sen et al. (1981) has shown that the relative dielectric permittivity of air, silica and water are approximately 1, 4.5 and 80, respectively. Changes in the percent water saturation of material, or contamination by a fluid other than water should therefore be readily seen by a GPR system. The relative permittivity of some common materials is listed in **Table 5.1.**

Of particular relevance to this project is that water has a far higher dielectric permittivity than most rock types (with the exception of ore), and is thus a common GPR target. Interfaces which are commonly mapped by GPR are lithological boundaries or interfaces, water table in unconfined aquifers, fractures and fracture zones and water bearing fissures.

The technique generally has an operating range of metres to 10's of metres, and a resolution of cm to 10's of cm, scales which are ideal for geotechnical and geohydrological work.

Table 5.1: Relative permittivity of some common materials (From Kraus, 1983)

Material	Relative permittivity
Vacuum	1
Air	1.0006
Paraffin	2.1
Rubber	3
Dry sandy soil	3.4
Quartz	5
Mica	6
Marble	8
Liquid ammonia	22
Glycerin	50
Water (distilled)	81

An important point is that the performance of a GPR system tends to be highly site specific. In particular, the technique has a ground penetrating capability which is inversely proportional to the bulk electrical conductivity of the rockmass. In areas of resistive surficial rock, the penetration may be in excess of 40 metres, while in areas of conductive surficial rock, the penetration can be a matter of a couple of metres or less. Thus GPR is not optimal when there is conductive overburden, or when the country rock itself is conductive.

There is a trade-off between penetration and resolution, or mapping accuracy, which can be regulated by the radiowave frequency which is used. As the frequency is increased the resolution improves due to the decrease in radio wavelength. Simultaneously, however, the operating range decreases. In general, the frequency is adapted for specific applications e.g. for fracture mapping a high frequency of 500Mhz would provide a penetration of up to 10 metres and a resolution of about 5cm, while for mapping lithological boundaries, a low frequency of 50MHz could provide a penetration of in excess of 40 metres, at a resolution of about 50 cm.

5.2 Principles of the Radiowave Tomography (RT) Technique

Radiowave tomography (RT) is a novel geophysical technique which utilizes radiowaves to interpolate geological information between boreholes by producing attenuation images of the intervening rockmass (Wedepohl, 1993). One of the first references to electromagnetic tomography appeared in 1981. This study by Lyttle et al, (1981) described the potential to trace fluid flow in rocks and presented some experimental theoretical results. However, the emphasis in geophysical tomography research during the 1980's centred on seismic cross borehole techniques and seismic tomography especially as it related to oil exploration. During the early 1990's there was renewed interest in the application of electromagnetic tomography. In a special edition of the geophysical journal *Geophysics* in 1995 (Vol. 60, no. 3) on cross well techniques, a few papers appeared, describing mainly basic and theoretical aspects of the technique (Spies and Habashy, 1995; Alumbaugh and Morrison, 1995; Wilt et al, 1995; Spies and Ellis, 1995; Newman, 1995; Nekut, 1995). According to the literature consulted, the application of RT in exploration studies has thus far been limited to the study of coal and base metal deposits (Thomson et al, 1995; Hatherly et al, 1991; Jeffreys and Thomson, 1995; Thomas et al, 1990; Young et al, 1994; Wedepohl, 1993). Apart from investigations related to this project (Wedepohl et al , 1994; Wedepohl et al, 1995, Mitchell, 1996), no other references to the application of RT to ground water studies have been found in the literature.

Since radiowave attenuation rate is primarily a function of conductivity, geological features which correlate to changes in conductivity are mapped. The technique has a higher resolution and smaller operating range than most conventional geophysical techniques, and is thus optimal for application to second phase exploration. It has limitations in that it only maps features having an electrical contrast to the host rock, given a suitable target geometry. For example, vertical features cannot be mapped using the technique if insufficient coverage is obtained around the target. In addition to this, resolution is proportional to frequency; however, operating range or penetration (maximum borehole separation), is inversely proportional to frequency.

In general the technique is most applicable to mapping conductive features in resistive country rocks. Features which fall into this category are weathered zones, fissures filled with saline water, base metal mineralization, and electrically distinct lithologies such as clays and sandstones. An alternative approach can be used for mapping out fresh water, which does not stand out as a conductive feature. This is radar tomography, which measures radar travel time in transmission mode, and produces images of radio wave velocity instead of attenuation rate. Radar tomography, although originally included in the research programme, was , however, not applied extensively in this project. Chapter 10 of this report is devoted to the experiments conducted with a borehole radar system.

These approaches have the potential for characterizing the country rock, and also degree of water saturation thus yielding spatial information on porosity variations. Another very powerful approach, alterant radio tomography has the potential to track water flow directly, and thereby yield spatial information on permeability variations. In this approach, a tomographic scan is performed before and after the injection of an electrically conductive (salt) water tracer, and a joint inversion of the two datasets highlights areas into which the salt tracer has moved. A major advantage is that direct discrimination is possible between electrical conductivity changes caused by water flow, and those related to variations in the host rock.

Three parameters determining the applicability of RT in a given environment are:

i) Operating range, or maximum borehole spacing which increases as the bulk electrical resistivity of the country rock increases.
ii) Target discrimination or minimum target thickness required for detectability, which is determined by the conductivity contrast between the target and the country rock;

iii) Resolution or mapping accuracy which is between one half and one quarter of the radio wavelength. The radio wavelength is inversely proportional to the *square of the dielectric constant of the rock.*

There is a trade-off between these parameters which can be regulated by the radiowave frequency which is used. As the frequency is increased, the resolution improves due to the decrease in radio wave length. Simultaneously, however, the operating range decreases due to increasing radio wave attenuation rate.

5.3 Principles of seismic tomography

The principle of seismic tomography (ST) is similar to that of RT. Whereas in RT the variations in electrical conductivity are mapped, the variation in seismic velocity is what is mapped in ST. Similar to RT a seismic source (Tx) is lowered in one borehole, while geophones (Rx) are lowered in the second borehole. Seismic borehole tomography provides a propagation seismic velocity section in the borehole plane, which can lead ultimately to the respective geologic section, using all other available information to construct a meaningful geological picture.

5.4 The RAMAC Borehole Radar System

The RAMAC short-pulse borehole radar was developed initially as part of the International Stripa Project in Sweden undertaken to develop techniques suitable for use in underground nuclear fuel waste repositories. Similar to GPR, borehole radar operates on the principle that electromagnetic waves, emitted from a transmitter antenna, are reflected from surfaces and objects in the rock and detected at another antenna, the receiver antenna. The differences ~~are, however, mainly~~ in the design where one of the challenges is to fit all equipment into a borehole.

6. EQUIPMENT AND FIELD PROCEDURE FOR RADIOWAVE AND SEISMIC TOMOGRAPHY

6.1 Radiowave tomography

6.1.1 General

The tomographic scans presented in this report, were produced with three RT systems operating at frequencies of 30 MHz, 50 MHz and 90 MHz. These systems were all developed and built at Miningtek, CSIR and modified specifically for this project. The systems comprise of 5 logical units:

i) down borehole radiowave transmitter (Tx) and receiver (Rx) probes;

ii) radiowave receiver unit located at the borehole collar;

iii) cabling and winches for lowering the two probes down the boreholes;

iv) PC based control unit and fibre optics link for recording the data and controlling the transmitter and receiver units;

v) software for processing the data which is collected, and producing the tomographic images.

The receiver (Rx) is located at the collar of one of the scan boreholes, and linked to the down-hole Rx probe by means of a coaxial cable. The control unit is located at the collar of the other scan borehole, and linked to the down-hole transmitter (Tx) probe by a fibre optics cable. Communications between the control unit and the receiver module is via a fibre optics cable strung out on surface (**Figure 1**).

The scans proceed by lowering the Tx probe down to a fixed point in one borehole and transmitting radiowaves through the survey area. A "fanbeam" profile of radiowave signal strength is then collected in the other borehole by profiling with the Rx probe. An example of a typical fanbeam profile is shown in **Figure 2.** Conceptually, the Tx probe illuminates the survey area from a fixed angle defined by its position in much the same way as does a torch-beam. Electrically conductive features absorb more radiowave energy than the surrounding rock, resulting in a radiowave "shadow zone" being cast behind these features (**Figure 3**).

Profiles are acquired for many different fixed Tx positions, in order to illuminate the ore zone from different angles. In general, the Tx and Rx spacing is approximately the same. This builds up a crisscross grid of radiowave coverage. By combining the different angular views using tomographic algorithms, a spatial map of variation in attenuation rate is produced, which depicts the position and geometry of geological features with distinct electrical conductivities.

In addition to acquiring the fanbeam profile data with the Tx position fixed, "parallel" profiles were also acquired for reconnaissance purposes. In this geometry, the Tx and Rx probes are moved in parallel at the same elevation, providing a rapid assessment of changes in the bulk rock conductivity as a function of depth.

Note that the tomographic images average over an area corresponding to the resolving power. As a consequence, the images are reliable indicators of horizon continuity, but may not detect isolated features which have dimensions less than the resolving power.

Attenuation images derived for individual borehole pairs are shown in **Figures 10a to 10e**. Note that an image processing package has been used to boost some of the more subtle features through the use of colour stretching and thresh-holding. The colour scales are thus not directly comparable between individual images. A temperature scaling has been used where the warm colours indicate high attenuation rates, or zones which are relatively electrically conductive, and the cold colours indicate low attenuation rates, or zones which are relatively electrically resistive.

6.1.2 Different RT systems used

As mentioned before, the different instruments used in different experiments and in different geological environments, operate at frequencies of 90 MHz, 50 MHz and 30 MHz.

In general, RT is applied at frequencies of between 1 and 30 MHz, where it has an operating range of up to 200 m, with a resolution of the order of metres. In the case of the Vaalputs study a much higher frequency of 90 MHz was used over an operating range of about 15 m. This was done so as to provide information of sufficiently high resolution. At 90 MHz the radio wavelength in granite is approximately 1 metre, providing a survey resolution of between 25 and 50 cm.

The 50 MHz system is a single-frequency system consisting of matched transmitter and receiver antennae, a receiver unit, cables and winches, and a control PC. The transmitter antenna acts independently of the receiver, and produces a constant signal of 50 MHz which is sampled at discreet depths by the receiver antenna. The received signal is converted to an intermediate frequency within the receiver which is then transmitted through a coaxial cable to the receiver unit. The receiver unit measures the signal and transmits the measurement to the control PC via fibre-optic cable.

The 30 MHz system is a multiple-frequency system which operates at 5 discrete frequencies, as preset by the operator according to site-specific conditions and maximum attainable resolution. The 30 MHz system is similar to the 50 MHz system in that it consists of the same basic components. However, the transmitter antenna is controlled by the control PC via a fibre-optic link; and due to the low frequencies used, no down-conversion of the signal before transmission to the receiver unit is necessary. The transmitter probe steps through the five preset frequencies as instructed by the control PC, while the receiver antenna passively measures the signal which is transmitted via coaxial cable to the receiver unit.

6.1.3 *Scanning modes*

A number of different scanning modes have been used during this project. These are

- *Reconnaissance parallel scans* used to determine operating ranges and in the second survey at IGS to choose optimum operating frequencies.
- *Background imaging* used for lithology characterization.
- *Differential tomography* produces images of the gradient of the attenuation of the rockmass with respect to frequency.
- *Alterant tomography* is used to track tracer flow directly, thereby giving an indication of flow paths and the porosity of the medium.

6.2 Seismic tomography

6.2.1 Equipment and data acquisition

The seismic source and receiver are a matched pair of piezoelectric transducers, with a resonant frequency of 50 kHz. Both source and receiver are lowered into water filled boreholes on reinforced coaxial cable. The source is pulsed by a high voltage pulse generator on surface, with the pulses being transmitted to the transducer down the coaxial cable. The pulse repetition rate is adjustable up to 100 pulses per second.

On the receiver side, the transducer is fed into an amplifier in the probe. The amplifier is powered via the coaxial cable, which also feeds the amplified signal back to surface. On surface, the signal is low pass filtered to remove mains interference, and amplified if necessary. It is then captured on a Tektronix TDS524 digital oscilloscope, triggered by the pulse generator.

The oscilloscope is connected to a portable computer, via an IEEE-488 to RS232 converter. The computer sets up the measurements to be made, and organizes data capture. The process is as follows:

On the computer, the user can choose various acquisition parameters, including sample time, number of samples and number of traces to average. Other parameters relating to the survey, such as depth in the transmitting and depth in the receiving borehole, are also entered on the computer. Once the parameters are entered, the user can command the oscilloscope to record a trace.

The trace is displayed on the oscilloscope screen, and a cursor is placed in the area near the first break. The user can zoom up the trace in amplitude and in time, and use the cursor to select the first break. If the trace is not suitable, the user can acquire another trace.

Once the first break is chosen on the 'scope, the user can record the trace under computer control. The computer records the time of the first break, as well as other ancillary information on its own hard disk drive, and instructs the oscilloscope to record the complete trace on its own internal 3.5 inch stiffy disk drive. Filenames are generated and logged automatically. The traces are not stored directly on the computer because of their size, and because of the time required to transfer a trace.

The summary information is available immediately for processing, and the complete traces are available for more sophisticated processing, if necessary.

6.2.2 Data processing

For this project P-wave arrival times were picked manually during data acquisition. For the sake of comparison, all three collected data sets were processed using the two different tomographic software packages developed and available at Miningtek. Firstly the data was analysed using a seismic processing package and secondly the software developed for the RT was used by replacing radiowave data with seismic travel time data. Like all tomographic software, the seismic package can also be divided into two main parts; a forward modelling part and an inversion part.

6.3 Borehole radar equipment

Although borehole radar equipment is commercially available, it is also still very much in a development phase. One off the available commercial systems is manufactured by the Malà Geoscience, a subsidiary of the well known Swedish geophysical equipment firm ABEM and marketed under the name of RAMAC. It is extremely expensive and definitely not a tool that will be used in normal ground water exploration applications. ABEM was contracted by the CSIR to bring their RAMAC borehole radar system to South Africa for controlled tests in the mining industry. This opportunity was also used to investigate the application of the technique to research into fractured rock aquifers. For this two sites were investigated; the one was the Karoo aquifer test site at the Institute for Groundwater Studies in Bloemfontein, and the second site was on the Archaean granites between Johannesburg and Pretoria.

The system which was brought to South Africa included a control PC, radar control unit, a 20 MHz dipole transmit and receive antenna system, a 60 MHz dipole transmit and receive antenna system, a 60 MHz directional receive antenna, an electric winch with 500m of cable, a manual winch with 150m of Kevlar cable for cross-hole work and a selection of battery packs.

Extensive use is made of fibre optics for communication between the various units of the system and the design is such that it ensures that there is no electrical connection between transmitter and receiver, or between either antenna and the control unit. The probe lengths are

60 MHz dipole system:

dipole antenna, short (1.3 metre) batteries and a 1 metre spacer: Total length approximately 6.9 metres.

20 MHz dipole system:

dipole antenna with 3 metre batteries, 5 metres of spacers: Total length can increase to 17 metres.

The system can be used in two modes: single-hole reflection or cross-hole measurements. In single-hole reflection applications the transmitter and receiver are lowered into the same hole, along with fibre-glass rods used as separators. Optical fibres are used for transmission of signals between the control computer and the borehole probes and to transfer data from the receiver to the control unit. The advantage of optical fibres are that they have no electrical conductivity and therefore do not cause wave propagation along the borehole. Moreover, since optical fibres are never disturbed by electrical noise, signals do not deteriorate along the cable, and signal quality is thus completely independent of cable length.

As a rule, the transmitter and receiver are separated by 3-6 metres in sedimentary and 5-15 metres in crystalline rock. Measurements are taken at fixed intervals, typically 0.5 metres. The RAMAC system uses a dipole antenna which radiates energy in all directions around the borehole as standard. Since the radar images contain cylindrical information, data from three boreholes is required to locate fractures or point source reflectors accurately. This may severely restrict the practical application of borehole radar, especially in the ground water industry, as it can increases the cost of the investigation significantly.

Cross-hole surveys provide information about the rock between the two boreholes. One of the probes is kept stationary in borehole 1, while the other is moved from measuring point to measuring point in borehole 2. The resulting set of measurements is called a borehole scan. After each scan is completed, the probe in borehole 1 is moved to the next measurement position, and the procedure is repeated. The processed data is shown as a tomogram, similar to those in RT tomography.

7. RADIOWAVE TOMOGRAPHY AND GROUND PENETRATING RADAR INVESTIGATIONS AT THE VAALPUTS SITE

7.1 Description of the site and research programme

The Vaalputs site was selected due to the availability of geological and geohydrological control, the fact that it is situated in a reasonably homogeneous geological setting, and because of the recommendation by the Steering Committee. Vaalputs is located in the Namaqua-Natal Metamorphic Complex within the Northern Cape, and hosts a fracture controlled secondary aquifer. The geology of the area consists mainly of granitic gneisses, with a fairly deep weathered layer (20 m on average), before fresh bedrock is encountered. The weathered material is often kaolinitic in nature and is thus electrically conductive. There are also isolated zones of weathered granite contained within the fresh granite. The water table in the area is variable, but around the disposal site itself, it is at approximately 50 metres. There is no primary porosity within the granites, and the aquifer is thus primarily controlled by the fracture geometries, with the degree of weathering of the granite being an important secondary control. The precise geometry and nature of these two controls are unknown.

The surface geophysical programme was conducted at an area overlying the Garing lineament to the west of the main disposal site. Various surface and borehole geophysical techniques were applied at Vaalputs, namely Ground Penetrating Radar (GPR), frequency domain electromagnetic profiling (FDEM), the magnetic method and radio wave tomography (RT). The main emphasis of the study was the use of the radio wave tomography and GPR techniques in detecting fractured zones. The FDEM and magnetic profiling techniques, being techniques of lower resolution were used mainly to provide additional background information to the study. A locality map of the Vaalputs study area is presented in **Figure 4** with the detailed grid that was used for the surface geophysics presented in **Figure 5.**

Five radio wave tomography scans were conducted between four sets of borehole pairs (indicated as V1 - V5 on **Figure 4**). One of the borehole pairs is located near the rest camp, and the other three borehole pairs are located at the waste disposal site itself. The objective of the RT scans was to interpolate the geometry of fractures and weathered zones between boreholes, and also if possible, to map possible flow paths for water along these zones.

Note that the ground water at the waste disposal site was saline, while the water at the other two sites was fresh.

7.2 Ground magnetic survey

The objective of the magnetics was to map out any lineaments which might be related to geological structures and thus influence the aquifer characteristics. Magnetic profiling was undertaken over the entire profile on a 10 m x 10 m grid and the data are presented in **Figure 6**.

The magnetic data indicates a clear distinction in magnetic signature to the north and south of the Garing Lineament. The frequency content of the magnetic data is much higher to the north of 70 m, indicating near surface magnetic variations in this region, possibly accompanied by an increase in magnetization. It is proposed that the basic intrusive rocks to the north are responsible for the change in the magnetic pattern.

7.3 Frequency Domain Electromagnetic (FDEM) profiling with the EM34 system

The objective of this profiling was to map the bulk electrical conductivity of the surficial rock, in order to map out lateral changes associated with fracturing or shear zones. A second objective was to provide an indication of the radar penetration which may be expected (radar penetration is inversely correlated to electrical conductivity).

7.3.1 Survey design and procedures

Data was recorded at Vaalputs using both horizontal and vertical dipole configurations at Tx-Rx coil separations of 10 m, 20 m and 40 m. Nine lines at a spacing of 10 m and station spacing 10 m were surveyed so as to cover a 10 m x 10 m grid over an area of 200 m x 80 m (**Figure 5**). The east-west trending Garing Lineament bisected the survey grid. The data for the horizontal dipole mode (i.e. vertical coplanar loops) and the vertical dipole mode (horizontal coplanar loops) for the 10 m, 20 m and 40 m coil separations are presented in Figs. 7a - 7c respectively, as contour plots of the apparent conductivity.

7.3.2 Presentation and discussion of results

The results indicate that the surficial rock in the survey area is conductive to moderately conductive. Although there is no obvious surface geological expression of the Garing Lineament, the FDEM data indicates that the rocks to either side of the Garing Lineament are electrically different. The conductivity values do not decrease markedly with increasing coil separation, which implies that the system is not penetrating through the clay overburden layer.

For the horizontal dipole mode, the apparent conductivities are higher to the north of the Garing Lineament, where they range from 10 mS/m to 30 mS/m, than to the south of the Garing Lineament, where in the region 20 m N to 60 m N they average 10 mS/m. The rock directly over the Garing Lineament is resistive.

It is believed that the higher conductivities to the north of the Garing Lineament result from weathering of the basic intrusives. It is also possible that the high resistivity of the rock directly over the Garing Lineament is caused by re-crystallization of the 80-100 metre wide fracture zone.

For the 10 m coil separation (**Figure 7a**) there is an anomaly with steep gradients centred around 130 m N, 50 m E to 110 m N, 70 m E which appears to be associated with a buried utility pipe close to surface. In vertical dipole mode, a similar conductivity variation is observed to that of the horizontal dipole mode, with conductivities to the north of the Garing Lineament averaging 20 mS/m to 30 mS/m, and values to the south averaging 10 mS/m. In general the vertical dipole data is noisier than the horizontal dipole data with more localized anomalies evident.

There is also an anomaly centred around 135 m N on the 20 m and 40 m coil separations (**Figures 7b and 7c**) which appears to be related to the presence of underground utility pipes. The "bulls-eye" anomaly observed in the 10 m coil separation data (**Figure 7a**) is thought to be corresponding to the same pipe, which is believed to be positioned as shown in **Figure 5**.

7.4 Ground Penetrating Radar (GPR)

The ground penetrating radar technique was employed with the specific aim of determining the applicability of the technique in detecting fracture zones in the host rock. For GPR profiling from surface the ideal fracture geometry would be horizontal or shallow dipping fracture zones. For steeply dipping fracture zones borehole radar techniques, in either transmission or reflection mode would be best suited for fracture detection.

7.4.1 Survey design and procedures

GPR radar data were collected over 4 profile lines spaced 25 m apart, viz. lines 0, 25, 50 and 75 (**Figure 5**). The instrumentation used was a pulseEKKO IV GPR system, incorporating a 400 V transmitter, with various antennae frequencies. Three frequencies were used in all: 50 MHz, 25 MHz and 12.5 MHz. Each profile was surveyed using at least two different frequencies.

7.4.2 Presentation and interpretation of results

Data collected with 50MHz, 25MHz and 12.5MHz antennae on Line 0 are presented in **Figures 8a to 8c** respectively. A clear feature which is common to all the figures is the diffraction patterns occurring between positions 35m to 60m north. A comparison between these three figures gives a clear illustration of how the penetration-resolution trade-off can be regulated by the frequency. It is also interesting to note that this feature correlates with relatively resistive zones as determined by the FDEM study and in the region of lower frequency magnetic variations. This is consistent with the fact that better radar penetration may be expected in the more resistive rockmass. The precise origin of this radar reflector is unknown, but it is certainly related to the Garing Lineament.

The reflectors observed from 150 ns (~8m) (for the 25 MHz data (**Figure 8b**) and from 250 ns (~12m) for the 12.5 MHz data can be related to differential weathering. The apparent "deep" reflector identified at 800 ns at position 90 m is a surface cultural effect caused by a nearby parked vehicle.

The 25 MHz and 12.5 MHz data for Line 25 are presented in **Figures 8d and 8e** respectively. The dominant feature noted on Line 0 is still observed, but is not as prominent. The reflector with apex at 550 ns at 90 m is caused by surface cultural effects.

On Line 50, the main feature observed on the previous two lines is no longer present for either the 25 MHz or 12 MHz data (**Figures 8f and 8g**). The reflectors with apices at 60 m and 100 m are surface cultural effects. No features of geological note are observed on Line 75 (**Figures 8h and 8i**).

In general there are no clear reflectors which can be identified relating to fractures in the granite. This indicates that the GPR is unable to penetrate through the 20 m clay overburden, an observation which would be consistent with theoretical calculations based on average conductivities for clays, and also with the FDEM data. This implies that GPR is of limited value to characterizing fracturing controlling this type of aquifer. More generally, the two parameters controlling the direct application of surface GPR to aquifer characterization will be the aquifer depth and the bulk conductivity of the overlying rock. By performing electrical property measurements on the overburden rocks, it will be possible to predict in advance whether GPR will penetrate through to the aquifer zone.

7.5 Summary of results from surface techniques

None of the surface geophysical techniques described above were able to directly characterize fracture geometries within the aquifer, and therefore cannot be used as primary tools for aquifer characterization in this environment. It is predicted that this statement will also hold for many other geohydrological environments in South Africa.

More positively, all of these techniques provided useful and complementary background information on the general rockmass structure at Vaalputs. The FDEM and magnetics showed that the rocks to the north and south of the Garing Lineament were physically distinct, while the GPR picked up a reflector associated with the Garing Lineament itself. In addition, the FDEM provided useful information in interpreting the GPR data. Since these techniques are fast and inexpensive to apply, it is suggested that they are used routinely in future studies, but in a support rather than a primary role.

7.6 Radio Wave Tomography (RT)

The objective of the RT scans was to interpolate the geometry of fractures (where and if weathered) and weathered zones between boreholes, and also if possible, to map the flow of water directly, by making use of a salt water tracer.

7.6.1 Survey design and procedures

Five RT scans named V1 to V5 were conducted at two sites at Vaalputs (**Figure 4**). The survey geometries in each case are summarized in Table 1 below. In all cases, the surveys started below the weathered clay layer. Thus the country rock was generally fresh granite, sometimes with isolated patches of weathered granite. (It was not possible to scan higher up, as the clay zone was generally cased with steel casing).

RT scans V1 and V3 were conducted at a borehole pair near the rest camp before and after the injection of a salt water tracer, in order to test the applicability of alterant radiowave tomography. The water level was approximately 10 m below ground surface. The water at these holes was fairly fresh, and water from the reverse osmosis plant proved to be adequate as a tracer. The procedure used was to fill one of the boreholes with saline water from a tanker, and then to pump from the other borehole to draw the water through the formation. This procedure was repeated iteratively for two days as the rock was relatively impermeable and resulted in the slow uptake of the saline water.

Tomographic scans V5, V4, and V2 (**Figure 4**) were conducted at the Waste disposal site itself between borehole pairs where the water yield from the boreholes was low-low, high-high, and low-high respectively. The objective of these three scans was to investigate if RT could provide a diagnostic regarding the different water yielding properties of the three boreholes. The water level at this site was approximately 55 metres, and the water is saline.

The RT system used in the tomographic scanning was operating at an frequency of 90 MHz. A Tx/Rx station spacing of 0.5 m was used for the alterant tomography, and a spacing of 1m was used for the other scans. In general RT is applied at frequencies of between 1 and 30 MHz, where it has an operating range of up to 200 metres, with a resolution of the order of metres. In the case of this study a much higher frequency of 90MHz was used over an operating range of about 15m. This was done so as to provide information of sufficiently high resolution; at 90MHz the radio wavelength in granite is approximately 1 metre, providing a survey resolution of between 25 cm and 50 cm.

Table 7.1: Summary of RT survey geometry at Vaalputs

Scan number	Borehole 1 and depths (m) surveyed	Borehole 2 and depths (m) surveyed	Borehole spacing (m)	Station spacing (m)
V-1	FW 26 (30-75)	FW 27 (30-53	~12	0,5
V-3	FW 26 (30-65)	FW 27 (30-53)	~12	0,5
V-5	GWB 9 (40-90)	PBH 16 (40-90)	~15	1
V-4	GWB 3 (20-77)	GWB 8 (20-63)	~15	1
V-2	GWB 7 (35-93)	GWB 5 (35-79)	~15	1

7.6.2 Presentation of results

7.6.2.1 Signal strength and attenuation images

Typical signal strength profiles from each RT scan are shown as **Figures 9a to 9e**. The profile geometry is indicated on the one side of the figure, and the data on the other side. The lines between the boreholes are the ray-paths linking the different Tx-Rx positions. Each ray-path is extrapolated onto the relevant data point on the profile. The profile is plotted in units of decibels relative to micro-volts. The arrows with numerals indicate radio wave shadow zones caused by specific conductive features (**Figures 9b to 9e**).

The corresponding tomographic images for each scan are shown as **Figures 10a to 10e**, together with the borehole logs provided by the AEC. A temperature scale is used: warm colours depict high attenuation rates of radiowaves indicating the presence of conductive material (e.g. weathered granite), while cold colours depict low radio wave attenuation rate indicating the presence of resistive material (e.g. fresh granite). Note that these images use independent colour mapping and are thus not directly comparable. Specific features are indicated by numerals which correspond to those used in **Figures 9a to 9e** (i.e. feature 1 on **Figure 9b** corresponds to feature 1 on **Figure 10b**).

*7.6.2.2 Alterant Tomography: Scans V1 and V3 **(Figures 10a and 10b)***

These two scans represent attenuation images before (**Figure 10a**) and after (**Figure 10b**) the injection of saline water tracer into one of the boreholes. The signal strength profile from V1 (**Figure 9a**) is typical of a homogeneous zone. The signal strength falls off as a smooth parabola, indicating increased attenuation as the Tx-Rx positions move further apart. The profile from V3 (**Figure 9b**) depicts the radiowave shadow zone caused by the thickest part of feature (1).

The pre-injection image (**Figure 10a**) from V1 is dominated by a linear conductive feature (1) running up towards borehole FW27. A faint trace of a linear conductive feature (2), almost perpendicular to feature 1 can be observed. In addition, the survey area can be divided into an upper more conductive zone (3) and a lower more resistive zone (4). It is postulated that feature (1) corresponds to slightly weathered granite and feature (4) represents fresh granite.

The post injection image from V3 (**Figure 10b**) is essentially unchanged from V1 except that the faint conductive feature (2) on **Figure 10a** is now dominant. This implies that the salt water tracer has flowed predominantly along feature (2) which is assumed to be an open fissure. Water flow has not taken place along feature (3) indicating that it is impermeable, and possibly related to clay or weathered granite. Interpretation of recent acoustic scans conducted by Mr N Andersen for the AEC on boreholes at Vaalputs, however, indicated that the present natural crustal stress field in these rocks, may also be responsible for the closed and/or open nature of fractures (pers. comm., N. Andersen). The way in which the fractures respond to the stress field, is a function of the strike and dip directions of the individual fractures, and the competency of the rock mass. A detailed reinterpretation of the RT images in conjunction with an analysis of the stress field conditions at Vaalputs may assist in resolving some of the unexplained phenomena.

*7.6.2.3 Low yielding boreholes: RT scan V5 (**Figure 10c**)*

RT scan V5 was conducted between two low yielding water boreholes GWB9 (Q=0,9 l/s) and PBH16. Both these boreholes are, based on packer tests, in the zone classified by Hodgson (1992) as being of low permeability. Water was struck at 73 m and at 63 m in boreholes PBH16 and GWB9 respectively.

The tomographic image (**Figure 10c**) shows two distinctly different zones. The upper is a relatively resistive zone (1) whereas the lower is a relatively conductive zone (2). The signal strength profile chosen from V5 (**Figure 9c**) depicts the distinct drop off in signal strength when the radiowaves travel through zone (2) as opposed to zone (1). The interface between the two zones is at approximately 58 m. This coincides well with the water levels in the two boreholes (55 m and 58 m in boreholes PBH16 and GWB9 respectively), implying a genetic link between conductivity and water saturation. The difference in conductivity between zones 1 and 2 therefore appears to be unrelated to weathering and the entire profile may represent a rather homogeneous rock mass. This agrees with the assessment made by Hodgson (1986) based on the packer testing that "the aquifer around PBH16 is fairly homogeneously fractured".

Within zone (2) are a series of linear conductive zones with a conjugate geometry (3). It is postulated that these are related to weathered zones along fractures in the granite.

*7.6.2.4 High yielding boreholes: RT Scan V4 **(Figure 10d)***

RT scan V4 was conducted between two high yielding boreholes. The resulting tomographic image (**Figure 10d**) shows two zones similar to those observed in V5: a relatively resistive zone (1), underlain by a relatively conductive zone (3). The water was struck at 55 m (Q=1,3 l/s) and 56 m in boreholes GWB3 and GWB8 respectively. The static water level in borehole GWB3 is at 51 m below ground level. The signal strength profile chosen from scan V4 (**Figure 9d**) depicts the radiowaves shadow zones associated with features (2) and (4).

A distinctive difference between the two scans is the presence of two sharply discontinuous conductive zones (2) and (4). Feature (2) which is above the water table level, appears to be related to weathering in the granite. Feature (4) correlates well to a water intersection in borehole GWB8, but it should also be noted that the zone does not extend through to the water intersection in borehole GWB3. It is thus not clear if (4) is directly associated with saline water or else with alteration of the rockmass.

Within (3) are a series of linear conductive zones with a conjugate geometry. It is postulated that these are related to weathered zones in the granite along fracture zones. A significant point to note from scan V4 is the association of a strong water yielding zone in borehole GWB9 (55-58 m) with the conductive zone being situated between 55 m and 62 m. This is also associated with sharp changes in geoelectrical character of the rockmass.

7.6.2.5 Low yielding/high yielding borehole combination: RT scan V2

RT Scan V2 was conducted between a low yielding (GWB9, Q<0,1 l/s) and a high yielding (GWB5, Q=1,23 l/s) borehole combination. Water was struck at 80 m and at 66 m in boreholes GWB9 and GWB5 respectively. The signal strength profile chosen from V2 (**Figure 9e**) depicts the radio waves shadow zones associated with feature (4).

The resulting tomographic image (**Figure 10e**) shows a relatively conductive zone (1) underlain by a localized resistive zone (2). This is the inverse situation to scans V5 and V4. Zone (1) is characterized by a series of relatively conductive linear features with a conjugate geometry, which may be associated with fracturing.

The most striking feature on the image is conductive zone (3/4) near the base of the survey area. This feature lies just below the water intersections in both boreholes and is thus probably genetically linked to the water. Zones 3 and 4 are relatively conductive near borehole GWB7 (3), the low yielding borehole and relatively resistive near GWB5 (4). A tentative explanation is that the zone represents a weathered layer in the granite which channels water: Feature (3) has been weathered to (electrically conductive) clay, making it impermeable to water, hence the low yield, while (4) is less weathered and is thus highly permeable, and therefore also a strong water yielding zone.

A significant point to note from scan V4 is that there is no absolute correlation between electrical conductivity and water occurrences. However, the spatial characteristics of the geoelectrical structure of the rockmass appears to be closely linked to the aquifer geometry.

7.7 Correlation between packer test and RT results

Hodgson (1986) conducted packer tests in three of the boreholes that were also used for RT scans. These boreholes were PBH16, GWB3 and GWB5. The packer test results are shown in **Figures 11 to 13.** The zone of higher permeability between 70 m to 75 m in borehole PBH16 (**Figure 13**) correlates well with the conductive zone marked (3) on **Figure 10c**. Similarly the high water take (increased permeability) near 40 m corresponds well with the electrically conductive zone on the RT. However, the two electrically conductive zones at 60 m and between 80 and 90 m correlate with water takes of <0,05 m^3/day.

In the packer test at borehole GWB3 no electrically conductive zone could be positively identified with the zones of large water takes. The fracture zone where high yield of water was encountered (~55 m) in borehole GWB3 correlates well with the packer test (**Figure 12**), but the RT data indicates a relatively resistive environment (**Figure 10d**).

In the RT scan of borehole GWB5 two electrically conductive areas can be seen. These are between 35 m and 40 m and between 75 m and 80 m. The former correlates well with the water take data (**Figure 13**). The zone over which water strikes were reported (63 to 66 m) correlates well with the packer data but not with the RT data.

In summary, there are both strong and weak correlations between hydraulic and electrical conductivity. The reason for this is probably in the degree of weathering or fracturing that occurs in granites. Electrically conductive zones may be representative of both highly weathered granite (clay with low hydraulic conductivity) or fractured zones filled with water (high hydraulic conductivity) and it is not possible to resolve these features on the available data.

7.8 Discussion of results

These initial radiowave tomography results were extremely promising, as they indicated an unequivocal link between the geoelectrical structure of the rockmass and the nature of the fracturing in the granites. It is also indicated, however, that this relationship can be complex and that the incorporation of geohydrological know-how and data is essential. Geophysical borehole logs could assist to distinguish further between whether the conductive zones identified on the tomograms are the result of fractures and fracture zones filled with water, and those areas where the granite is weathered to a clay. In general, water occurrences appeared to be spatially related to sharp geoelectrical discontinuities. There is not, however, a direct correlation between the electrical conductivity and water transmissivity of rock. In fact, water appears to occur predominantly in moderately conductive zones: it may be that very high electrical conductivities indicate impermeable clay, while high electrical resistivities indicate unfractured and therefore impermeable rock.

These factors imply that alterant radio tomography will be extremely important in identifying the genetic origins of geoelectric changes - the first experiment performed as a part of this study already demonstrated the ability of this approach to discriminate directly between water and lithology. Another implication is that incorporation of geohydrological data and know-how is critical when interpreting the results.

8. TOMOGRAPHY INVESTIGATION AT THE IGS SITE AT BLOEMFONTEIN

8.1 Geology and geohydrology at the IGS site

The IGS site is situated on the campus of the University of the Orange Free State. The test site covers an area of about 2 ha and is underlain by rocks of the Lower Beaufort Group (Colliston, personal communication). A representative lithological description is shown in **Figure 14**. A total of 22 percussion boreholes as well as three inclined diamond cored boreholes have been drilled on the site. Their distribution is shown in **Figure 15**. The boreholes in which most of the RT experiments were conducted are shown on **Figure 16**, which is an enlargement of a portion of **Figure 15**. In broad terms, the succession consists of a carbonaceous shale (2-4 m) separating an upper mudstone layer (6-8 m) and a lower sandstone layer (8-9 m). The "basement rocks" (for the purpose of this investigation) is a dark blue shale succession. A thin layer (3-6 m) of sandstone is usually also present between the carbonaceous shale and the upper mudstone. Geological profiles of the percussion boreholes are shown in **Figure 17**.

Three aquifers have been identified in this geological succession at the test site. These are commonly referred to as aquifers A1, A2 and A3. The main semi-confined aquifer is developed in the lower sandstone and is separated from the upper phreatic aquifer developed in the mudstone and upper sandstone by the carbonaceous shale layer which forms an aquitard. The third aquifer is developed in the blue shale succession of the basement rocks and is also confined. Different piezometric levels are recorded for all three aquifers (Viviers *et al*, 1995).

The conceptual model of the aquifers constructed by researchers from the IGS describes essentially a fractured rock aquifer in which the majority of the fractures are believed to be near horizontal and often of limited lateral extent (Verwey *et al*, 1993; van der Voort, 1995). In addition to the ground water associated with normal sedimentary structures in the Karoo formations, the fracturing and weathering associated with the dyke structures dictate the flow patterns to a large extent. Dykes do not occur within the IGS test site and therefore water movement is restricted to structures associated with the sedimentary succession. Most of the research at the IGS site has concentrated on establishing the interplay between lithology, fracturing, pore space, aquifer parameters and borehole yield. In broad terms, a model has been inferred whereby the water flow is controlled largely by well connected horizontal fracturing and bedding planes, with the storage being provided by the pore space within the sedimentary rocks. Consequently, the most important aquifers, in terms of storage, occur preferentially in the sandstones with the low hydraulic conductivity siltstone, shale an clay layers often forming aquicludes.

Blow as well as tested yields indicate highly variable conditions; from 7 l/s to virtually dry. The difference between a "dry" and a successful borehole is only determined by the presence or absence of a fracture.

Hydraulic properties of the aquifer have been determined through pumping (Viviers *et al*, 1995) and cross-borehole and double packer tests (Verwey *et al.* 1993). Average hydraulic conductivity values for the confining carbonaceous shale were found to be around 3×10^{-8} m/s, for the sandstone aquifer 3×10^{-4} m/s and for the lower aquifer 1×10^{-7} m/s. The hydraulic conductivity for the fracture is given as 1×10^{-4} m/s by Botha *et al* (1994). The hydraulic conductivity for the upper unconfined aquifer varies between 2×10^{-6} and 9×10^{-6} m/s.

From the studies on the IGS site conducted and reported on by the IGS, it is evident that there are significant lateral changes in the aquifer characteristics which appear to be associated with changes in fracturing, and to some extent changes in lithology. The detailed linkage between these factors is at present poorly understood, however the following general empirical observations have been made:

i) There is a large lateral change in water level, with boreholes UO1, UO2, UO3, UO10, and UO17 having a water table level of about 5m, and the other boreholes having a water level of about 12m. There is thus a 7m ground water gradient between boreholes UO3 and UO4, spaced only 2,8m apart. It is inferred that this differential is related to the absence of aquifer A1 in borehole UO4.

ii) Boreholes UO5, UO16, and UO20 reportedly have yields of up to 25 m^3/h. Boreholes UO6, UO7, UO8 and UO9 have moderate yields of about $5 m^3/h$. Boreholes UO3 and UO4 have very low yields of about 0,5 m^3/h.

iii) It is inferred that the lateral changes in both water level and yield are both related to more intensive fracture development in the centre of the test site, and in particular more intensive development of the major horizontal fracture in the centre of aquifer A2. This does however not explain the differences observed over the short distance between boreholes UO3 and UO4. The increased yield would be due to an increase in hydraulic conductivity, while the water table change would result from the black shale aquicludes being disrupted thereby eliminating the perched aquifer A1. It has been suggested that the overall aquifer recharge is along a northwest trending lineament of intensified fracturing running from boreholes UO16 to UO20.

iv) Borehole samples show oxidation down to a depth of 17m, indicating that this is the lowest water level which has occurred historically.

v) Potentiometric levels in almost all boreholes (except UO-1, UO-3, UO-10, UO-17, UO-18 and UO-19 which are between 1402,8 to 1405,4 mamsl) are all close to 1400 mamsl and no clear flow direction can be established from these measurements.

vi) The potentiometric level in Aquifer A2 is lower that both Aquifers A1 and A3. There would thus be a tendency for ground water to move towards Aquifer A2.

8.2 Objectives and programme at the IGS site

Two series of investigations were done at the IGS site. The first investigation focussed on testing of the Radiowave Tomography and Ground Penetrating Radar methods under the local geological conditions in order to evaluate the efficiency of the techniques in identifying and delineating flow paths and fracturing within Karoo aquifers. A second objective was to be assess the design parameters for the different techniques to be able to optimally design future experiments in similar geological conditions.

The second series of experiments conducted at the IGS site can be regarded as verifying and extending the geohydrological findings of the initial 50 MHz RT conducted at the site and had as main objectives the following:

- to map the different lithologies and lateral variations in a concentrated region within the centre of the IGS test site (in the region bound by boreholes UO3, UO5, UO8, UO9);
- to obtain additional structural information from differential-mode data obtained using the 30MHz system between boreholes UO3 to UO5 and UO3 to UO6; and
- to map water flow directly within the region using alterant tomographic data obtained with both the 30 MHz and the 50 MHz systems.

At the IGS site, a frequency of 50 MHz was optimal for the borehole spacings and rock types encountered at this site. This has a wavelength of about 1 metre in these rocks, giving a resolving power of between 25 and 50 cm, and an operating range of about 10 metres at the IGS site. Compared to the granitic rocks of the Vaalputs area discussed earlier, the shale and siltstone dominant formations of the Karoo Supergroup are generally at least one to two orders of magnitude electrically more conductive, reducing the operating ranges for RT which are achievable at a given frequency. In more resistive tock types (e.g. granites) a more favourable range resolution tradeoff would be achievable. The higher moisture and salt content, combined with the conductive nature of clay minerals, is responsible for the higher conductivities of the shale and siltstone sequences present in the Karoo Supergroup formations, compared to for example, the more crystalline and dense, dry granitic or quartzitic rocks.

A Tx/Rx station spacing of 50cm was generally used at the IGS site to correspond to the half wavelength. In some cases a spacing of 25cm was initially used, but later discarded when no additional benefit was realized. In most cases the boreholes were surveyed from 5 to 35 metres depth (with small deviations), so as to scan all three aquifers. Using these parameters it was possible to scan a single borehole pair in approximately 6 hours.

The second phase thus saw the implementation of two RT systems: the 50 MHz system as used to obtain more complete and concentrated information, and for comparison with the initial 50MHz work; and the use of the multifrequency 30 MHz system to obtain additional structural and water-flow information at a number of frequencies.

Ultimately, the aim of the tomography surveys was to provide information that could benefit the development of appropriate geohydrological models for Karoo aquifers present at the site and elsewhere, when used in conjunction with additional geohydrological and geological information.

8.3 Field programme and results for first series of experiments

The initial investigation was split into two sections. The first section consisted of the exploratory GPR survey, whereas the second included the RT work which consisted of three phases, namely:

- reconnaissance scanning to calibrate the system and determine operating ranges;
- background tomographic imaging to characterise lithologies;
- and alterant scanning to track water movement directly.

8.3.1. Results from the GPR survey

From previous experience of GPR surveys in Karoo environments, although geographically different areas, it was not expected that the GPR results would be of great advantage to provide additional information to unravel the geological conditions. The technique was nevertheless tried to assess whether it could help in detecting fractures in the sandstone aquifer below the electrically more conductive upper shale and weathered horizons. The survey in the end proved to be unsuccessful as the high electrical conductivity of the Karoo sediments limited the radar ground penetration to a couple of metres only. On this basis it is predicted that conventional GPR will be of limited value in studying Karoo aquifers.

8.3.2 Presentation and analysis of Radiowave Tomography results

The objective of the RT work programme was to provide information along two perpendicular lines through the survey area. One line passed through boreholes CH1, UO2, UO3, UO4, UO5, UO6, UP15, UO19 and UO12. The other line passes through boreholes UO14, UO20, UO7, UO6, and UO18. The RT work programme was divided up into three phases:

Phase (i): Reconnaissance parallel scans

During this phase, parallel scans were conducted between all targeted boreholes pairs. The first objective was to calibrate the RT system in this environment. The second objective was to provide a quick reconnaissance of the geoelectrical structure of the lithological succession. The final objective was to establish the operating range. These data are, however, insufficient for tomographic imaging.

Phase (ii): Background tomographic imaging for lithology characterization

Full tomographic imaging was conducted between borehole pairs selected by considering the output from Phase (i). The primary objective was to characterize the host rock lithology, and consider the link to the behaviour of the aquifer.

Phase (iii): Alterant tomography to track water movement directly

Alterant tomographic imaging was conducted between boreholes selected by considering the output of Phase (ii). These images represent the difference between the rock before and after the injection of a salt water tracer, which in effect allows the water flow to be tracked directly.

8.3.3 Phase (i): RT background calibrations and range tests

The parallel profiles conducted during phase (i) are summarized in Table 2 below.

8.3.3.1 Penetration

It was not generally possible to obtain penetration above about 10 metres depth due to the presence of casings and highly conductive clay overburden (**Figure 18a**). This precluded the possibility of imaging aquifer A1.

Radiowave penetration through all lithologies below the overburden was obtained for borehole spacings of 5 metres and less (**Figure 18a**). Radiowave penetration was only obtained through the relatively resistive sandstone A2 for borehole spacings of 5 to 10 metres (see also **Figure 22d** where most of the profile is at the system noise level of -15 dB microvolts). No radiowave penetration was obtained for borehole spacings of more than 10 metres. It was thus concluded that a frequency of 50 MHz RT could be used up to a borehole spacing of 10 metres for scanning the main aquifer A2, and up to a borehole spacing of 5 metres for scanning the complete succession. The remaining phases (ii) and (iii) were planned accordingly.

Table 8.1: Summary of different scans completed during first survey

Borehole 1 (transmitter)	Borehole 2 (receiver)	Spacing between boreholes (m)	Radio Wave Penetration
UO14	UO20	10	Aquifer A2
UO20	UO7	10	Aquifer A2
UO7	UO6	5	Full
UO6	UO18	20	-
UO15	UO6	15	-
UO6	UO5	5	Full
UO5	UO3	5	Full
UO6	UO4	7.5	Aquifer A2
UO6	OU3	10	Aquifer A2
5	4	2.5	Full
4	3	2.5	Full
14	7	20	-
20	6	15	-

Notes: 1. "Full" indicates radiowave penetration up to a depth of 10 metres; "Aquifer A2" indicates penetration only through the main aquifer A2; and "-" indicates no penetration whatsoever.

2. The lower 6 profiles were for calibration and cross checking only.

8.3.3.2 Lithological characterization

Typical parallel scans for boreholes spaced about 5 metres apart are shown in **Figure 18.** The signal strength profiles are indicated in units of decibels relative to microvolts. The Tx and Rx probes are kept at the same elevation, thus each data point "samples" the bulk rock at a specific elevation. Remembering that the signal strength will be inversely correlated to total radiowave attenuation between Tx and Rx, and that radiowave attenuation is in turn inversely correlated to electrical resistivity, it can be deduced that the signal strength is correlated to bulk electrical resistivity.

The parallel plots thus, in effect, provide uncalibrated logs of the variation of bulk electrical resistivity as a function of depth.

Figure 18 also shows the effect of injecting the salt water tracer, by superimposing profiles collected at different times after salt water injection in different colours. The discussion on this aspect is deferred to Section 7.3.5.

An important point is that clay is electrically highly conductive. Thus more argillaceous layers tend to be relatively electrically conductive, while more arenaceous layers tend to be relatively electrically resistive. Weathering and/or oxidation often result in the formation of clay leading to a raised electrical conductivity. Radiowave tomography will **not** be able to map out fracturing directly unless this fracturing is associated with clay mineralization, or a salt water tracer is used. Seismic tomography is better suited for mapping out fracturing directly.

It is observed that the signal strength through the upper mudstone layer is very low, in fact about at the system noise level of about -15 dB microvolts. This implies that limited information can be obtained about the mudstone and the sandstone layer A1 which underlies it, despite the fact that the mudstone is highly electrically conductive. The signal strength rises steadily through the black shale layer, indicating that this layer becomes progressively more resistive with depth. This may indicate a reduction in the level of oxidation with depth until the lowest oxidation level of 17m. There is a distinct signal strength high associated with the sandstone aquifer A2. This implies that A2 is relatively electrically resistive, which is consistent with an arenaceous layer. The signal strength drops off sharply within the siltstone layer A3, and then even further within the shale layer. This is consistent with an increase in clay content with depth.

8.3.3.3 Lateral changes

It is observed from the data that both large and even very subtle features are generally repeated almost exactly in profiles derived from different borehole pairs. This can be seen for borehole pairs UO3-UO5, UO5-UO6, and UO7-UO6 by comparing **Figures 18a, 18b and 20b.**

One lateral change which is observed is the presence of a conductive zone at a depth of about 22m (in the centre of A2) between boreholes UO14-UO20 and UO20-UO7, and is best developed between boreholes UO20-UO7. This feature is indicated by the arrow in **Figure 21.** This feature is absent from all other borehole pairs which were scanned. After discussions with IGS researchers and a study of the geophysical logs, it is postulated that this feature is related to clay infilling in the major fracture zone which occurs at this depth, and is thought to be an important water transport mechanism.

8.3.3.4 System calibration, data repeatability and data consistency

Table 2 indicates that there is multiple coverage of some areas. This is for the purpose of calibrating the system in this environment, and also for checking the data consistency and repeatability. Additional checks which were performed were to repeat certain profiles over a period of several days, and also to perform reciprocity checks, where the Tx and Rx boreholes were interchanged.

Figure 18a shows an example where data were re-acquired 4 times over a period of 2 days. (This was a part of phase 3, the salt water injection, but since the salt did not penetrate between these boreholes, this data can be used as a repeatability check). It is observed that the data are almost identical on each occasion. Statistically it was determined that the data variance for repeatability checks was better than 0.5dB, while the data variance for reciprocity checks was better than 1.0dB. This figure is better than the specification of the electronic receiver itself. The calibrations required for the tomographic imaging were successful, and also indicated a data consistency of better than 1.0 dB.

It is thus deduced that the data is of a very high quality, and thus a high confidence can be placed on the conclusions derived from manipulating the data.

8.3.4 Phase (ii): Background tomographic imaging for lithology characterization

Based on the results from Phase (i), only borehole pairs spaced 10 metres or less apart were tomographically scanned. For boreholes spaced 5 metres or less apart the complete succession was scanned, while for borehole spaced 5-10 metres apart, only the aquifer A2 was scanned. The borehole pairs were selected so as to provide information along two perpendicular lines; from UO14 to UO18 and from UO3 to UO6.

These results largely confirmed the geoelectrical features and boundaries observed during Phase (i), and also verified that the major lithological units were horizontally layered as had been expected. In fact, no inclined features were observed (This does not preclude the presence of non-horizontal fracturing, which would only show up if it had significant clay infilling).

8.3.4.1 Lithological characterization

The electrical characteristics of the lithology is clearly shown in **Figure 19a**, where results from boreholes 3 to 6 are overlain on the geological boundaries The following geoelectrical structure is observed:

- The upper clay layer and sandstone A1 are electrically highly conductive, probably due to the clay content, and the associated oxidation/weathering.

- The black shale grades from highly to moderately electrically conductive, possibly due to a decrease in oxidation with depth.

- The sandstone A2 is depicted as a distinct relatively electrically resistive layer, as would be expected for an arenaceous rock. It is significant to note that whereas at Vaalputs the water level interface coincided with the transition from resistive (unsaturated) to conductive (saturated) the intrinsic resistive nature of the sandstone layer dominates in this case. The lithology therefore controls the electrical character, whether it is water saturated or not. It must also be remembered that at Vaalputs the water is much more saline than at the IGS site.

- The siltstone aquifer A3 is depicted as a distinct electrical unit of moderate conductivity.

- The underlying shale is depicted as a distinct electrically conductive unit.

Table 8.2: Summary of scan geometry

Borehole 1 (transmitter)	Borehole 2 (receiver)	Spacing between boreholes (m)	Radio Wave Coverage
UO14	UO20	10	Aquifer A2
UO20	UO7	10	Aquifer A2
UO7	UO6	5	Full
UO6	UO18	20	Full
UO5	UO3	5	Full
UO6	UO4	7.5	Aquifer A2
UO6	UO3	10	Aquifer A2
UO5	UO4	2.5	Full
UO4	UO3	2.5	Full

Notes: 1. *"Full" indicates radiowave coverage up to a depth of 10 metres; and "Aquifer A2" indicates coverage only through the main aquifer A2.*
2. *The lower 6 profiles were for calibration and cross checking only*

There is no obvious lithological feature between boreholes UO3 and UO4 to explain the water table differential between these two boreholes. It should be noted, however, that the current geohydrological hypothesis is that this differential is due to the absence of water in aquifer A1 in borehole UO4, which implies that any associated lithological feature which causes the differential would be located in the upper 10 metres. Since RT cannot penetrate through this region, it implies that the it cannot be used to test this hypothesis.

There is no clear electrical expression of the major fracture zone between 21 and 25 metres depth between boreholes UO3-UO5, or UO5-UO6. This is expected, and merely implies that the fracture zone does not have significant clay infilling in this area.

8.3.4.2 Lateral changes

The geoelectrical structure is remarkably consistent from borehole pair to borehole pair. This can be seen, for example, by comparing results from boreholes UO3-UO5, and UO5-UO6 in **Figure 19a**, and UO6-UO7 in **Figure 20a** which are virtually indistinguishable. This implies that most lateral changes in the aquifer are either unrelated to lithological changes, or result from lithological changes which are too subtle or localized to be detected by the RT.

One change which is observed is the existence of a conductive feature in the centre of aquifer A2, between borehole UO14-UO20 and UO20-UO7. As noted in the previous section, *it is postulated that this relates to clay infilling within the major fracture zone.* It is noted that this feature is not developed near borehole UO14, and that there is a gap in the feature between boreholes UO20 and UO14. This could imply that there is a lateral variation in the degree of clay infilling.

8.3.4.3 Consistency of results

Multiple coverage of some areas was conducted as a check on the RT method itself, as indicated in Table 2. These results indicated that the RT technique was self consistent.

8.3.5 Phase (iii): Alterant tomography to track water movement directly

Alterant tomography is a differential approach where the difference in conductivity of the rock is imaged before and after the injection of a salt water tracer. This will highlight the movement of the water itself, rather than the lithological units. In view of the lateral uniformity of the lithological units, it was decided to concentrate on only four borehole pairs, UO14-UO20 and UO20-UO7 (to examine the effect of the clay infilling of the fracture zone), UO3-UO5 (where relatively low hydraulic conductivities were expected) and UO5-UO6 (where relatively high hydraulic conductivities were expected). Boreholes UO4 and UO7 were used as injection boreholes.

The procedure used was as follows:

i) Mix up a few hundred litres of completely saturated salt solution in a tanker belonging to the IGS.

ii) Inject about 100 litres of the salt water solution into the injection borehole through a hosepipe, using a pump connected to the tanker. A pressure head sufficient to just ensure water flow was utilized. The hosepipe was moved up and down the borehole from 5-35 metres to ensure even injection throughout all three aquifers.

iii) Monitor the selected borehole pairs by means of parallel scans, after salt injection. (The salt was not pumped through from any of the other boreholes - this was an attempt to allow the water to move slowly enough so that the process could be monitored).

iv) Conduct full tomographic imaging at the borehole pairs where changes were noted.

Strictly speaking, the experiments map the movements of the ions in the salt water, rather than the water itself. Due to binding of the ions to the rocks, and diffusion of the ions, the water flow may be somewhat different to the ionic flow.

8.3.5.1 Injection from borehole UO7

The effect was noted almost immediately for borehole pair UO20-UO7 (**Figure 22d**) and a few hours later for UO5-UO6 (**Figure 18c**). No change was noted from boreholes UO3-UO5 (**Figure 18a**), and for boreholes UO14-UO20. It may be inferred that there is a higher hydraulic conductivity between boreholes UO20-UO7, and UO5-UO6 than between boreholes UO3-UO5 and UO14-UO20. This is consistent with the geohydrology data which is available. It may also be inferred that the water movement is in two directions at the same time. This implies that there is no clear flow direction, and that the water must be moving mostly by the slight head introduced by pumping the water into the injection hole.

The changes as seen in the parallel scans (**Figures 18c and 22d**), indicate that the change in signal strength induced by the tracer reaches a maximum very rapidly (within hours) and then decays back to the base level much more slowly. This would support the idea of fast water flow along fractures, induced by the increased head in the injection hole, followed by a diffusive movement of the tracer away from the boreholes.

8.3.5.2 Injection from borehole UO4

After the injection from borehole UO7 was unsuccessful in inducing a change between boreholes UO3-UO5, injection from borehole UO4 was conducted in order to try and probe these boreholes. This injection did not produce a result for boreholes UO14-UO20, UO20-UO7, or UO5-UO6, indicating that there may be some impermeable or unfractured zone around borehole UO4 causing this borehole to be low yielding. The injection did induce a change between boreholes UO3-UO5 (**Figure 18b**). It is interesting to note that this change has a different temporal signature to that observed during the previous injection; the change in signal strength builds up slowly to a maximum over a period of a day, with no obvious decay. This may imply that the water is moving diffusively, and supports the concept of an impermeable zone around borehole UO4.

Verwey *et al* (1993) describe the results of packer tests in a selection of the boreholes at the IGS site. Although they did not use borehole UO4 as an injection borehole for cross borehole packer tests, their results are consistent with the RT results in that very limited hydraulic connection between UO4 and the surrounding boreholes exists. They did, however, find that hydraulic connection does exist between UO4 and UO3, and UO4 and UO5 at a depth of 20 m and 24 m respectively. The difference between the RT and packer tests is that in the former no pressure head was created by the injection of the fluid, whereas during the alterant tomography experiments only a slight pressure head was sustained.

Full differential imaging was then performed on three borehole pairs UO3-UO5, UO5-UO6, and UO20-UO7. Originally it was hoped to monitor the complete water flow process in a "snapshot" way. Unfortunately, the data could not be acquired fast enough, and the results thus indicate the "before" and "after" situations. The results of the three differential scans are discussed in the following section. The warm colours in the alterant image (**Figures 19c and 22c**) indicate areas of maximum tracer ingression, while the cold colours indicate areas of minimum tracer ingression. Obviously the colour scaling cannot be compared to the lithological images.

8.3.5.3 Alterant scan between boreholes UO3-UO5, and boreholes UO5-UO6

Two tests were done:

(i) Injection at borehole UO4 and observation in boreholes UO3-UO5;

(ii) Injection at borehole UO7 and observation in boreholes UO5-UO6.

Borehole UO3-UO5 represents a situation when one hole is very low yielding, (UO3), and one hole very high yielding (UO5). Movement of the tracer between the two boreholes was only obtained by injecting the water through the intermediate borehole UO4. Boreholes UO5-UO6 represents a situation when one borehole is very high yielding (UO5), and one borehole moderately yielding (UO6). Movement of the tracer between the two boreholes was obtained by injecting the water through borehole UO7. The "before" and "after" scans are collated in **Figures 19a and 19b**, while the differential scans are collated in **Figure 19c**. It is important to remember when comparing the images that the injection points were different.

The parallel scans indicate that most of the water flow is through the bottom of aquifer A2 and the top of aquifer A3 (**Figure 18**). There is also water flow through the shale, which is unexpected. It is observed that there appears to be almost no water flow above 17 metres, which corresponds to the oxidation elevation - this may imply that oxidation has resulted in a closure of pore space above the oxidation level.

Note that there is very little difference observable between the "before" and "after" scans, due to the fact that the changes induced by the tracer are relatively subtle. The changes are, however, clearly seen on the differential images. This can be visualized by examining the parallel profiles of **Figure 18** and recognizing that the before and after images are generated from the individual parallel scans acquired at different times, while the alterant images are generated from the differences between data acquired at different times.

The following observations can be made:

- The water movement is dominantly along well defined lineations of complex geometry, which are often inclined. This is in contrast to the regular horizontal layering of the lithological units.

- It is inferred that this movement is related to flow along fracturing, but that this fracturing is not strictly only horizontal as expected. This observation is supported by the results from the packer testing by Verwey *et al.* (1993).

- The water movement is predominately through the bottom of aquifer A2 and the top of aquifer A3.

- *The inclination for the lineations between boreholes UO3 and UO5 mirrors the* change in water table level between these boreholes.

- There is also a more subtle but pervasive water movement throughout the rock below an elevation of about 17 metres. The lack of water flow above this elevation may be related to closure of pore space by oxidation. It is inferred that this water movement is diffusive. There are some subtle features within the bulk rock which mirror the inclination of the lineations controlling the major water flow.

8.3.5.4 Alterant scan between boreholes UO20-UO7

Boreholes UO20-UO7 represents a situation when one borehole is very high yielding (UO20), and one borehole is moderately yielding (UO7). Note that only the main aquifer A2 could be imaged because of the borehole spacing. The conductive lineation present in the middle of aquifer A2, is inferred to relate to clay infill within a major fracture zone. Movement on the tracer between the two boreholes was obtained by injecting the water through borehole 7. The before and after scans are shown in **Figures 22a and 22b**, while the differential scan is shown in **Figure 22c**.

The following observations can be made:

- The water movement occurs predominately above and below the conductive lineation shown in **Figure 22a**. This implies that there is limited water flow through this zone, and that the zone may even act as aquicludes to some extent.

- *It is inferred that this movement is related to flow along fracturing due to the* speed at which the changes are monitored.

- The water movement is most intense below the conductive lineation.

9. SECOND RADIOWAVE TOMOGRAPHY SURVEY AT THE IGS

9.1 Objectives

The overall objective of the second-phase RT work was to test and verify the initial hypotheses and findings, and then to extend the current knowledge of Karoo aquifers by applying a larger range of RT techniques to the site.

The main aim of the second-phase RT survey at the IGS site was to map the lithologies toward the centre of the test site as well as lateral variations therein, and to provide information on time and spatial variations regarding the flow of a tracer through the aquifers present at the site under steady-state conditions. To provide the required information the following field procedure for the phase-two RT was followed. The fieldwork was centred around boreholes for which the largest amount of integrated geohydrological, geological, and geophysical information was available (these are boreholes UO3, UO5, UO6, UO8, and UO9). This configuration of boreholes allowed for the pseudo 3-D imaging of flow processes within the region.

A concentrated salt solution was used as the conductive tracer. Each injection consisted of spreading the tracer throughout the length of the surveyed region within the borehole using approximately 70 litres of pre-mixed salt solution. Individual injections lasted approximately five minutes.

9.2 Equipment and field procedure specific to the Phase 2 experiments

Two tomography systems developed at Miningtek were used in the second-phase RT fieldwork conducted at the IGS test site; these are the 50 MHz (single-frequency) and 30 MHz (multifrequency) systems. The second system, generally referred to as the 30 MHz system has the capability of measuring the response at five preset frequencies between 10 and 30 MHz. There is an inherent trade-off between range and resolution with regard to frequency; the higher the frequency, the smaller the range and the better the resolution (and vice-versa).

The fieldwork consisted of the following five stages:

Stage 1 - 50 MHz

The first stage involved obtaining parallel as well as full background scans from 5 m to 35 m between boreholes UO5-UO3, UO3-UO9, UO8-UO5 and UO8-UO9, and from 10 m to 35 m between boreholes UO9-UO5 and UO3-UO8 using the 50 MHz system. The first set of scans cover the sides of the square region, while the second two cover the diagonals. Tomographic scans across the diagonals of the square were limited from 10 m to 35 m due to a loss of penetration at 50 MHz between 5 m and 10 m due to the high conductivity of the sediments located in this region. Included in this stage was a full reciprocity scan (UO3-UO5) for comparative purposes with Phase 1 data and for a reciprocity check on later alterant data. Two additional parallel scans were performed as reciprocity and repeatability checks on the 50 MHz system. Other additional parallel scans were conducted between boreholes UO3-UO4 and UO4-UO5 to enable the calculation of E_o values at 50 MHz in the region. The parallel scans between UO3-UO5 were also used for comparative purposes against the same data acquired with the 30 MHz system (to compare range advantages and characteristic features which should be present in both datasets).

Stage 2 - 30 MHz

The second stage involved obtaining parallel as well as full background scans from 5 m to 34 m between boreholes UO3-UO5, and UO3-UO6 using the 30 MHz system. This included selecting the five optimum frequencies in the range 10-30 MHz for the remainder of Phase 2 as well as parallel-scan range tests for further spaced boreholes (UO14-UO6 and UO3-UO10). An additional parallel scan was conducted between UO5-UO6 to enable the calculation of E_o values for the region at the five selected frequencies. All parallel scans (excluding the range tests) were repeated in reverse mode (swapping transmit and receive positions) as reciprocity and repeatability checks on the system. Range tests were conducted with the 30 MHz system in parallel-scan mode between boreholes UO14-UO6 and UO6-UO10 to determine attainable ranges in Karoo sediments.

Stage 3 - Injection of tracer using 50 MHz equipment

The third stage involved the injection of the tracer into borehole UO5 and the continuous monitoring of the square region with the 50 MHz system (in parallel-scan mode) across all boreholes until it was determined that the progression of the tracer through the region had stabilised.

Stage 4 - Alterant tomography using 50 MHz equipment

In this stage, full alterant imaging was conducted in the square region with the 50MHz system. Re-injections of the tracer were performed at UO5 before acquiring alterant data. Alterant images were conducted at a time after the salt injection such that the solution had not dissipated and/or relaxed into some equilibrium position within the aquifer. Data acquired during the third phase indicated that there was no penetration of the tracer between borehole pairs spatially separated from UO5; thus, for alterant scans of the spatially separated boreholes, a re-injection of the tracer was performed at UO8.

Stage 5 - Alterant tomography using 30 MHz equipment

Full alterant imaging was performed between UO3-UO5 and UO3-UO6 with the 30 MHz system, with a re-injection of the tracer at UO5. This stage was conducted before the injection of the tracer at UO8 (as detailed in stage 4) to keep the source of the tracer constant.

9.3 Presentation of results

9.3.1 System calibration, range tests and penetration

9.3.1.1 The 50 MHz system

Figure 23 shows the parallel scans for the block scanned using the 50 MHz system. Separations between boreholes bound by the block vary between 4.63 m (along the sides of the block) to 7.0m (along the diagonals). Throughout the block, penetration was achieved between depths of 10 m and 30 m along both the sides and the diagonals, while only limited penetration was achieved between 30 m and 35 m along the sides. Above a noise level of approximately -13 dBµV, maximum signals obtained were at a level of approximately 70 dBµV at 50 MHz. Thus, at 50 MHz, and at borehole separations of between 4.63 m and 7.00 m, full tomographic imaging was possible between depths of 10 m and 30 m.

9.3.1.2 The 30 MHz system

Figures 24 and 25 show parallel scans performed with the 30 MHz system between boreholes UO3-UO5 and boreholes UO3-UO6 at borehole separations of 4.83 m and 9.87 m respectively. Frequencies were chosen for the remainder of the survey according to the trade-off between range and resolution. The highest frequency was set to 29.1 MHz as this was the highest frequency at which penetration through the majority of the succession was still achieved. This highest frequency corresponds to the highest possible resolution achievable using the 30 MHz system. The lowest possible frequency (11.1 MHz) was chosen in order to broaden the frequency range investigated. Parallel scans from these two surveys (**Figures 24 and 25**) indicate that above a noise floor in the region of -35 dBµV, the maximum signal obtained was approximately 86 dBµV at 11.1 MHz for the closer-spaced boreholes. The three highest frequencies used (29.1 MHz, 24.1 MHz and 20.1 MHz) did not achieve penetration above 9 m for the further-spaced boreholes, while the highest frequency did not achieve penetration below 26 m for the further-spaced boreholes. Thus, for the closer-spaced boreholes (UO3-UO5) full tomographic imaging was possible between 5 m and 34 m; while for the further-spaced boreholes (UO3-UO6) full tomographic imaging was only possible between 9 m and 26 m at 29.1 MHz, 9 m and 34 m at 24.1 MHz and 20.1 MHz, and between 5 m and 34 m at 11.1 MHz and 16.1 MHz. Range tests were performed with the 30 MHz system in parallel-scan mode between boreholes UO6-UO14 and boreholes UO6-UO10. The results of these are detailed in **Tables 9.1** and **9.2.**

9.3.2 Background scanning

It should be kept in mind that each individual image within all figures in this report were processed separately, and thus have slightly different colour histogram functions. Thus, in determining the continuity of a marker horizon across a borehole, geoelectric layers should be viewed relative to other layers within the same image.

Table 9.1: Range test at a borehole separation of 25.2 m (UO6-UO14)

Frequency (MHz)	Penetration achieved between depths of:
10.1	10 m - 25 m
12.1	11 m - 24 m
14.1	13 m - 22 m
16.2	14 m - 21 m
18.1	14 m - 21 m

Table 9.2: Range test at a borehole separation of 50.6 m (UO6-UO10)

Frequency (MHz)	Penetration achieved between depths of:
10.1	None
11.1	None
12.1	None
14.1	None
16.2	None

9.3.2.1 Lithological characterisation and lateral variations

50 MHz Background parallel scans

Figure 23 shows a comparison of all background parallel scans obtained using the 50 MHz system in the region enclosed by the block. These are plots of radiowave attenuation along horizontal paths. All six background scans in this plot have been calibrated (via a conversion to attenuation values in dBμV/m) and should look identical for a horizontally-layered, homogenous earth. There are some discrepancies between the plots which provide information on lateral variations in the sub-surface. What is important in these plots is that conductive and resistive marker horizons are observed in parallel scans acquired across spatially-separated borehole pairs; this implies that throughout the surveyed region there is horizontal layering, although there are lateral variations in the geoelectrical composition of the individual geoelectric layers. The interpretation of the plots has been done in conjunction with information available from core samples. The interpreted stratigraphic section is maintained throughout the report, and it should be kept in mind that the depths of lithological boundaries and the thickness of geoelectric layers may vary slightly through the surveyed region.

Near the top of the diagram, two of the plots (those for the diagonals of the square) have a far lower attenuation value than those for the sides of the square. This is due to the fact that the attenuation values of the plots in this region of the subsurface are calculated while the system is operating in noise; and in the calibration of the data to attenuation values, the responses recorded along the side of the square are divided by a smaller number (borehole separation). In this region of the subsurface, the stratigraphy is dominated by a highly electrically-conductive lithology (interpreted as being a mudstone from core samples). This region exists from above 5 m to a maximum depth of 10.5 m, after which the mudstone grades into a more resistive lithology between 10.5 m and 11.5 m. This second layer is interpreted as being a sandstone (aquifer A1). After this thin marker, there is a decrease in the attenuation to the resolvable base of a layer at approximately 14.5 m. This is interpreted as being a black shale from the available borehole core.

Below the black shale, there is a further decrease in the attenuation as is expected from the presence of a series of different sandstones between the depths of 14.5 m and 24 m. This series of sandstones was previously interpreted as being aquifer A2. Some of the sandstones in this series are weathered (from the core samples) and there is evidence of this in the attenuation profiles. There are two regions within this sandstone that are interpreted as being weathered; these are between 17 m and 18 m, and 19.5 m and 22 m. These regions show an increase in attenuation, attributed to a higher clay content with respect to the surrounding sandstone. Of particular interest here is the weathered region between 19.5 m and 22 m. This region is extremely prominent between some borehole pairs, and less between others. After discussions held with IGS researchers, it was revealed that this conductive signature marks the position of a horizontal fracture which may now, and as a result of the core drilling technique applied here, contain some highly electrically-conductive drilling mud. Although radiowave tomography does not directly map fractures, it can detect fractures that are infilled with material having a conductivity contrast to the surrounding host rock. Thus the detectability of this region across the test site is dependent upon the distribution of the clay mineral (which may act as an aquicludes) throughout the test site, and thus on the location of the core boreholes with respect to the surveyed region.

Below the sandstone series, there occurs a more conductive layer (between the depths of 24 m and 27.5 m) which is interpreted as being a siltstone layer corresponding to the lower aquifer (A3). After the siltstone there is an even more conductive layer (identified as a grey shale) which continues to the base of the profile. From the attenuation profiles, there is another layer between the approximate depths of 31.5 m and 34 m having a higher resistivity than the overlying grey shale, very similar to that of the siltstone. This geoelectric layer is not recorded in the available borehole core, and is followed by a layer having a similar resistivity to that of the grey shale. From the borehole core, it is evident that below depths of approximately 30 m, the lithology is dominated by shale which is occasionally interbedded with siltstones. The layer between 31.5 m and 34 m may be a representation of this.

In terms of lateral variations, there are significant deviations between the plots shown in the above diagram between 10.5 m and 14 m, and below 19.5 m. In general, a higher bulk attenuation is expressed in profiles obtained towards the southern portion of the square (between boreholes UO5 and UO8), while lower attenuations are observed toward the north (between boreholes UO9 and UO3). Intermediate profiles (between boreholes UO9-UO8, UO3-UO8, UO5-UO9, and UO5-UO3) have the same bulk attenuation. What this implies is that in general, lithologies to the north of the region have a lower clay content than those to the south. This is consistent with the existence of core boreholes CH2 and CH3 (drilled using bentonite) to the southwest of the region. This difference in attenuation is particularly well developed in the sandstone A1, the black shale below A1, towards the base of the sandstone series A2 (including the identified weathered region between 19.5 m and 22 m), and is extremely well developed in the lower siltstone (A3) and grey shale units. If these lower attenuations are indeed related to the contamination of the aquifers with bentonite, then higher hydraulic conductivities may be expected in the northern portion of the region with respect to those in the south.

30 MHz Parallel scans

Figures 24 and 25 are parallel scans obtained between boreholes UO3-UO5 and UO3-UO6 respectively, using the 30MHz system. Individually, these plots show the response (in dBμV) at the five preset frequencies between a single borehole pair, and have not been converted to attenuation values (as with the 50 MHz plots). These 30 MHz plots have the same bulk trends as were observed in the 50 MHz plots, but at a lower resolution (as would be expected at lower frequencies). In each of these plots, the frequencies plotted range from 11.1 MHz to 29.1 MHz. At higher frequencies in this range, there is a greater attenuation of the signal, and thus a lower response. Thus, the highest response recorded in the plot is that at 11.1 MHz.

9.3.2.2 Background imaging

The images presented in this section were obtained both as background images (prior to the injection of the tracer) and as post-injection images. Both background and post-injection images show the same features, however, in the latter case, certain features are often highlighted. The reasons for this are twofold. Firstly, in the post-injection images, as the lower boundary of the conductivity of the rockmass is raised as a whole, the colour table used in the image processing spans a smaller range of attenuation values. This has the effect of boosting features having intermediate conductivities towards the higher end of the colour table. Secondly, features along which migration of the tracer is taking place will naturally be highlighted with respect to the background attenuation.

50 MHz Background images

These images (presented in **Figures 26 to 28**) confirm the geoelectrical features, marker horizons and boundaries identified in the 50 MHz background parallel scans. In general, these images show evidence of large-scale horizontal layering in the subsurface. **Figure 26** shows a typical 50 MHz background image acquired between the boreholes UO8 and UO5. As can be seen in this figure, the top aquifer A1 is not resolved from the highly conductive mudstone (red) near the top of the image. The black shale appears as a more resistive (blue-green) layer beneath the mudstone, and there are apparent cross-cutting features in this layer. Beneath the shale is a gradational boundary with the middle sandstone A2, which appears as a dark-blue layer with faint cross-cutting conductive features (particularly highlighted in **Figure 26** is the "weathered zone" between 19.5 m and 22 m). The middle sandstone has a sharp lower contact with the underlying, more-conductive (blue-green) siltstone. The grey shale beneath the siltstone has a higher conductivity than the siltstone and apparent cross-cutting features are also present within this layer. The last two layers (the lower siltstone and shale) are clearly resolved toward the base of the image, having similar conductivities to the overlying siltstone (A3) and grey shale.

Of interest in these tomographic images are a number of thin, undulating layers within some of the geoelectric layers. Two thin, faint, undulating layers are present within the main aquifer A2. These appear as electrically conductive layers within the more resistive sandstone. They are interpreted as being either weathered zones or zones contaminated with bentonite within the main sandstone aquifer (A2) as determined in the analysis of the 50 MHz parallel scans. These features present in the grey shale may either be fracture-related or may be representative of large-scale cross beds within the unit. Faults are not directly detectable by radiowave tomography, but may be inferred from additional information such as: (i) the offsetting of electrically resistive or conductive layers across a fault; (ii) the movement of a conductive tracer along a fault; or (iii) the existence of sufficient amounts of a conductive mineral within the fault. At this particular test site, there is no evidence of faulting in the surveyed region, although this does not preclude the possible existence of fractures within the rockmass as a whole.

30 MHz Background images

In broad terms, the 30 MHz background images (**Figures 29 to 32**) exhibit the same features as are observed in the 50 MHz images. The major discrepancies between these and the 50 MHz images is in the lower resolution attained with the 30 MHz system, and the manner in which the base of the geoelectric sequence is imaged. The latter is imaged as a series of dipping layers, and whether or not these imaged layers have any physical significance is not certain. These may only be artefacts, as they are not imaged with the higher frequencies using the 30 MHz system. In general, the 30 MHz images show three distinct layers; a middle resistive layer with a gradational upper boundary, and a generally sharp lower contact, located between two more conductive layers, the lower of which may have physically-significant cross-cutting features. The lowermost layer is not imaged as four distinct layers (with the exception of the 29.1 MHz image between boreholes UO3 and UO6, in which three layers are resolvable beneath the middle sandstone A2), and the black shale beneath the top mudstone is not resolved from the middle aquifer A2.

Figures 29 and 30 show the 30 MHz images acquired between UO3 and UO5 prior to and after the injection of the tracer respectively, and can be directly compared to the

50 MHz images acquired over the same region. **Figures 31 and 32** show the 30 MHz images acquired between boreholes UO3 and UO6 and show the same broad features as are present in the 30 MHz images between UO3 and UO5. In general, dipping features in the background images (**Figures 29 and 31**) are somewhat "flattened" in the post-injection images. This would imply that the tracer raises the conductivity in the broad region surrounding the dipping features, and the dipping features are not preferred paths for the tracer in the base of the profile.

9.3.3 Differential tomography

9.3.3.1 30 MHz differential images

Differential tomography produces images of the gradient of the attenuation of the rockmass with respect to frequency. The images presented in **Figure s 33 to 36** are thus images of the change in conductivity attributed to a change in frequency.

Figure 33 shows the differential images acquired between boreholes UO3-UO5 prior to the injection of the tracer. The differential images at the lower end of the frequency spectrum highlight the dipping layers towards the base of the image as are observed in **Figure 29**. Two of these dipping layers are also observed in the 50 MHz background image between UO3 and UO5. These layers are not present in the differential images towards the higher end of the spectrum (on the right of **Figure 33**). Rather, these higher-frequency differential images tend to highlight some of the horizontal boundaries between the defined geoelectric layers. In particular, these are the boundaries between the sandstone A1 and the units above and below it, the boundary between the black shale and the sandstone A2, the boundary between the sandstone A2 and the siltstone, the boundary between the siltstone and the grey shale, and the boundary between the lowermost siltstone and underlying shale at the base of the imaged succession. The most prominent feature in the higher frequency differential images is a horizontal, red marker at 19.5 m; this corresponds to the upper limit of the "weathered" zone identified in the 50 MHz background scans. The post-injection difference images (in **Figure 34**) are much the same as the background difference images, the only difference being in the relative colour representations of the identified features.

Figures 35 and 36 show the background and post-injection difference images acquired between UO3-UO6. These images show the same features as those acquired between UO3-UO5. Again, the higher-frequency images tend to highlight horizontal layer boundaries, while the lower-frequency images highlight broad, dipping features towards the base of the images.

9.3.4 Alterant tomography to track water movement directly

9.3.4.1 Continuous monitoring of the tracer

Figures 37a to 39b show parallel scans obtained between different borehole pairs at different times after a single injection of the tracer. **Figures 37a and 37b** are different representations of the time series obtained between boreholes UO3-UO5. **Figure 37a** shows the progression of the tracer as a set of conventional parallel scans. **Figure 37b** shows the progression of the tracer relative to background; these are plots of the difference between the background parallel scan and the time series of post-injection parallel scans. These "difference to background" plots show the progression of the tracer more clearly.

In **Figure 37b,** soon after the injection of the tracer, there is a sharp change in the attenuation values. This, particularly toward the top of the profile, is interpreted as being mostly due to the salt present in the solution within the borehole, immediately surrounding the antenna. As time increases, the tracer migrates into the surrounding rockmass and in general, the plots show the concentration of the tracer within a number of regions of the aquifer.

Figure 37b shows parallel scans acquired across a single borehole pair (UO3-UO5) at successive time increments during the continuous monitoring of the tracer from 5 minutes to 24 hours after the injection of the tracer. In this case, UO5 was used as the injection point. These have been differenced from the background parallel scan for the same set of boreholes (acquired prior to the injection of the conductive tracer) and are in units of additional path attenuation (dBµV). In this figure, there is an initial sharp rise in attenuation with respect to the background below 10 m. This is interpreted as being due to the initial concentration of salt solution within the borehole and around the antenna. The 9,5 m level marks the water level within the borehole, and no conductivity variation would be expected above this. In time the tracer migrated and diffused into the subsurface in three dimensions, accounting for the slowly decreasing attenuation levels with respect to background within the two-dimensional plane of measurement. During this decay process, the tracer preferentially concentrated in specific regions (these being the flow paths within the aquifers). The attenuation fall-off in the other regions is interpreted as being predominantly due to the decreasing concentration of the salt solution within the injection borehole.

The most noticeable anomalous region in **Figure 37b** is a broad region extending from 10,5 m to 22,5 m depth, in which the tracer was highly concentrated for extended periods of time. This was interpreted as a diffusive region in which the slow flow of the tracer was due to diffusive or porous flow. Within this region, smaller regions may occur, exhibiting behaviourally different flow patterns. At 10 m there was a rapid initial influx and rapid fall-off of the tracer. This occurred at the base of the upper mudstone, and was interpreted as being representative of bedding-plane flow. The rapid fall-off of the tracer in this region may have been due to the limited supply of the tracer at the top of the water column within the injection borehole, as the salt solution stagnated towards the base of the borehole after injection. A similar type of behaviour was observed at the interface between sandstone aquifer A1 and the black shale (at 11,5 m), and also towards the base of the black shale (at 14,5 m). In the latter case the fall-off of the tracer was more restricted. The existence of these anomalous regions indicated that although there was diffusive flow into broad regions, bedding planes could be preferred paths for flow within the latter. This type of flow may also be related to fracture-type flow in which case the fractures were associated with the bedding planes. This type of behaviour was again observed outside the broad, diffuse region at 24 m and 34 m, both of which coincided with bedding planes. In these two cases, the fall-off of the tracer was very slow, and hence it could be assumed that the fall-off rate of the tracer in these regions was directly related to the supply of tracer, as the level of the salt solution stagnated towards the base of the injection borehole.

The flow of the tracer within the different regions as described above indicates the possibility of three mechanisms accounting for the flow of the tracer through the rockmass. The first of these is a slow, diffusive mechanism operating within the black shale and middle sandstone A2. The second mechanism is one of fracture flow, or flow within weathered regions within the middle sandstone A2. The third appears to be bedding-plane related flow at the base of sandstone A1, the base of the black shale, the base of sandstone A2, and at the base of the lowermost siltstone.

The tracer was only observed in parallel scans obtained across borehole pairs including borehole UO5 (the borehole in which the injection of the tracer was performed). This indicates that the diffusive mechanism is slow or physically restricted between spatially separated borehole pairs, and that fracture flow or bedding plane related flow far from the injection point is restricted to thin regions not detectable at 50 MHz.

The explanation presented above for **Figure 37b** *also applies to* **Figures 38b and 39b** as the profiles are almost identical.

9.3.4.2 50 MHz alterant scans

The alterant scans obtained at the IGS test site are shown in **Figures 40 to 42**. The figures span injections from two distinct injection points (namely UO5 and UO8). **Figure 40** shows all alterant scans obtained using UO5 as the injection point; **Figure 41** shows all alterant scans obtained using UO8 as the injection point; and **Figure 42** is both sets of alterant scans displayed together.

Two distinct features relating to the flow of the tracer are highlighted in the images in **Figure 40**. The first of these is related to broad diffusive flow between 11 m and 19 m. These depths span sandstone aquifer A1, the black shale, and the region of sandstone aquifer A2 above the identified "weathered zone" between 19.5 m and 22 m. The alterant scans between UO8-UO5 and UO9-UO5 in this figure show features within this "diffusive zone" which correlate to a cross-cutting feature observed in the black shale in the background scans acquired across these boreholes (see **Figure 27**). Clearly, the movement of the tracer preferentially occurs along the conductive marker located within the black shale. In the analysis of the background scans, the conductive feature within the black shale was tentatively identified as a large-scale cross-bed; however, the feature may simply represent the distribution of the black shale. Diffusive flow occurs to a greater extent between boreholes UO5-UO3 than between the other boreholes pairs in this series of alterant scans; this may relate to a greater hydraulic conductivity between these two boreholes.

The second major feature in the alterant scans in **Figure 38** is a linear feature close to the base of the middle aquifer (A2), which crosses the boundary between the middle sandstone (A2) and the underlying grey shale; this is thought to be related to fracture-type flow. The linear feature dips to the northwest, and spans the lower portion of the middle aquifer (A2), below the identified "weathered zone" between 19.5m and 22m, and crosses the boundary between the middle sandstone and the grey shale. This feature is continuous throughout the entire region enclosed by the block, although it appears to thin between UO9-UO5; however, this may simply relate to the extent to which the tracer is stored within the feature at a particular location. That this cross-cutting features observed in the scans between UO8 and UO5 (**Figure 40**) and between UO9 and UO5 (**Figure 38**) plays a role in the recharge of aquifer A2 cannot be ruled out entirely.

The diffusive flow is more concentrated around the borehole in which the injection was performed (UO5), as can be seen in the three-dimensional view of the images, while the fracture-type flow spans the entire image. The images show no evidence of the tracer toward the base of the image, as would be expected from the continuous monitoring of the tracer (**Figures 37a to 39b**).

Figure 41 shows all alterant images acquired using UO8 as the injection point together with the 50 MHz Background parallel scans for the region. All alterant scans in this figure were acquired from a single injection at UO8. Directly after the injection, UO8-UO3 were scanned, followed by UO8-UO9, and lastly UO9-UO3. In these images, there is again evidence of diffusive and fracture-type flow; however, the diffusive flow is more restricted than that shown in **Figure 40.** The alterant scan between boreholes UO8-UO9 shows that there is no penetration of the tracer into the black shale. Rather, the diffusive flow of the tracer is restricted to that portion of the middle sandstone aquifer (A2) above the identified "weathered zone". Between UO8-UO3, diffusive flow is further restricted; however, this may be due to the short time-lapse between the injection of the tracer and the subsequent scanning of the borehole pair. The alterant scan between UO9-UO3 does not show evidence of diffusive-type flow; this may be due to the time at which the scan was performed, and that sufficient time had not passed to allow for the diffusion of the tracer between these two boreholes spatially removed from the injection point. Fracture-type flow is evident between UO9-UO3 and UO8-UO3. The linear feature imaged in these scans is identified as a similar feature to that discussed in the analysis of **Figure 40**, and exhibits the same behaviour.

Figure 42 shows all alterant scans acquired during the second-phase radio tomography. Of interest in this figure is the manner in which the linear features discussed in the analyses of **Figures 40 and 41** appear to cross-cut one another; what these features represent is uncertain. However, they always exist beneath the identified "weathered zone" which may represent the infilling of a fracture with bentonite; this being true, the "weathered zone" may act to some extent as an aquicludes.

From the continuous monitoring of the tracer, it was postulated that three types of flow existed within the region. These were diffusive flow, fracture flow, and flow associated with bedding planes. The alterant scans provide evidence of diffusive and fracture-type flow. In the discussion of the continuous monitoring of the tracer, an additional zone of flow was identified between 33.5 m and 34.5 m; this was not imaged in the 50 MHz alterant scans. This may be due to the small dimensions of the zone, or the low concentration of the tracer within the zone; however, it is certain that the zone exists, and its behaviour is probably very similar to the linear features identified in the analysis of the alterant scans.

In order to test the reciprocity of the technique and at the request of the Steering Committee, a reciprocal alterant scan was performed between boreholes UO3 and UO5. The result of this was an alterant image very similar to that obtained with the Tx and Rx reversed indicating that the reciprocity of the technique is not violated under these conditions. The differences in the two images are minor and can easily be accounted for by the time at which the images were acquired after the injection of the tracer.

9.3.4.4 30 MHz alterant scans

No meaningful results were obtained from the 30 MHz alterant data. It was found that the difference in the attenuation values prior to and after the injection of the tracer was not sufficient to be imaged with the 30 MHz system. A possible reason for this is that regions in which the tracer was concentrated were not large enough to be resolved using the 30 MHz system. Although there was a constant offset in the attenuation values over both of the surveys, which would not be imaged, there was not significant deviation in the values from this DC offset, which would have been the features that would have been preferentially imaged.

9.4 Results from the seismic tomography experiments

The survey started with the one metre spacing parallel scan between boreholes UO5 and UO6. **Figure 43a** presents this profile where the travel time is plotted against depth. Two additional parallel scans were carried out covering the space between boreholes UO4 and UO5 and between boreholes UO3 and UO4. The parallel scan between UO4 and UO5 was also done at one metre intervals (**Figure 43b**), whereas the parallel scan between UO3 and UO4 shown in **Figure 43c** is a more comprehensive scan with a 20 cm spacing between consecutive positions.

After the acquisition of the parallel profiles, tomographic profiles, starting with the one between boreholes UO3 and UO4, 2.30 m apart, were acquired. The receiver probe was lowered in the UO3 borehole at 20 cm intervals from a depth of 11,8 m to 37 m. The transmitter was lowered in the UO4 also at 20 cm intervals from a depth of 10.8m up to a depth of 37 m. These depths represent the bottom of the boreholes and the respective water levels.

Because of its geometry (the unusually large depth/width ratio), the tomographic profile between boreholes UO3 and UO4 was subdivided in three segments in order to get a stable solution in terms of reconstructed velocity images. **Figure 44** presents all three segments showing the velocity images, where **Figure 44a** shows it between depths 12 m and 20 m, **Figure 44b** presents it between depths 20 m and 30 m, and finally **Figure 44c** gives it between depths 30 m and 37 m.

The most outstanding recovered feature is depicted in **Figure 44b** where a low velocity zone, probably corresponding to fractured rocks, crosses from depth 22 m at borehole UO3 down to 23 m in borehole UO4 with an average thickness of 1,3 m . In the same **Figure 44b**, a high velocity zone, that crosses from a depth 25.9 m at borehole UO3 nearly horizontally up to borehole UO4, displays an average thickness of ~0,7 m.

In **Figure 44c** a very steep (approximately 60°) low velocity zone, that crosses from a depth of 35,8 m in borehole UO3 up to 31,7 m at borehole UO4 has an average thickness of 2,3 m. There is also a strong indication that this structure shows some kind of dislocation at a depth of 34,1 m.

The travel time data was also interpreted using radiowave tomography interpretation software. The similarity of the two sets of tomographic scans interpreted by two different software packages, is illustrated in **Figure 45**. The same discussion as given above is also valid for the tomographs resulting from the interpretation using the radiowave software.

9.5 Correlation between RT and Packer test results

Verwey et al. (1993) conducted a series of double packer tests and cross borehole packer tests in a selected number of boreholes on the IGS Test Site. The set of hydraulic conductivity values calculated for borehole UO5 from these tests are graphically displayed in **Figure 46.** From these results two zones can be identified which have significantly higher hydraulic conductivity compared to the rest of the borehole. These zones extend from 5 m to 12 m and from 17 m to 25 m.

By means of cross borehole packer tests, Verwey et al. (1993) were able to establish at what depths and between which boreholes hydraulic connections are present. The relative value of the connection could also be established. This is illustrated in **Figures 47 and 48.** These figures should be compared to the alterant images shown in **Figures 19c and 40.** From **Figure 19c** it is clear that water movement occurred freely over the zone from 17 m to 24 m. This corresponds almost exactly with that of the largest hydraulic conductivities determined from the packer tests (**Figure 46**). In the zone between 11 m to 15 m no water movement could be observed during the injection of the salt water tracer. However, between 5 m and 11 m, some flow could be identified. Again, both these zones correspond almost exactly with those identified from the packer tests. Unfortunately no packer test derived hydraulic conductivities are available for borehole UO3, UO6 or UO8, so that the inclined flow direction indicated on the alterant scans could be verified. However, from **Figure 47** it is clear that a number of inclined flow paths are present especially between UO5 and UO6, UO5 and UO7, UO5 and UO8, and UO5 and UO9. This is in agreement with the information derived from the alterant scans.

The alterant images also indicate that within Aquifer A2 horizontal as well as inclined flow occurs. This is in contrast to the almost only horizontal flow observed in the siltstone Aquifer A3. It is therefore concluded that bedding plane as well as fracture flow dominates in Aquifer A2, whereas only bedding plane flow occurs in Aquifer A3.

10. BOREHOLE RADAR EXPERIMENTS

10.1 Background information

During 1996, The Division of Mining Technology (Miningtek) of the CSIR undertook a feasibility study into the application of low frequency borehole radar to achieve long range or deeper penetration of rock formations than is normally achieved with conventional GPR systems. This investigation was primarily focussed on the gold and base metal mining environment However, *as water filled fractures in the mining environment are one of the targets of these investigations*, it was also thought to test the systems on shallower targets presented in the ground water exploration and research environment. Low frequency GPR suffers from noise or "clutter" being generated by the antennas and there is no simple way to reduce this noise. The lower frequencies typically used cover the frequency range 10 to 80 MHz.

As its name implies, borehole radar operates in a borehole. The antenna is thus closely coupled to the rock, isolating the system from clutter caused by local metal or air spaces. Borehole radar offers some advantages over conventional GPR:

- Once the decision is made to place the antenna in a borehole, the length of the antenna is no longer a practical obstacle. Low frequencies can thus be used for long range probing.
- Since a borehole is required, it can be sited to achieve the best geometry in relationship to the target. Underground GPR always has to be operated from tunnels or other openings. Often, these openings do not offer a good geometry with respect to the target.

On the other hand, borehole radar also suffers from some disadvantages which are related to the advantages:

- Borehole radar requires boreholes. The cost of acquiring data is often substantially less than the cost of drilling the borehole.
- At present, diamond drilled holes or small diameter holes are required. In a mineral exploration application it is best to site radar boreholes outside the target. However, there is a reluctance among geologists to drill diamond holes beyond the orebody. The

requirement of a small diameter borehole is important as the airspace around the antennas need to be restricted as much as possible. This poses a problem for the application in conventional water supply boreholes.

10.2 Discussion of results

10.2.1 Chloorkop Waste Disposal Site

The Chloorkop waste site is situated on Halfway House Granites where a new hazardous waste disposal site was developed. As part of the geohydrological investigations numerous boreholes with depths up to 50 metres were drilled. Ground water occurs in the upper weathered sections of the granite as well as in fractures in the more solid granite.

Since borehole radar is well suited to imaging fracturing, it was hoped that it would provide further information about fracturing at the site. A good understanding of the role fractures in the granite play in the ground water flow mechanisms in this aquifer are of particular importance in terms of their ability to transport contaminants within the aquifer.

The borehole radar was also tested in both single borehole mode to investigate possible reflections from fractures and diabase dykes (Boreholes CH-15, Ch-16, Ch-17, Ch-27 and Ch-31), as well as cross-hole mode (Boreholes Ch-16 and Ch-32) to determine whether it might be possible to use it to monitor potential leakages from the site.

A number of the radargrams obtained from single borehole experiments are displayed in **Figures 49 to 53**. It appears that in most of the boreholes there was a lack of targets or water filled fractures. A notable feature in the radargrams is antenna ringing (shown as "A" in **Figure 51**). Antenna ringing is the repetition of signal caused by the reverberation of the antenna when the receiver is struck by a reflected wave and is an artefact of the antenna. The ringing observed in the Chloorkop radargrams are aggravated because the boreholes used were of large diameter (165 mm), and a wave is set up in the borehole. The problem is similar to the tube wave in seismic reflection studies.

Any trace of fracturing was obliterated by the effect of ringing. However, definite changes in the reflection patterns are visible on the radargrams. The most notable feature is the low penetration in the upper weathered zone compared to the more solid, unweathered granite. In an attempt to correlate the degree and depth of weathering and the depths at which water strikes were encountered, with the radargram features, **Table 10.1** was drawn up. For this correlation the change in reflection pattern was taken as the point where a definite increase in the two-way reflection time occurs.

A reasonable correlation of the features listed in **Table 10.1** is apparent, but no reflection pattens from fractures are visible. The most promising reflections were obtained from borehole Ch-27 which is drilled a few metres away from a thin intrusive diabase dyke (**Figure 52**). However, the reflections were probably damped by the weathered transition zone between the granite and the diabase. An attempt to image the dyke was not successful, probably because the interface is not a sharp transition. There is evidence of significant weathering along the interface of the dyke.

Table 10.1: Correlation between radargrams and weathering depth, Chloorkop

Borehole number	Depth at which radargram pattern change occurs (m)	Depth of weathering (m)	Water strike (fractures) depths (m)
Ch-15	26 (?)	27	27-29; 40-42
Ch-16	5	5	17 (minor); 25
Ch-17	16	15	30 (minor)
Ch-27	22	28	23 (minor)
Ch-31	30	32	26 (minor)

In conclusion it can be said that the electrical performance of the borehole radar system at the Chloorkop site was good, but the targets did not lend themselves to good interpretation and imaging. The site also illustrated the ringing problem which occurs when borehole radar is used in oversize boreholes.

10.4.2 Aquifer Test Site: Bloemfontein

The second test was done at the Institute for Groundwater Studies' Karoo aquifer test site on the Campus of the University of the Free State. The same boreholes that were described in earlier experiments were again used for the borehole radar tests. Based on the results of the radio wave tomography experiments, it was not expected that the borehole radar would add significantly to the existing knowledge of the structural aspects of the aquifer. Earlier RT results did indicate that there may be fractures cutting across the horizontal layering and in so doing, providing hydraulic pathways for fluid migration. The test site has been studied extensively and geohydrologically it is well understood. It therefore provided a good opportunity to test the borehole radar technique as good control on the interpreted results was available and to determine whether the application of borehole radar techniques could provide any additional information on the aquifer under these geological conditions.

Success was, however, not expected for the following reasons:

- the electrical conductivity in Karoo sediments is generally high, which would limit the range and penetration depth; and
- the main fractures (in this case the target for the borehole radar technique) is perpendicular to the borehole. This is a poor geometry to expect high quality radargrams from.

Nevertheless, in order to compare test results from the more electrically conductive Karoo formations with those from the more resistive environments where the borehole radar had been tested thus far (Witwatersrand quartzites and Halfway House granitic environments), it was decided to also some limited tests at the IGS site.

In practice, the first problem was exacerbated by the horizontal layering of the sediments. The relatively resistive sandstone layers are thin, which meant that the long antenna string could not fit entirely into the sandstone zone. Either the transmit or the receive antenna was not in the resistive layer, and sometimes only one arm of the electric dipole was in the resistive sandstone layer. Tests were conducted in the following boreholes: Core borehole CH1 and CH2, and the 165 mm diameter boreholes UO5, UO8 and UO20. In addition cross-borehole tests were done using boreholes UO5 and UO8. In all test the 60MHz antennas were used. Radargrams are displayed in **Figures 54 to 59** (Also refer to **Figures 15 and 16** showing the positions of the boreholes).

The best results were found in borehole UO5. A prominent horizontal fracture is present at a depth of 22m in this borehole. This fracture, shown as a 'break' in the radargram, is clearly visible in the radargram. A similar feature is visible at a depth of about 21m in the radargram of borehole UO8.

In the crosshole radargram between borehole UO5 and UO8 a distinct change in reflection pattern occurs at a depth of 24m. This coincides with the transition from the sandstone aquifer (A2) to the siltstone aquifer (A3). The RT tomograms across this section (**Figure 40**) indicate a prominent fracture at a depth of 24.5m in borehole UO8 and at 22m at borehole UO5. Although the packer tests conducted by staff of the IGS confirmed the presence of this inclined hydraulic, the most prominent hydraulic connection between these two boreholes is horizontal and occurs at a depth of 20m. This fracture is, however, not visible on the RT tomograms .

The aim of introducing a new geophysical tool should always be to provide information that is not available using other tools, or to provide the same information at less cost, in time or resources. At this site, the borehole radar proved that the technique is capable of showing the presence of fractures, but not their extent or geometry. Similar, more detailed results are available from conventional borehole logging techniques, such as caliper and sonic log, and at much reduced costs. Results of the radiowave tomography (RT) matched those of borehole radar poorly at the IGS site. Based on what is known about the electrical properties and geometry of the fracturing, the result was, however, expected.

11. CONCLUSIONS AND RECOMMENDATIONS

In terms of the main objectives of the project, the following main conclusions of a general nature can be made from the information presented in this research report:

- Three pilot studies using the high resolution geophysical techniques of Radiowave and

Seismic Tomography, have been conducted successfully to test whether these techniques can assist in characterizing the nature of aquifers at a micro-scale (over ranges of metres, with resolutions of 10's of centimetres) compared to the more traditional geohydrological techniques available. This work was supported by the use of more conventional geophysical techniques.

- No surface geophysical technique (including GPR, seismic reflection and refraction, magnetics, and frequency domain EM) can, at present, characterize aquifers directly at this scale. These techniques can, however, provide useful background information. Since these techniques are fast and inexpensive to apply, it is suggested that they are used routinely in future studies, but in a supporting rather than a primary role.

- The Radiowave Tomography results proved that it is a flexible technique which not only finds application in secondary-phase mineral exploration, for which it was originally developed, but which can equally well be applied in the environmental field.

- Radiowave and Seismic Tomography (RT and ST), in contrast to other more conventional geophysical techniques, demonstrated the potential to interpolate the aquifer geometry between boreholes. This was proven in two contrasting geological environments, namely fractured Proterozoic granite gneiss and Karoo age sedimentary successions.

- The characterisation of the physical nature of the aquifer can be done indirectly by pin-pointing lithological controls on the aquifer geometry, and directly by using alterant tomography to track water flow. It was demonstrated that RT and ST, when used in combination, have the ability to map different lithologies and lateral variations therein, major fractures, and water flow directly. Alterant scans confirmed that the water flow could be directly mapped using a conductive tracer.

- RT is at a stage where the efficiency, consistency and repeatability of results is sufficiently high to render the technique useful as a monitoring tool. The technique produces information essential in the development of both geologic and geohydrological models, and can be used in combination with Seismic Tomography, to further constrain these models.

- RT has proved itself in the field of geohydrology and may facilitate a major advance in the formulation of geohydrological models of flow, which are usually derived from sparse and often incomplete datasets. It can be applied to the identification and delineation of flow paths within aquifers as an aid to the identification, definition and refinement of appropriate geohydrological models.

More specific conclusions emanating from the studies done at the two test sites are:

- The results of Ground Penetrating Radar were disappointing at both test sites and did not contribute at all to our knowledge of the physical nature of the rock formations or the aquifer(s) itself.

- The selection of frequencies for each type of geological environment is primarily dependant on the prevailing geological conditions and physical parameters of the rock type, as well as the scale of detail or resolution required in the study of the aquifer. It is often a trade-off between resolution and depth penetration (horizontally) that determines the frequencies selected.

- The reconnaissance scans in a Karoo environment indicated that at 50 MHz, RT can be applied for imaging the full succession (approximately 40 m) for boreholes spaced 5 m. apart. However, at a borehole spacing of 10 m at the IGS test site, penetration was only achieved through the second aquifer (A2) situated within a sandstone and roughly in the middle of the succession.

- Repeatability checks indicated that the data was of a high quality. Reciprocity test were also conducted and indicated that minor discrepancies occur when transmitter and receiver positions are interchanged. These discrepancies were found to be negligible. Consistency checks indicated that the RT method was internally self-consistent, and that a high confidence could thus be placed on conclusions derived from the manipulation of the data.

- Background scans indicated that it was possible to image lithological units on the basis of their electrical conductivity contrasts.

- The images indicated that the geoelectric structure is horizontal in the case of the Karoo geology with little variation from borehole pair to borehole pair, although this did not preclude non-horizontal fracturing. It was concluded that changes in aquifer characteristics and behaviour are unrelated to major lithological changes, although they may be related to subtle lithological variations.

- It was determined that sediments in the region of the IGS test site are horizontally layered and that lateral conductivity variations within individual geoelectric layers do exist; cross-cutting features were observed within the black shale, the middle sandstone aquifer (A2), and the grey shale.

- A laterally varying conductive feature was identified between boreholes UO14, UO20 and UO7 within the middle aquifer (A2) of the IGS test site. This was interpreted as being related to the infilling of a major fracture with clay.

- Alterant scans confirmed that the water flow could be directly mapped using a conductive tracer. From these scans, it was inferred that there is no strong flow direction near the centre of the test site. The results provided some evidence of an impermeable zone in the region of borehole UO4 which relates to the low yield of this borehole, and the variation of the water depth of the IGS test site within these boreholes. It was not possible to characterise the upper aquifer (A1) as penetration was not achieved through this conductive horizon.

- From the initial RT conducted at the site, it was determined that water movement between boreholes UO3 and UO6 of the IGS test site occurs predominantly along well defined lineations near the base of aquifer A2 located within a sandstone, and the top of aquifer A3 located within a siltstone. These features were interpreted as being related to flow along fractures. The lineations were identified as having complex boundaries, are not horizontal, and cut across the defined boundaries of aquifers A2 and A3. Flow between boreholes UO3 and UO5 was identified as being diffusive, while flow between boreholes UO5 and UO6 was identified as being more genuinely "flow-like". Pervasive water movement was identified below the determined oxidation level, which was apparently related to a diffusive mechanism.

- Between boreholes UO20 and UO7 of the IGS test site, a major conductive feature in the centre of A2 was identified. This was interpreted as being related to the infilling of a major fracture zone with clay. From the alterant scans conducted between these boreholes, this was interpreted as acting to some extent as an aquicludes. Water flow between these boreholes was interpreted as being related to flow within well-defined zones, these possibly being fractures.

- In the case of the electrically resistive granite aquifer at Vaalputs, the water saturation of the granite influences the radiowave images significantly, whereas in the case of the more electrically conductive Karoo formations no distinction can be made between the saturated and unsaturated parts of the formation.

- No physical "barrier" between borehole UO3 and UO4 of the IGS test site could be seen on any of the RT or ST images to explain the significant difference in potentiometric level (~7 m) observed in the two boreholes.

- The continuous monitoring of the progression of the tracer was performed under steady-state conditions at the IGS test site, and three major zones of flow were identified: The first of these is a broad-diffusive zone spanning the black shale and the upper portion of the middle aquifer A2. The second is a narrow zone crossing the boundary between the middle aquifer and the siltstone aquifer A3, existing below the identified "weathered zone" within the middle aquifer A2. The third zone exists towards the base of the imaged succession, and has a character similar to that of the second zone. The latter two zones were associated with fracture-type flow, this implying that flow within these regions is more genuinely flow-like as opposed to diffusive.

- Alterant data was acquired throughout the surveyed region at the IGS Test Site at both

30MHz and 50MHz. The 50MHz alterant scans confirmed the existence of the upper two zones of flow observed in the continuous monitoring of the tracer, and it was possible to deduce the types of flow from the images. The 30MHz alterant data did not produce any meaningful results due to the small change in the system, induced via the introduction of a tracer, at these frequencies.

- The tomography results agree in broad terms with current geohydrological thinking; however, there are deviations in terms of the placement of the three aquifers, and flow along non-horizontal fracturing towards the lower portion of the middle sandstone aquifer A2 at the IGS test site. There are apparent deviations in the results of the first and second series of tomography experiments. However, it appears that the choice of injection point for the alterant scans affects the results to a large extent, this depending on the connectivity between the injection point and the aquifers (ie. whether or not the chosen borehole intersects the aquifers). In agreement are the flow-types observed at the site in both datasets; both surveys indicate that diffusive and fracture-type flow occur in close proximity.

- The seismic tomography data set was interpreted with software specifically designed for the application to seismic data, as well as with the software developed to interpret the RT data sets. The two software packages yielded virtually the same results, thereby adding confidence in the soundness of the interpretations.

- For both the Vaalputs and IGS sites, a good correlation between the results from packer tests and that of tomography was found. Areas of high and low hydraulic conductivity correlated well with high flow and low flow zones identified on the alterant scans.

The experience gained with applying borehole radar to ground water and other mining investigations, confirmed that geophysical tools should be used within their range of applications. Some of the important observation made include the following:

- Best results are achieved when the host rock is electrically resistive. The RAMAC system delivered good ranges in the Witwatersrand quartzites, Halfway House granites, and other resistive hosts, but gave very little penetration in various Karoo sediments.

- If there is layering, with the borehole crossing resistive and conductive layers, the resistive layers should be substantially thicker than the antenna system is long. In the Karoo aquifer for example, the resistive layer was not thick enough for effective use of the borehole radar.

- The target should be semi-parallel to the borehole. In the Karoo aquifer, the target crossed the borehole at right angles, so the radargram provided no more information than conventional borehole logging, or even careful core logging. By contrast, some fractures in the Witwatersrand quartzites could be well imaged because of their semi-vertical nature.

- The borehole should be long enough for profiling and of small diameter. Radar returns echo from any discontinuity encountered. Only by profiling a sufficiently long borehole can desired echoes be separated from short discontinuities. Borehole radar works most successfully in small diameter holes. In larger holes, such as the 150 mm holes at the Chloorkop waste site, the holes cause reverberations which reduce the data quality.

The feasibility study has shown that borehole radar is an exciting technique, which can definitely take its place for some in-mine problems where the results have proven it to be an excellent tool for fracture and fissure mapping. In terms of ground water applications, its usefulness will be governed by the economics of the project. It will probably be best suited for applications in a research and not so much in a production environment.

Some recommendations resulting from this project are the following:

- The results of the RT and ST experiments have been very promising and it is recommended that these techniques be employed as the prime high-resolution geophysical tool in obtain detailed information on rock and aquifer structure when the demands on the project are such that detailed information is required.

- More surveys of this nature will have to be conducted to test the technique under different geological and geohydrological environments in order to become more familiar with the interpretation of the results in terms of their geohydrological meaning.

- One aspect that was not addressed in this project although initially envisaged, was to develop techniques to calculate from RT derived information, hydraulic parameters for the aquifer or specific sections thereof. Much more work in this respect will be required in terms of the development of the necessary theoretical base for such calculations, the effect that the geological environment has on the calculated values, and ultimately on the the verification of the calculated values. Geostatistical techniques may perhaps be a suitable route to follow in this regard. In this respect, more emphasis should be placed on the application of Seismic Tomography, as some work has already been done in the oil exploration industry to determine permeability and storage from cross borehole seismic surveys.

As a final and overall conclusion it can be said that the results obtained using RT in a Karoo geological environment indicated that the physical nature of the aquifer agrees in broad terms with the current geohydrological thinking. Significant deviations from this were, however, identified, such as flow along non-horizontal fracturing which now needs to be incorporated into the conceptual model, as well as taken into account when developing any mathematical techniques to analyse fluid flow in fractured rocks of this nature.

The project further demonstrated the importance and power of working as a team comprising members from of a wide variety of disciplines (geohydrologists, geophysicists, geologists (structural geologists, sedimentologists), mathematicians, electronic engineers, numerical data specialists). In many cases there was no direct interaction between these disciplines and there may be no reference to their work in this report, but in some way their expertise was incorporated into the end product. In this regard the workshops and field visits of South African researchers in fractured rock aquifers organised and funded by the Water Research Commission plays a vital role and needs to be further supported and expanded.

REFERENCES

Alumbaugh, D.L. and Morrison, H.F. (1995) Theoretical and practical considerations for crosswell electromagnetic tomography using a cylindrical geometry. Geophysics, 60, 3, 846-870.

Botha, J.F. (1992). The geometry and physical nature of fractured aquifers. A few introductory remarks. Institute for Groundwater Studies, UOFS, Bloemfontein.

Brandt, M.B.C. and Coetsee, VdA. (1993). Progress report on the project: The Application of *Seismic Tomography and Ground Penetrating Radar for the Determination of Fractures and Hydraulic Properties of Fractured Rock Aquifers.* Submitted to the Water Research Commission at the Steering Committee Meeting on 12 May 1993. Report EMAP-C-93018, CSIR, Pretoria.

Carneiro, D., Mitchell, G. and Vogt, D. (1995). Application of Seismic Travel Time Borehole Tomography at the IGS Test Site; CSIR Miningtek, Internal Report, 1995

Crampin, S. and Lovell, J.H. (1991). A decade of shear wave splitting in the Earth's crust: What does it mean? What can we make of it? And what should we do next? Proc. Of the 4th Intern. Workshop on Seismic Anisotropy, Geophys. J. Int., 107, 387-407.

Daniels, Jeffrey J. (1990). Fundamentals of Ground Penetrating Radar. SoftEarth Associates Inc., Westerville Ohio.

Hay, R., Levin, M. and Faurie, J.N. (1987). Site selection program for the disposal/storage of radioactive waste in South Africa. Site Suitability Phase Progress Report No. 53. Geohydrology and water management of the Garing fault and the adjoining aquifer in the Orchard area north of the Vaalputs airfield. Atomic Energy Corporation of SA. Restricted Report PIN-1063(B/R), GEA787.

Hodgson, F.D.I. (1986). Site selection program for the disposal/storage of radioactive waste in South Africa. Site Suitability Phase Progress Report No. 54. Design and installation of a borehole monitoring system at the Vaalputs Nuclear Waste Disposal Site. Atomic Energy Corporation of SA. Restricted Report PIN-1070(B/R), GEA799.

Kraus, J.D. (1984). Electromagnetics. McGraw Hill, New York, 775pp.

Levin, M. and Jamieson, B. (1986). Site selection program for the disposal/storage of radioactive waste in South Africa. Site Suitability Phase Progress Report No. 46. Borehole data in the vicinity of the Vaalputs Radioactive Waste Disposal Facility. Atomic Energy Corporation of SA. Restricted Report PIN-976(B/R); GEA717.

Lytle, R.J., Lager, D.L., Laine, E.F., Salisbury, J.D. and Okada, J.T. (1981) Fluid-flow monitoring using electromagnetic probing. Geophys. Prosp., 29, 627-638.

Mitchell, G.B. (1996). Internal report on the project: The Application of Seismic Tomography and Ground Penetrating Radar for the Determination of Fractures and Hydraulic Properties of Fractured Rock Aquifers. Miningtek, CSIR.

Mitchell, G.B., Wedepohl, E. and Carneiro, D. (1996). The characterization of aquifers using Radio Tomography. Paper submitted for presentation at the Soc. of Exploration Geophysicists Meeting, San Francisco, December 1996.

Nekut, A.G. (1995) Crosswell electromagnetic tomography in steel-cased wells. Geophysics, 60, 3, 912-920.

Sen, P.N., Scala, C. and Cohen, M.H. (1981). A self-similar model for sedimentary rocks with application to the dielectrc constant of fused glass beads. Geophysics, vol. 46, p. 781-795.

Spies, B.R. and Ellis, R. G. (1995) Cross borehole resistivity tomography of a pilot-scale, in-situ vitrification test. Geophysics, 60, 3, 886-898.

Spies, B. R. and Habashy, T. R. (1995) Sensitivity analysis of crosswell electromagnetics. Geopysics, 60, 3, 834-845.

Van der Voort, I. (1995). The influence of the geometry of Karoo aquifers on their ability to yield water. Unpublished MSc thesis, University of the Orange Free State, Bloemfontein, 85pp.

Verwey, J.P., Botha, J.F. and Buys, J. (1993) The analysis and interpretation of aquifer tests in secondary aquifers. Progress report to the water research Commission. Institute for Groundwater Studies, Univ. Of the Orange Free State, 19pp.

Vogt, D. (1997). Final report: A preliminary investigation into the applicability of borehole radar. CSIR Division of Mining Technology, CSIR Report no. MS/5/97 (2 volumes).

Wedepohl, E. (1993). Radio Wave Tomography: Imaging Ore Bodies Using Radio Waves. Proceedings of the 3rd Technical Meeting of the South African Geophysical Association in Cape Town.

Wedepohl, E., Meyer, R., and Mitchell, G. (1995) Interim report on the project: The Application of Seismic Tomography and Ground Penetrating Radar for the Determination of Fractures and Hydraulic Properties of Fractured Rock Aquifers; Submitted to the Water Research Commission at the Steering Committee Meeting on 10 May 1995.

Wedepohl, E., Pitts, B. and Meyer, R. (1994). Interim report on the project: The Application of Seismic Tomography and Ground Penetrating Radar for the Determination of Fractures and Hydraulic Properties of Fractured Rock Aquifers. Submitted to the Water Research Commission at the Steering Committee Meeting on 17 June 1994. Report no. EMAP-C-94035, CSIR, Pretoria.

Wilt, M.J., Alumbaugh, D.L., Morrison, H.F., Becker, A., Lee, K.H., and Deszcz-Pan, M. (1995) Crosswell electromagnetic tomography: System design considerations and field results. Geophysics, 60, 3, 871-885.

FIGURES

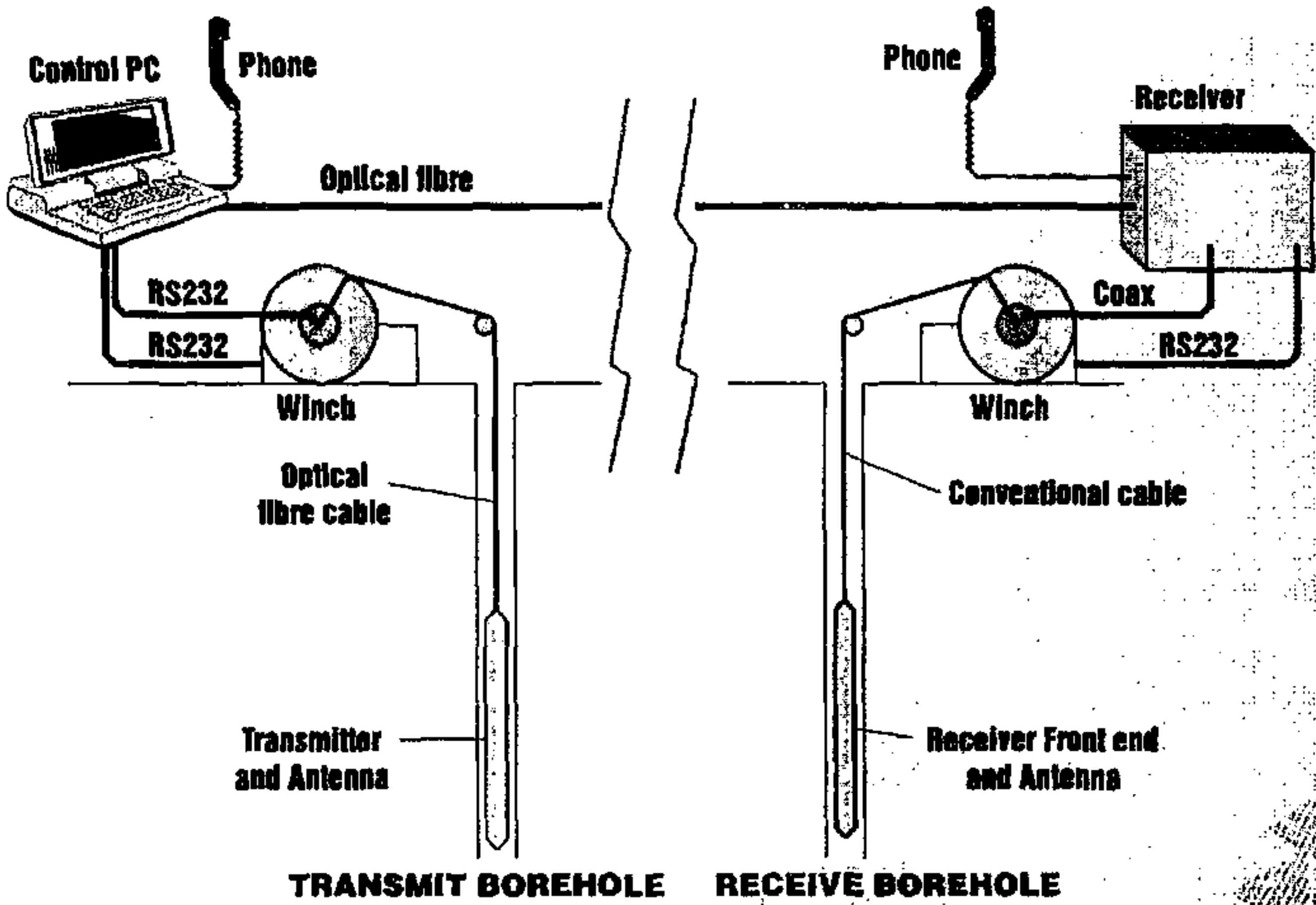

Figure 1: Instrument layout for cross borehole Radiowave Tomography surveys.

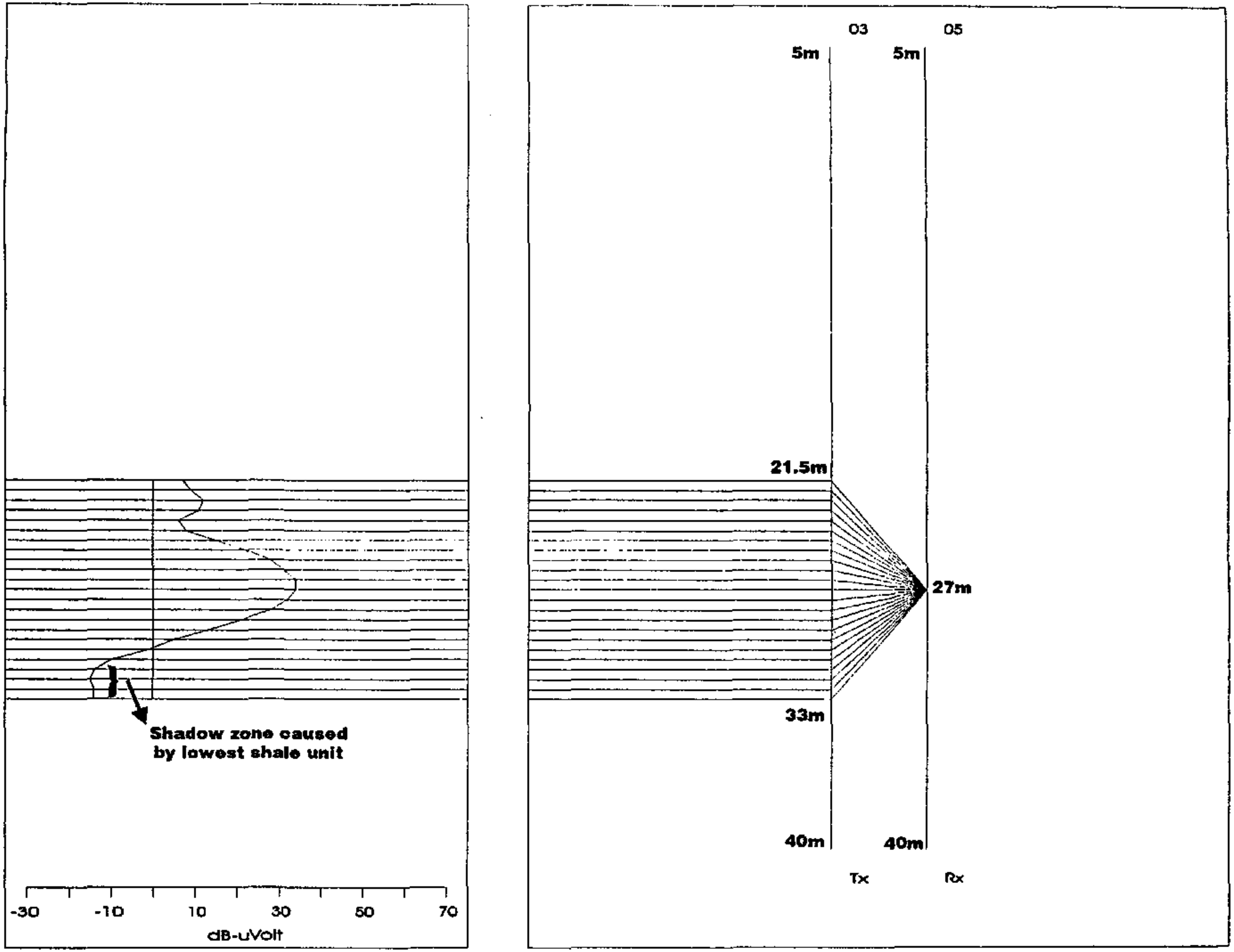

Figure 2: Example of a RT "fan-beam profile" between two boreholes.

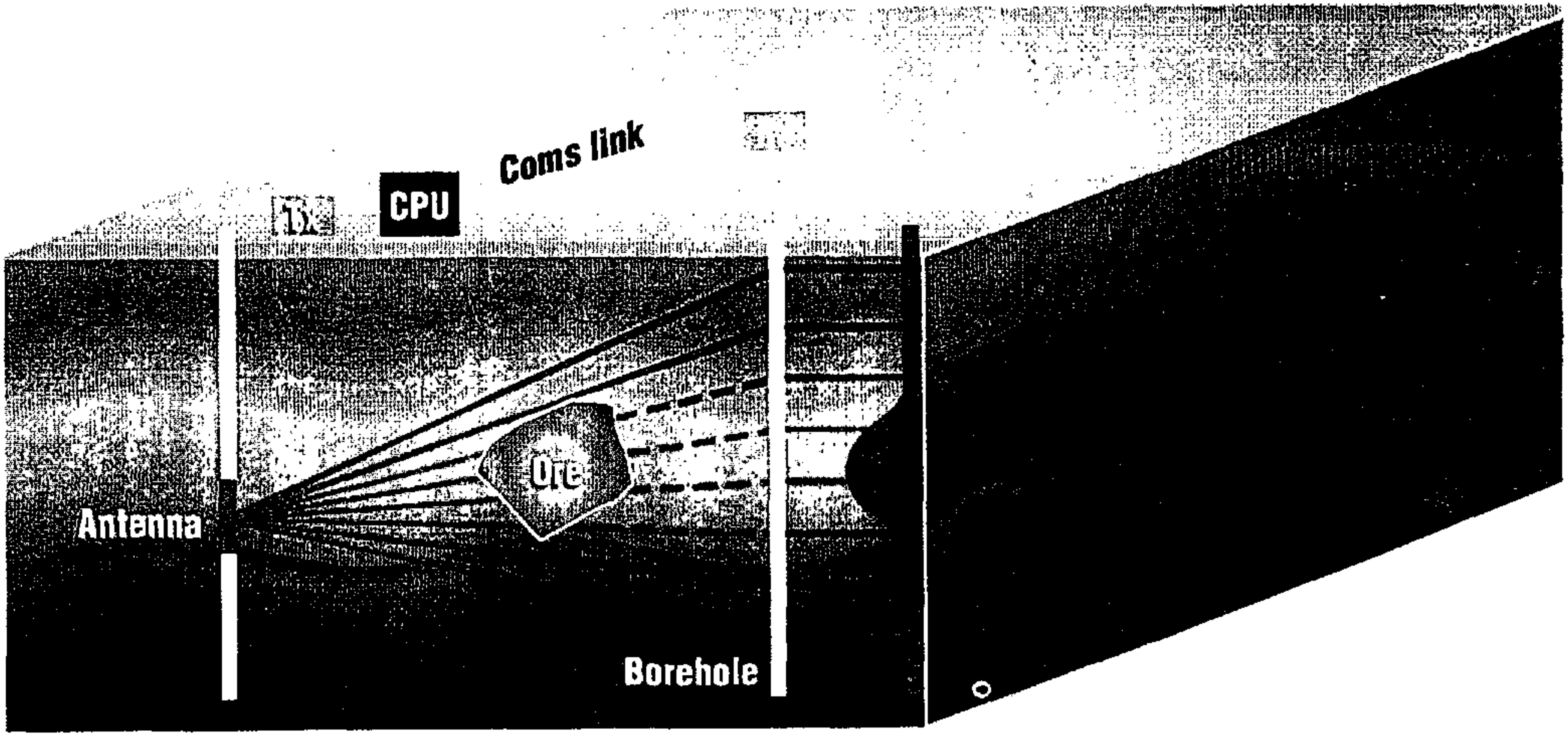

Figure 3: Schematic diagram to illustrate the "radiowave shadow zone" being cast behind a body between the Transmitter (Tx) and Receiver (Rx).

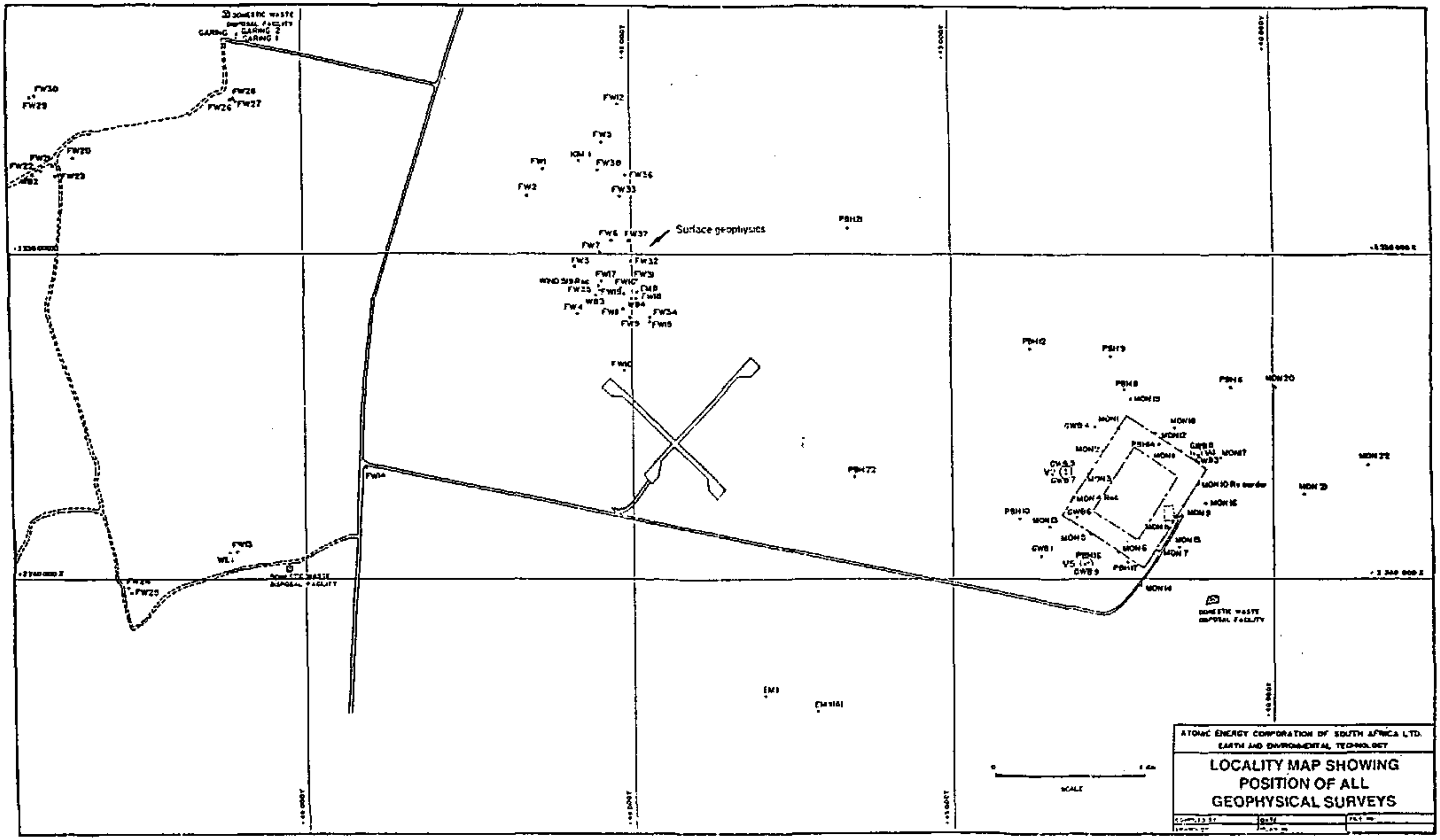

Figure 4: Locality map for the Vaalputs survey area.

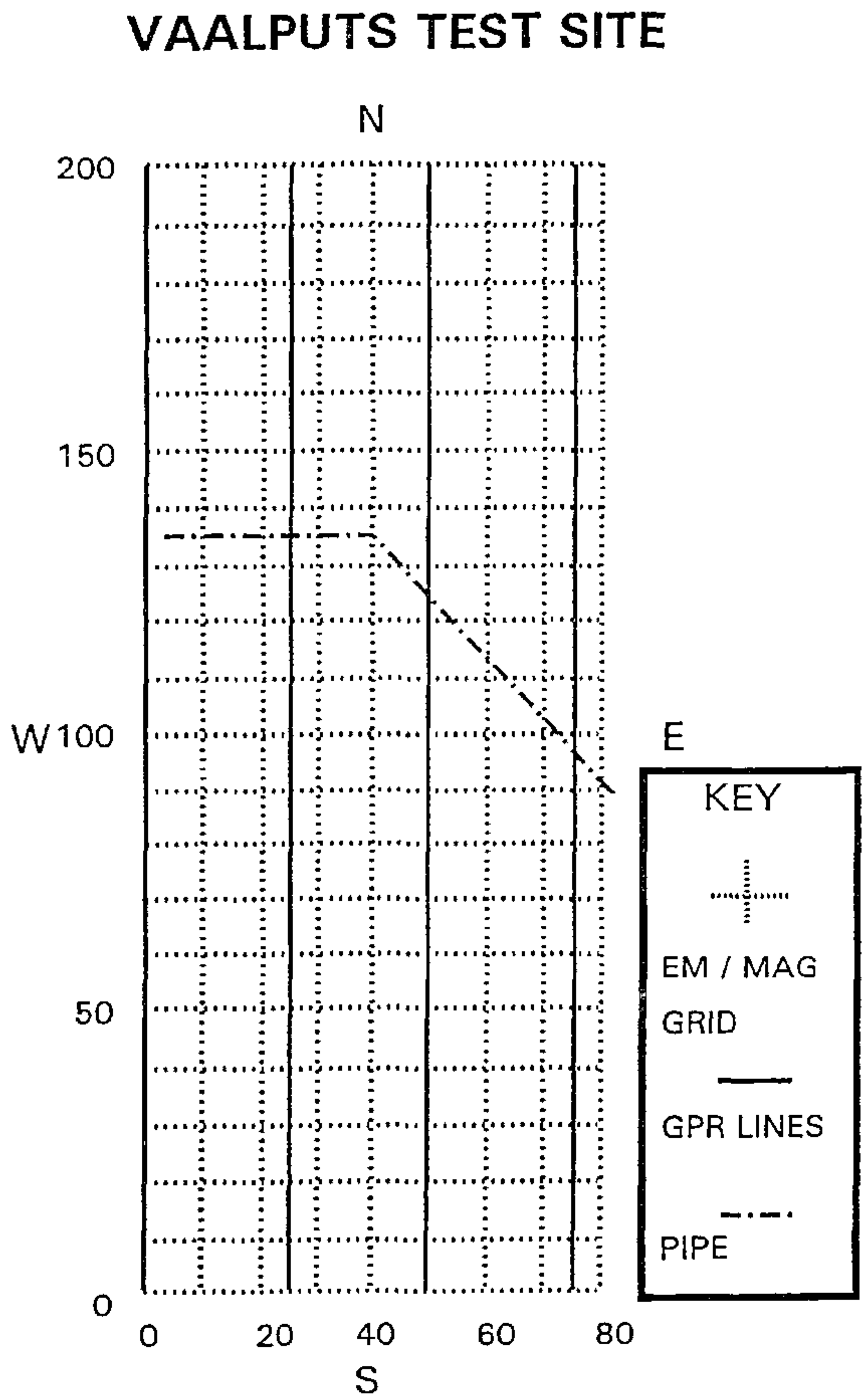

Figure 5: Grid layout at Vaalputs indicating the survey lines for the surface geophysical surveys.

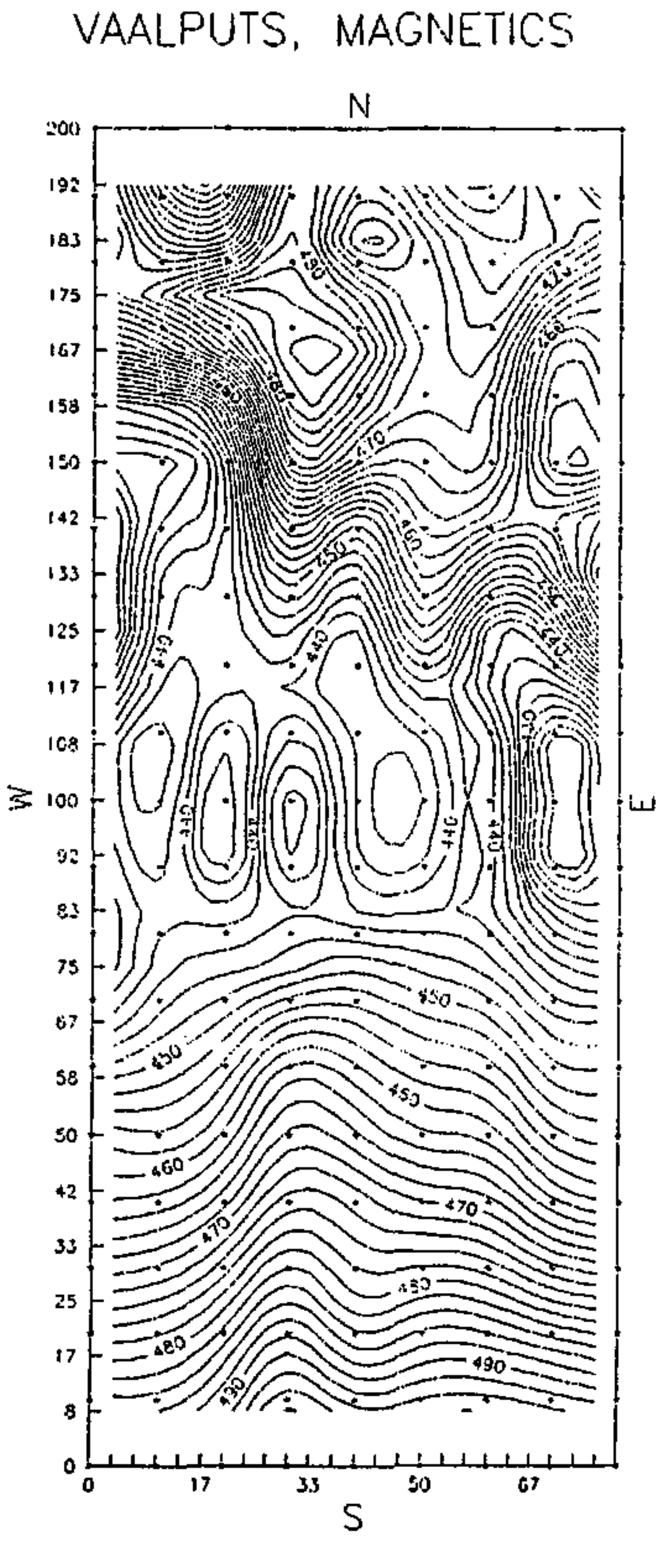

Figure 6: **Contoured residual ground magnetic field intensity in nT over the survey grid at Vaalputs.**

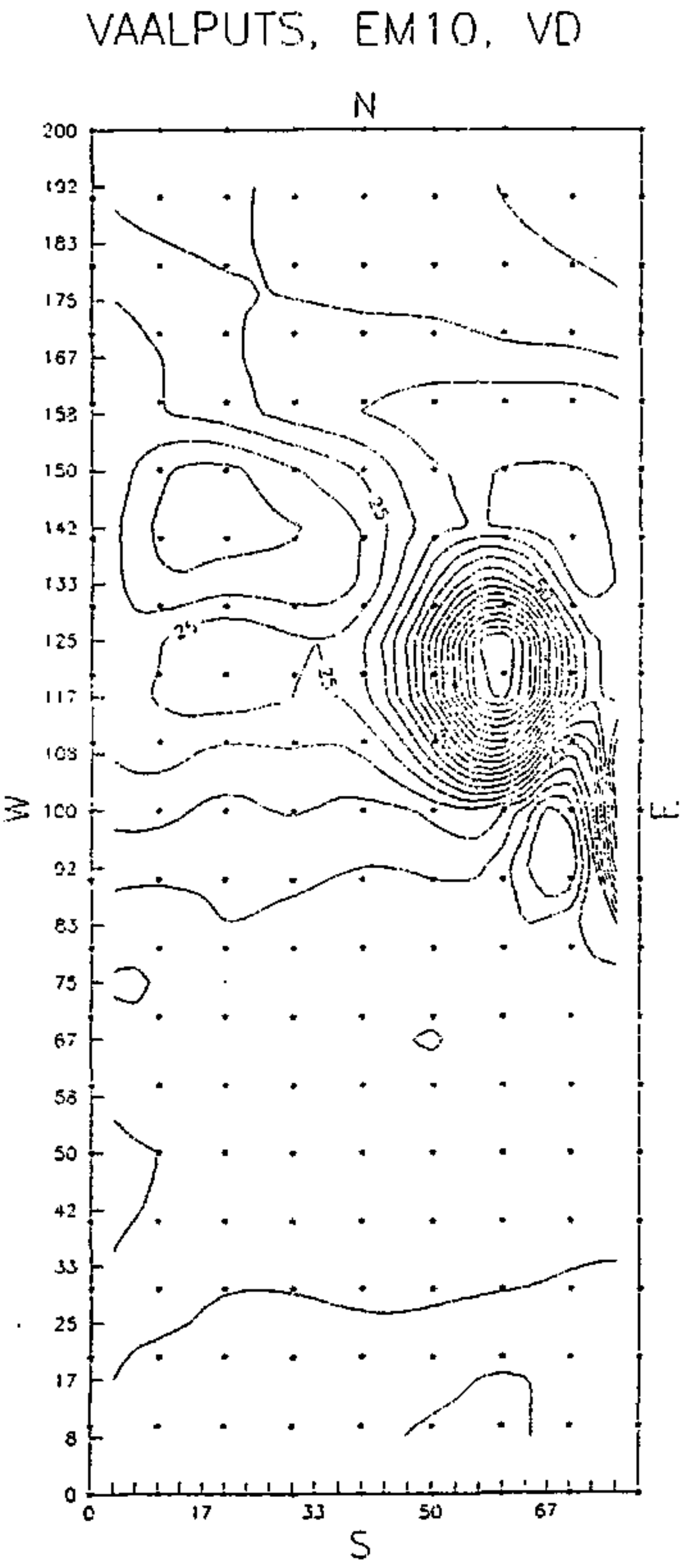

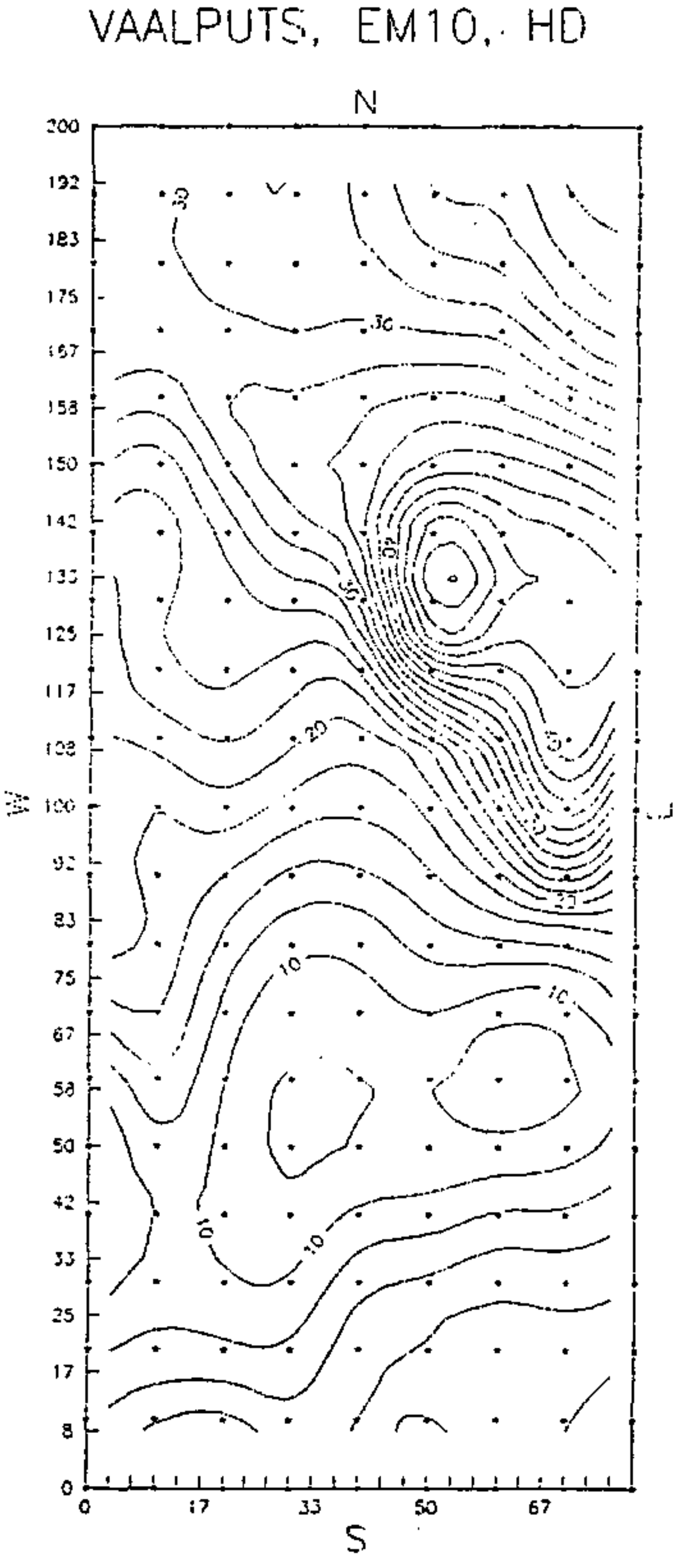

Figure 7(a)&7(b): **Contoured apparent electrical conductivity values in mS/m for the 10 m spacing EM34 horizontal and vertical dipole modes at Vaalputs.**

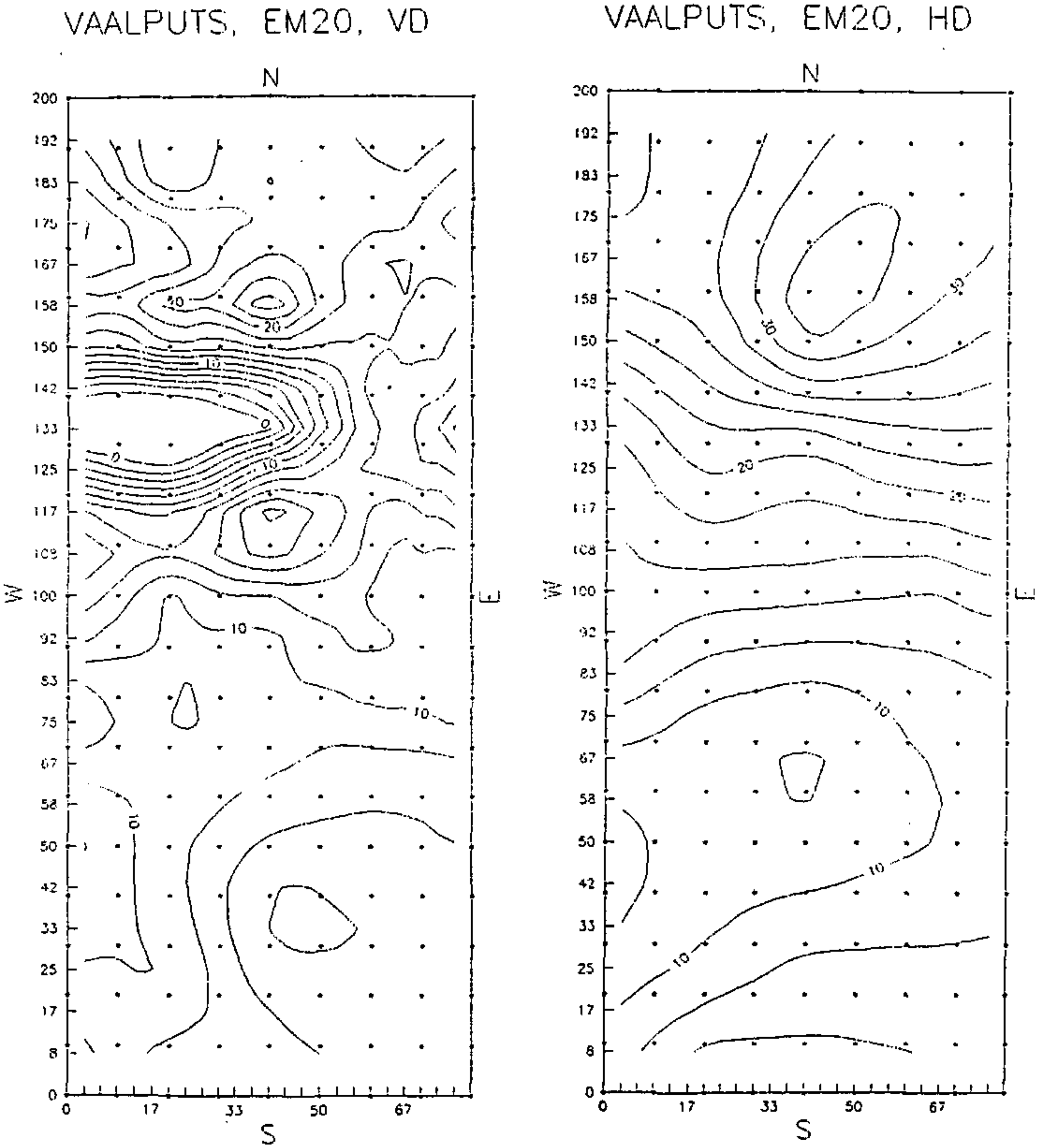

Figure 7(c)&7(d): **Contoured apparent electrical conductivity values in mS/m for the 20 m spacing EM34 horizontal and vertical dipole modes at Vaalputs.**

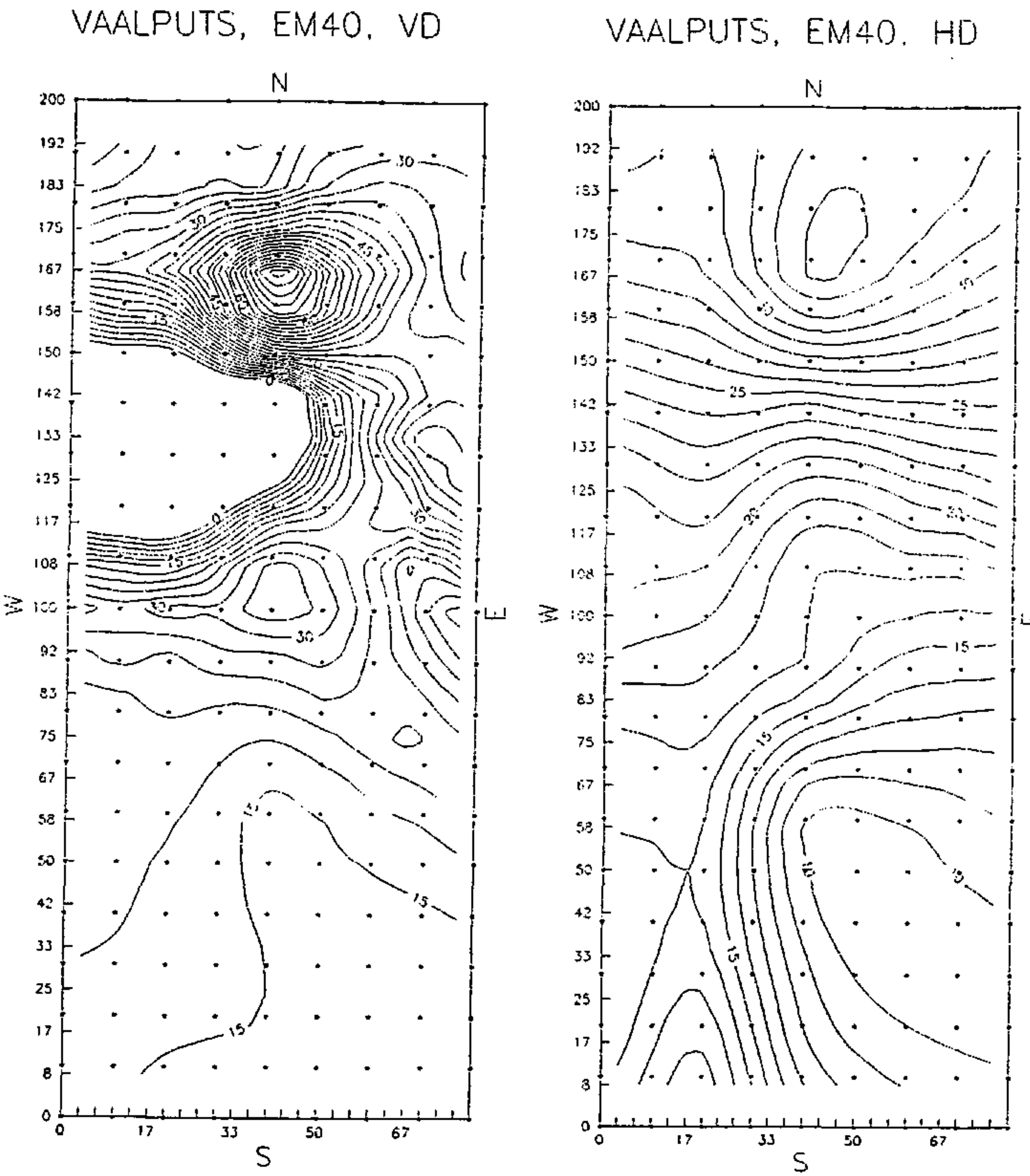

Figure 7(e)&7(f): **Contoured apparent electrical conductivity values in mS/m for the 40 m spacing EM34 horizontal and vertical dipole modes at Vaalputs.**

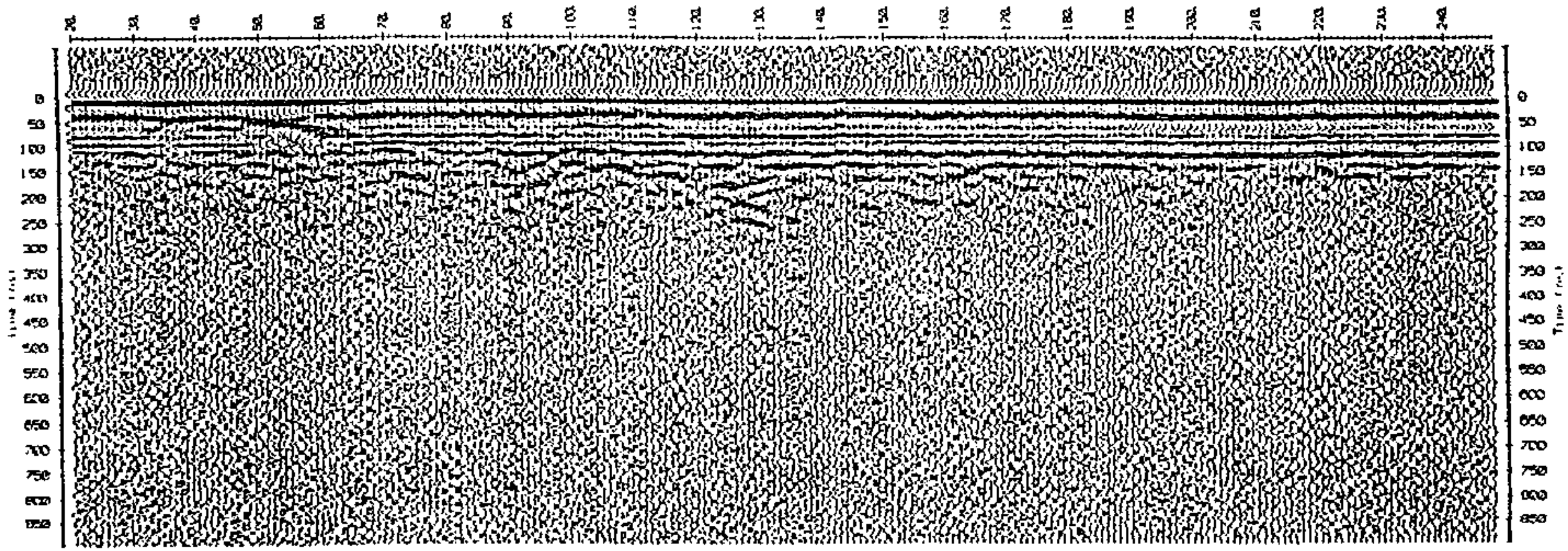

Approximate depth conversion:
20 nS = 1 metre (based on a
dielectric constant of 8).

Figure 8(a): 50 MHz bistatic antennae GPR Radargram (S-N) along Line 0 (Figure 5), Vaalputs.

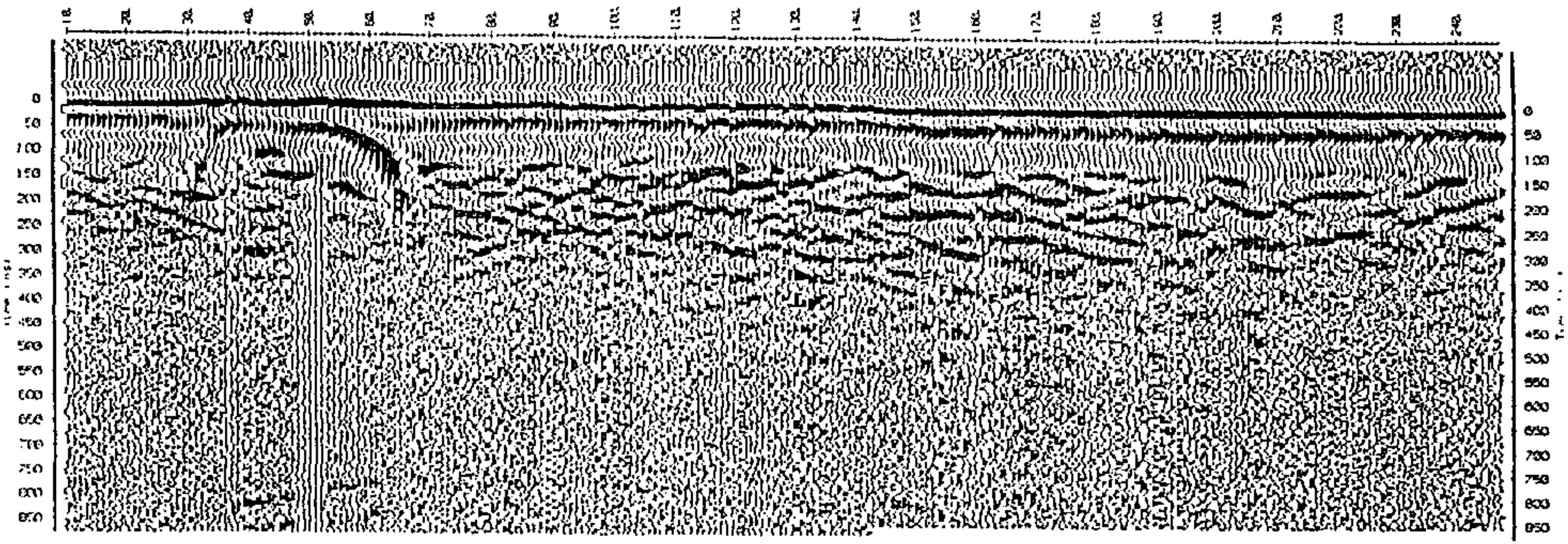

Approximate depth conversion:
20 nS = 1 metre (based on a
dielectric constant of 8).

Figure 8(b): 25 MHz bistatic antennae GPR Radargram (S-N) along Line 0 (Figure 5), Vaalputs.

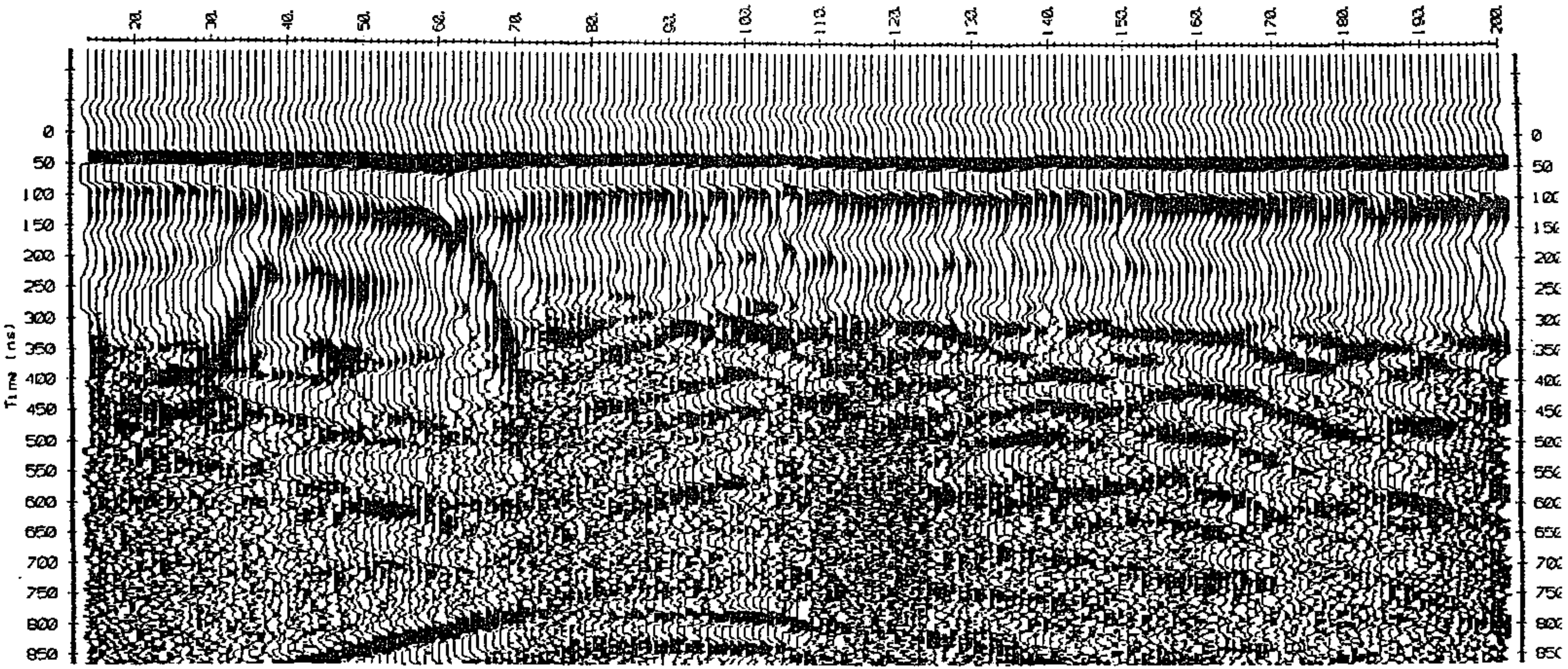

Approximate depth conversion:
20 nS = 1 metre (based on a
dielectric constant of 8).

Figure 8(c): 12,5 MHz bistatic antennae GPR Radargram (S-N) along Line 0 (Figure 5), Vaalputs.

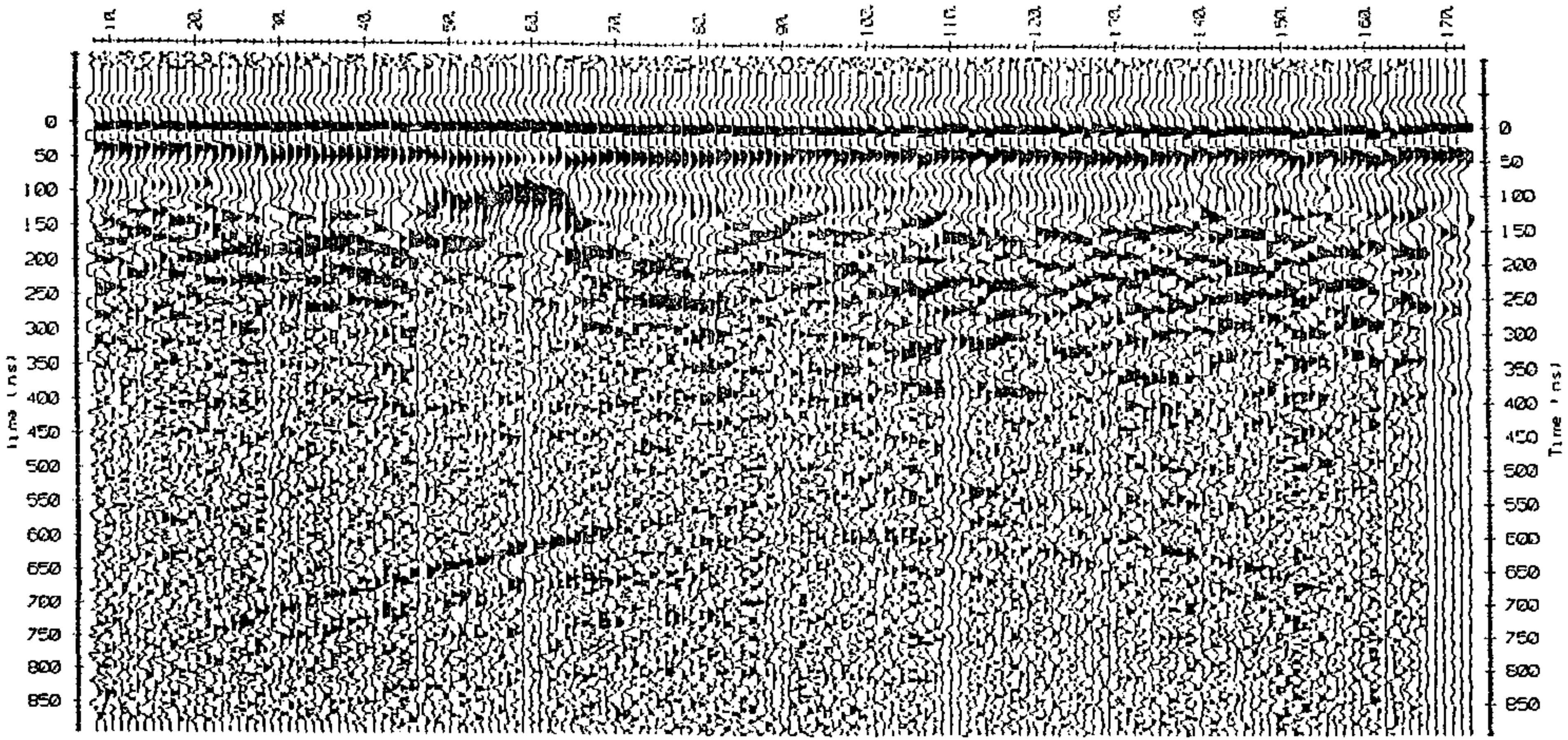

Approximate depth conversion:
20 nS = 1 metre (based on a
dielectric constant of 8).

Figure 8(d): 25 MHz bistatic antennae GPR Radargram (S-N) along Line 25 (Figure 5), Vaalputs.

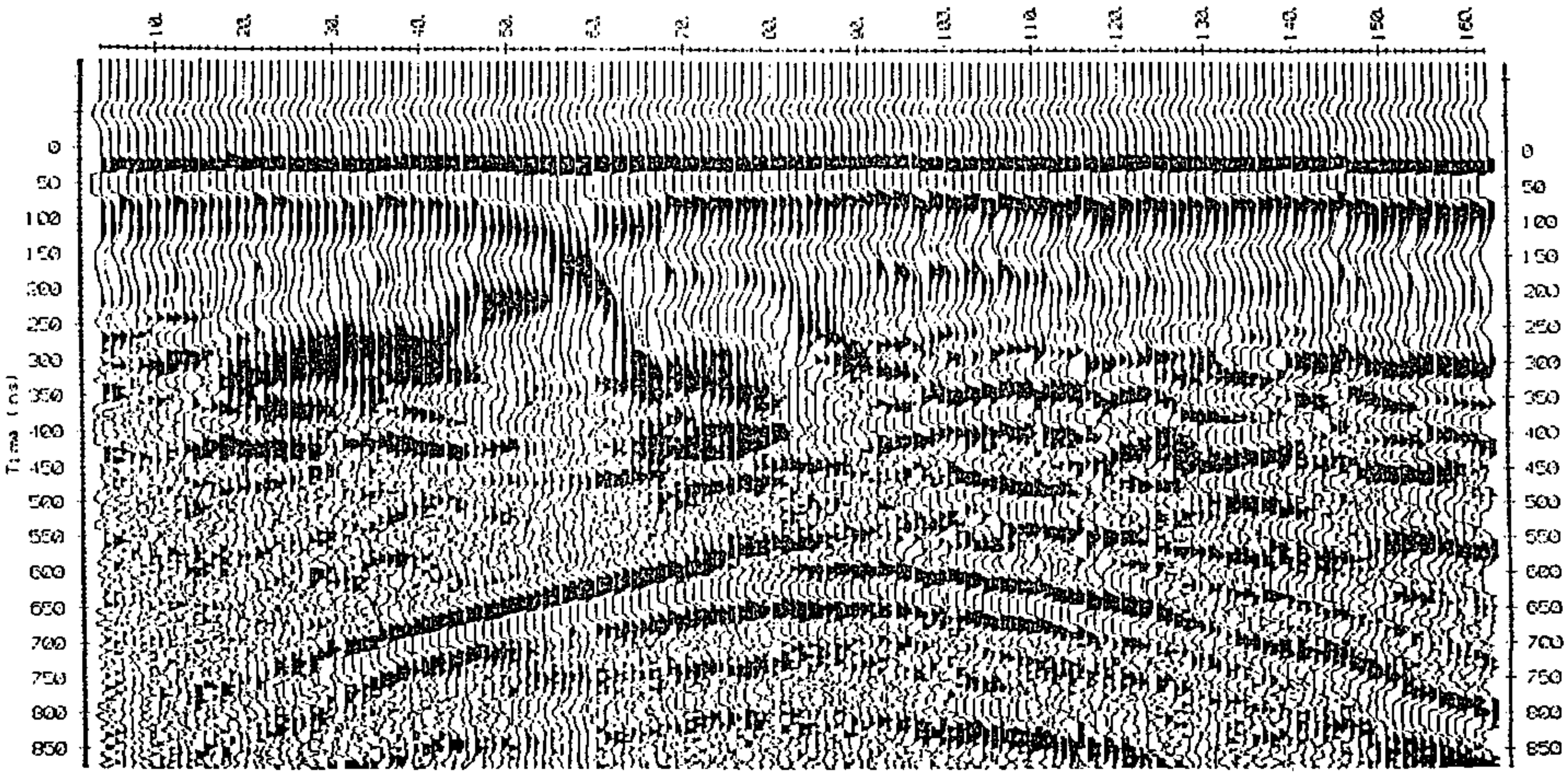

Approximate depth conversion:
20 nS = 1 metre (based on a
dielectric constant of 8).

Figure 8(c): **12,5 MHz bistatic antennae GPR Radargram (S-N) along Line 25 (Figure 5), Vaalputs.**

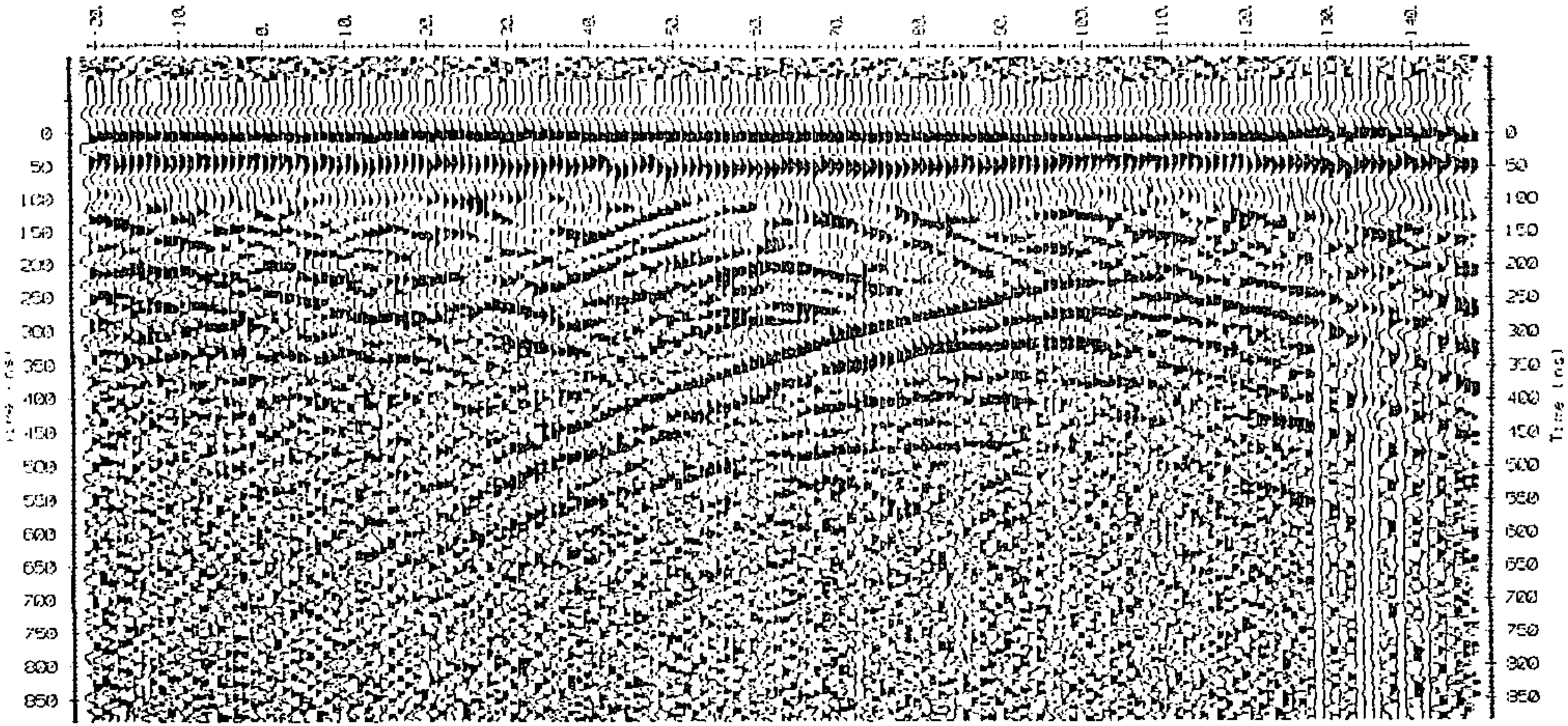

Approximate depth conversion:
20 nS = 1 metre (based on a
dielectric constant of 8).

Figure 8(f): 25 MHz bistatic antennae GPR Radargram (S-N) along Line 50 (Figure 5), Vaalputs.

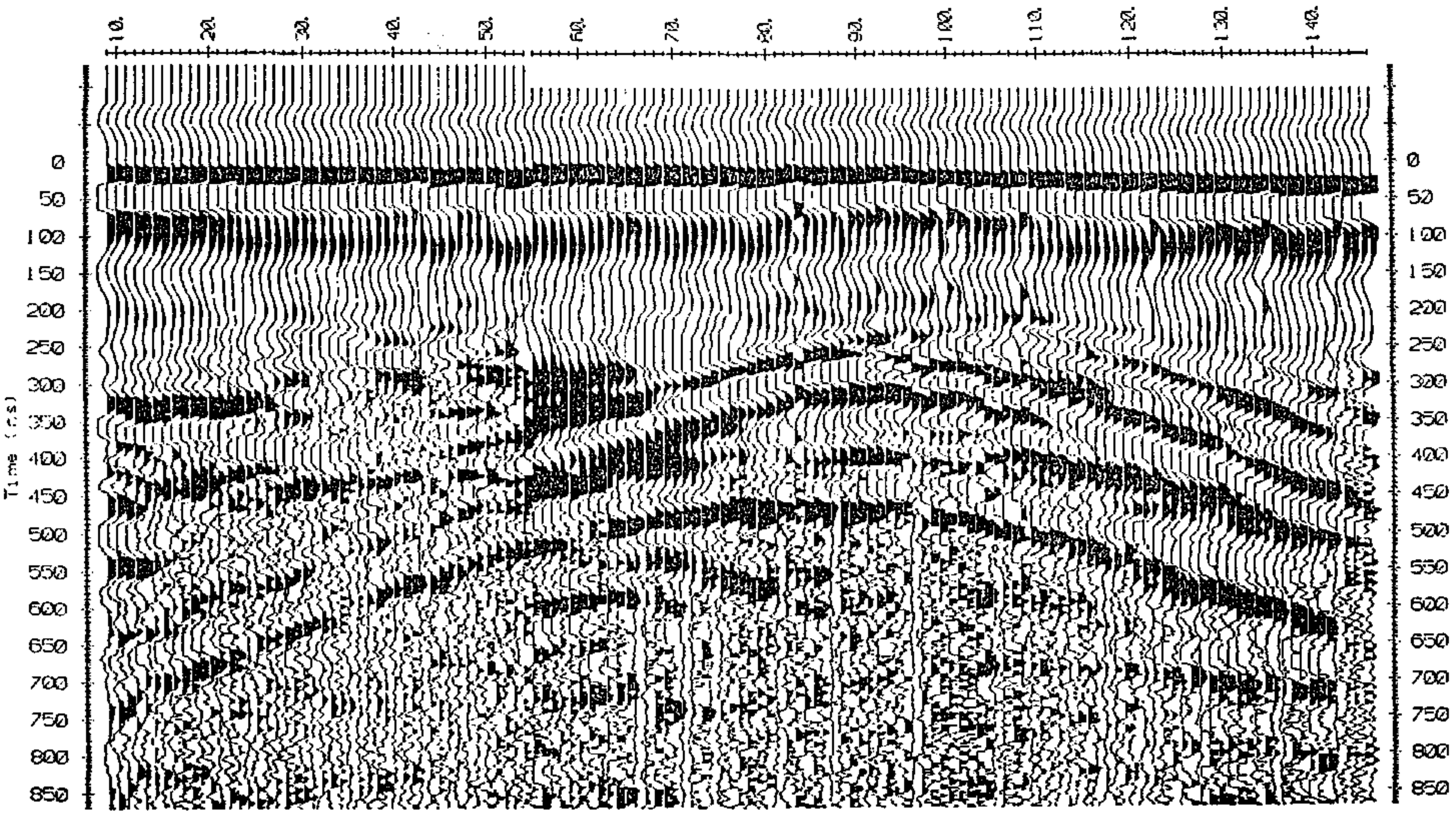

Approximate depth conversion:
20 nS = 1 metre (based on a
dielectric constant of 8).

Figure 8(g): 12,5 MHz bistatic antennae GPR Radargram (S-N) along Line 50 (Figure 5), Vaalputs.

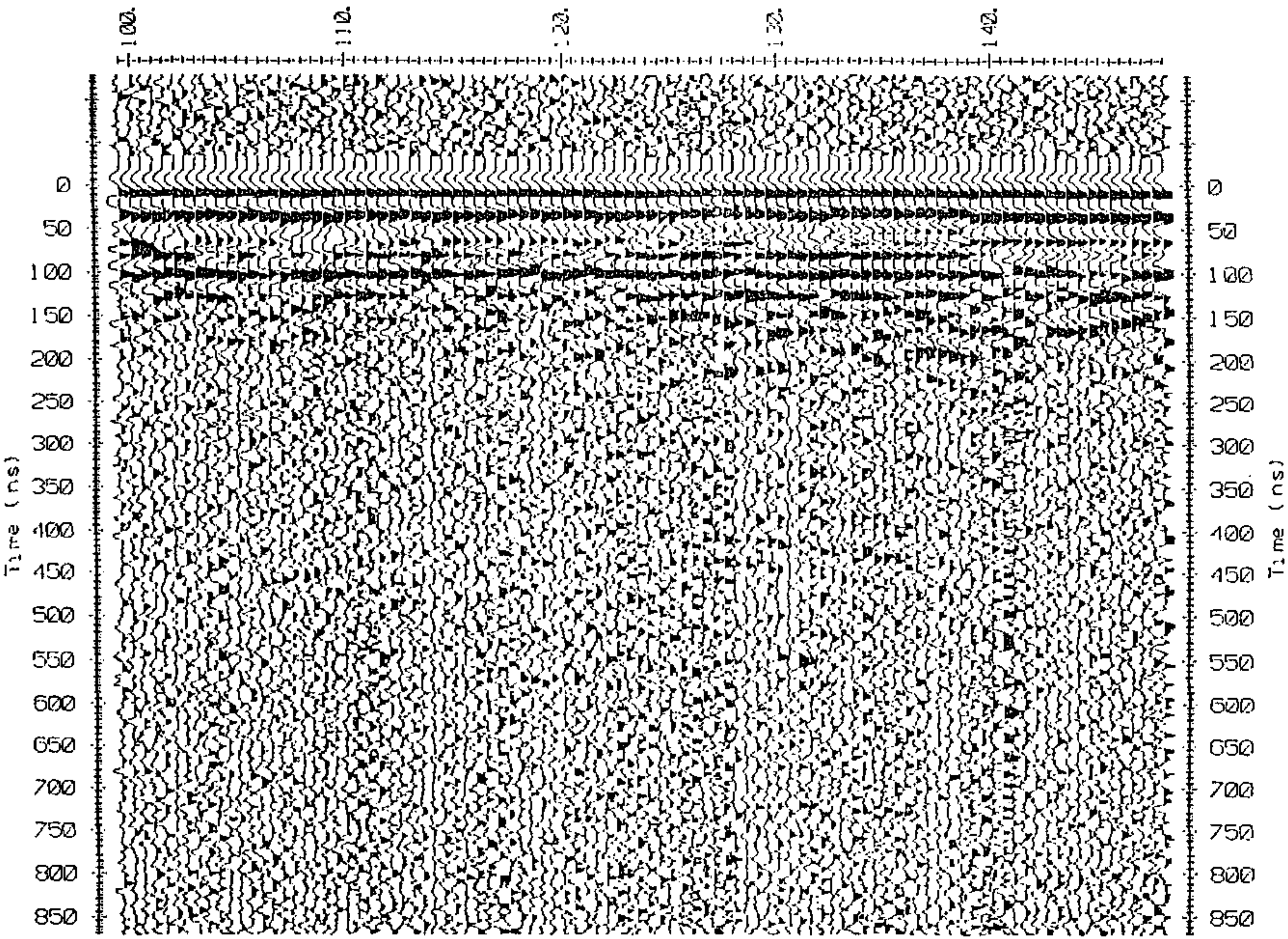

Approximate depth conversion:
20 nS = 1 metre (based on a dielectric constant of 8).

Figure 8(h): **25 MHz bistatic antennae GPR Radargram (S-N) along Line 75(Figure 5), Vaalputs.**

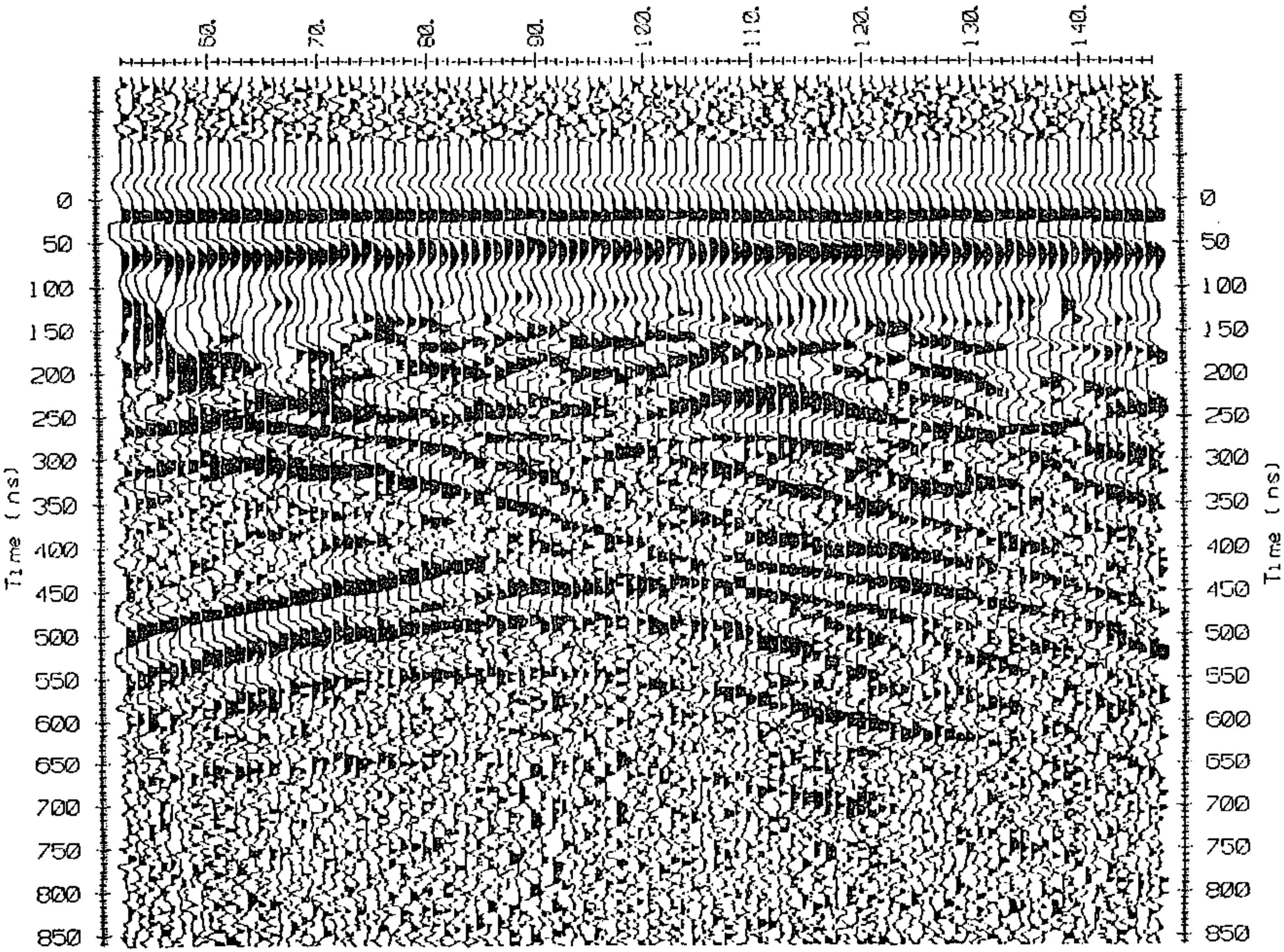

Approximate depth conversion:
20 nS = 1 metre (based on a dielectric constant of 8).

Figure 8(i): **12,5 MHz bistatic antennae GPR Radargram (S-N) along Line 75 (Figure 5), Vaalputs.**

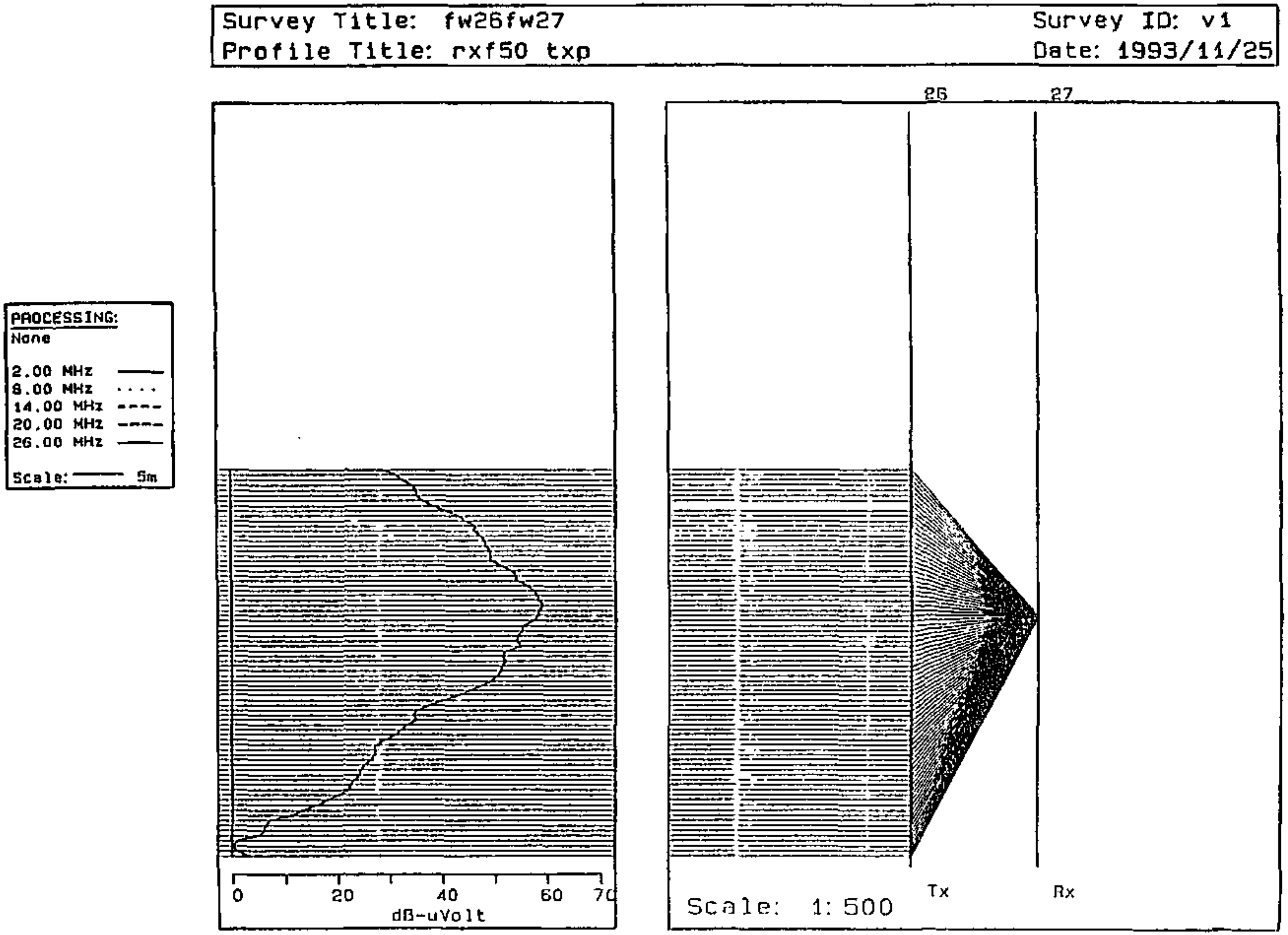

Figure 9(a): Representative RT signal strength profile from Scan V1 at Vaalputs.

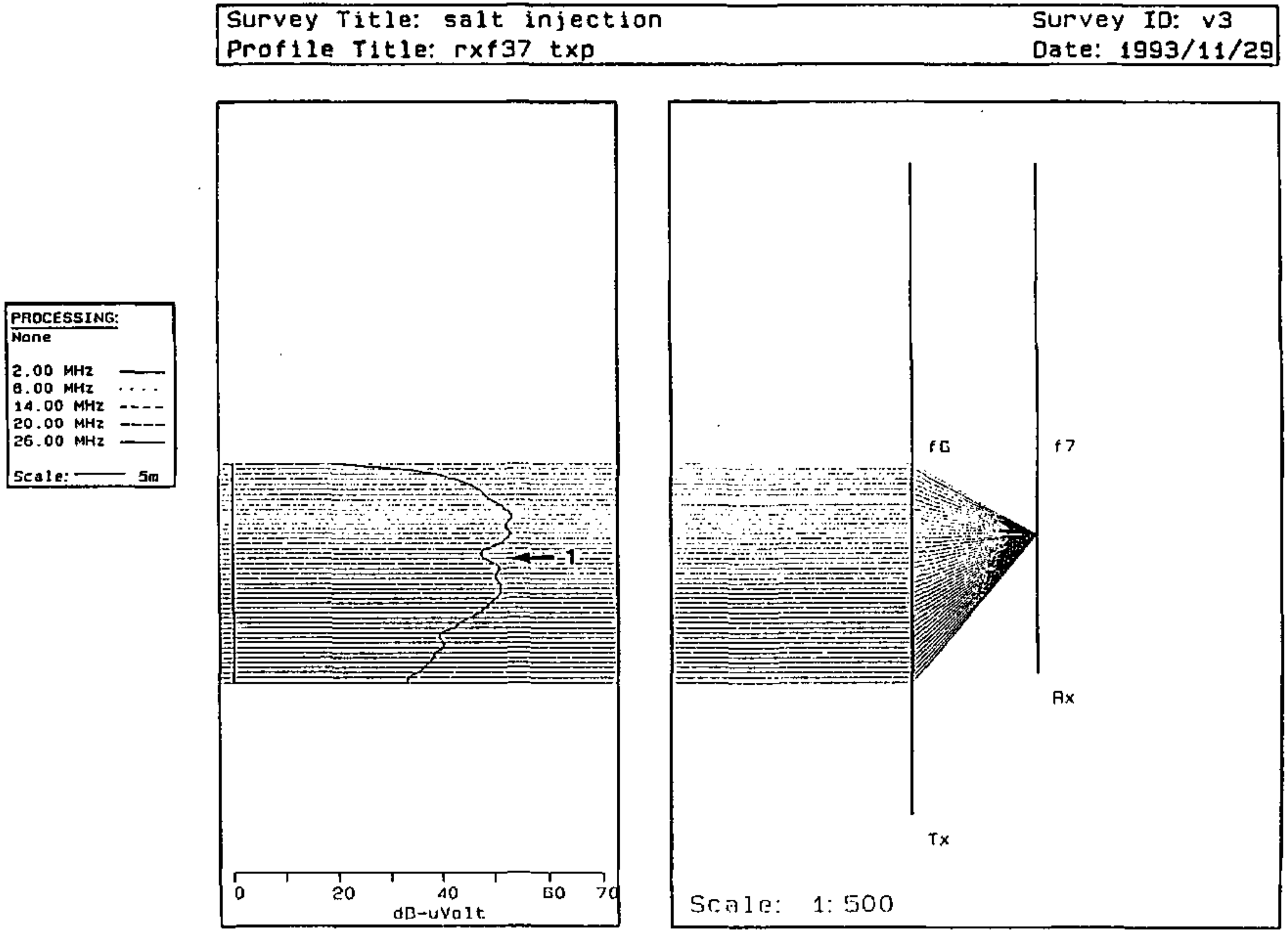

Figure 9(b): Representative RT signal strength profile from Scan V3 at Vaalputs.

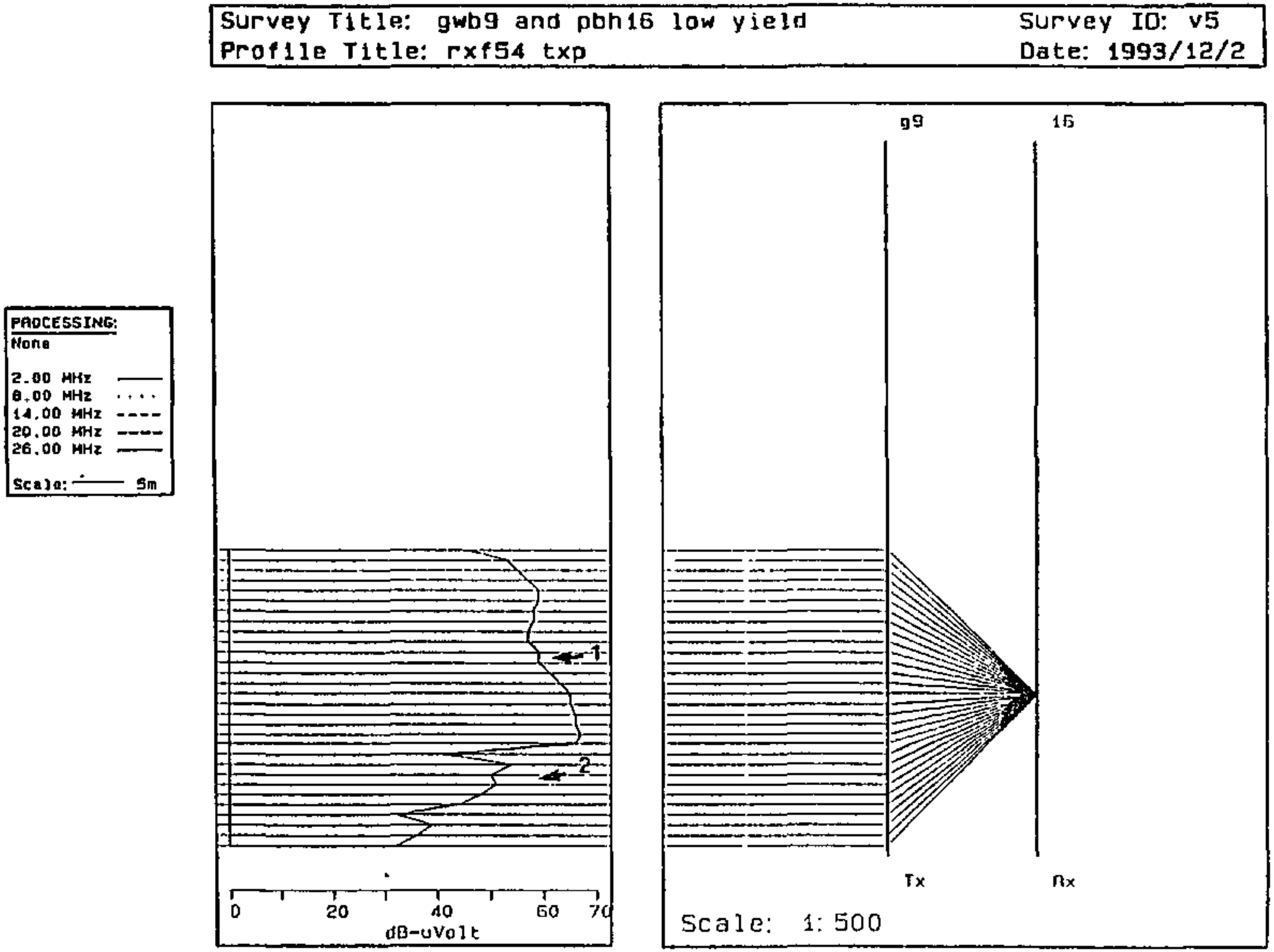

Figure 9(c): **Representative RT signal strength profile from Scan V5 at Vaalputs.**

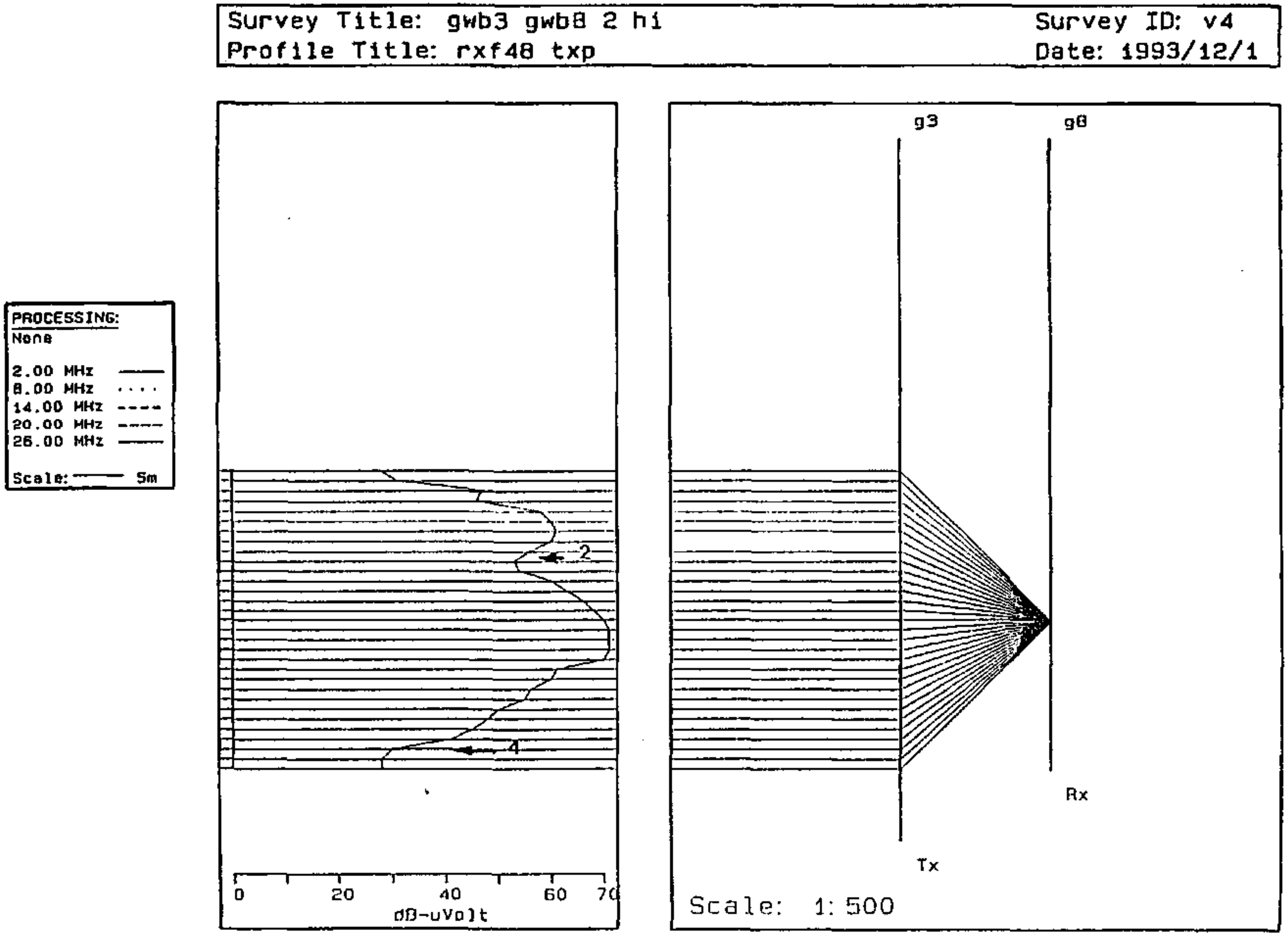

Figure 9(d): Representative RT signal strength profile frcm Scan V4 at Vaalputs.

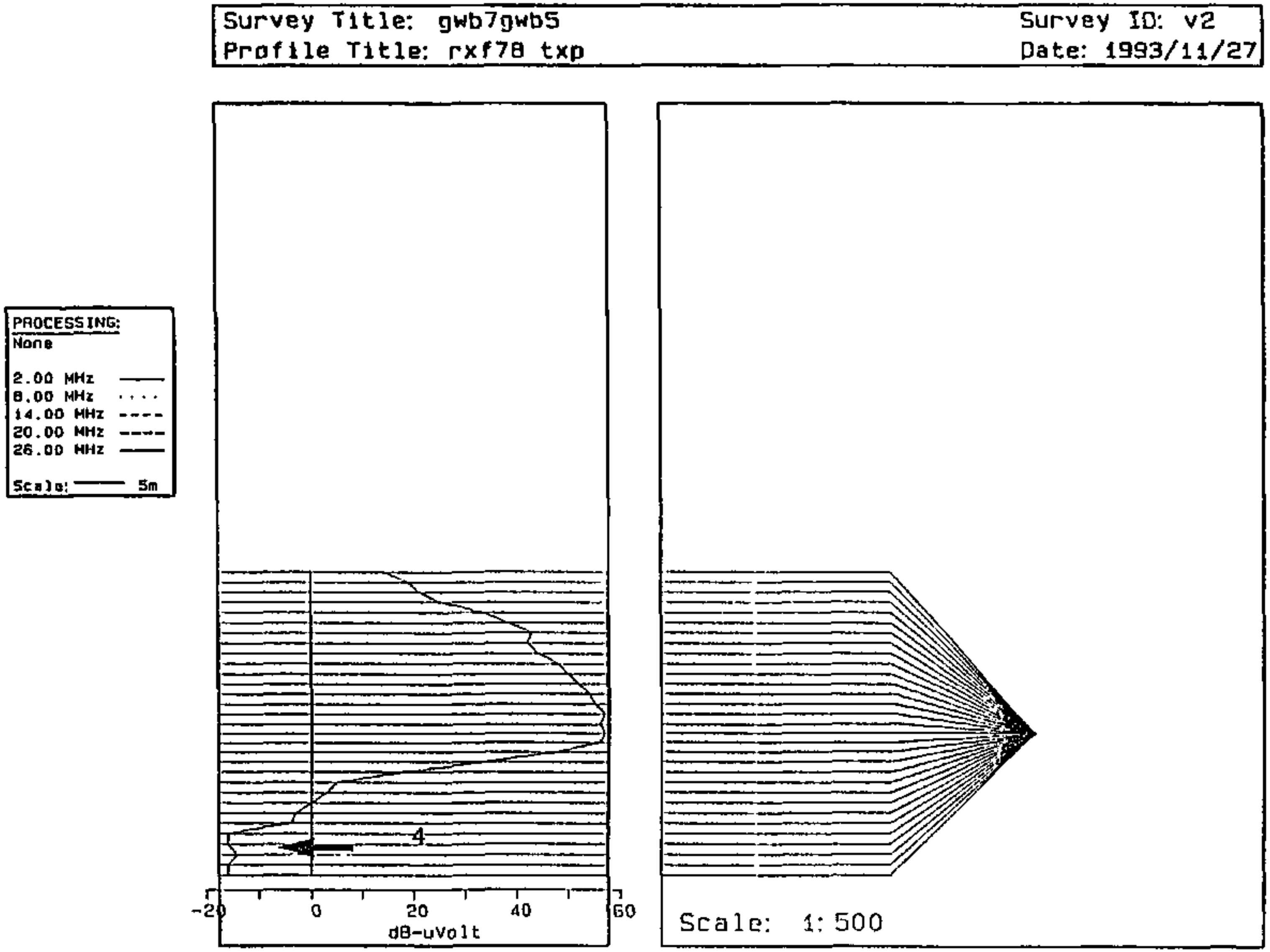

Figure 9(e): Representative RT signal strength profile from Scan V2 at Vaalputs.

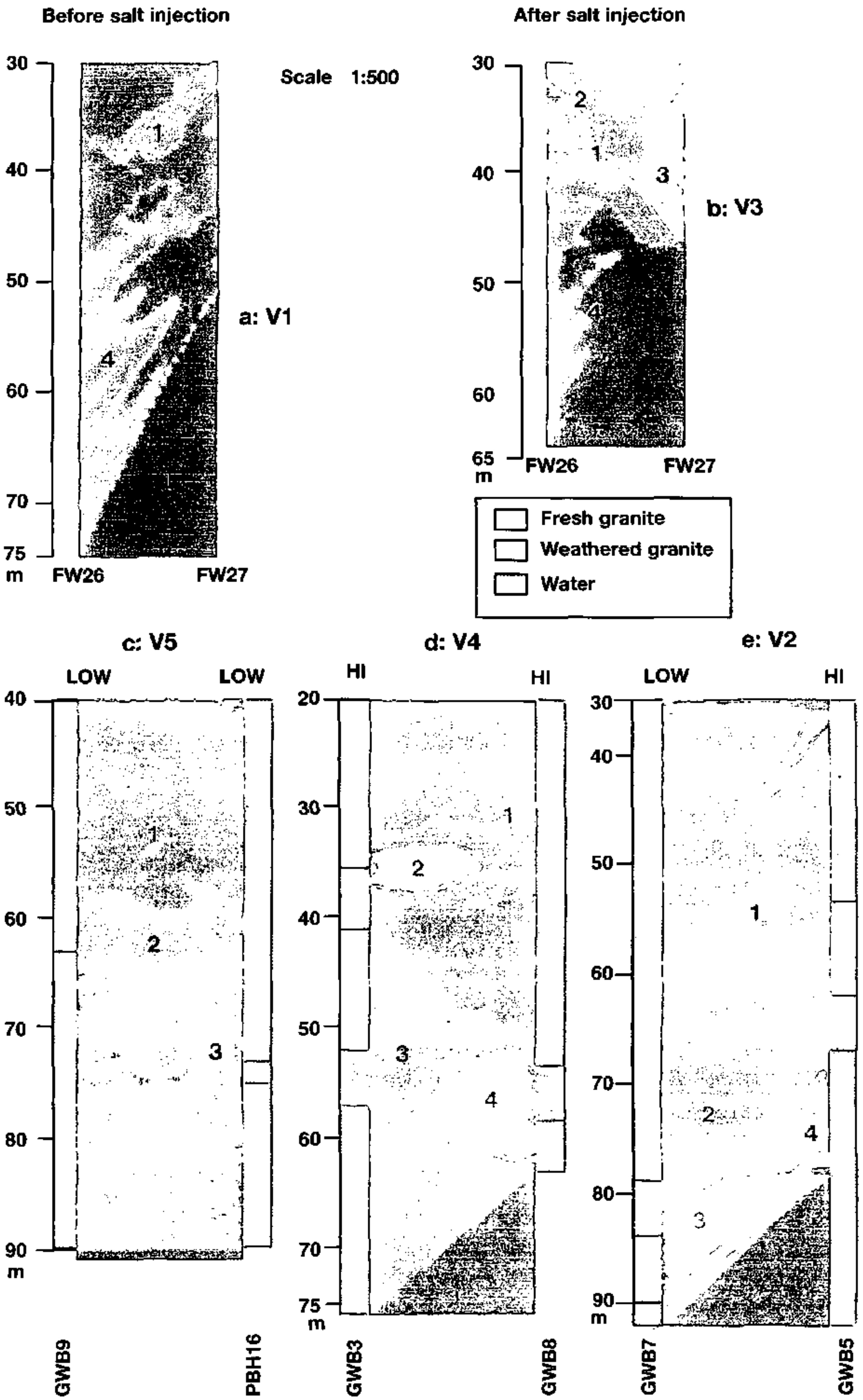

Figure 10(a-e): Tomographic images between a selection of boreholes at the Vaalputs Site

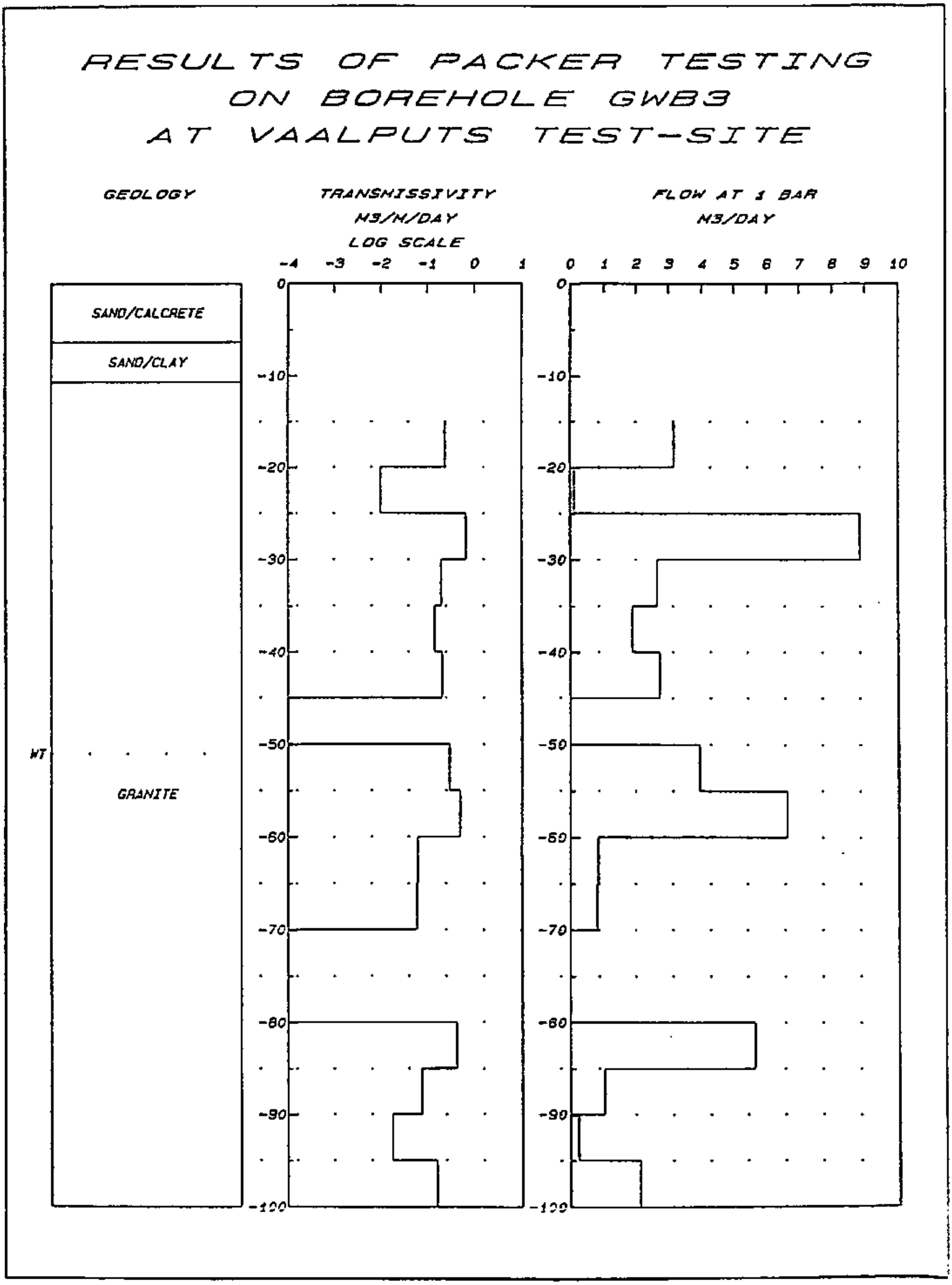

Figure 11: Results of Packer testing on borehole GWB3, Vaalputs.

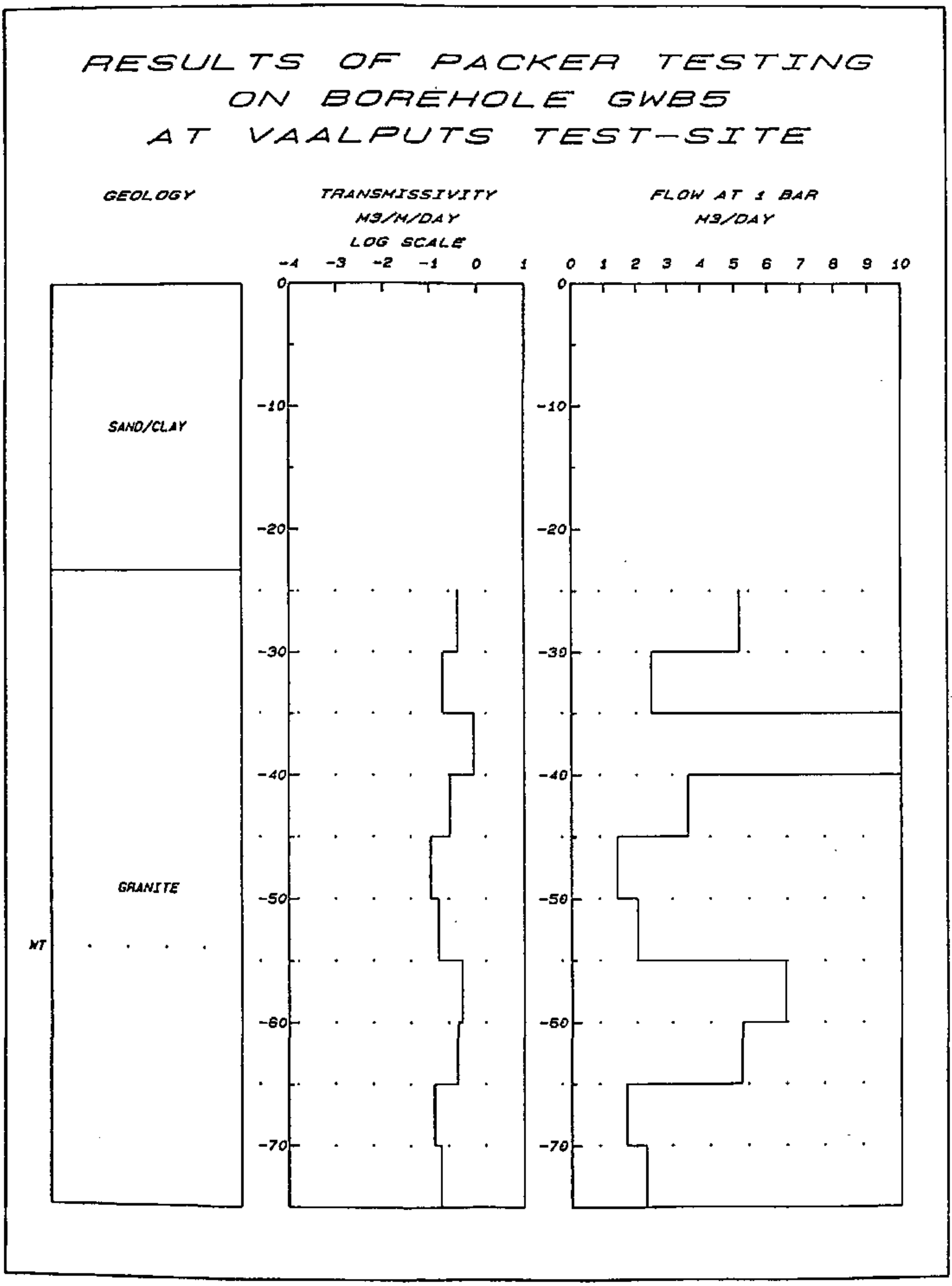

Figure 12: Results of Packer testing on borehole GWB5, Vaalputs.

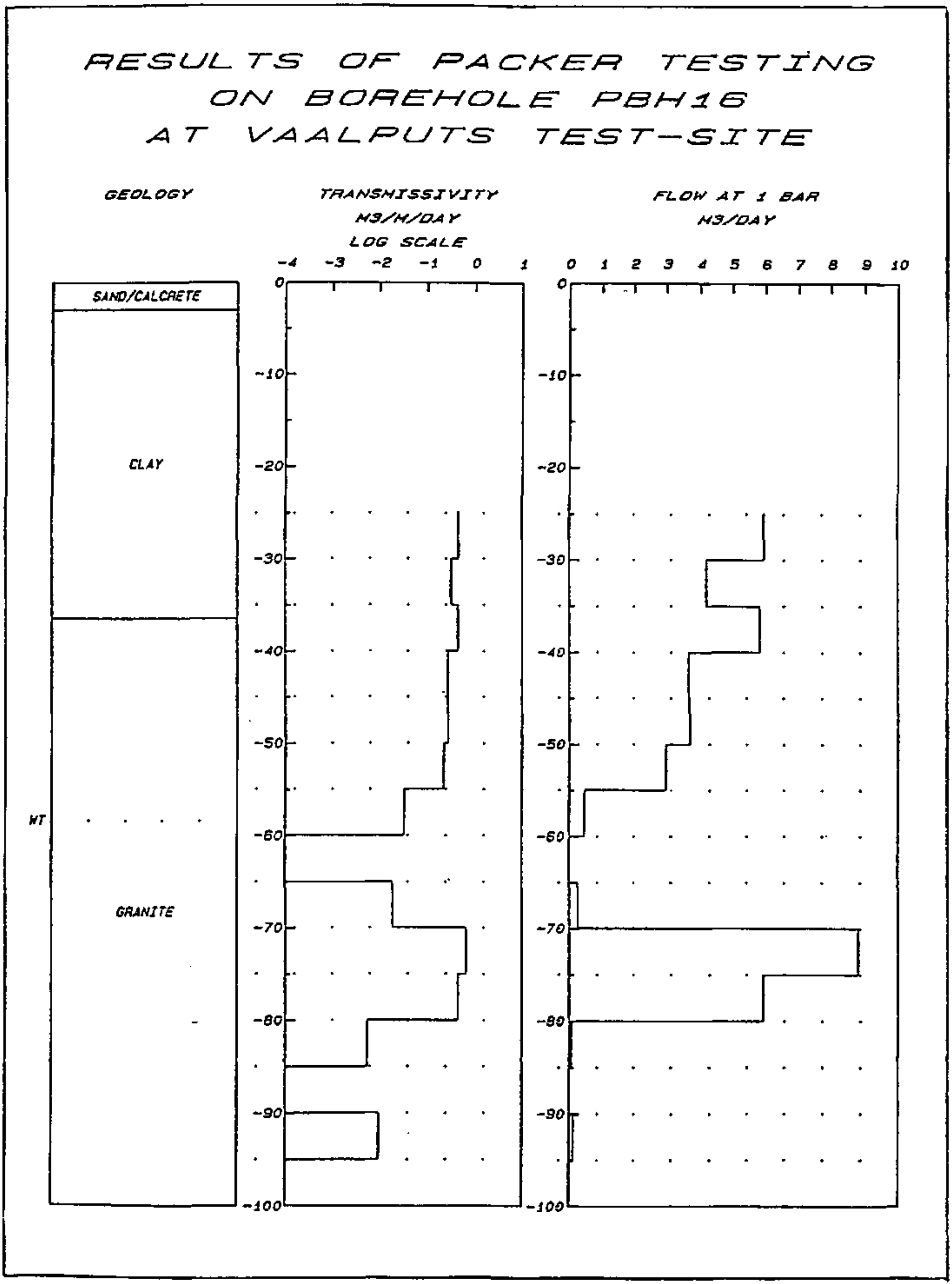

Figure 13: Results of Packer testing on borehole PBH16, Vaalputs.

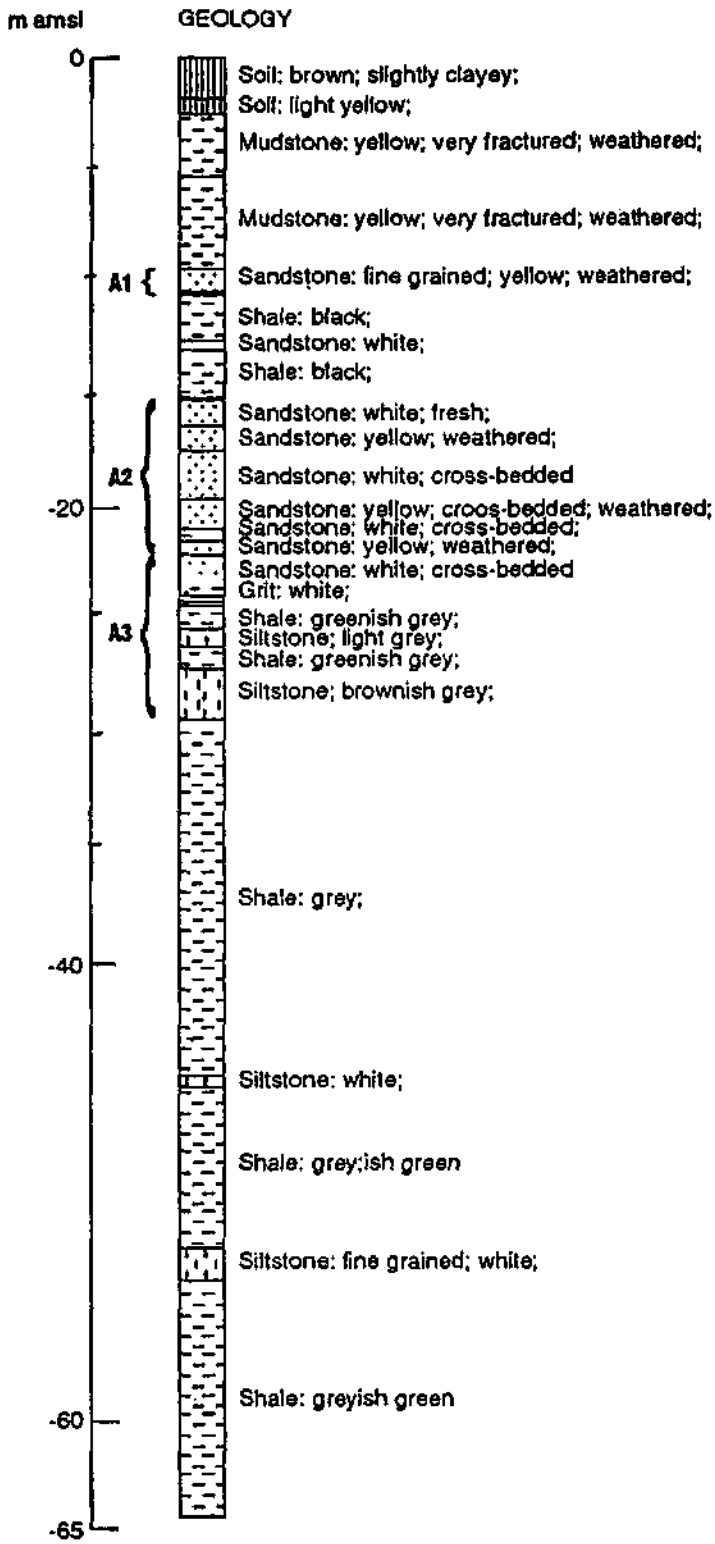

Figure 14: **Representative geological section at the IGS Test Site. The position of the three aquifers A1, A2 and A3 are indicated.**

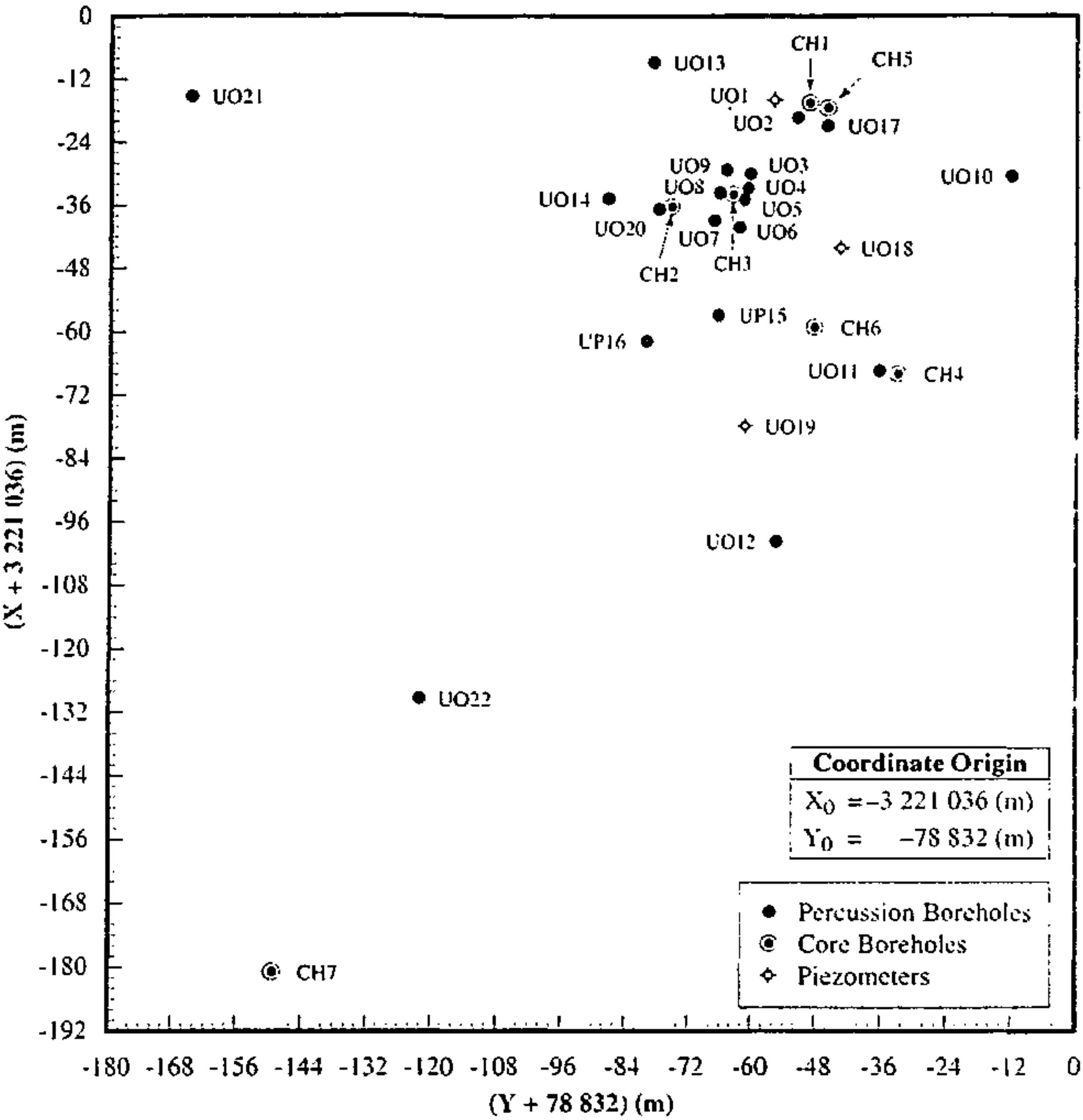

Figure 15: **Map showing the positions and types of boreholes drilled on the Campus Test Site at the University of the Orange Free State.**

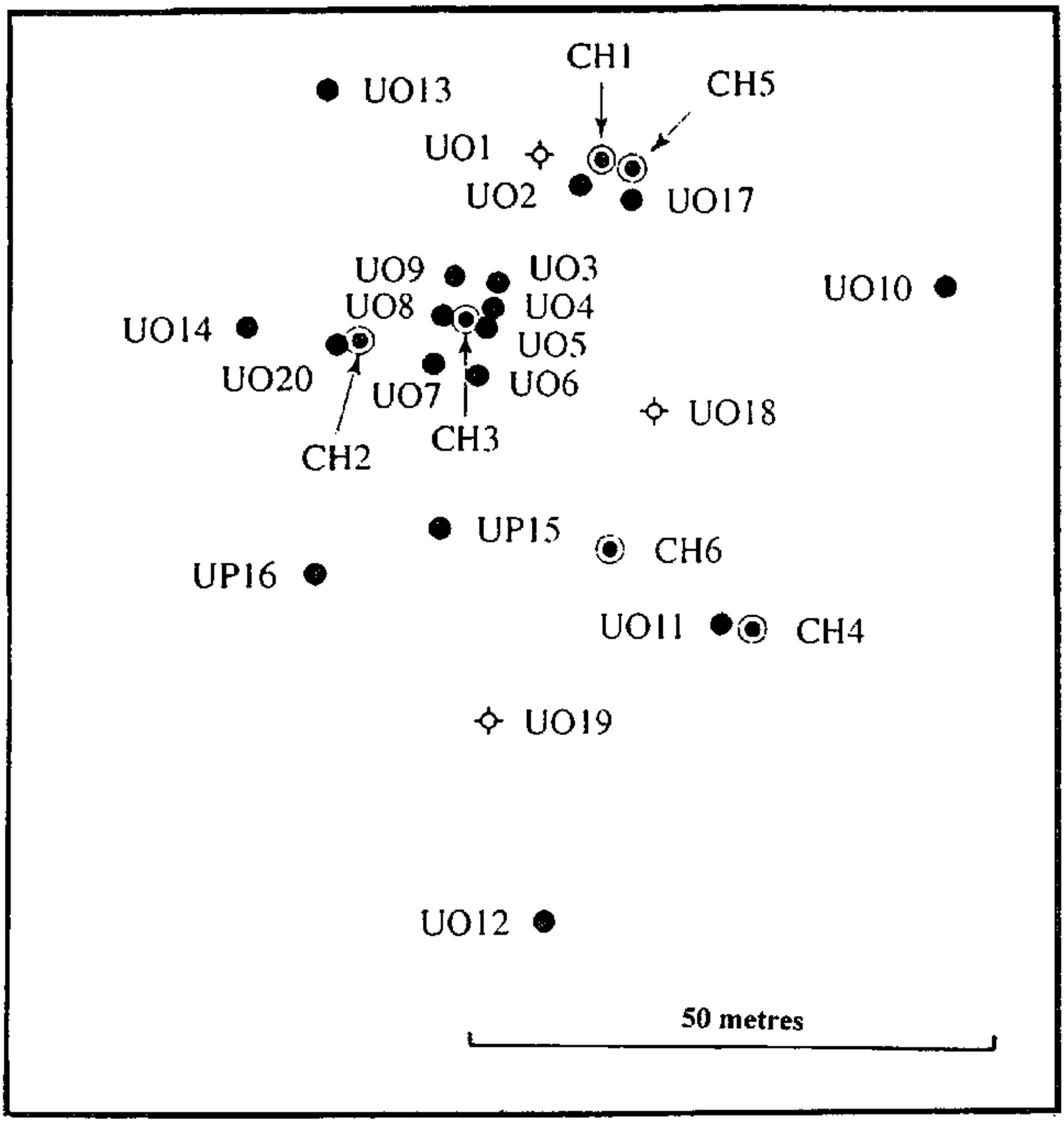

Figure 16: **Enlarged section of part of Figure 15 showing the positions of the boreholes where the RT work was concentrated, IGS Test Site.**

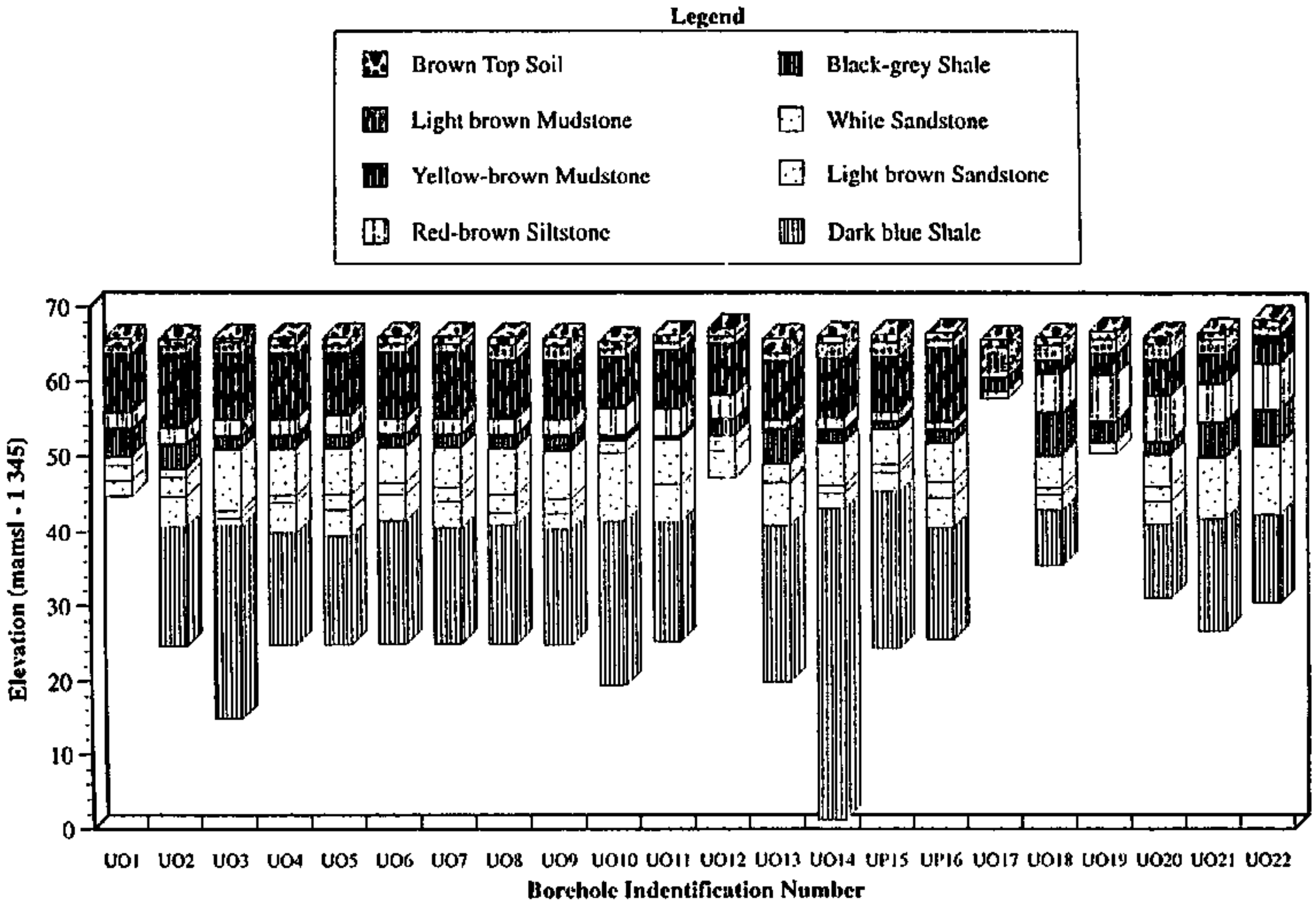

Figure 17: **Geological profiles of the percussion boreholes on the UOFS Campus Test Site.**

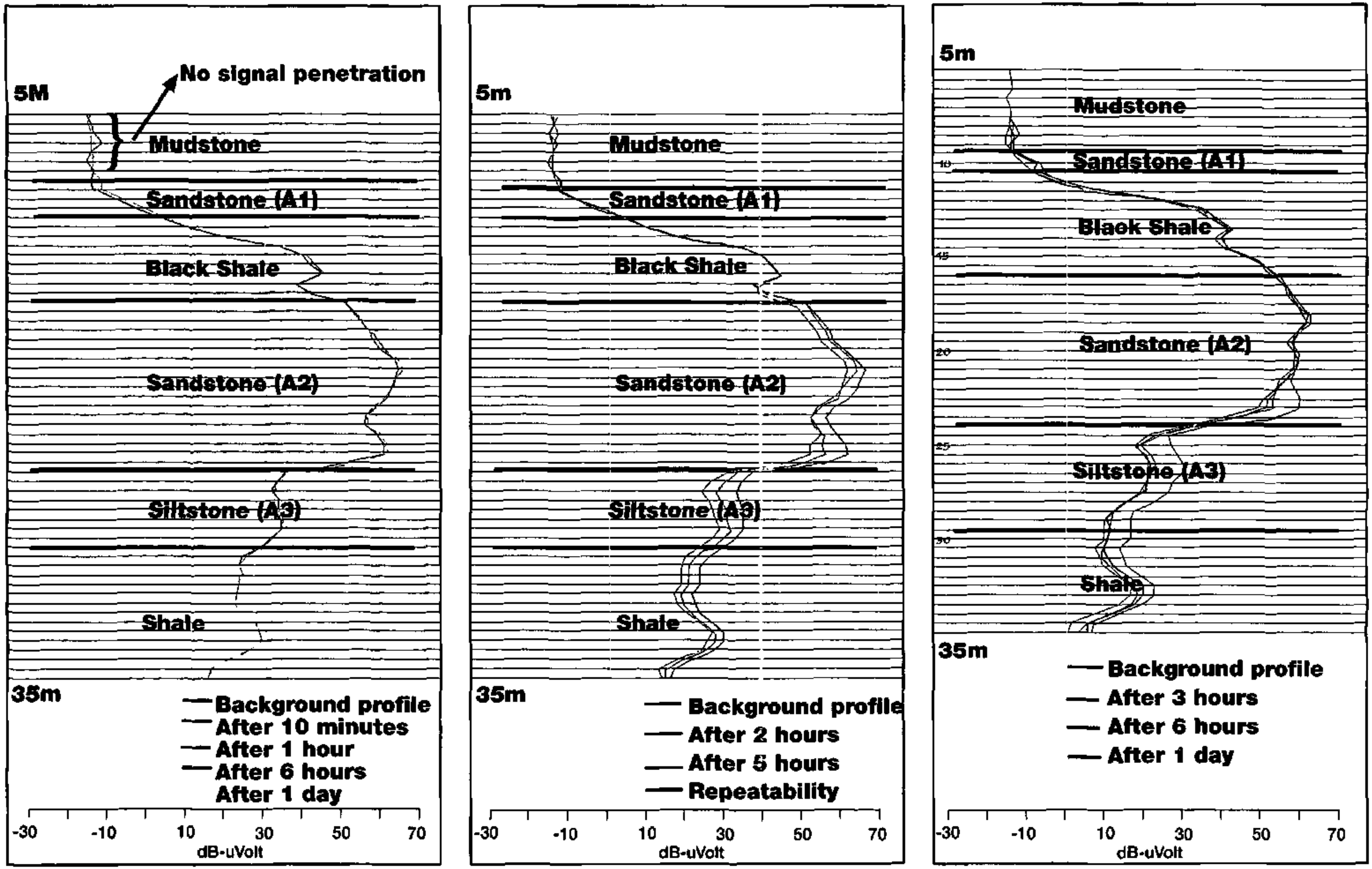

a) Boreholes 3 to 5 after salt injection 1 (from 7) b) Boreholes 3 to 5 after salt injection 2 (from 4) c) Boreholes 5 to 6 after salt injection 1 (from 7)
Figure 18: Parallel scans between boreholes UO3 and UO5 and UO6, IGS Test Site

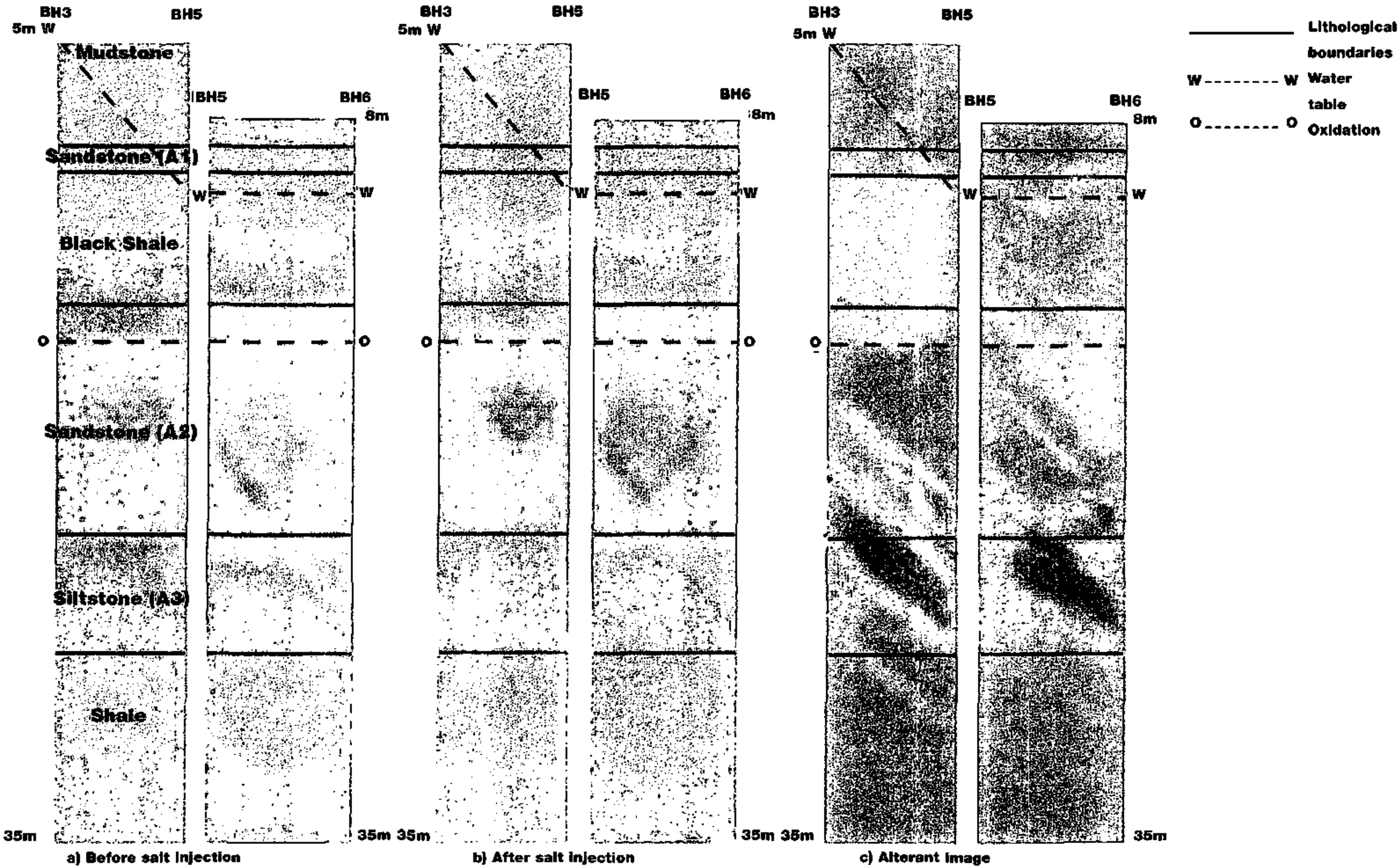

Figure 19: RT images between boreholes UO3 and UO5, and between UO5 and UO6 before and after salt water injection, together with the resulting alterant images, IGS Test Site

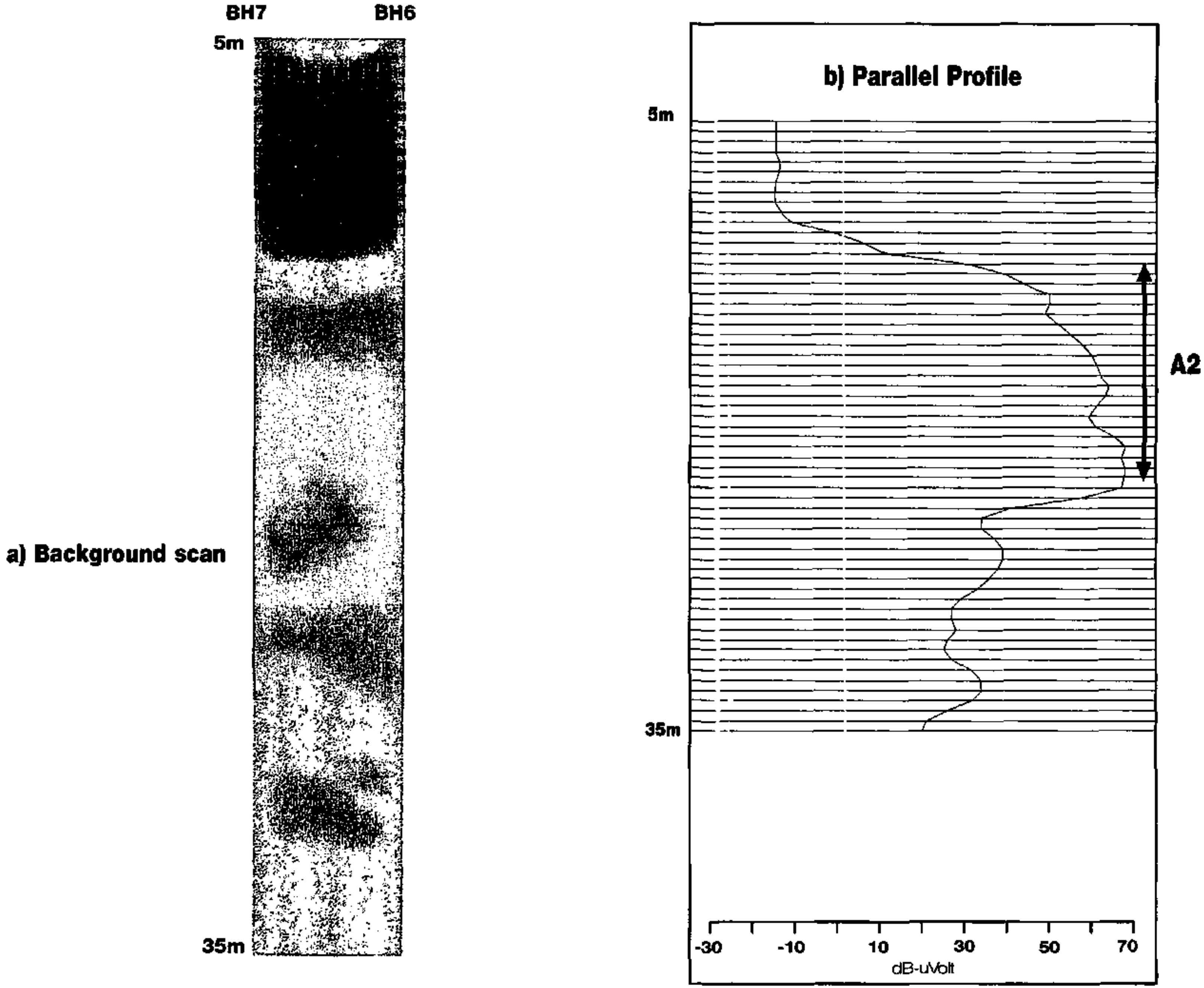

Figure20: Background and parallels tomographic scans between boreholes UO7 and UO6, IGS Test Site.

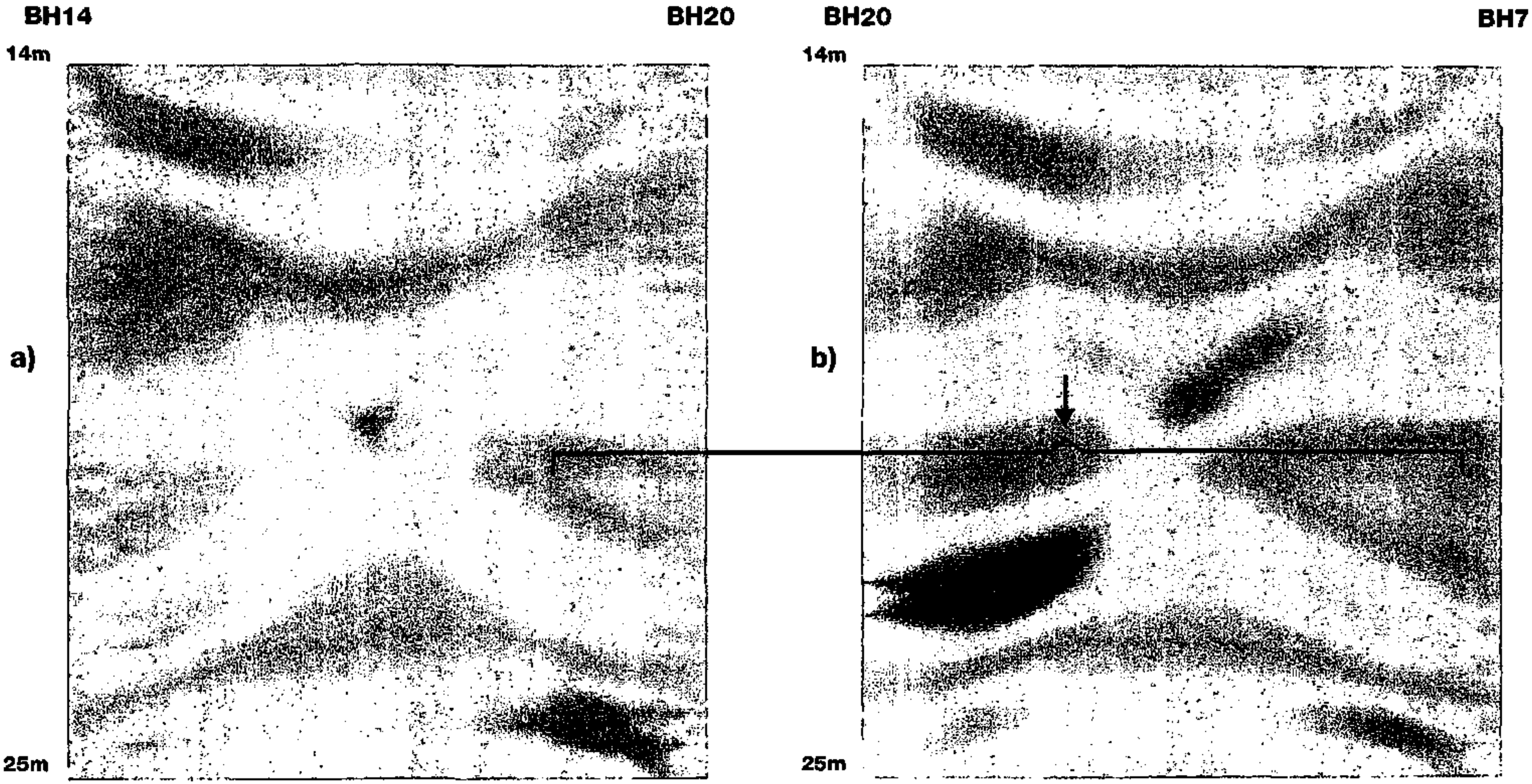

Figure21: Background and parallel tomographic scans between boreholes U014 and UO20, and between UO20 and UO7, IGS Test Site.

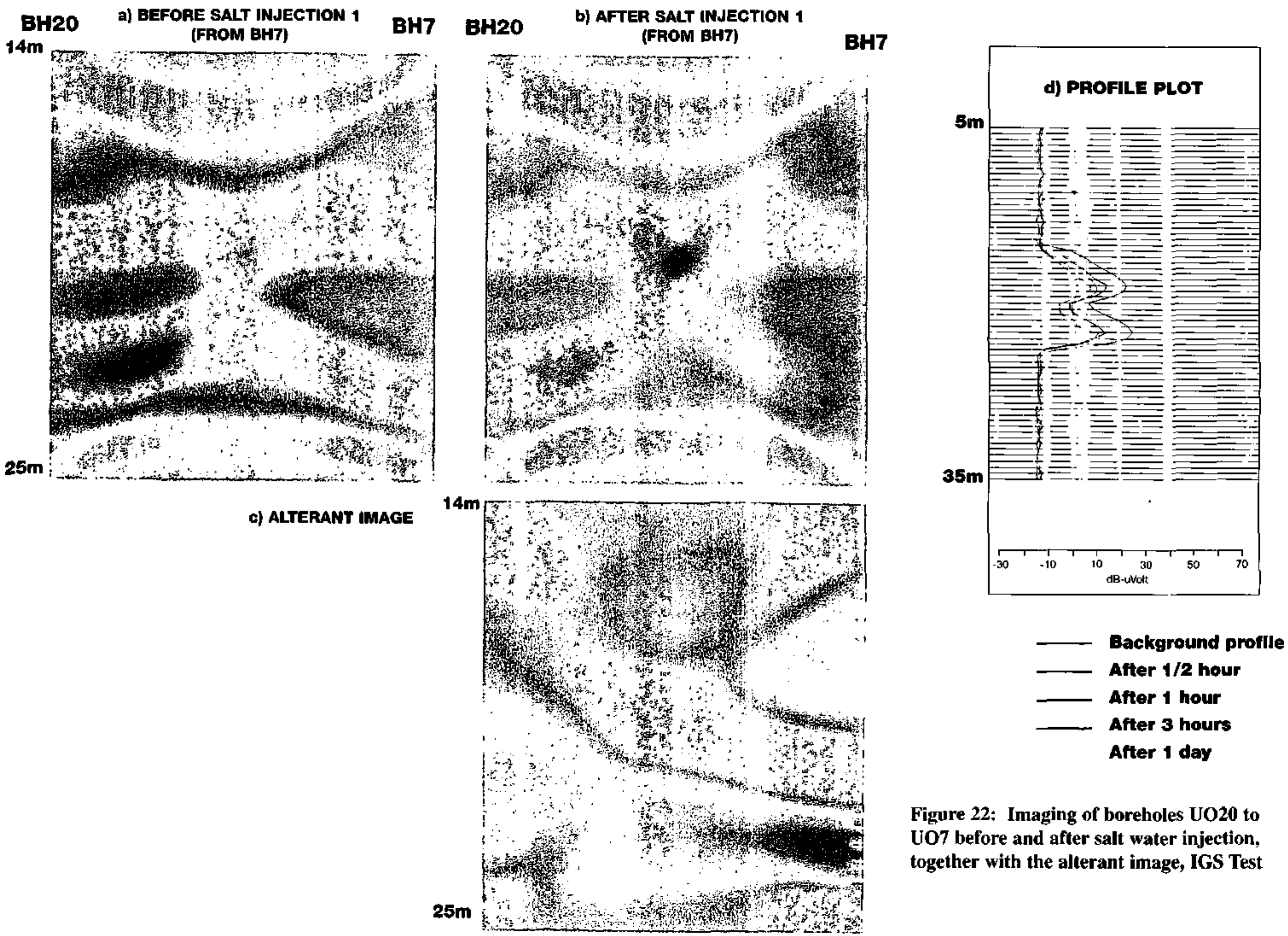

Figure 22: Imaging of boreholes UO20 to UO7 before and after salt water injection, together with the alterant image, IGS Test

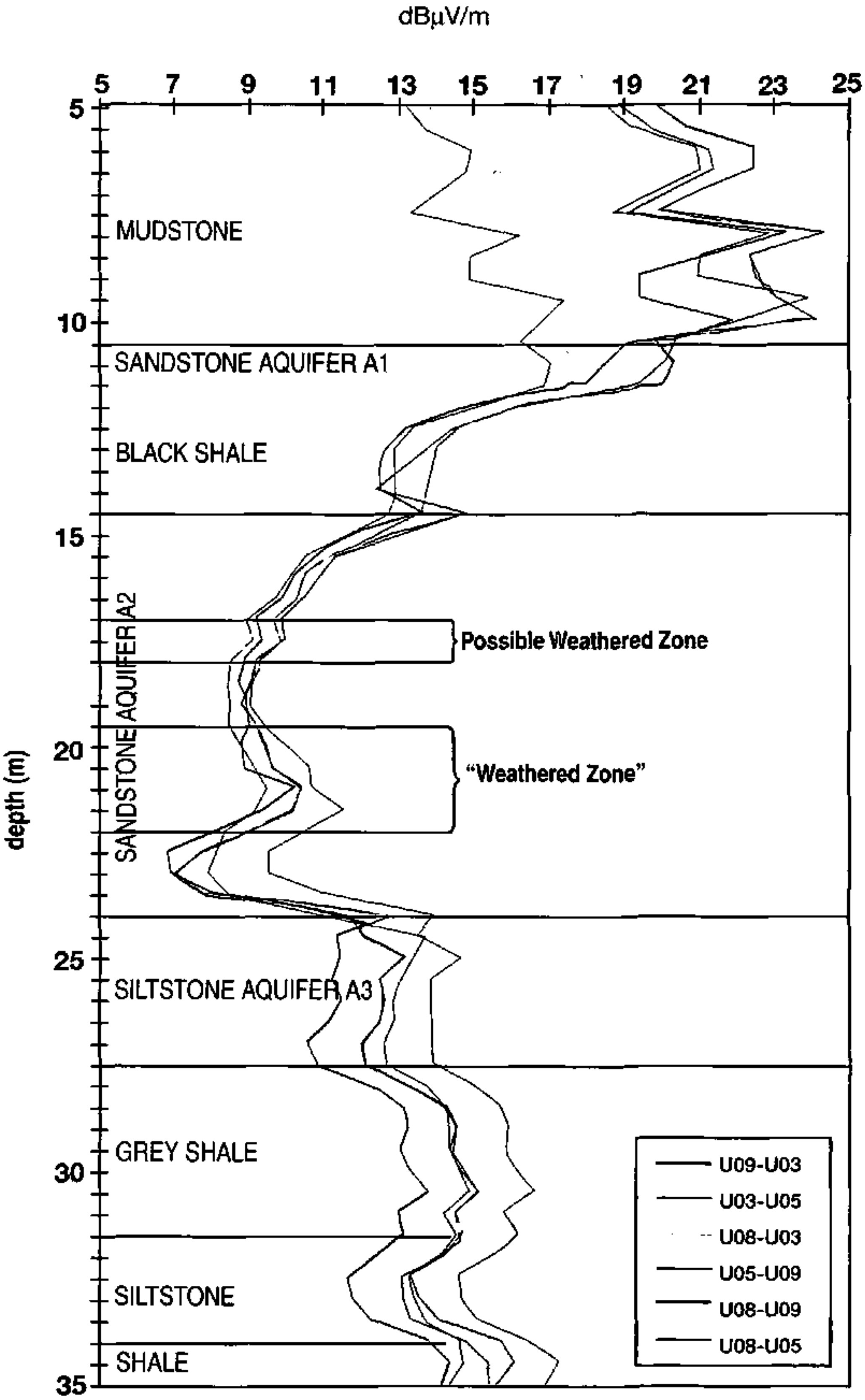

Figure 23: 50 Mhz calibrated background parallel scan

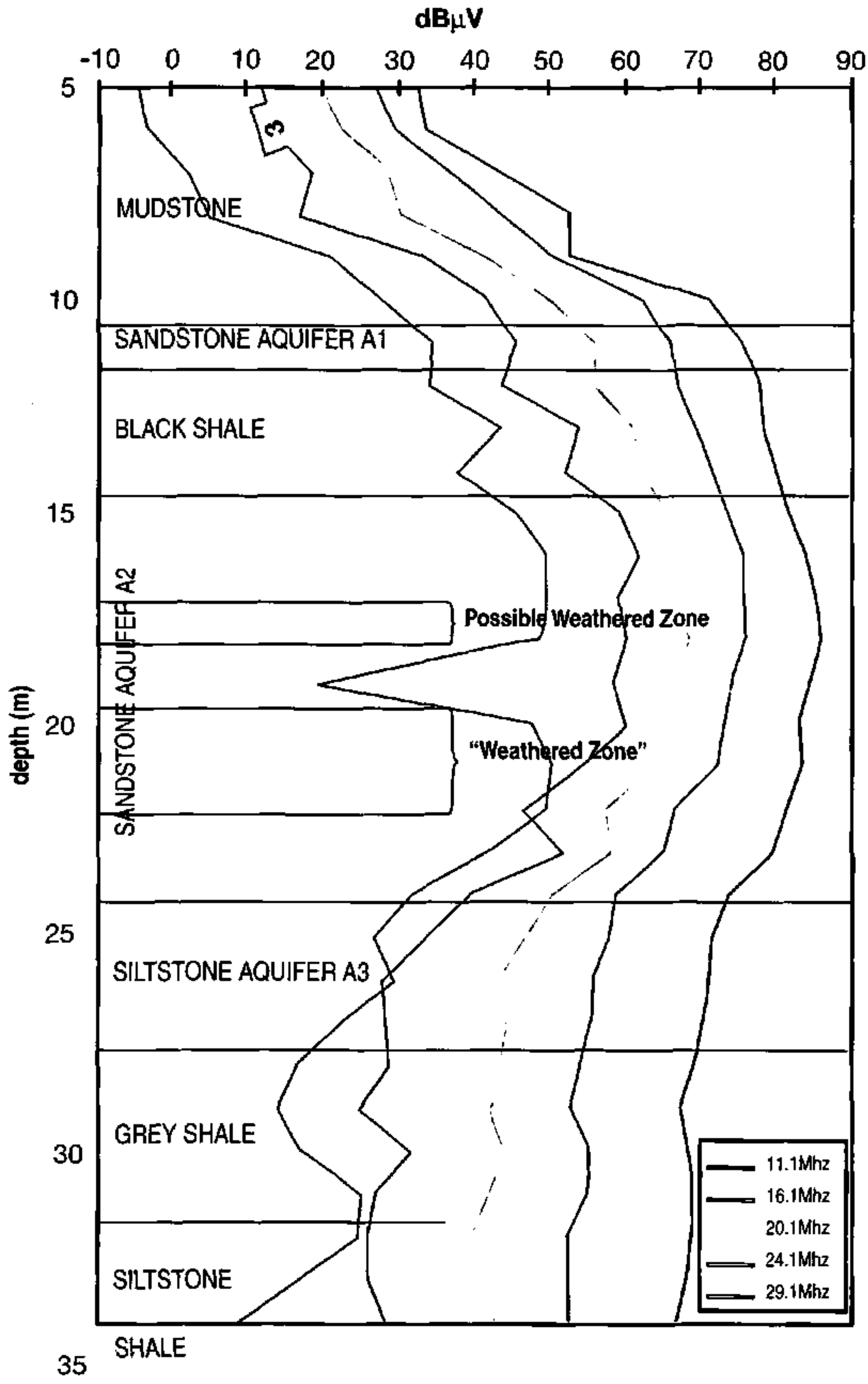

Figure 24: 30 MHz background parallel scan between boreholes U03 and U05

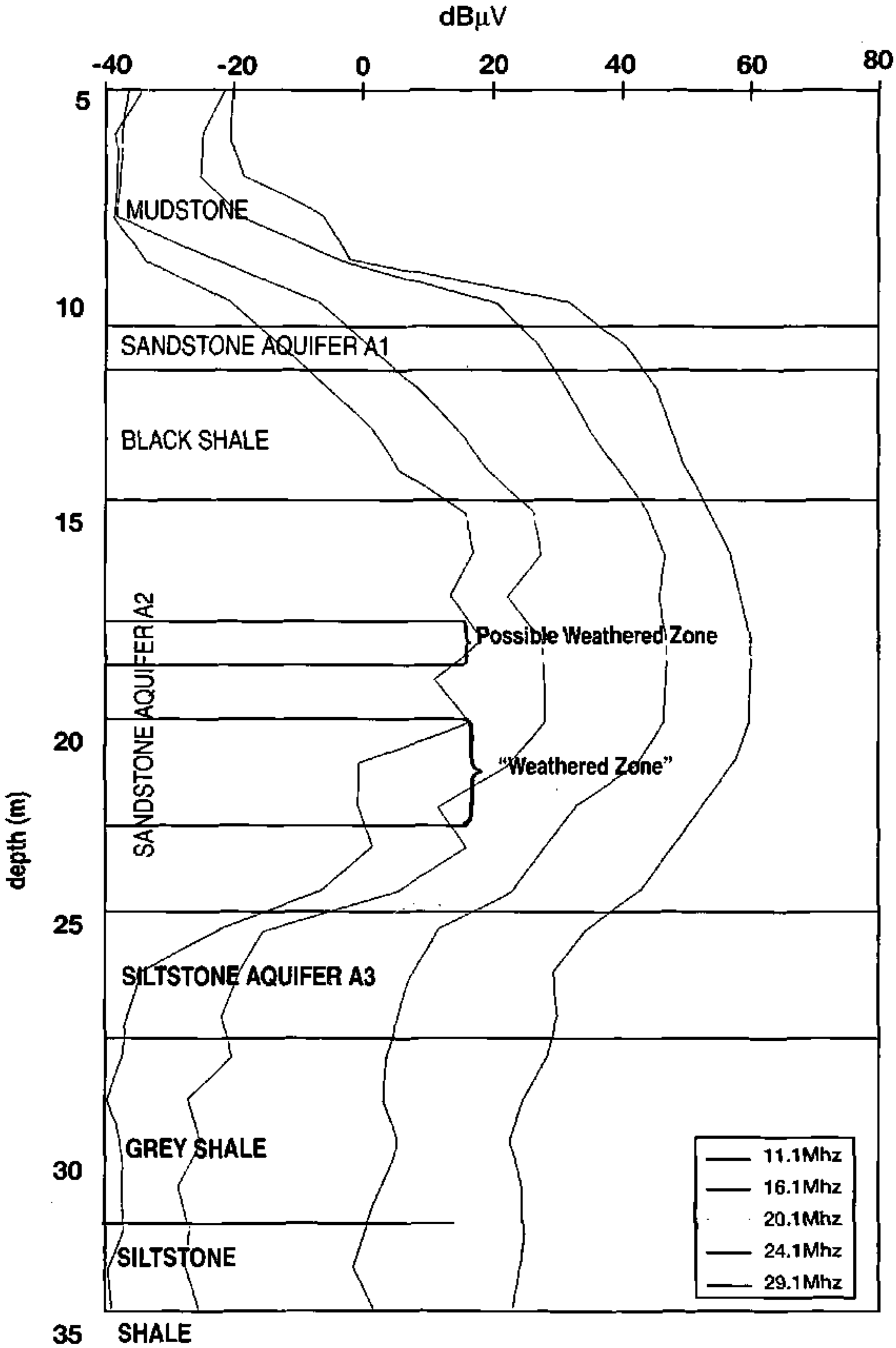

Figure 25: 30 MHz background parallel scan between boreholes UO3 and UO6

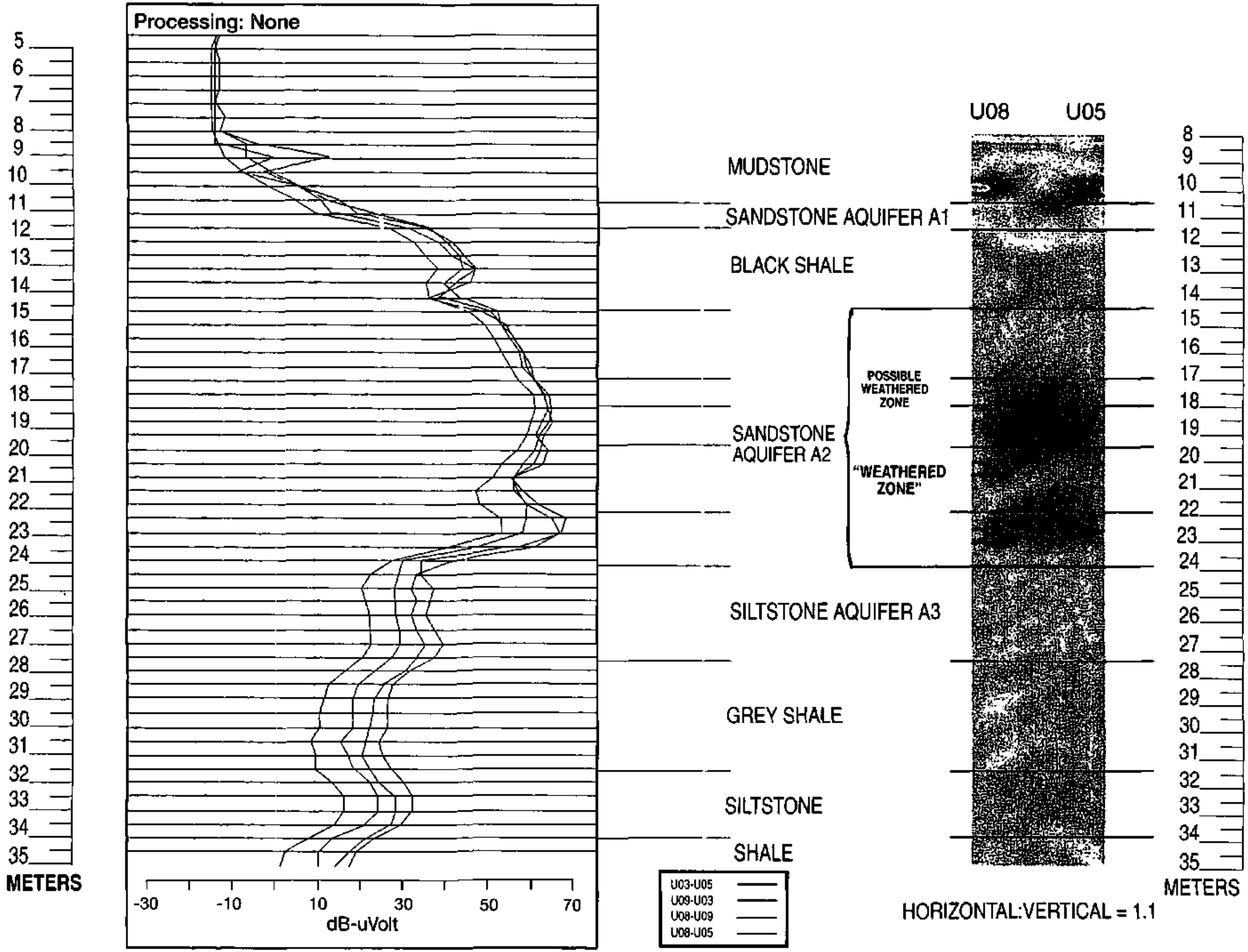

Figure 26: Typical 50 MHz background image (Boreholes U08 to U05)

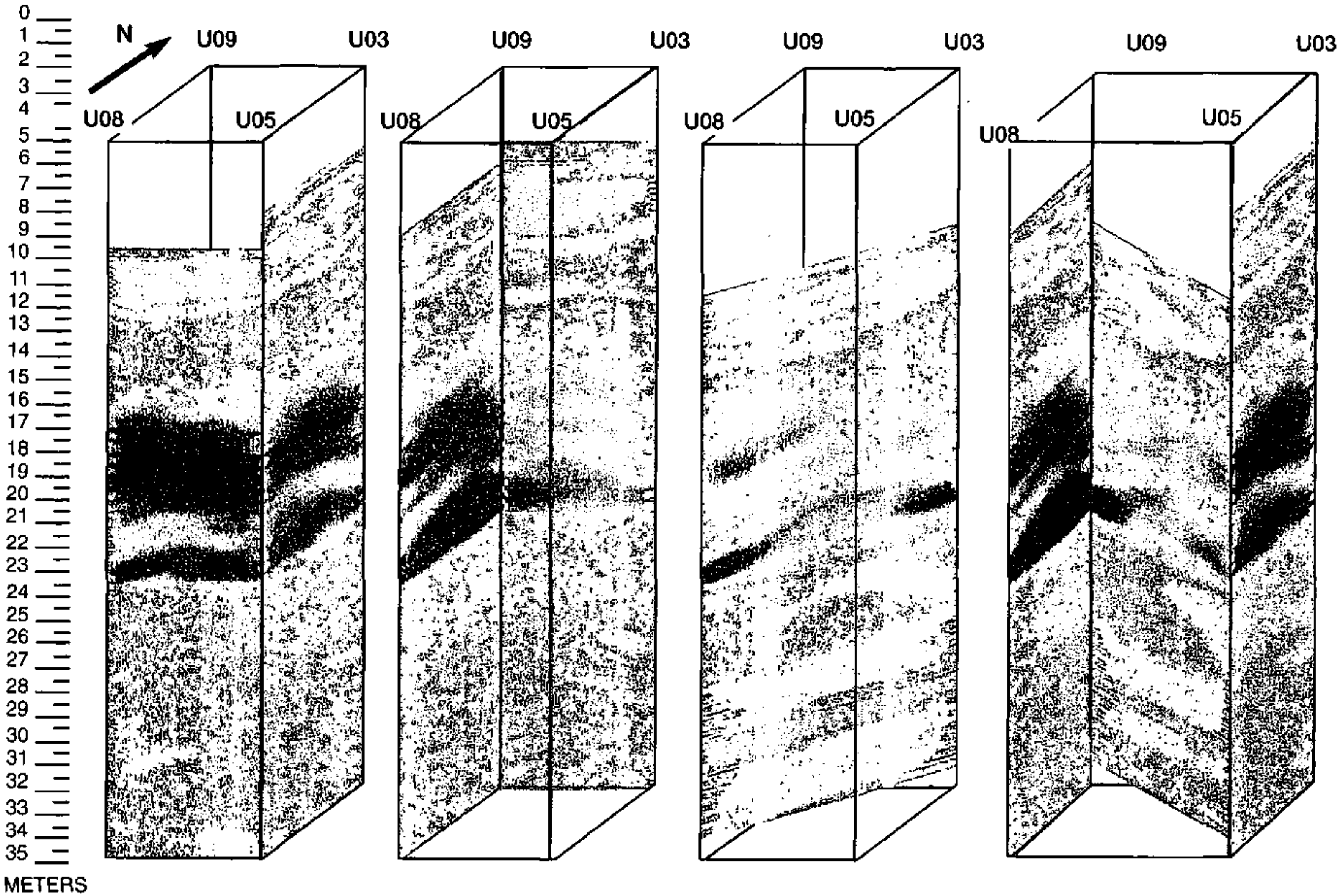

Figure 27: 50 MHz background images

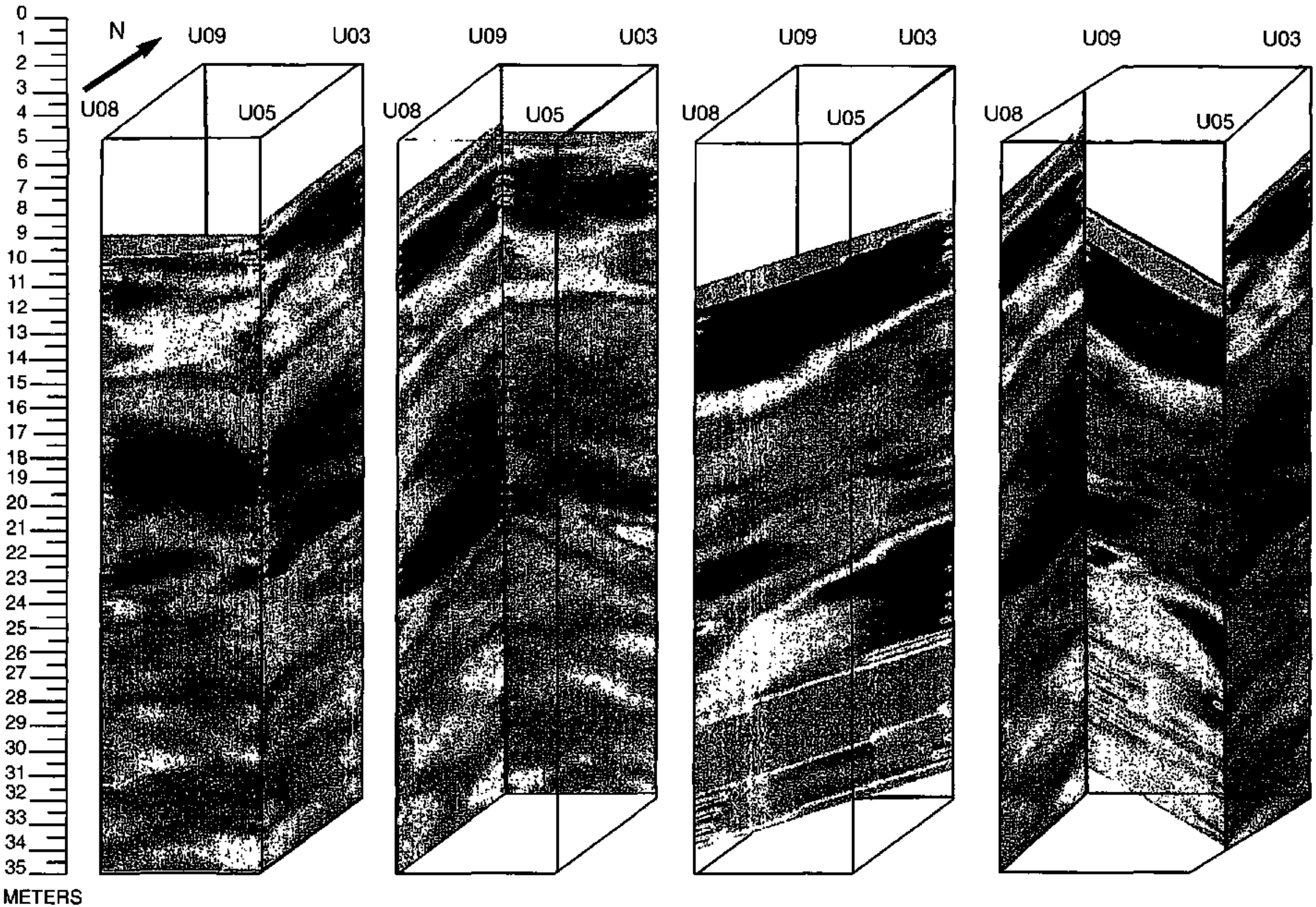

Figure 28: 50 MHz post-injection images

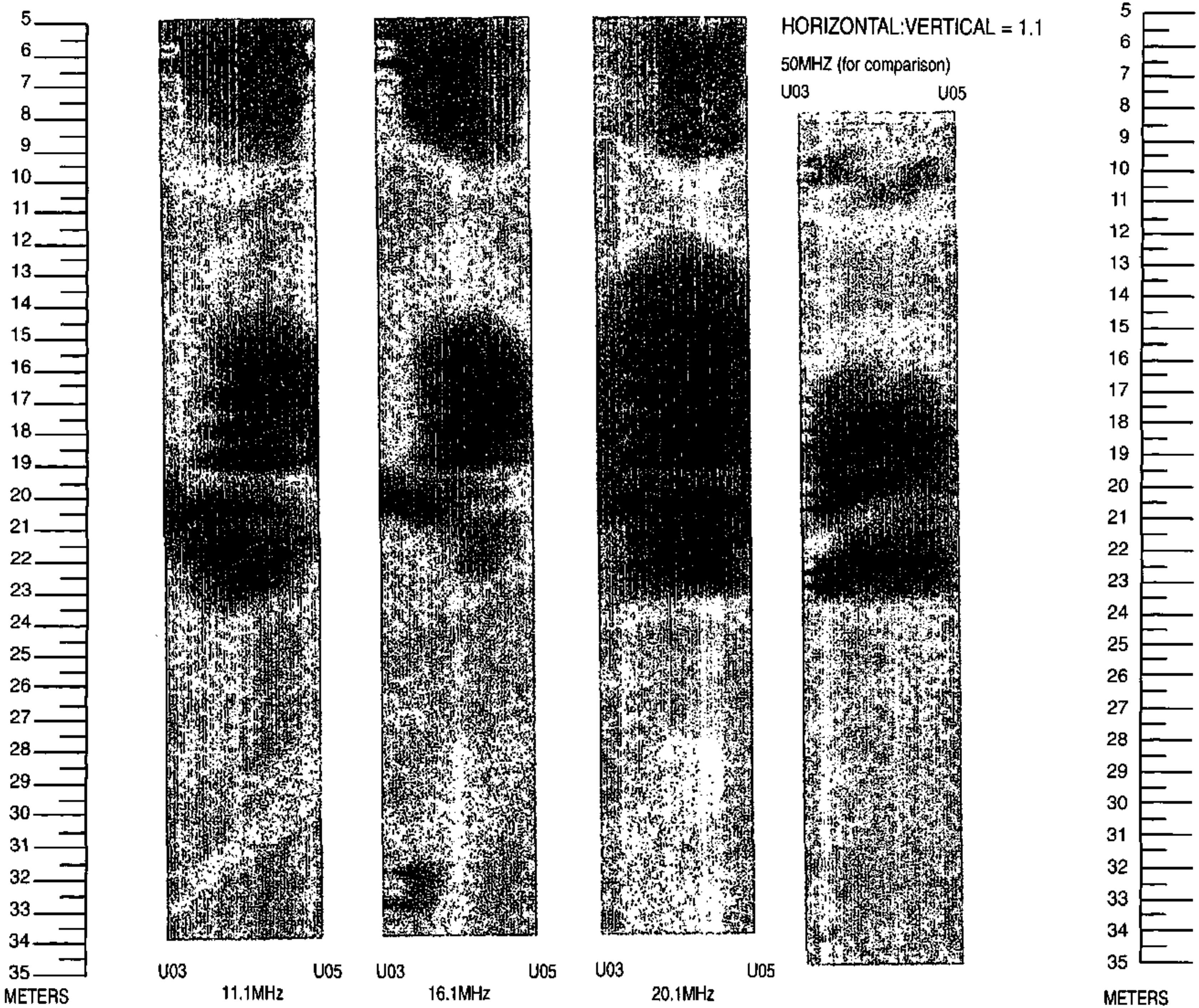

Figure 29: 30 MHz background images (boreholes U03 to U05) at three frequencies.

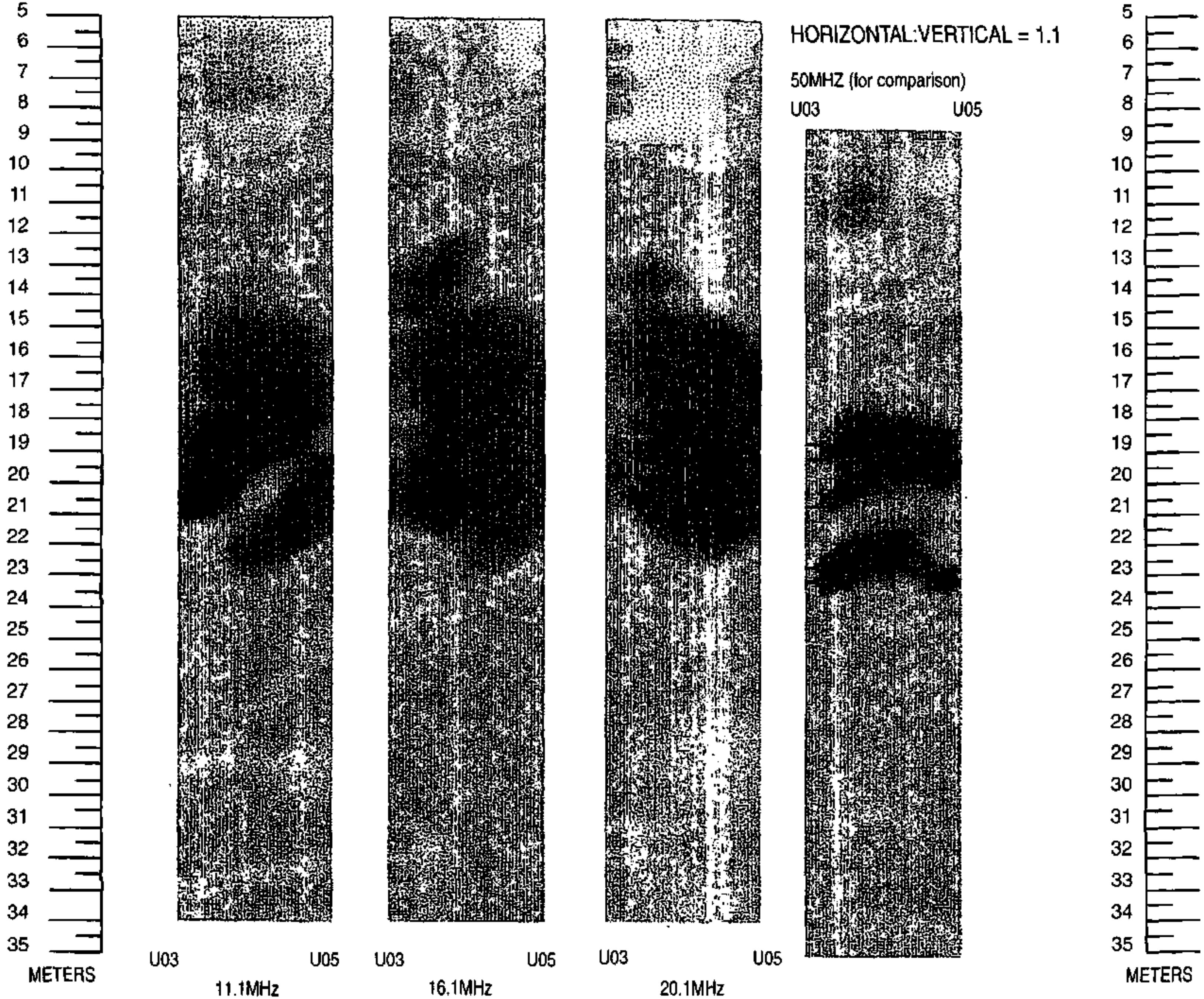

Figure 30: 30 MHz post-injection images (boreholes U03 to U05) at three frequencies.

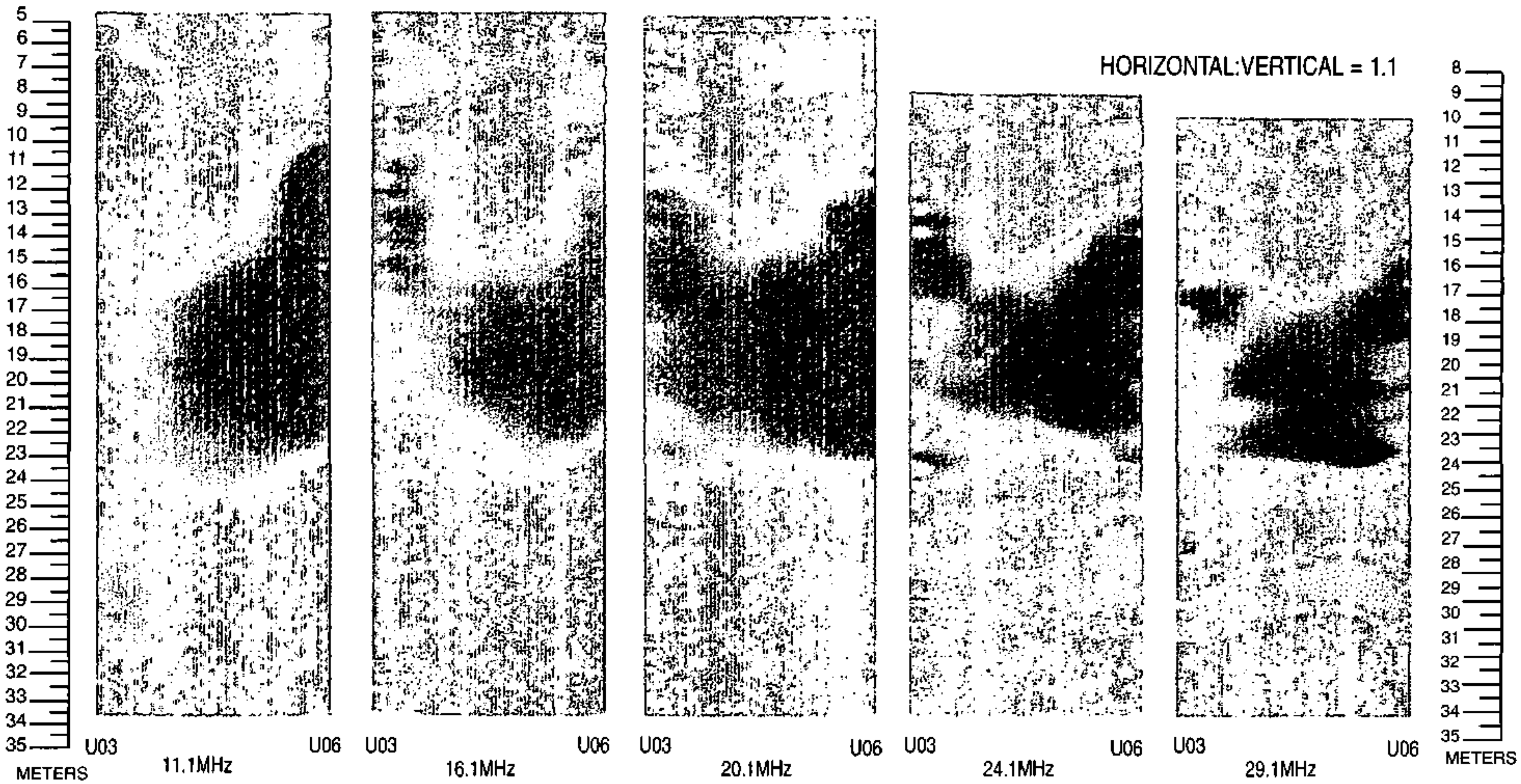

Figure 31: 30 MHz background images (boreholes U03 to U06) at five frequencies.

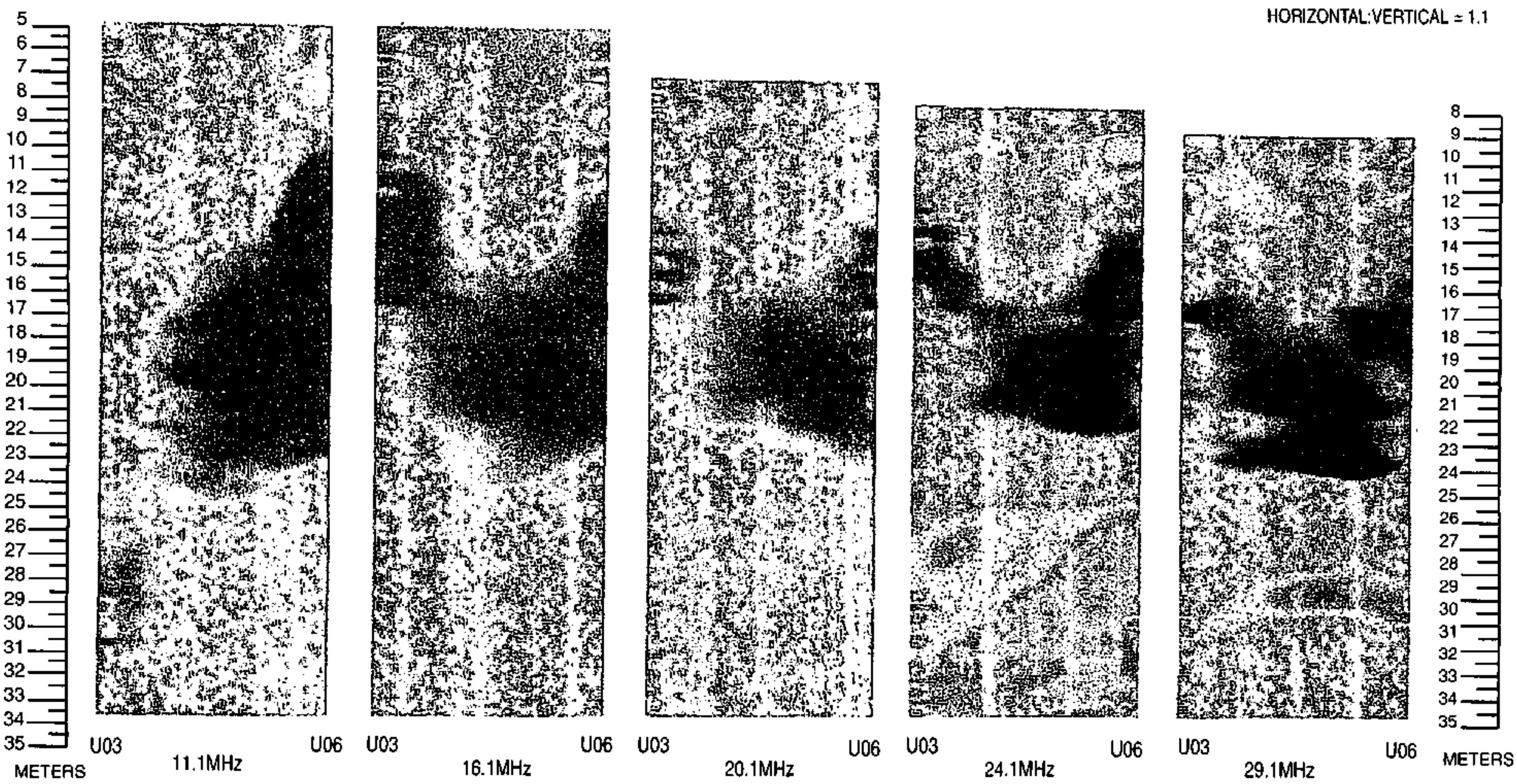

Figure 32: 30 MHz post-injection images (boreholes U03 to U06) at five frequencies.

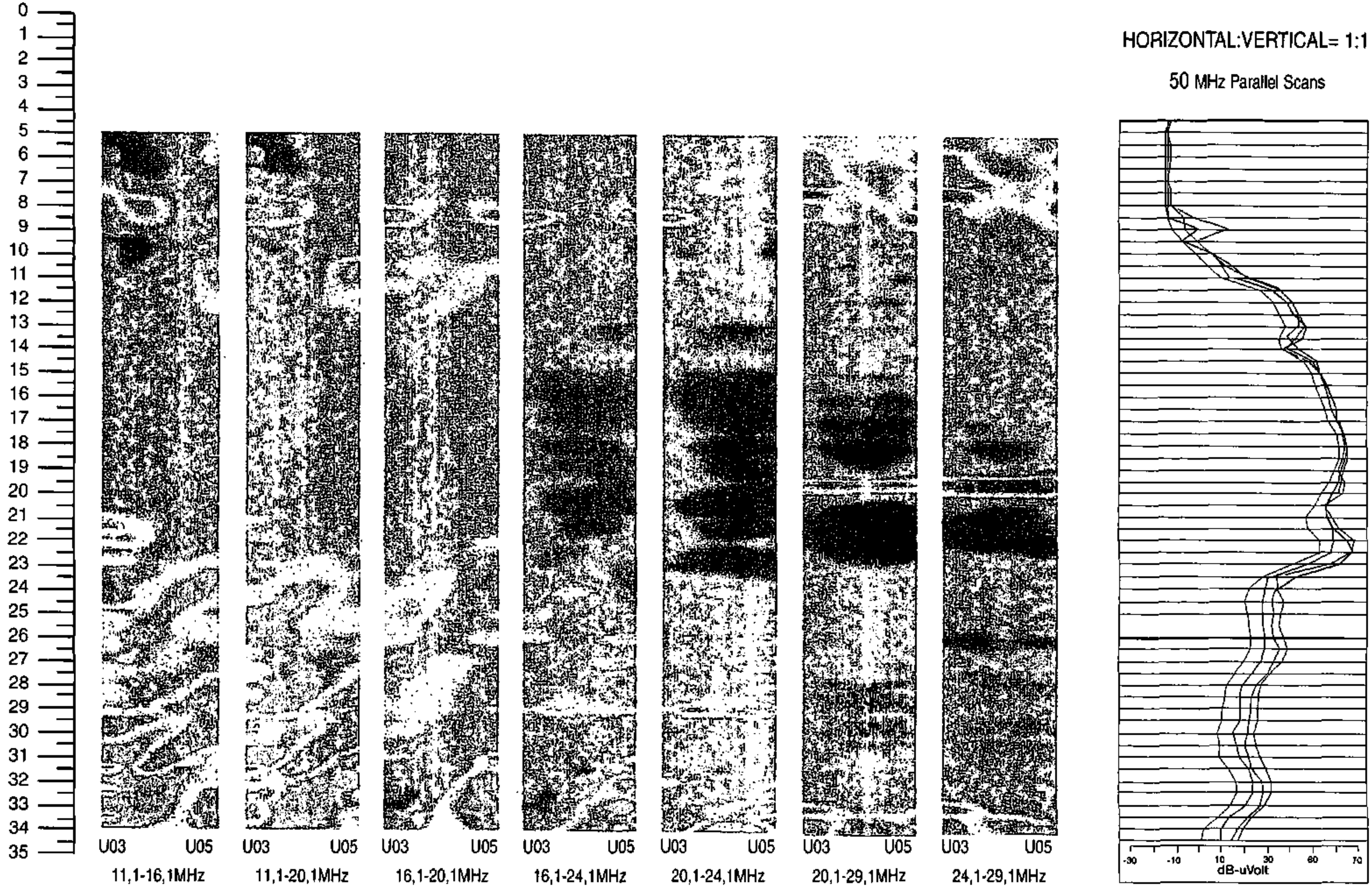

Figure 33: 30 MHz background difference images (between boreholes U03 to U05)

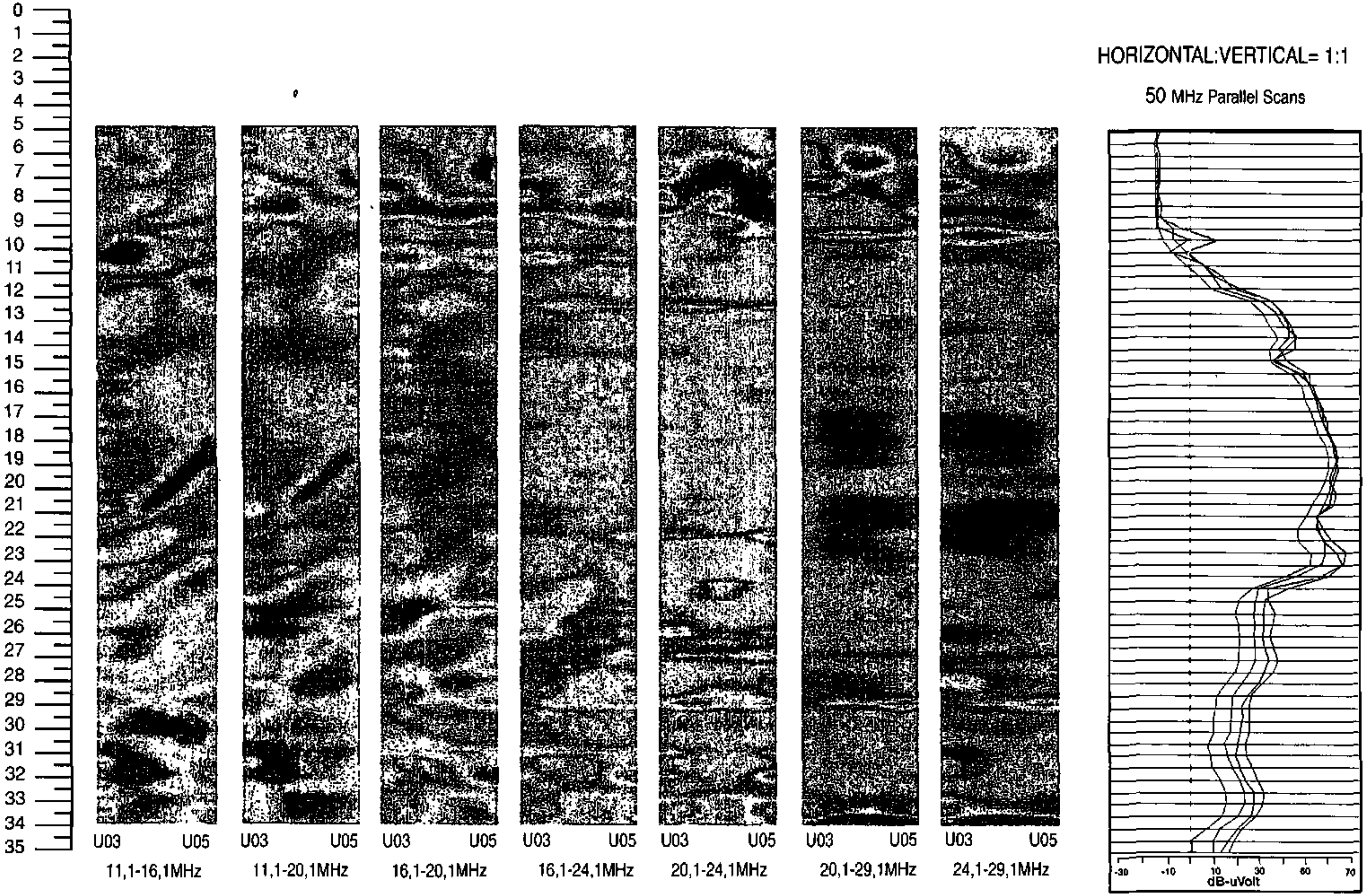

Figure 34: 30 MHz post-injection difference images (between boreholes U03 to U05)

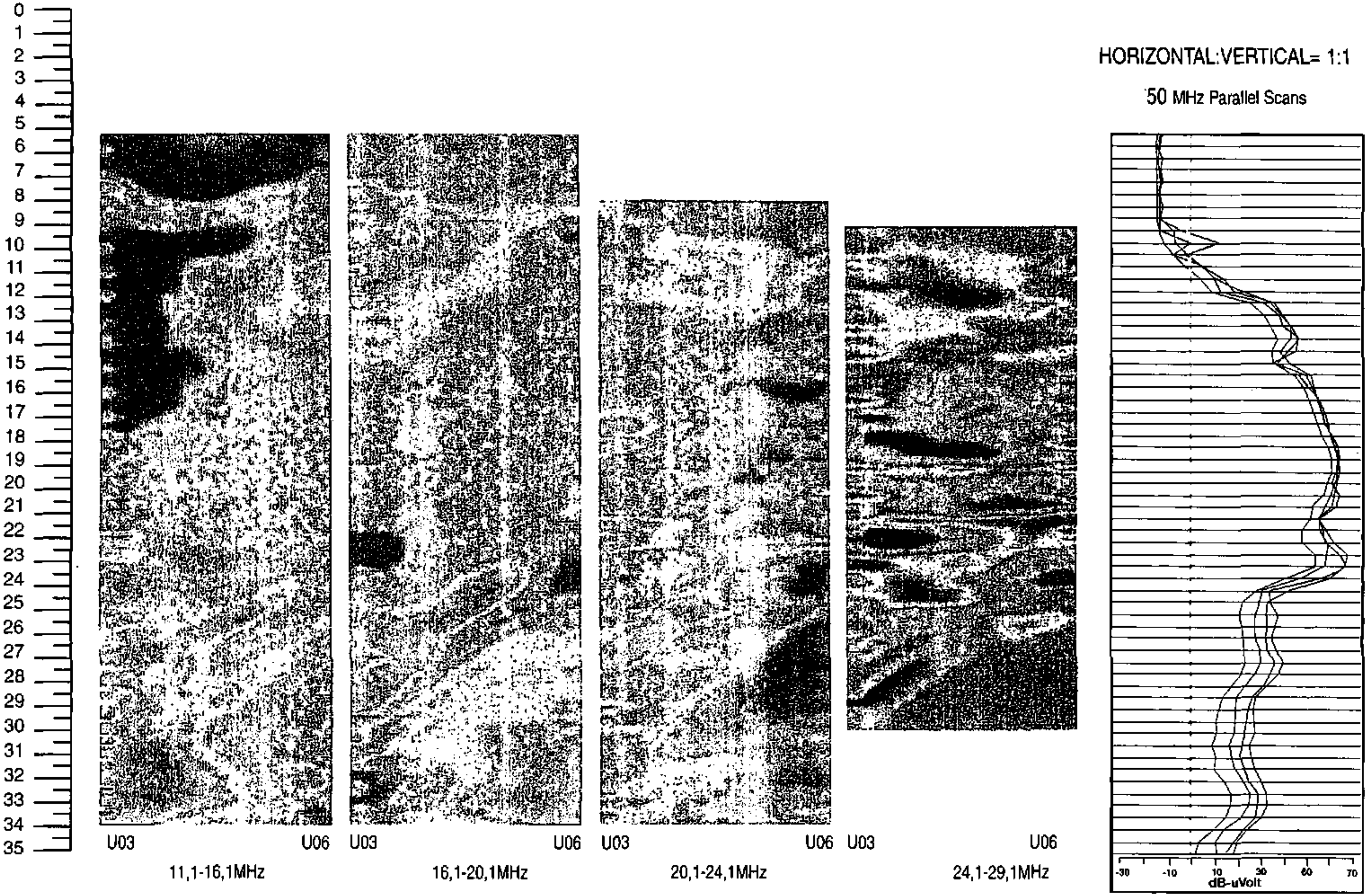

Figure 35: 30 MHz background difference images (between boreholes U03 to U06)

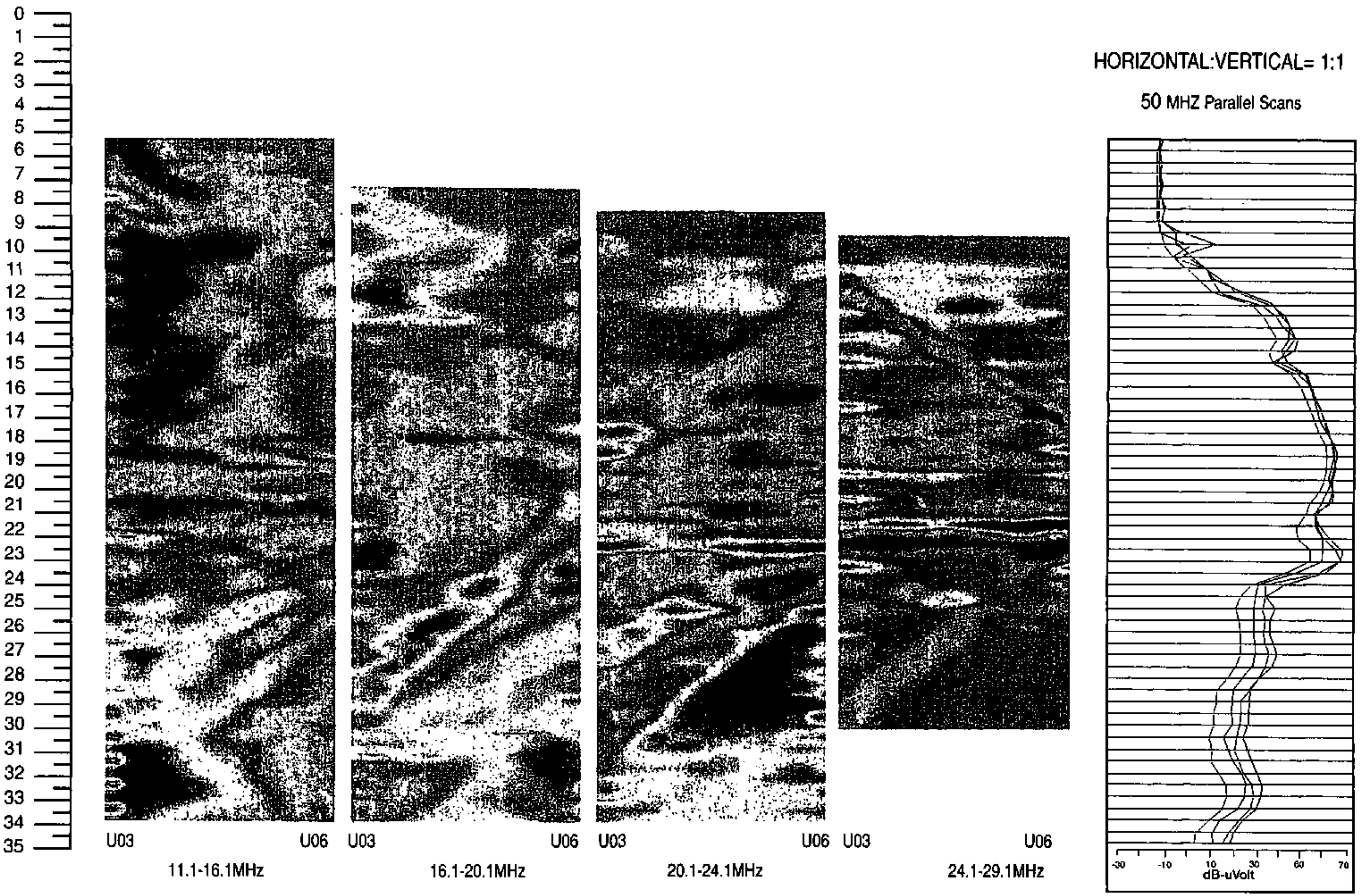

Figure 36: 30 MHz post-injection difference images (between boreholes U03 to U06)

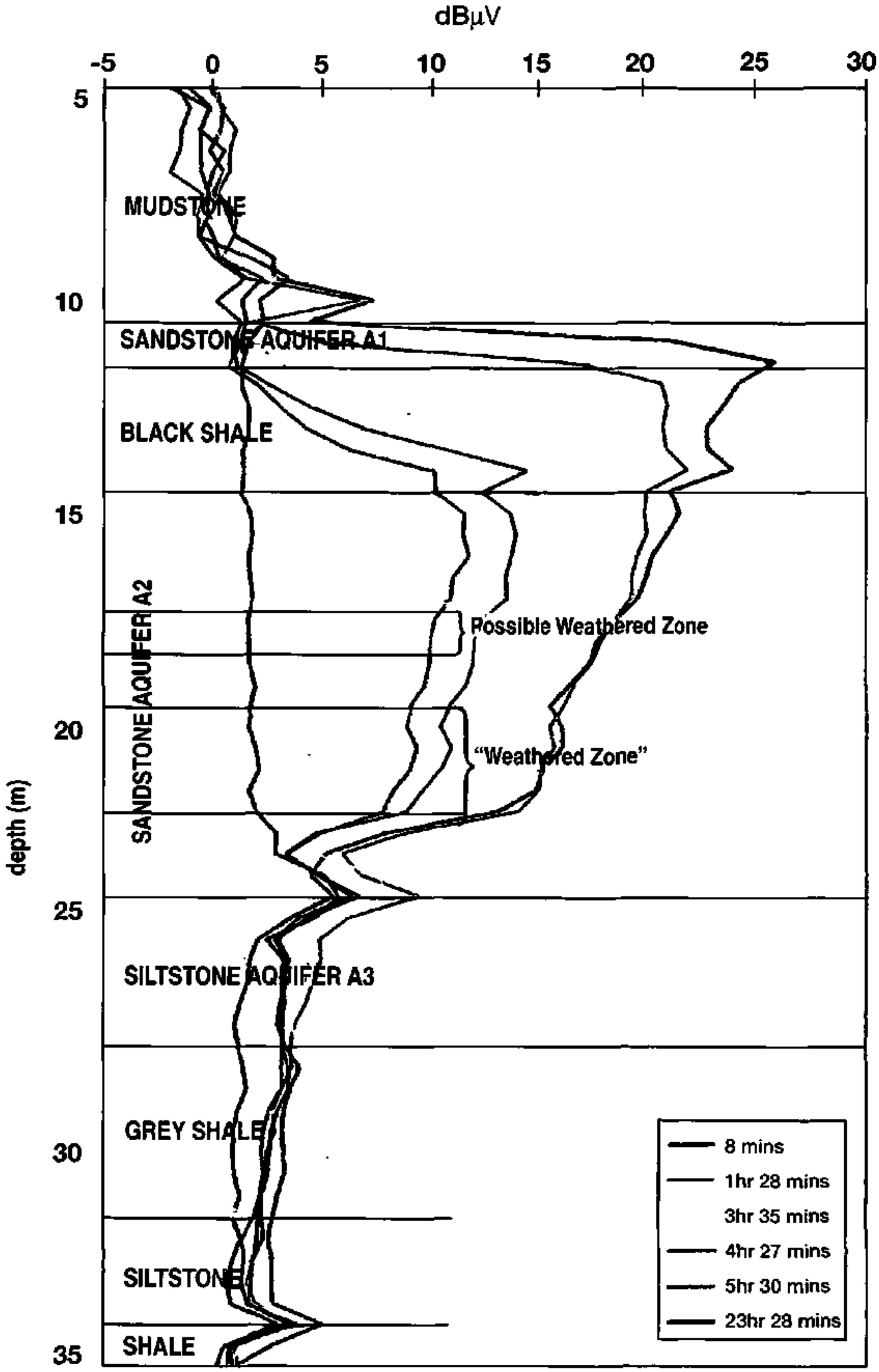

Figure 37(a): 50 MHz tracer progression monitoring (between boreholes UO3 and UO5)

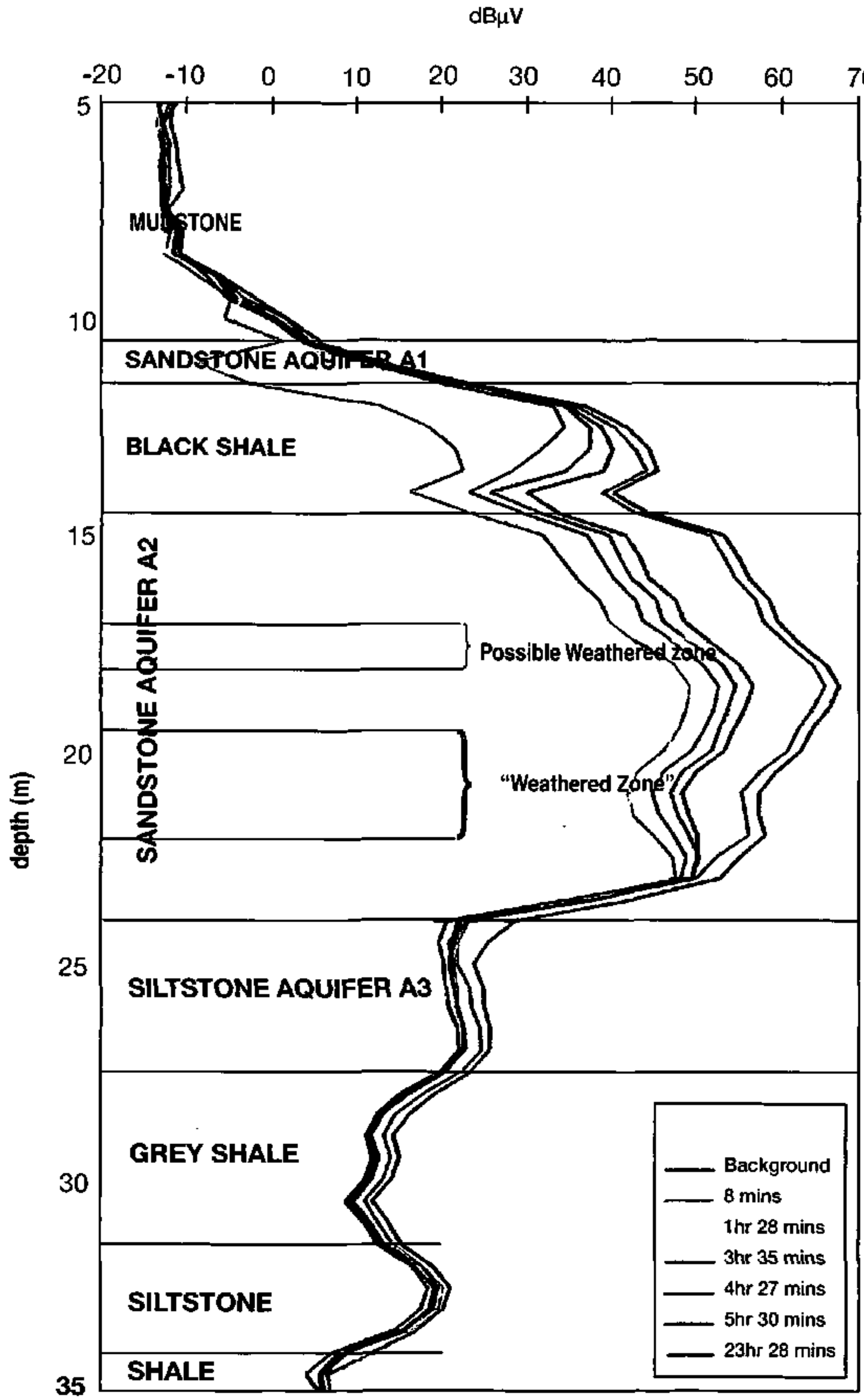

Figure 37(b): Difference to background image (between boreholes UO9 and UO5)

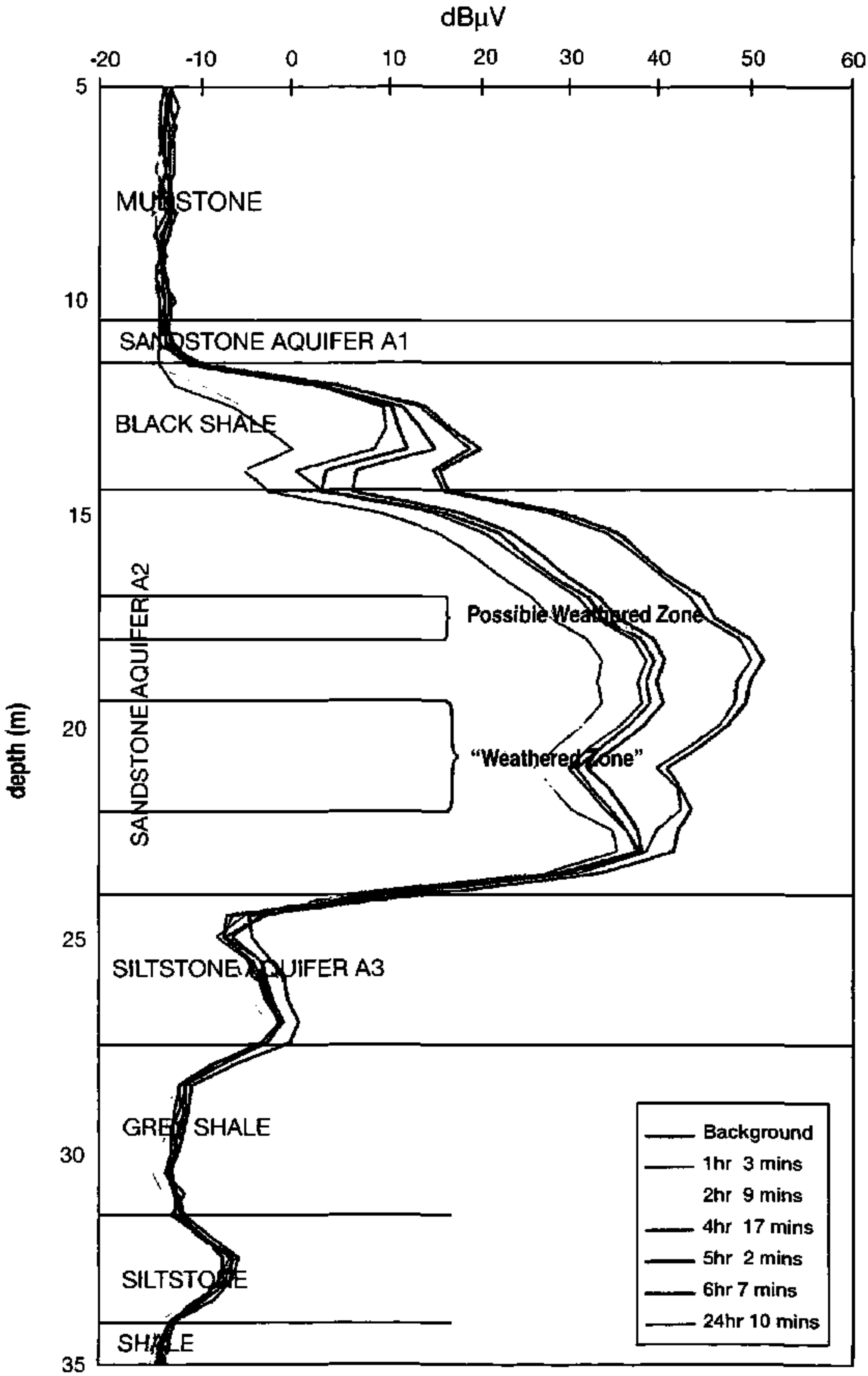

Figure 38(a): 50 MHz tracer progression monitoring (between boreholes UO9 and UO5)

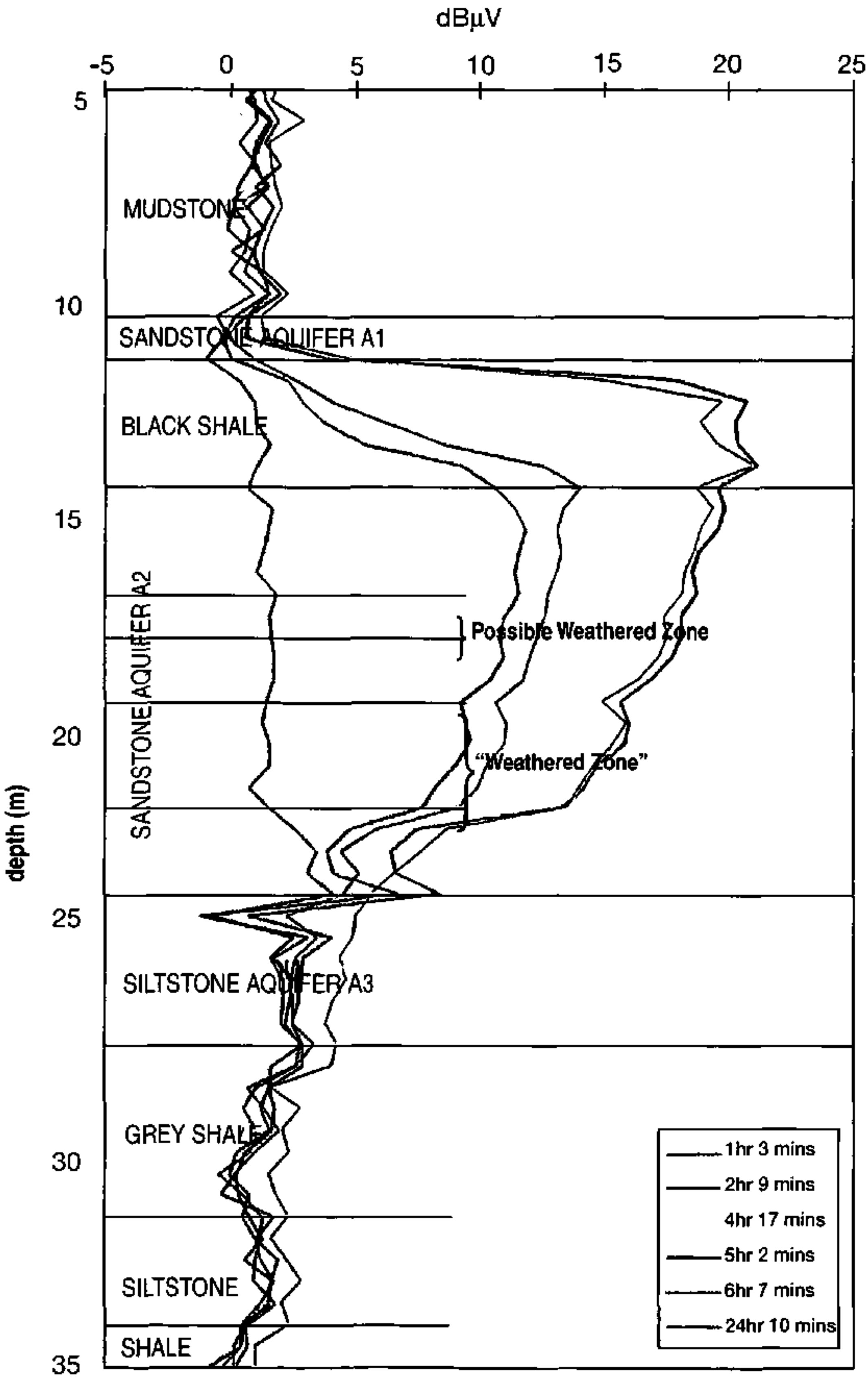

Figure 38(b): Difference to background image (between boreholes UO9 and UO5)

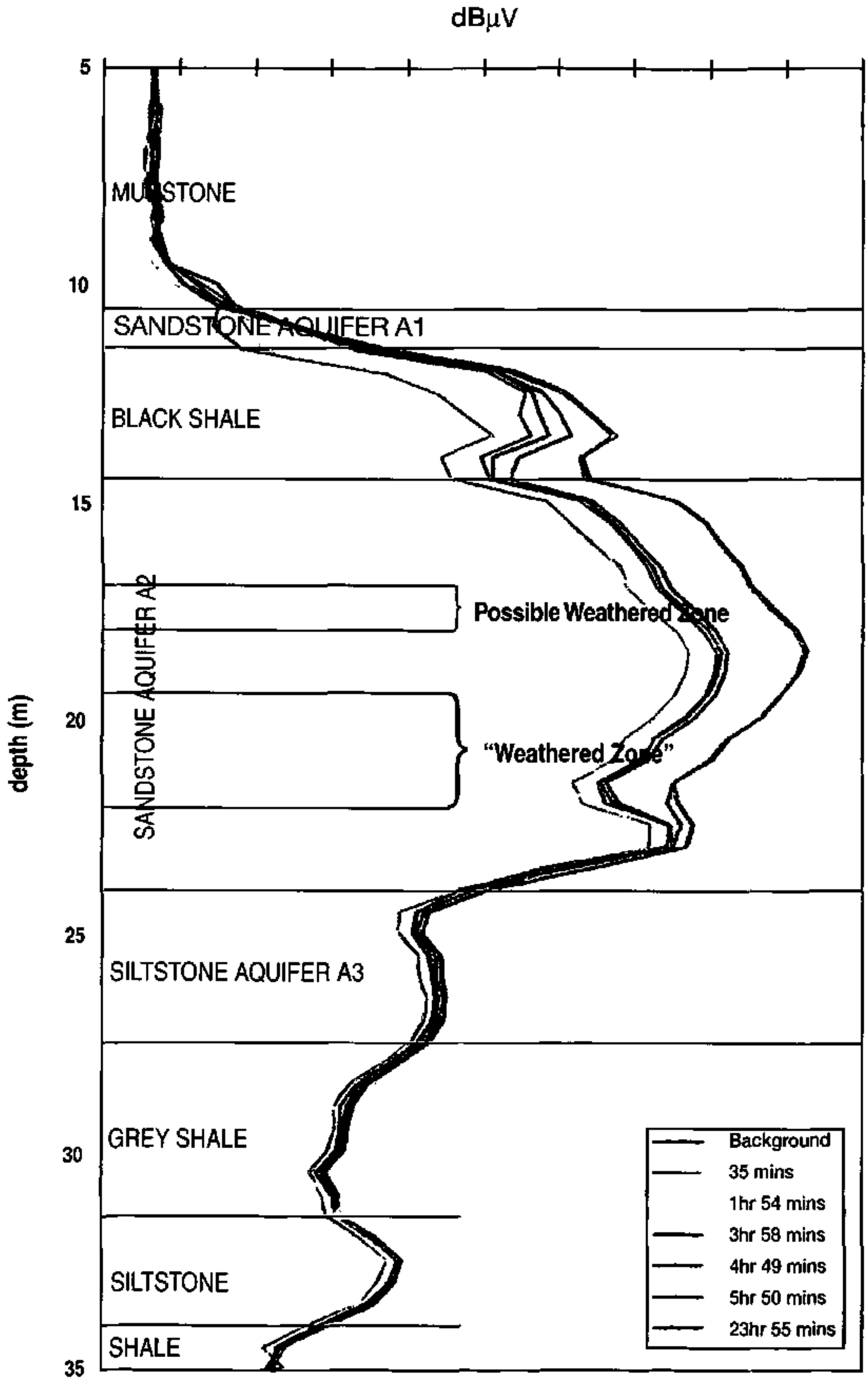

Figure 39(a): 50 MHz tracer progression monitoring (between boreholes U08 and U05)

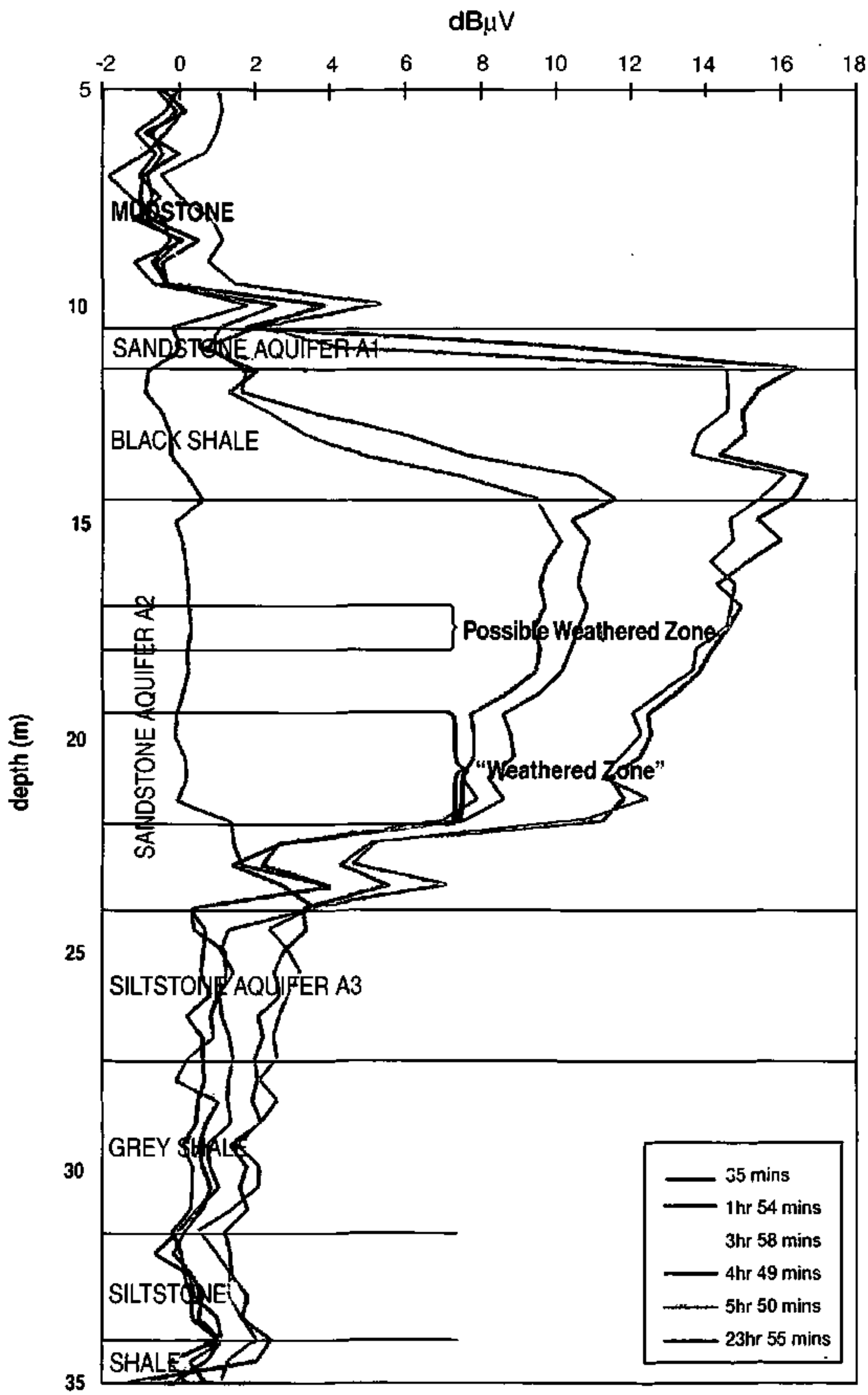

Figure 39(b): Difference to background image (between boreholes U08 and U05)

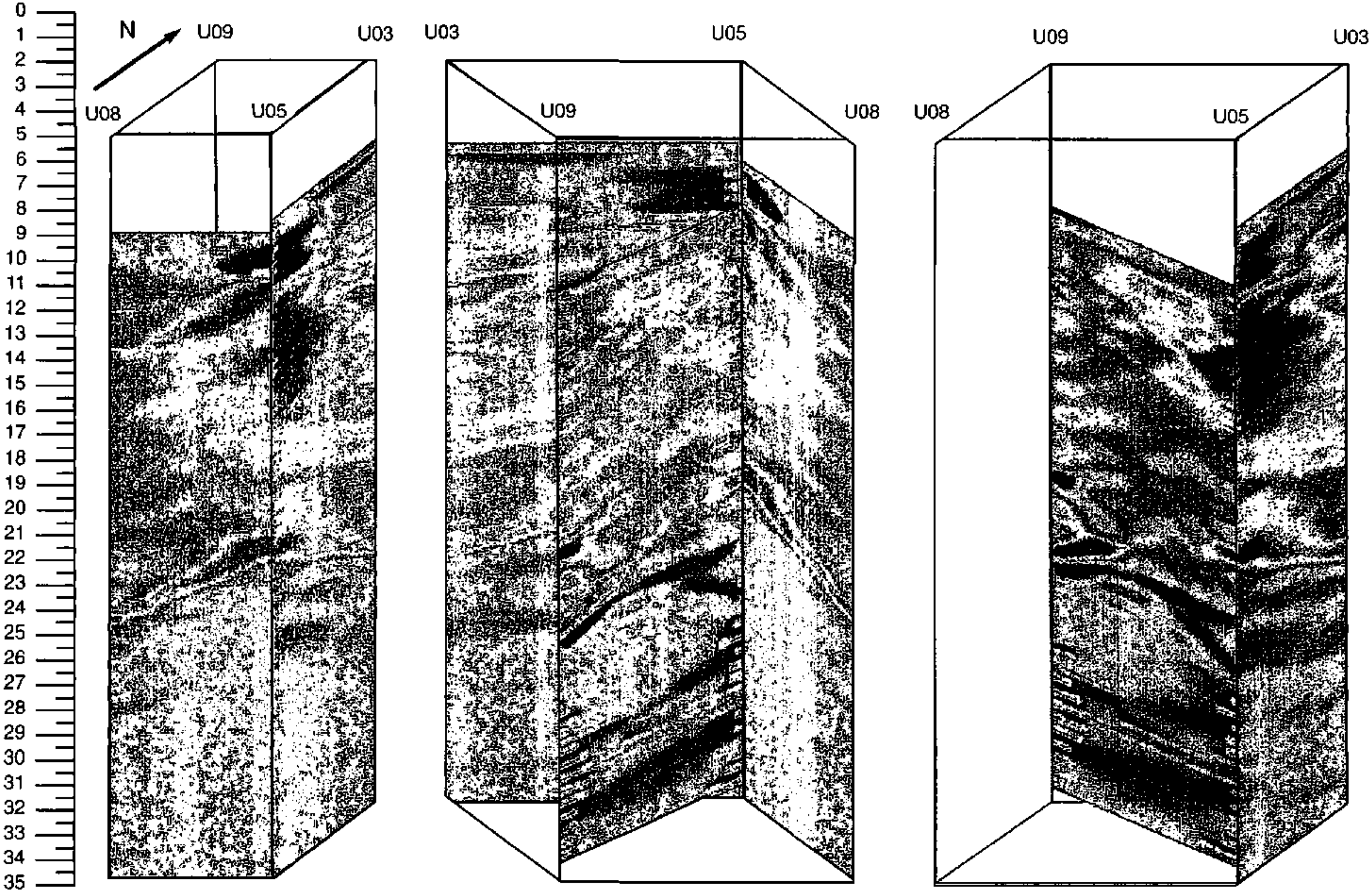

Figure 40: 50 MHz alterant images from salt water injection at borehole U05

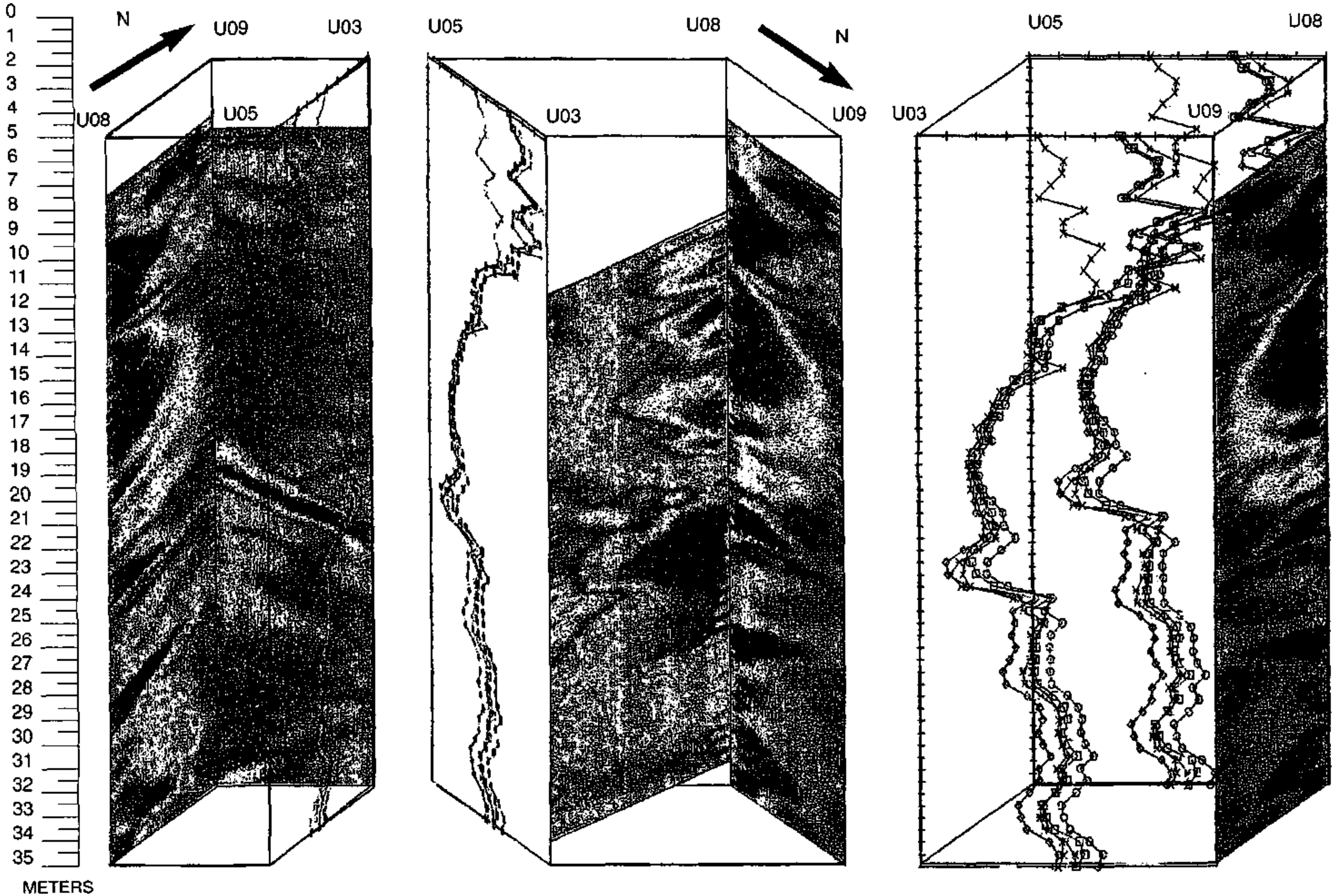

Figure 41 : 50 Mhz alterant images fro salt water injection at boreholes U08

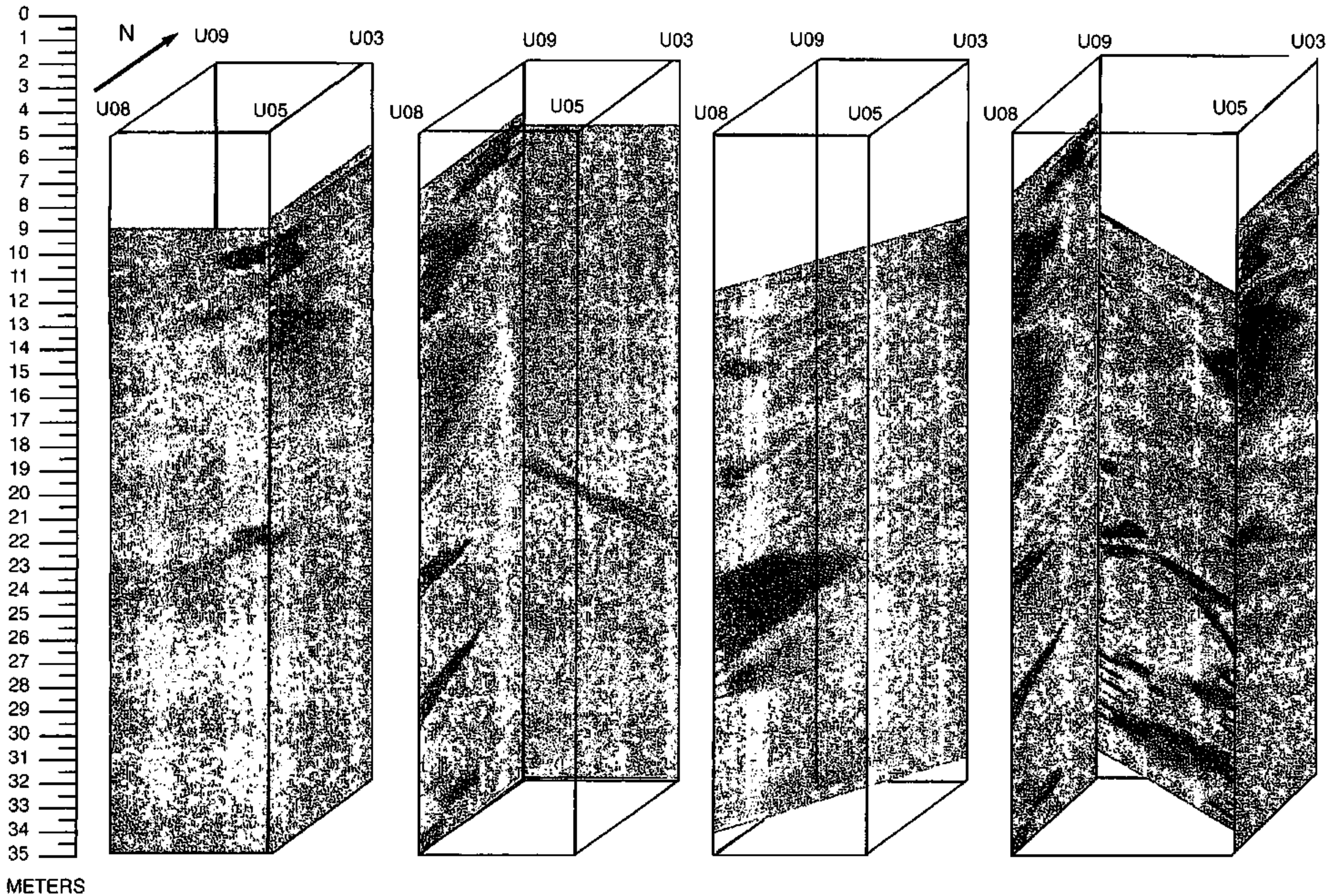

Figure 42: Composite diagram showing all 50 MHz alterant images

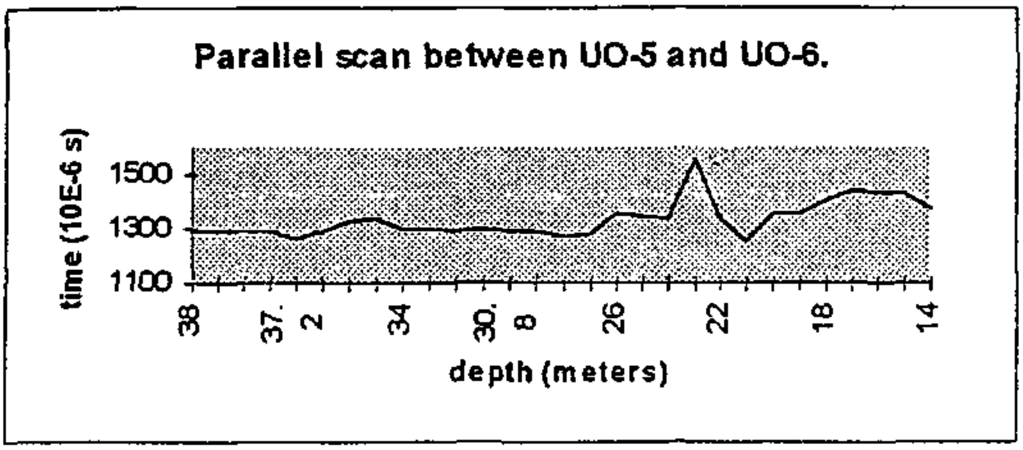

Figure 43(a): Parallel seismic scan between boreholes UO5 and UO6.

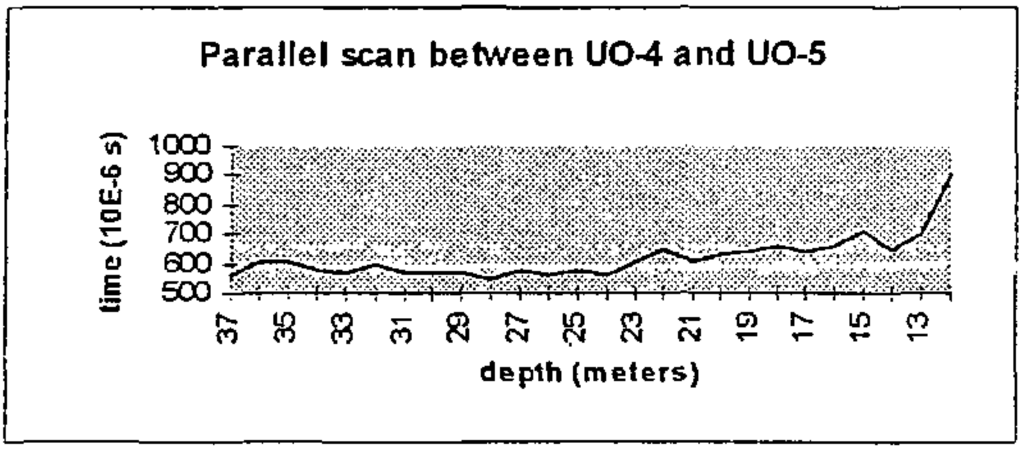

Figure 43(b): Parallel seismic scan between boreholes UO5 and UO6.

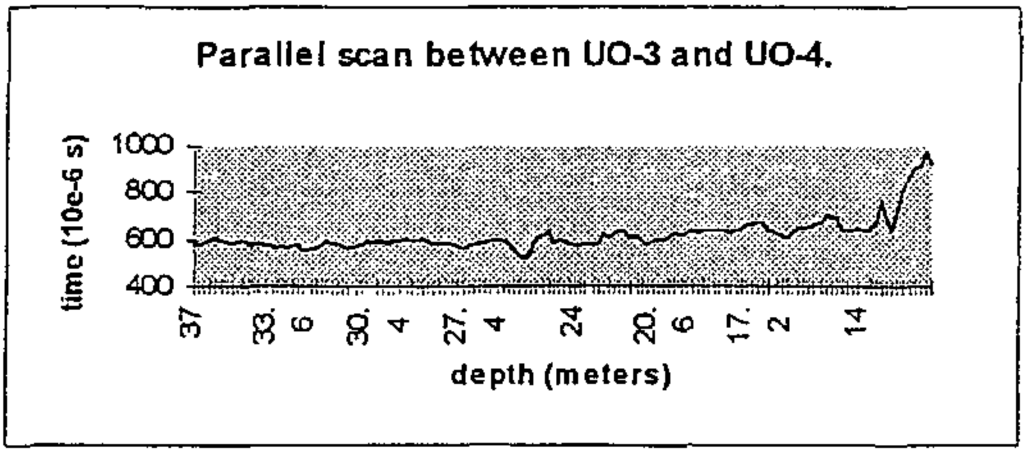

Figure 43(c): Parallel seismic scan between boreholes UO5 and UO6.

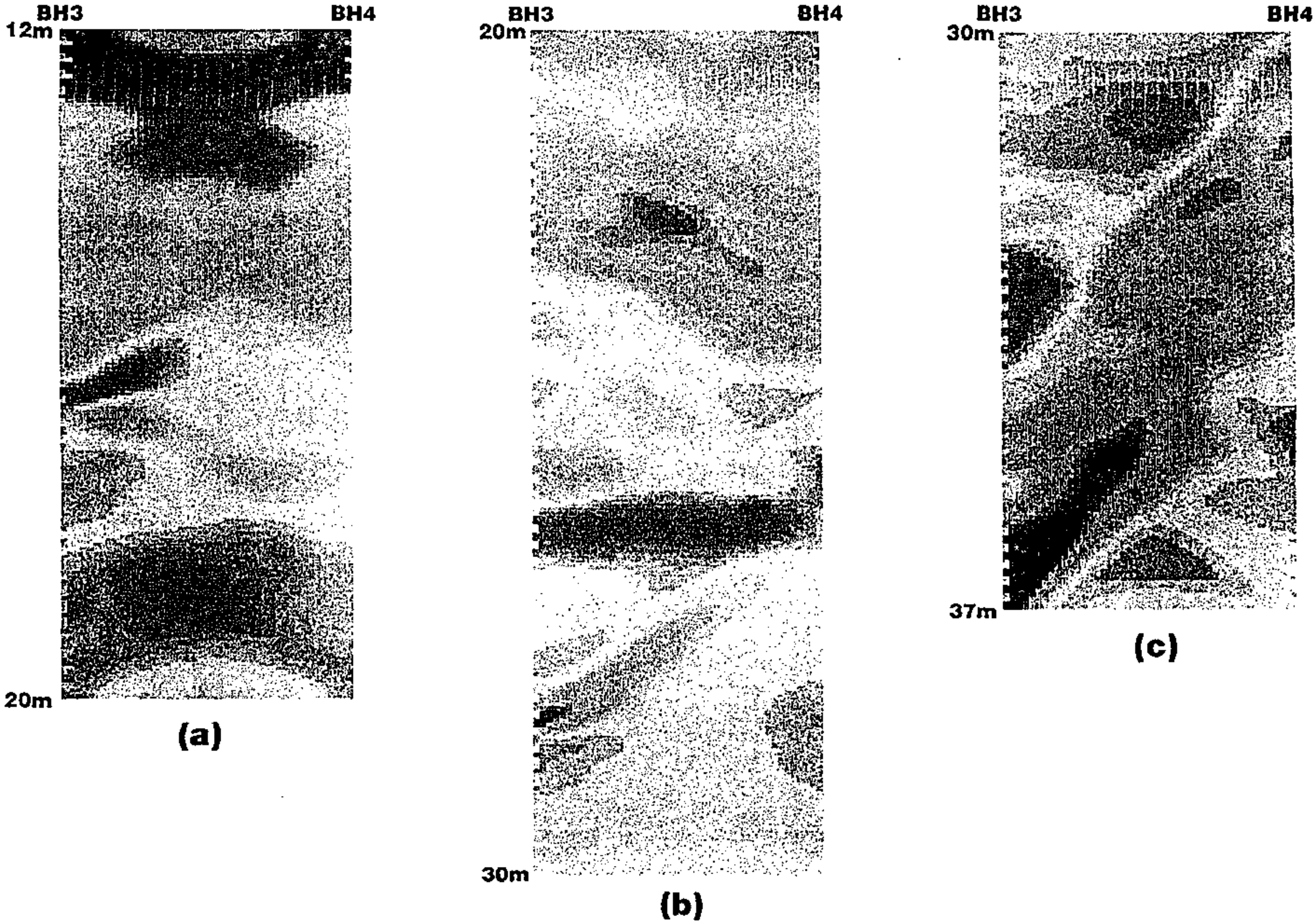

Figure 44: Tomographic images for boreholes UO3-UO4 reconstructed from the seismic scans.

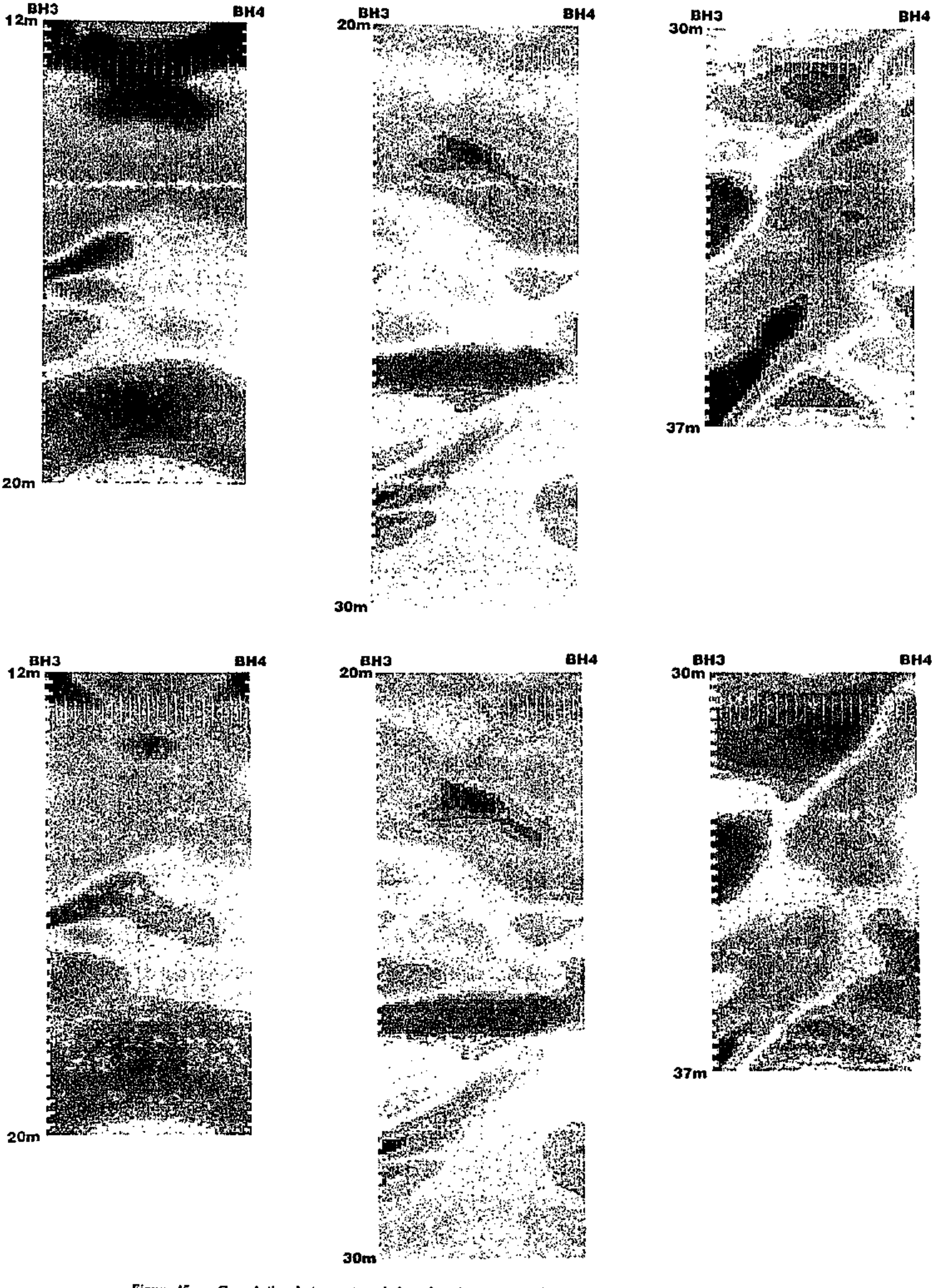

Figure 45: **Correlation between travel time data between boreholes UO3 and UO4 interpreted with tw different software packages. Upper scan interpreted with a seismic software package, and th lower scan interpreted with a RT software package adapted for seismic data.**

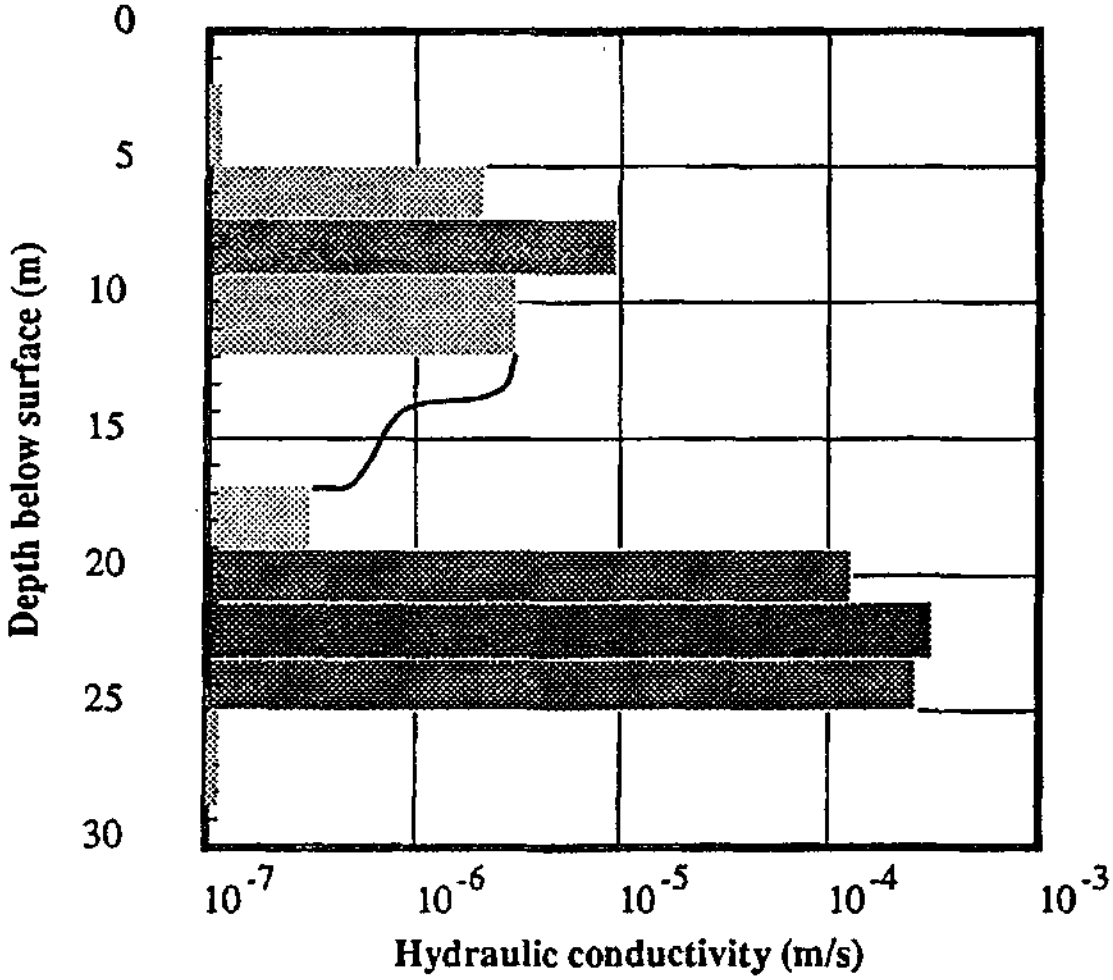

Figure 46: A graphical representation of the distribution of the hydraulic conductivity of borehole UO5, using the data from a single borehole, double packer test.

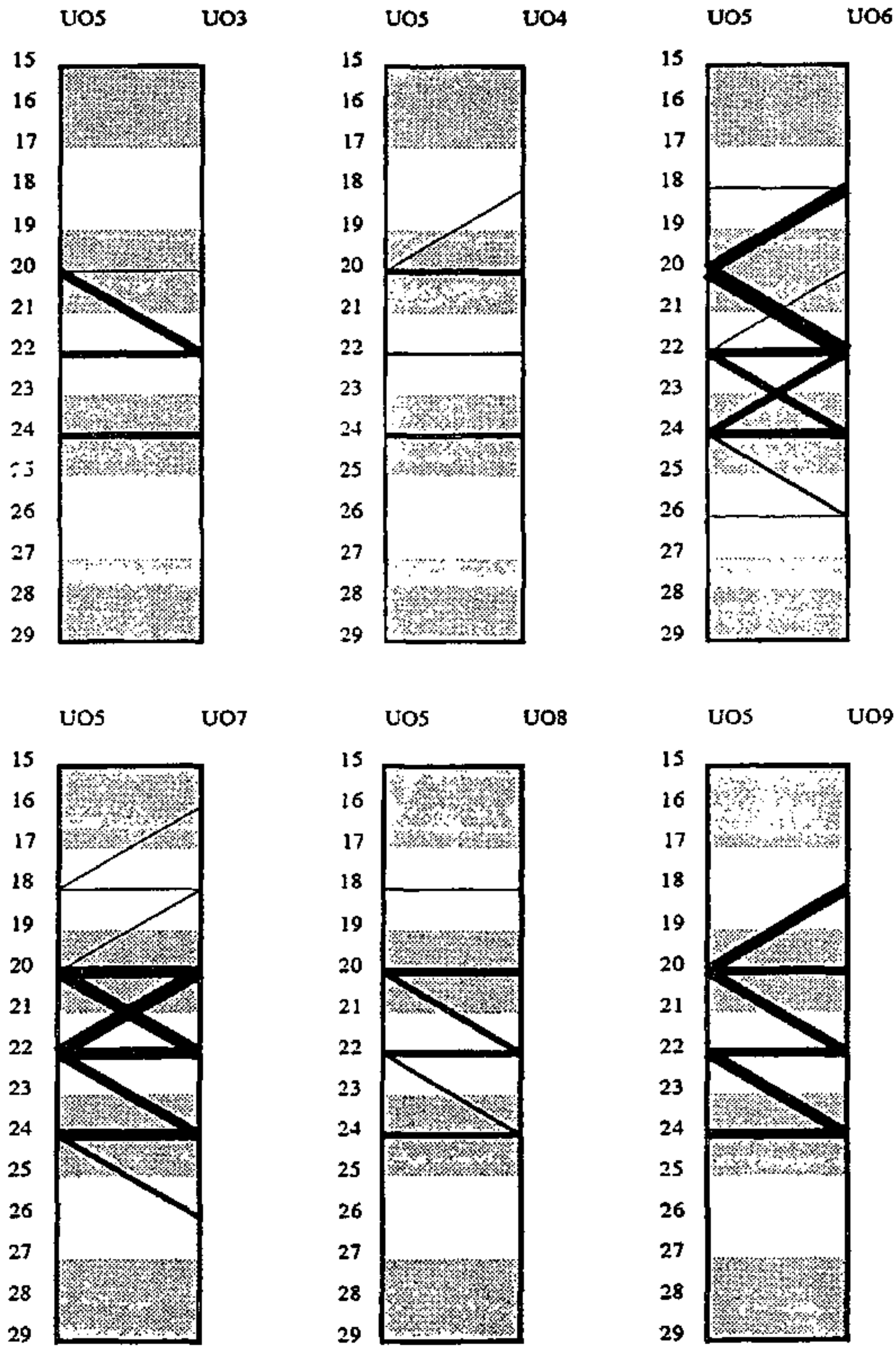

Figure 47: **Vertical sections where cross borehole packer tests were conducted. The thickness of the connecting lines indicates the relative magnitude of the hydraulic connection between the boreholes.**

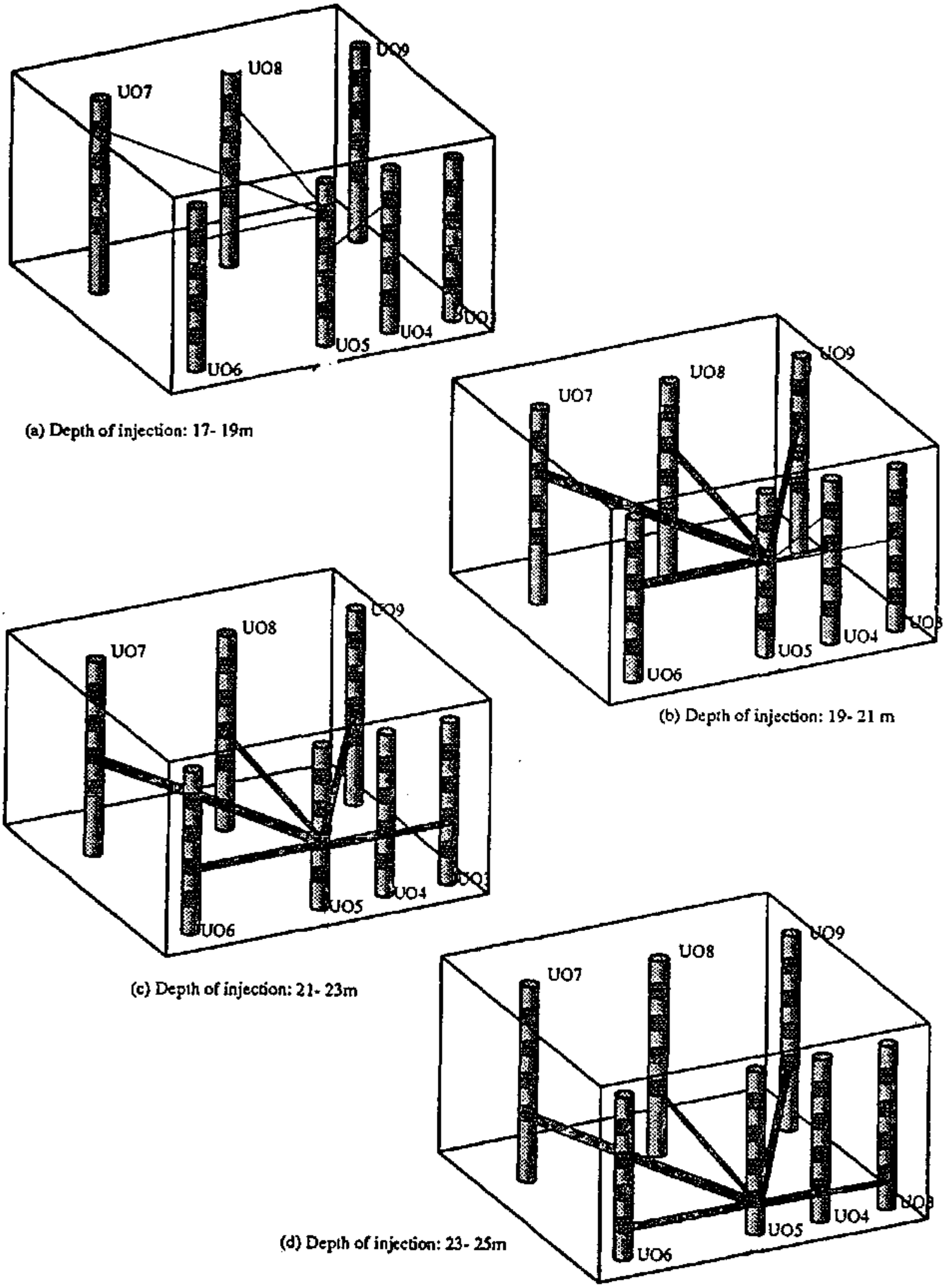

Figure 48: **A graphical representation of the connections observed during the cross borehole packer tests.**

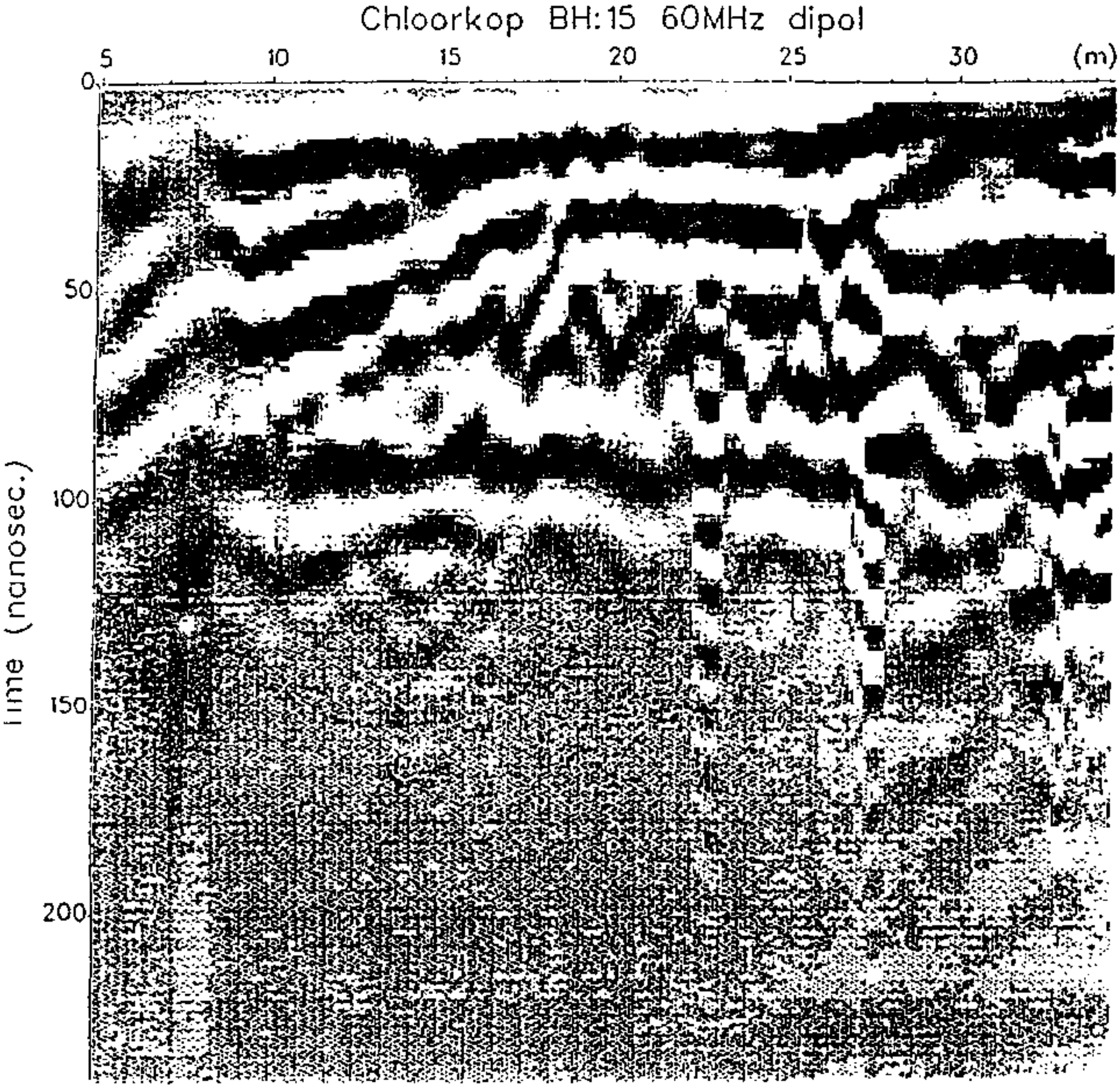

Figure 49: Radargram from Chloorkop. Borehole Ch-15, 60 MHz dipole antenna.

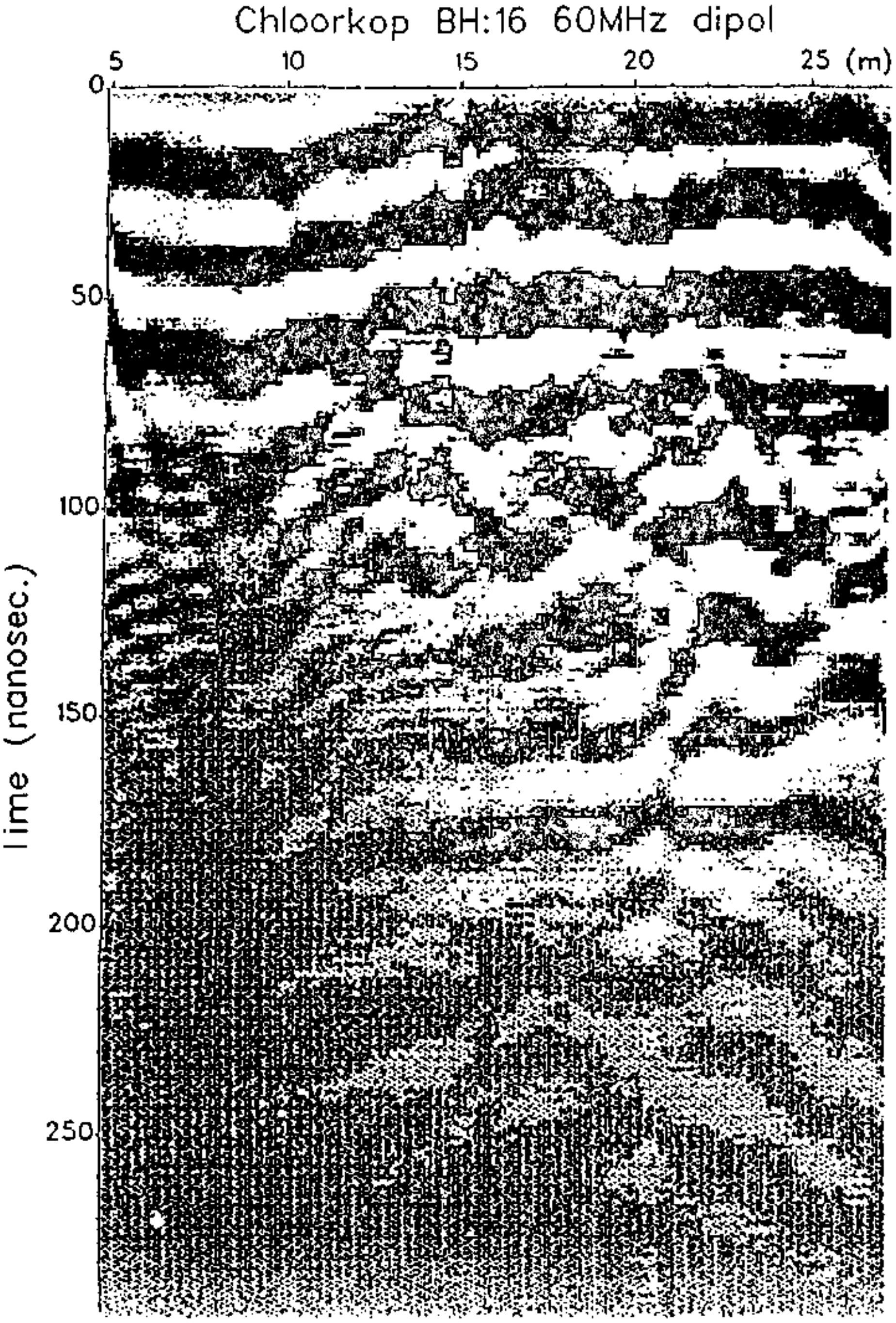

Figure 50: Radargram from Chloorkop. Borehole Ch-16, 60 MHz dipole antenna.

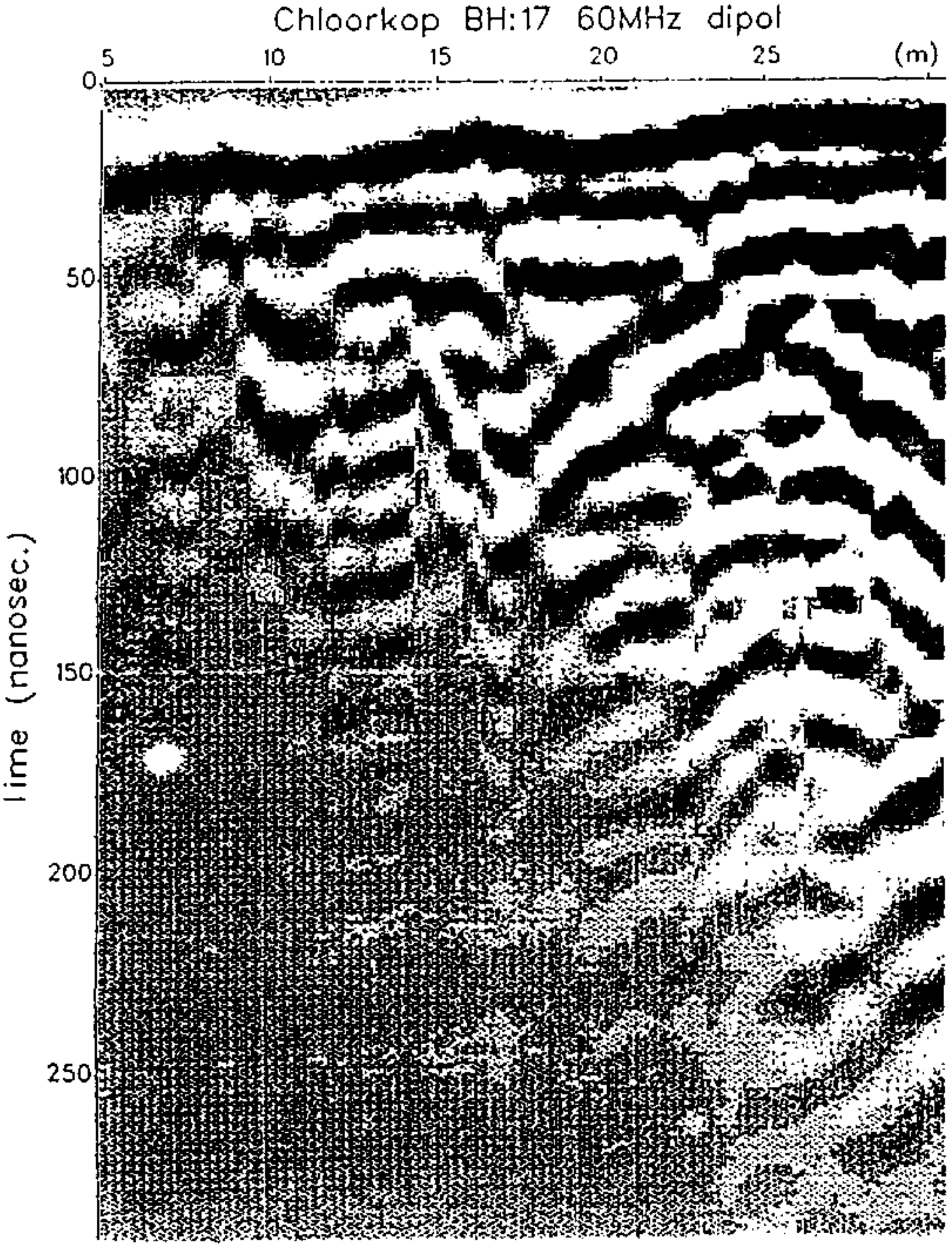

Figure 51: Radargram from Chloorkop. Borehole Ch-17, 60 MHz dipole antenna.

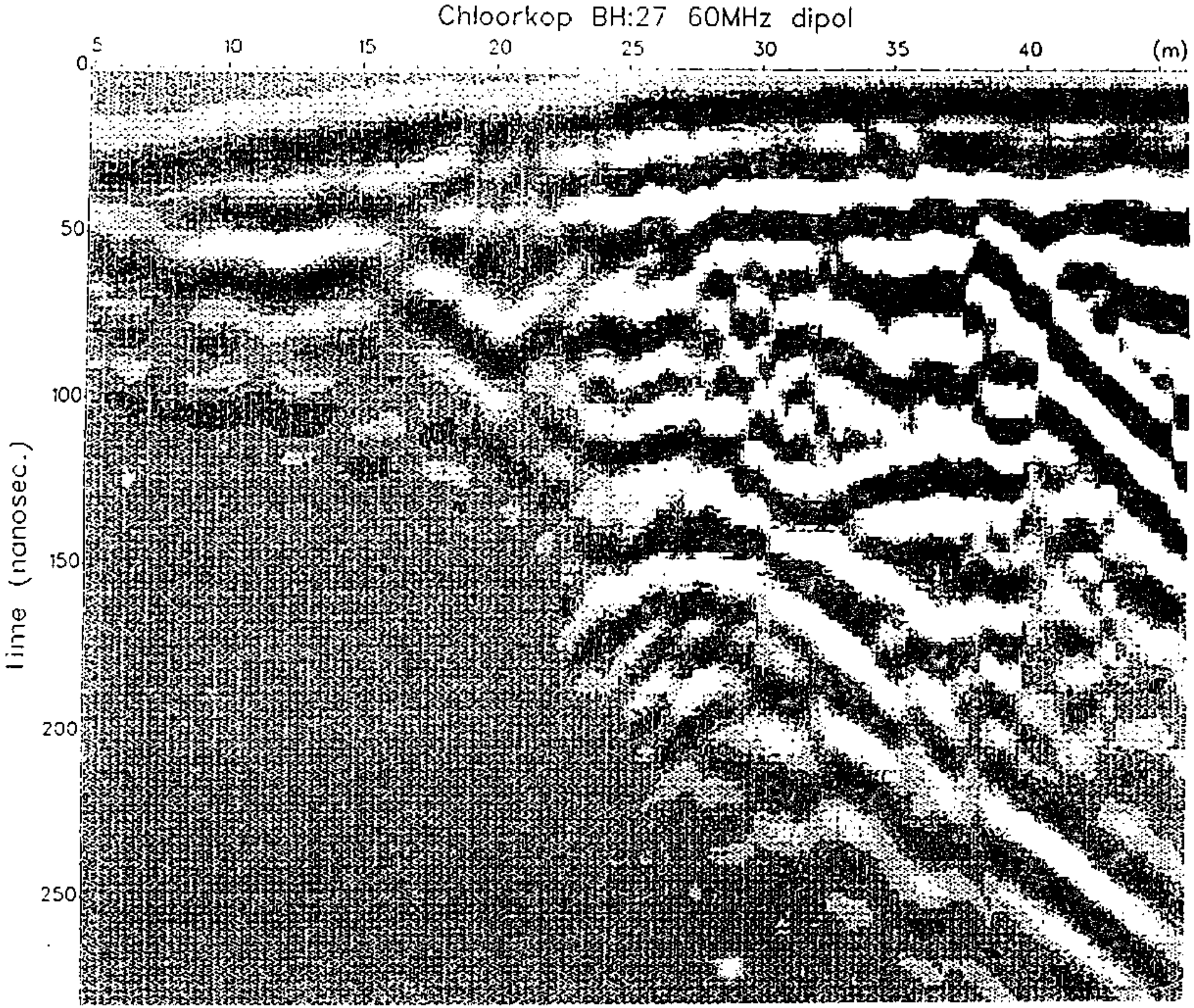

Figure 52: Radargram from Chloorkop. Borehole Ch-27, 60 MHz dipole antenna.

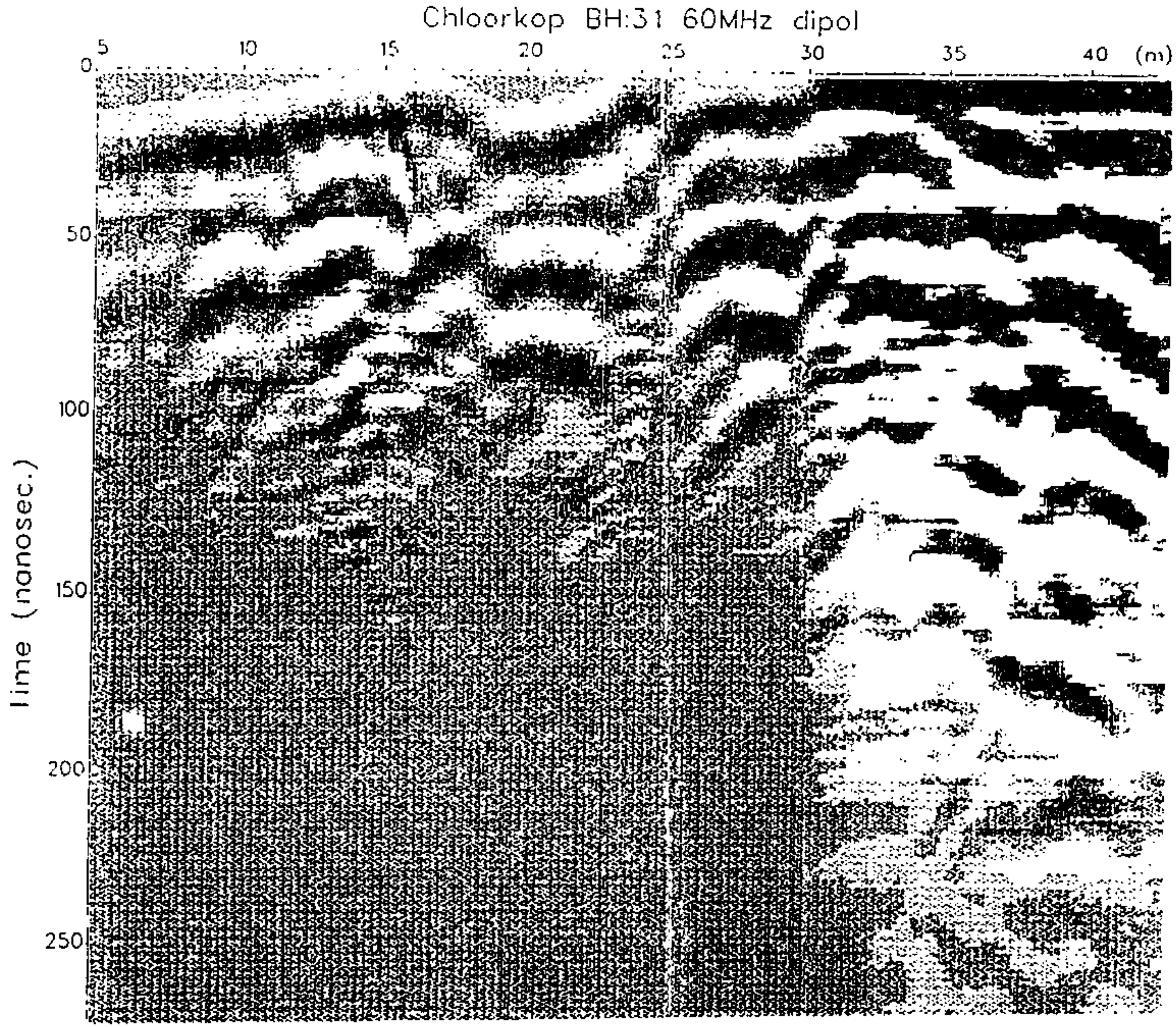

Figure 53: Radargram from Chloorkop. Borehole Ch-31, 60 MHz dipole antenna.

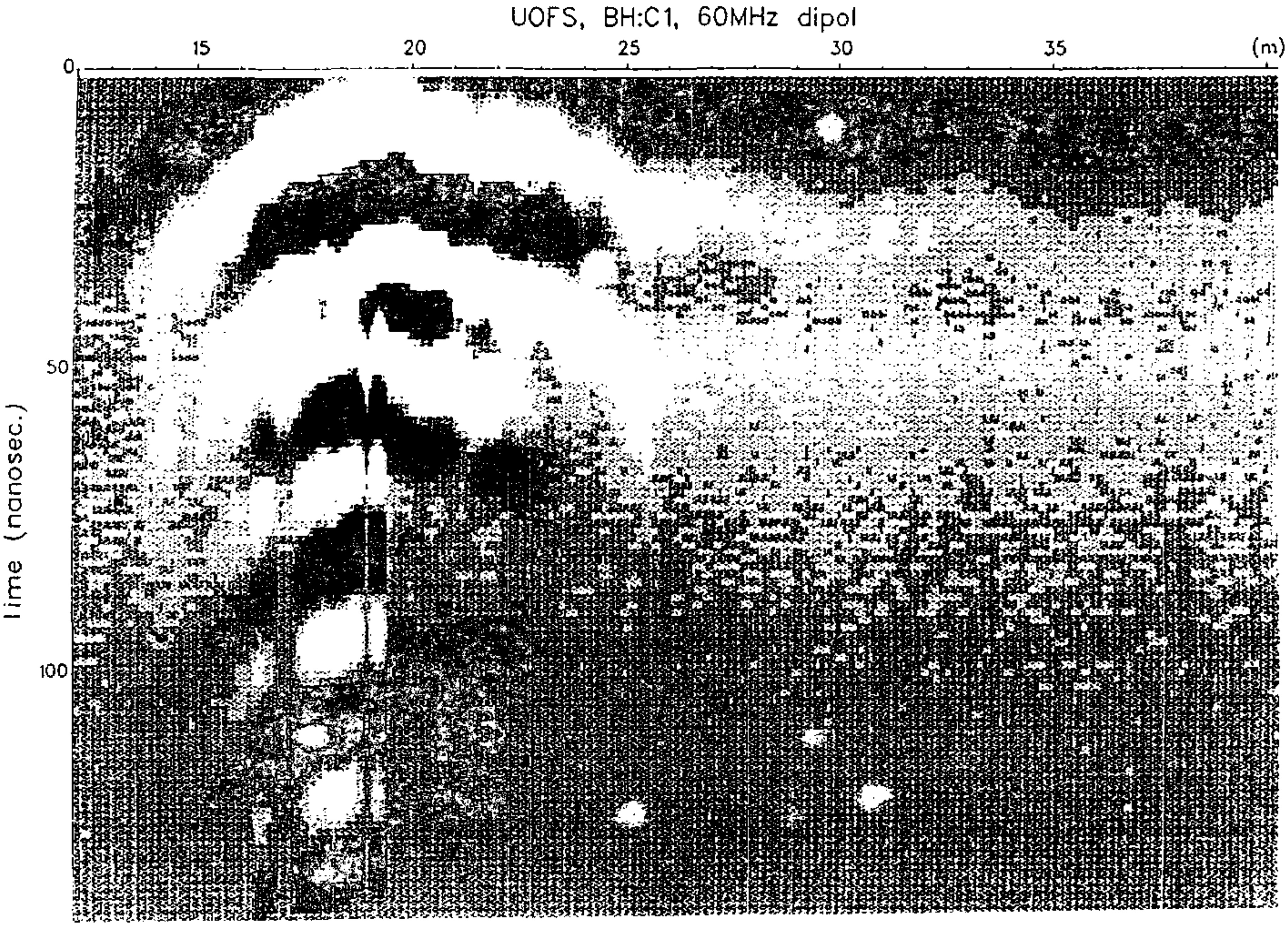

Figure 54: Radargram from IGS Karoo Test Site Borehole C1, 60 MHz dipole antenna.

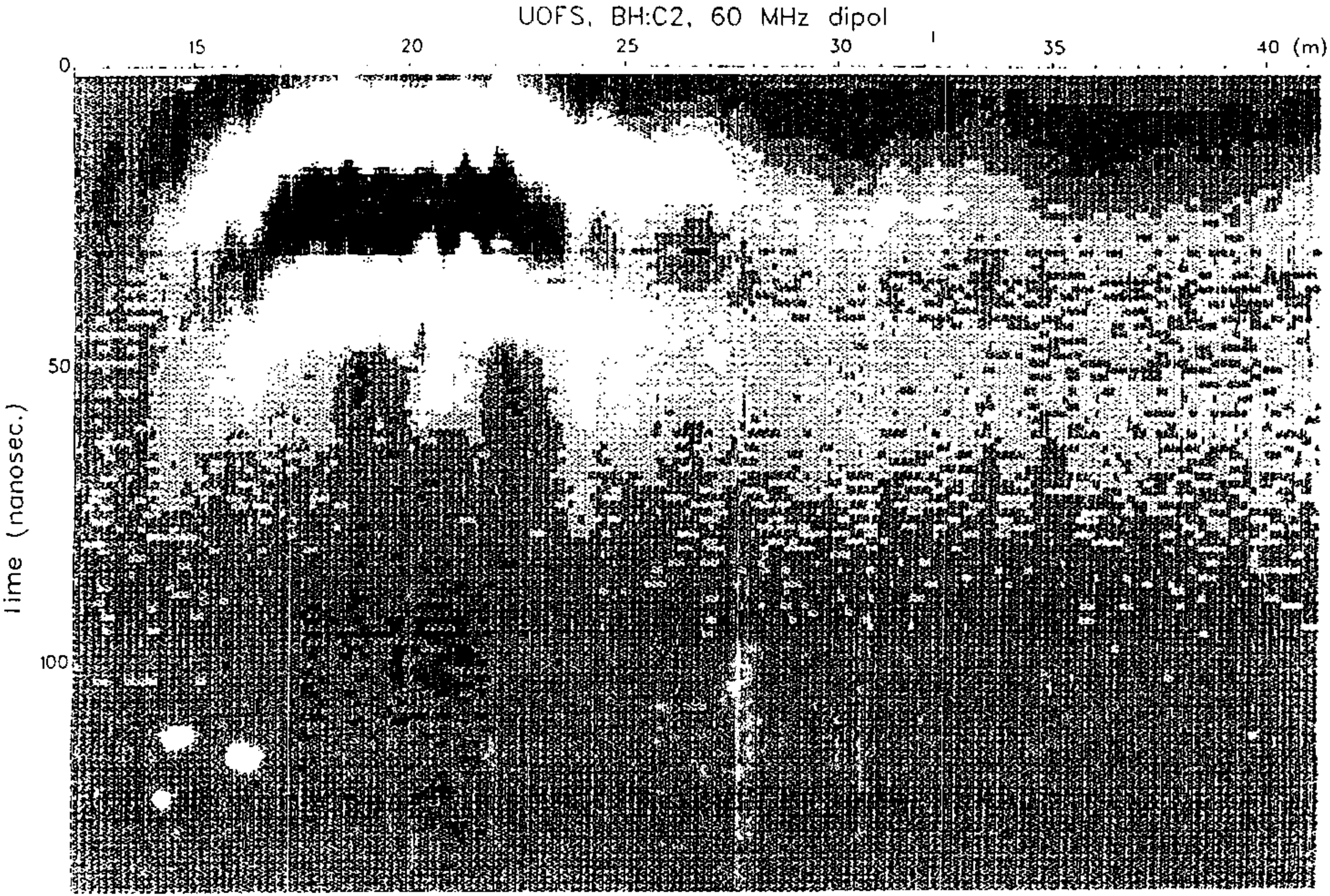

Figure 55: Radargram from IGS Karoo Test Site Borehole C2, 60 MHz dipole antenna.

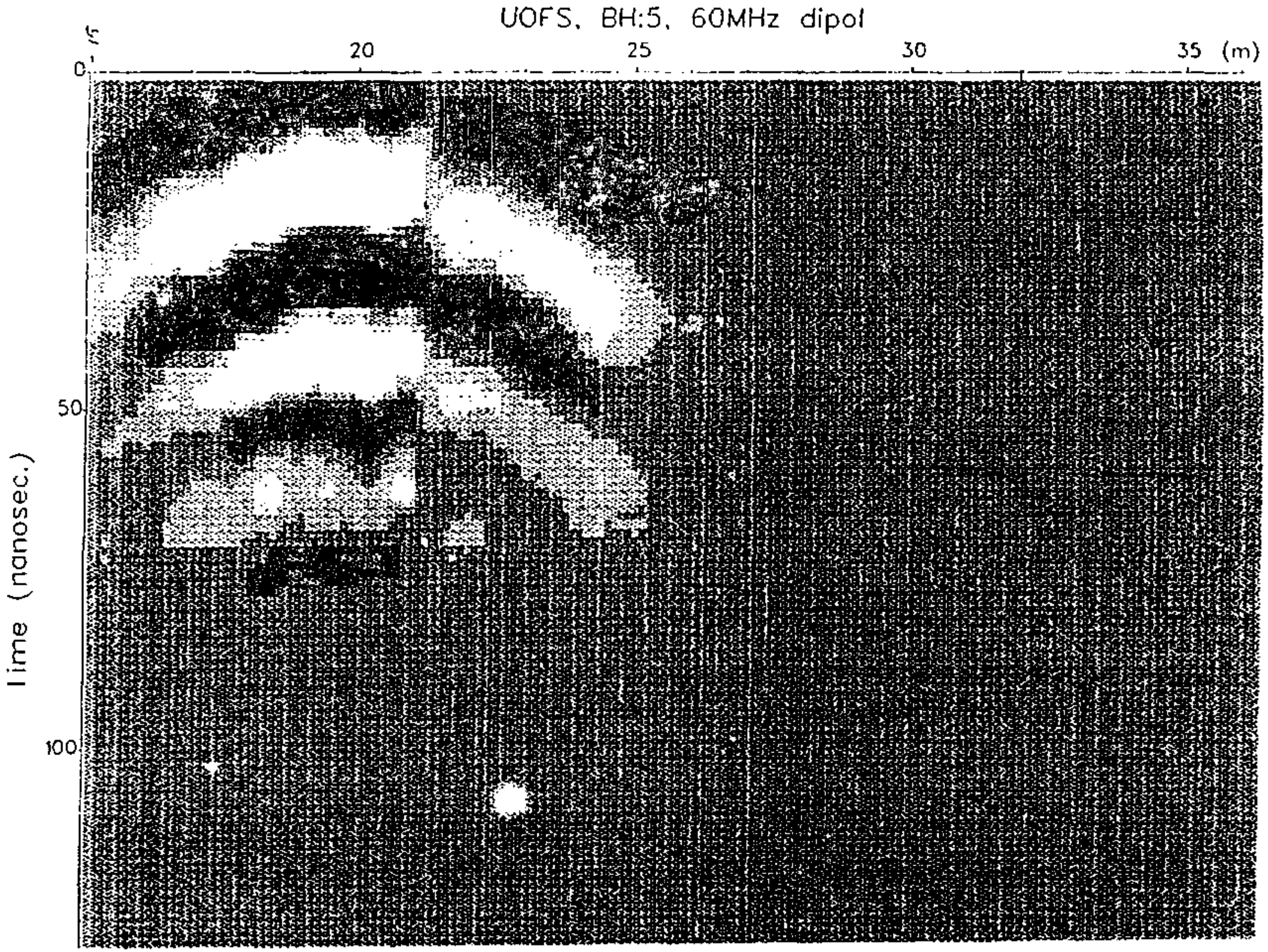

Figure 56: Radargram from IGS Karoo Test Site Borehole UO5, 60 MHz dipole antenna.

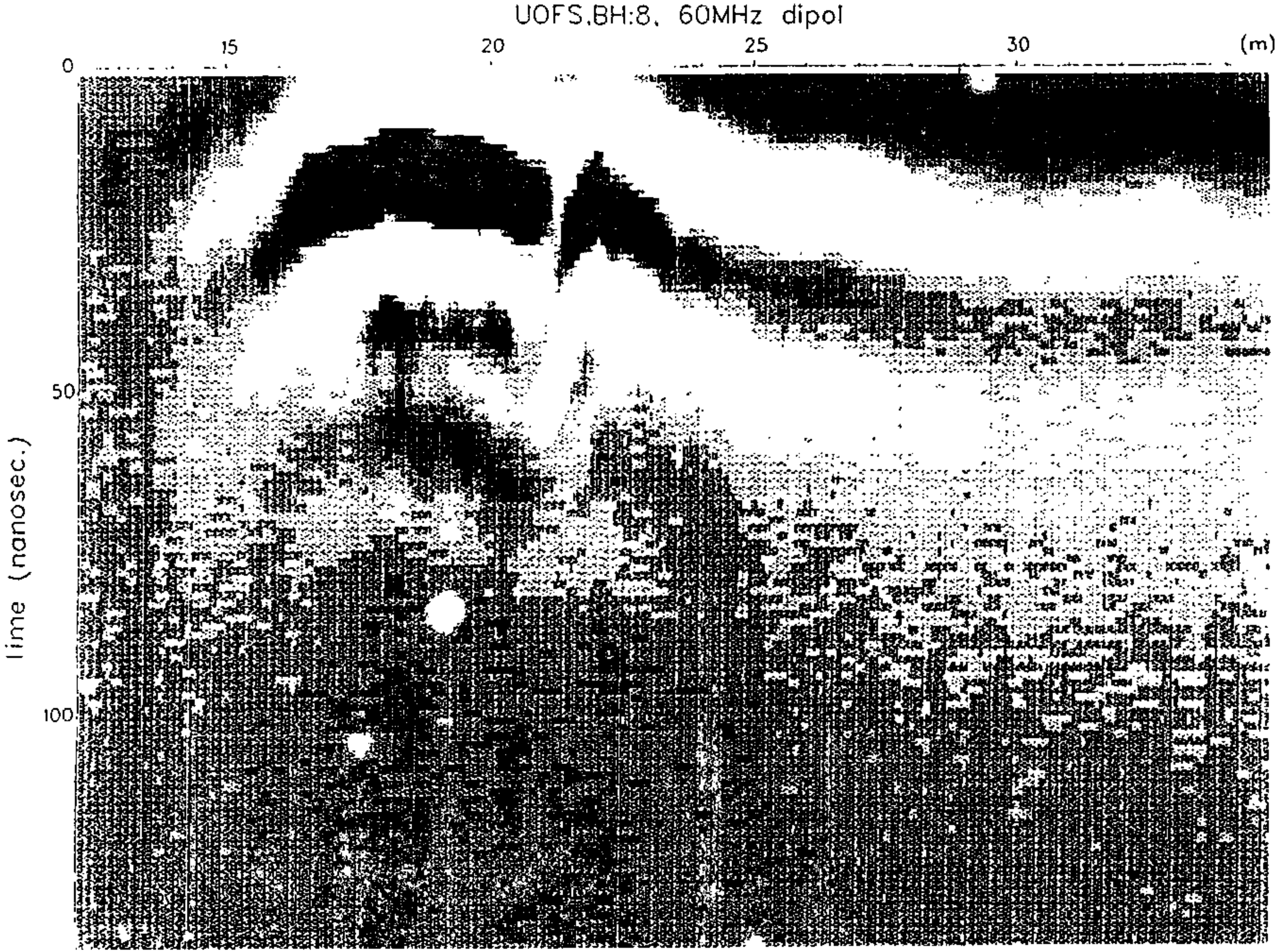

Figure 57: Radargram from IGS Karoo Test Site Borehole UO8, 60 MHz dipole antenna

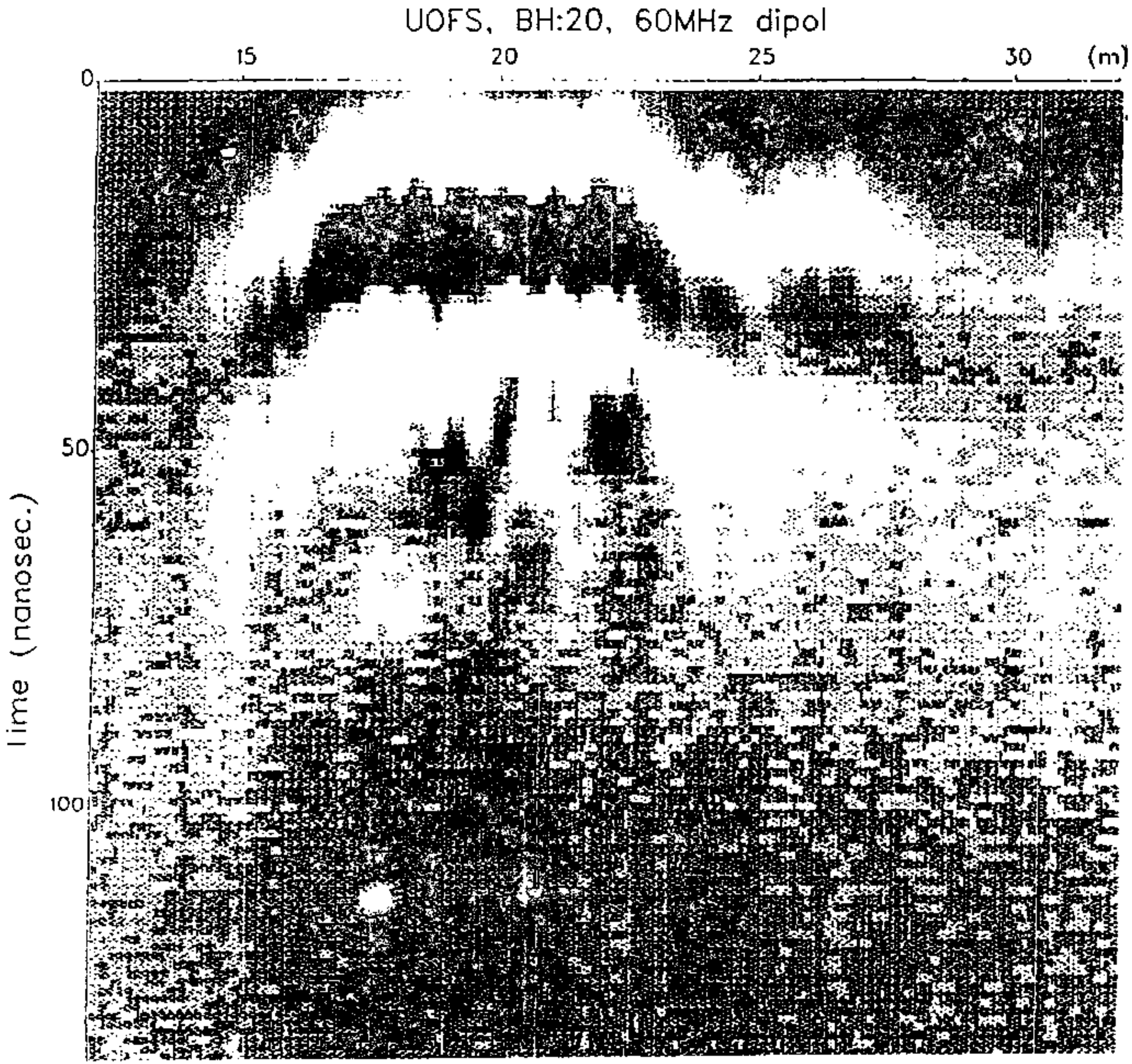

Figure 58: Radargram from IGS Karoo Test Site Borehole UO20, 60 MHz dipole antenna.

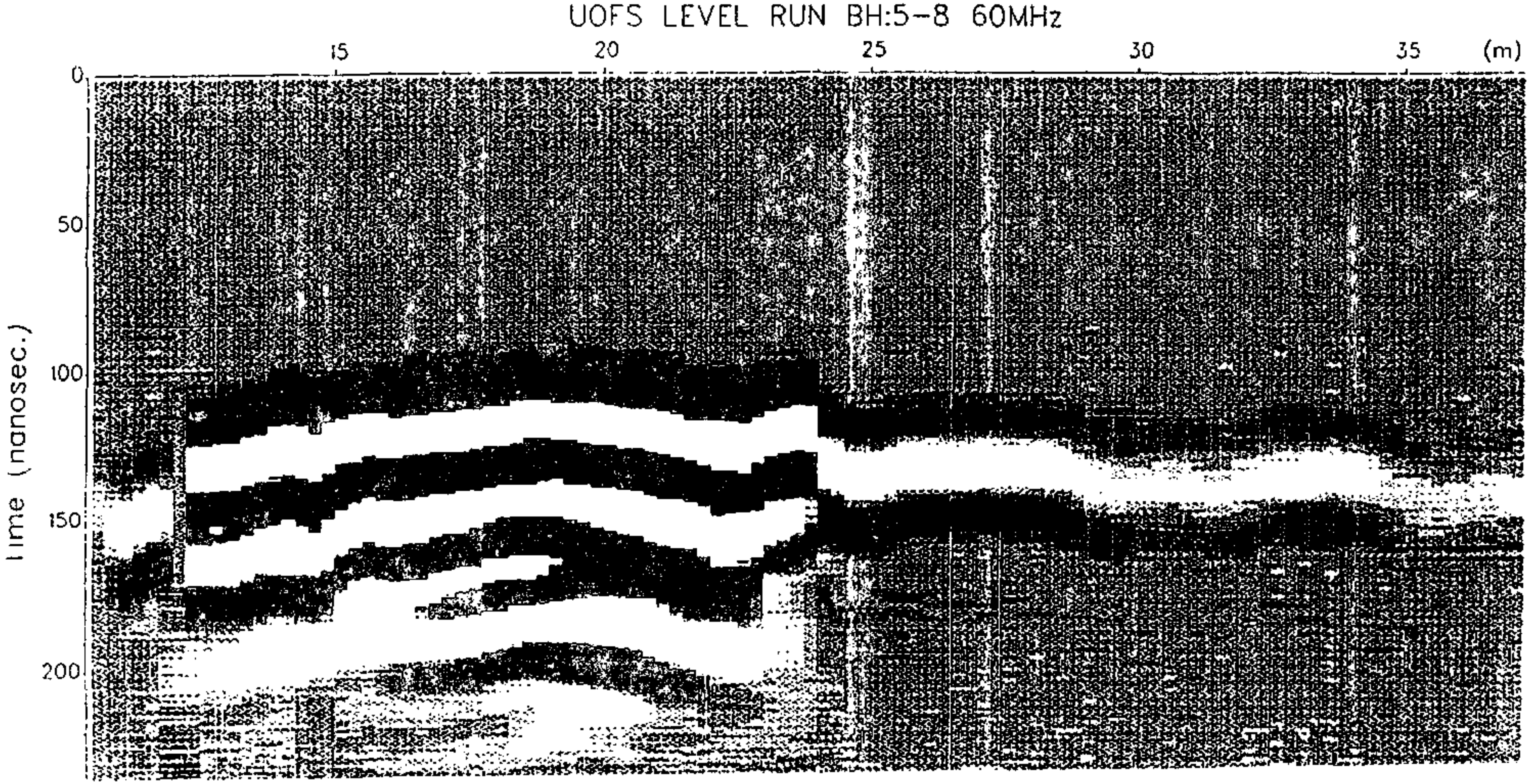

Figure 59: Radargram from IGS Karoo Test Site Borehole UO5, 60 MHz dipole antenna, parallel scan.